TOPICS IN HETEROCYCLIC CHEMISTRY

**Series Editor** R. R. Gupta **Volume Editors** K. Matsumoto · N. Hayashi

# Heterocyclic Supramolecules II



## 18 Topics in Heterocyclic Chemistry

Series Editor: R.R. Gupta<sup>†</sup>

## **Editorial Board:**

D. Enders · S.V. Ley · G. Mehta · K.C. Nicolaou

R. Noyori · L.E. Overman · A. Padwa

## **Topics in Heterocyclic Chemistry**

Series Editor: R. R. Gupta<sup>†</sup>

Recently Published and Forthcoming Volumes

### Phosphorous Heterocycles I

Volume Editor: R.K. Bansal Volume 20, 2009

### **Aromaticity in Heterocyclic Compounds**

Volume Editors: T. Krygowski, M. Cyrański Volume 19, 2009

#### Heterocyclic Supramolecules II

Volume Editors: K. Matsumoto<sup>†</sup>, N. Hayashi Volume 18, 2009

#### Heterocyclic Supramolecules I

Volume Editor: K. Matsumoto Volume 17, 2008

#### **Bioactive Heterocycles VII**

Flavonoids and Anthocyanins in Plants, and Latest Bioactive Heterocycles I Volume Editor: N. Motohashi Volume 16, 2009

### **Bioactive Heterocycles VI**

Flavonoids and Anthocyanins in Plants, and Latest Bioactive Heterocycles I Volume Editor: N. Motohashi Volume 15, 2008

## **Heterocyclic Polymethine Dyes**

Synthesis, Properties and Applications Volume Editor: L. Strekowski Volume 14, 2008

## Synthesis of Heterocycles via Cycloadditions II

Volume Editor: A. Hassner Volume 13, 2008

## Synthesis of Heterocycles via Cycloadditions I

Volume Editor: A. Hassner Volume 12, 2008

### Bioactive Heterocycles V

Volume Editor: M.T.H. Khan Volume 11, 2007

### **Bioactive Heterocycles IV**

Volume Editor: M.T.H. Khan Volume 10, 2007

## **Bioactive Heterocycles III**

Volume Editor: M.T.H. Khan Volume 9, 2007

#### **Bioactive Heterocycles II**

Volume Editor: S. Eguchi Volume 8, 2007

### **Heterocycles from Carbohydrate Precursors**

Volume Editor: E.S.H. ElAshry

Volume 7, 2007

#### **Bioactive Heterocycles I**

Volume Editor: S. Eguchi Volume 6, 2006

#### **Marine Natural Products**

Volume Editor: H. Kiyota Volume 5, 2006

## **QSAR** and Molecular Modeling Studies

## in Heterocyclic Drugs II

Volume Editor: S.P. Gupta Volume 4, 2006

### **QSAR** and Molecular Modeling Studies

in Heterocyclic Drugs I Volume Editor: S.P. Gupta Volume 3, 2006

#### **Heterocyclic Antitumor Antibiotics**

Volume Editor: M. Lee Volume 2, 2006

## Heterocyclic Supramolecules II

**Volume Editors:** 

K. Matsumoto<sup>†</sup>, N. Hayashi

## With Contributions by

R. Bishop · M. R. Caira · N. Hayashi · H. Higuchi

M. Iyoda · K. Ninomiya · T. Nishinaga · H. Suga

M. Takase · K. Tanaka



The series *Topics in Heterocyclic Chemistry* presents critical reviews on "Heterocyclic Compounds" within topic-related volumes dealing with all aspects such as synthesis, reaction mechanisms, structure complexity, properties, reactivity, stability, fundamental and theoretical studies, biology, biomedical studies, pharmacological aspects, applications in material sciences, etc. Metabolism will also be included which will provide information useful in designing pharmacologically active agents. Pathways involving destruction of heterocyclic rings will also be dealt with so that synthesis of specifically functionalized non-heterocyclic molecules can be designed.

The overall scope is to cover topics dealing with most of the areas of current trends in heterocyclic chemistry which will suit to a larger heterocyclic community.

As a rule, contributions are specially commissioned. The editors and publishers will, however, always be pleased to receive suggestions and supplementary information. Papers are accepted for *Topics in Heterocyclic Chemistry* in English.

In references, Topics in Heterocyclic Chemistry is abbreviated Top Heterocycl Chem and is cited as a journal.

Springer www home page: springer.com Visit the THC content at springerlink.com

Topics in Heterocyclic Chemistry ISSN 1861-9282 ISBN 978-3-642-02040-7 e-ISBN 978-3-642-02041-4 DOI 10.1007/978-3-642-02041-4 Springer Dordrecht Heidelberg London New York

Library of Congress Control Number: 2009931323

#### © Springer-Verlag Berlin Heidelberg 2009

This work is subject to copyright. All rights are reserved, whether the whole or part of the material is concerned, specifically the rights of translation, reprinting, reuse of illustrations, recitation, broadcasting, reproduction on microfilm or in any other way, and storage in data banks. Duplication of this publication or parts thereof is permitted only under the provisions of the German Copyright Law of September 9, 1965, in its current version, and permission for use must always be obtained from Springer. Violations are liable to prosecution under the German Copyright Law.

The use of general descriptive names, registered names, trademarks, etc. in this publication does not imply, even in the absence of a specific statement, that such names are exempt from the relevant protective laws and regulations and therefore free for general use.

Cover design: WMX Design GmbH, Heidelberg, Germany

Printed on acid-free paper

Springer is part of Springer Science+Business Media (www.springer.com)

## **Series Editor**

Prof. R. R. Gupta<sup>†</sup> 10A, Vasundhara Colony Lane No. 1, Tonk Road Jaipur 302018 India

## **Volume Editors**

Prof. Dr. Kiyoshi Matsumoto<sup>†</sup>

Chiba Institute of Science Faculty of Pharmaceutical Sciences 15-8 Shiomi-Cho Chiba, Choshi-Shi 288-0025 Japan Dr. Naoto Hayashi

Associate Professor of Chemistry Graduate School of Science and Engineering University of Toyama 3190 Gofuku Toyama 930-855 Japan nhayashi@sci.u-toyama.ac.jp

## **Editorial Board**

Prof. D. Enders

RWTH Aachen Institut für Organische Chemie 52074, Aachen, Germany enders@rwth-aachen.de

Prof. Steven V. Ley FRS

BP 1702 Professor and Head of Organic Chemistry University of Cambridge Department of Chemistry Lensfield Road Cambridge, CB2 1EW, UK svl1000@cam.ac.uk

Prof. G. Mehta FRS

Director
Department of Organic Chemistry
Indian Institute of Science
Bangalore 560 012, India
gm@orgchem.iisc.ernet.in

Prof. K.C. Nicolaou

Chairman
Department of Chemistry
The Scripps Research Institute
10550 N. Torrey Pines Rd.
La Jolla, CA 92037, USA
kcn@scripps.edu
and
Professor of Chemistry
Department of Chemistry and Biochemistry
University of CA
San Diego, 9500 Gilman Drive
La Jolla, CA 92093, USA

vi Editorial Board

Prof. Ryoji Noyori NL

President RIKEN (The Institute of Physical and Chemical Research) 2-1 Hirosawa, Wako Saitama 351-0198, Japan and University Professor

University Professor
Department of Chemistry
Nagoya University
Chikusa, Nagoya 464-8602, Japan
noyori@chem3.chem.nagoya-u.ac.jp

Prof. Larry E. Overman

Distinguished Professor Department of Chemistry 516 Rowland Hall University of California, Irvine Irvine, CA 92697-2025 leoverma@uci.edu

Prof. Albert Padwa

William P. Timmie Professor of Chemistry Department of Chemistry Emory University Atlanta, GA 30322, USA chemap@emory.edu

## **Preface**

Explanation of the structure-property relationship of a given molecule is generally simple because the characteristics of the atomic groups and chemical bonds and the effects emerging from their interaction have long been known, both from theoretical studies and numerous experimental results. In contrast, it is often difficult to analyze, estimate, and account for the structure-properties relationship in supramolecules. The characteristics of supramolecules are governed both by the nature of the constituent molecules and by their configuration while the characteristics of the constituent molecules are usually evident as mentioned above; their configurations are difficult to control, predict, and accurately estimate because of insufficient knowledge regarding the intermolecular forces. Moreover, since most of the intermolecular forces constructing supramolecules are weak, the supramolecular structure may vary depending on various factors, such as modification of the molecular structure, auxiliaries, and experimental conditions. Thus, in order to obtain supramolecules with the desired structures and properties, theoretical investigations on the intermolecular forces and accumulation of experimental studies on the relationship between the supramolecular structure and properties are both important.

In line with this, the present volume, *Topics in Heterocyclic Chemistry:* Supramolecular Chemistry II, which is a continuation of Supramolecular Chemistry I, is a review of recent studies on intermolecular interactions connecting (and occasionally repelling) the molecules together with a few individual topics including formation, structure, and function of crystalline-state host-guest supramolecular systems and intelligent supramolecular nano assemblies and highly stereoselective 1,3-dipolar cycloaddition catalyzed by supramolecular complex. In all chapters, the unique characteristics of heterocyclic moieties play a significant role.

The first chapter, " $X/\pi$  Interactions in Aromatic Heterocycles: Basic Principles and Recent Advances" by N. Hayashi, H. Higuchi, and K. Ninomiya, reviews recent theoretical and (partly) experimental studies on inter- and intramolecular interactions as the constructing forces of the supramolecules, which include  $\pi/\pi$ ,  $CH/\pi$ , cation/ $\pi$ , anion/ $\pi$ ,  $OH/\pi$ ,  $NH/\pi$ , and lone-pair/ $\pi$  interactions, and the interplay of  $\pi/\pi$  interaction and hydrogen bonding. Unlike the other chapters in Volumes I and II, which have no apparent relationship, this chapter can be regarded as an introduction to the overall theoretical fundamentals.

viii Preface

The second chapter, "Supramolecular Host–Guest Chemistry of Heterocyclic V-Shaped Molecules" by R. Bishop, describes crystalline-state inclusion behavior of  $C_2$ -symmetrical V-shaped host compounds consisting of heterocyclic moieties. The guidelines of the design and synthesis of the host molecules are also documented.

The third chapter, "Inclusion and Optical Resolution of Guest Molecules by Selected Synthetic Dihydroxy- and Trihydroxy-Host Compounds Containing Heterocyclic Scaffolds" by M. Caira and K. Tanaka, describes inclusion properties and crystal structures of TADDOL host compounds, which have a heterocyclic backbone and bear two or more hydroxy groups. The optical resolution of guest components is also discussed with reference to the structure of the host molecules.

The fourth chapter, "Supramolecular Structures and Nanoassemblies of Oligothiophenes and Tetrathiafulvalenes" by M. Iyoda, T. Nishinaga, and M. Takase, describes structure, conductivities, and optical properties of intelligent supramolecular nano-self-assemblies (nanofibers, nanoparticles, etc.) consisting of oligothiophenes and tetrathiafulvalene (TTF) derivatives. The results will provide important information for developing molecular electronics based on organic molecules.

In the final chapter, "Asymmetric 1,3-Dipolar Cycloaddition Reactions Catalyzed by Heterocycle-Based Metal Complexes" by H. Suga, highly enantioselective 1,3-dipolar cycloadditions are described, where the supramolecular catalysts consisting of metal cation and chiral heterocyclic ligands play a significant role.

This volume was originally edited by Professor Kiyoshi Matsumoto, who was also an Editor of *Topics in Heterocyclic Chemistry: Supramolecular Chemistry I.* Unfortunately, however, he died in the summer of 2008, before its completion. It was then taken over by us and completed according to his original plan, except for the missing chapter by Prof. Matsumoto himself. This volume, as well as *Supramolecular Chemistry I*, incorporates all the latest advances in heterocyclic supramolecular chemistry. We believe that the articles published in the two volumes will encourage progress in this area, and are sure that they will become an enduring monument of Prof. Matsumoto, a great master of heterocyclic supramolecular chemistry.

Toyama, May 2009

Naoto Hayashi

## **Contents**

$X/\pi$ Interactions in Aromatic Heterocycles:	
Basic Principles and Recent Advances	1
Naoto Hayashi, Hiroyuki Higuchi, and Keiko Ninomiya	
Supramolecular Host–Guest Chemistry	
of Heterocyclic V-Shaped Molecules	37
Roger Bishop	
Inclusion and Optical Resolution of Guest Molecules by Selected	
Synthetic Dihydroxy- and Trihydroxy-Host	
Compounds Containing Heterocyclic Scaffolds	75
Mino R. Caira and Koichi Tanaka	
Supramolecular Structures and Nanoassemblies	
of Oligothiophenes and Tetrathiafulvalenes	103
Masahiko Iyoda, Tohru Nishinaga, and Masayoshi Takase	
Asymmetric 1,3-Dipolar Cycloaddition Reactions Catalyzed	
by Heterocycle-Based Metal Complexes	119
Hiroyuki Suga	
Index	155

Top Heterocycl Chem (2009) 18: 1–35

DOI: 10.1007/7081\_2008\_15

© Springer-Verlag Berlin Heidelberg 2009

Published online: 14 March 2009

## $X/\pi$ Interactions in Aromatic Heterocycles: Basic Principles and Recent Advances

Naoto Hayashi, Hiroyuki Higuchi, and Keiko Ninomiya

**Abstract** This article outlines the basic principles and recent advances of  $XH/\pi$  interactions involving heteroaromatic molecules or moieties, which include  $\pi/\pi$  interactions,  $CH/\pi$  interactions, cation/ $\pi$  interactions, anion/ $\pi$  interactions,  $NH/\pi$  and  $OH/\pi$  interactions, and lone-pair/ $\pi$  interactions. Their fundamental features (such as interaction energies and favorable geometries) investigated by means of high-level theoretical calculations and statistical studies are described and compared to interactions involving aromatic hydrocarbons. Several typical or unique examples, where  $XH/\pi$  interactions play a significant role in construction of crystal and supramolecular structures and/or in modulating the properties are shown. The interplay of  $\pi/\pi$  interaction and hydrogen bonding is also mentioned.

**Keywords** Database analysis, Theoretical calculations,  $X/\pi$  interactions, X-ray structure

#### **Contents**

1	Intro	oduction: Classification of $X/\pi$ Interactions and Methods	2
2	$\pi/\pi$	and CH/π Interactions	6
	2.1	Geometry and Interaction Energy of Two Aromatic Molecules	6
	2.2	Theoretical Studies on $\pi/\pi$ and CH/ $\pi$ Interactions of $\pi$ -Deficient	
		Heteroaromatic Molecules	7
	2.3	Theoretical Studies on $\pi/\pi$ and CH/ $\pi$ Interactions of $\pi$ -Excessive	
		Heteroaromatic Molecules	10
	2.4	Substituent Effects in $\pi/\pi$ and CH/ $\pi$ Interactions	12
	2.5	Statistical and Experimental Studies on $\pi/\pi$ and $CH/\pi$ Interactions	15
3	Cati	on/π Interactions.	17

Graduate School of Science and Engineering, University of Toyama, Gofuku,

Toyama, 930-8555, Japan

e-mail: nhayashi@sci.u-toyama.ac.jp

K. Ninomiya

Graduate School of Engineering, Kyoto University, Katsura, Kyoto, 615-8510, Japan

N. Hayashi ( ) and H. Higuchi

Top Heterocycl Chem (2009) 18: 1–35

DOI: 10.1007/7081\_2008\_15

© Springer-Verlag Berlin Heidelberg 2009

Published online: 14 March 2009

## $X/\pi$ Interactions in Aromatic Heterocycles: Basic Principles and Recent Advances

Naoto Hayashi, Hiroyuki Higuchi, and Keiko Ninomiya

**Abstract** This article outlines the basic principles and recent advances of  $XH/\pi$  interactions involving heteroaromatic molecules or moieties, which include  $\pi/\pi$  interactions,  $CH/\pi$  interactions, cation/ $\pi$  interactions, anion/ $\pi$  interactions,  $NH/\pi$  and  $OH/\pi$  interactions, and lone-pair/ $\pi$  interactions. Their fundamental features (such as interaction energies and favorable geometries) investigated by means of high-level theoretical calculations and statistical studies are described and compared to interactions involving aromatic hydrocarbons. Several typical or unique examples, where  $XH/\pi$  interactions play a significant role in construction of crystal and supramolecular structures and/or in modulating the properties are shown. The interplay of  $\pi/\pi$  interaction and hydrogen bonding is also mentioned.

**Keywords** Database analysis, Theoretical calculations,  $X/\pi$  interactions, X-ray structure

#### **Contents**

1	Intro	oduction: Classification of $X/\pi$ Interactions and Methods	2
2	$\pi/\pi$	and CH/π Interactions	6
	2.1	Geometry and Interaction Energy of Two Aromatic Molecules	6
	2.2	Theoretical Studies on $\pi/\pi$ and CH/ $\pi$ Interactions of $\pi$ -Deficient	
		Heteroaromatic Molecules	7
	2.3	Theoretical Studies on $\pi/\pi$ and CH/ $\pi$ Interactions of $\pi$ -Excessive	
		Heteroaromatic Molecules	10
	2.4	Substituent Effects in $\pi/\pi$ and CH/ $\pi$ Interactions	12
	2.5	Statistical and Experimental Studies on $\pi/\pi$ and $CH/\pi$ Interactions	15
3		on/π Interactions	

Graduate School of Science and Engineering, University of Toyama, Gofuku,

Toyama, 930-8555, Japan

e-mail: nhayashi@sci.u-toyama.ac.jp

K. Ninomiya

Graduate School of Engineering, Kyoto University, Katsura, Kyoto, 615-8510, Japan

N. Hayashi ( ) and H. Higuchi

4 Anion/π Interactions .....

3 OH/It and	NH/\(\pi\) Interactions				
	$r/\pi$ Interactions				
	of $\pi/\pi$ Interaction and Hydrogen Bonding				
	ng Remarks				
References					
Abbreviati	on				
Arg	Arginine				
B3LYP	Becke's three-parameter method with Lee-Yang-Parr correlation functional				
BSSE	Basis set superposition error				
CCSD	Coupled cluster with single and double excitations				
CCSD(T)	Coupled cluster with single, double, and perturbative triple excitations				
CSD	Cambridge structural database				
CT	Charge transfer				
DF-DFT	Density fitting DFT				
DFT	Density functional theory				
DFT-D	DFT methods explicitly including dispersion terms				
HOMO	Highest occupied molecular orbital				
LMP2	Local MP2				
LUMO	Lowest unoccupied molecular orbital				
Lys	Lysine				
MEP	Molecular electrostatic potential				
MO	Molecular orbital				
MPn	<i>n</i> th order Møller–Plesset methods ( $n = 2$ or 4)				
NICS	Nucleus-independent chemical shift				
PDB	Brookhaven protein databank				
Phe	Phenylalanine				
RI-MP2	-MP2 Resolution of identity MP2				
SCS-MP2	Spin-component-scaled MP2				

## 1 Introduction: Classification of $X/\pi$ Interactions and Methods

Trp

Tyr

VDZ VTZ Tryptophan Tyrosine

Valence double zeta

Valence triple zeta

Molecular complexes have attracted much attention recently because they frequently have properties that go beyond the mere sum of constituent molecules. Molecular complexes that are structurally interesting or bear intriguing properties are referred to as *supramolecules*. The nature of supramolecules is determined by the character of the constituent molecules and how they interact, as the molecule is

characterized by the constituent atoms and the covalent bondings connecting them. Generally, it is easy for us chemists to estimate the character of molecules approximately, because of accumulated knowledge of the atom, functional groups, and chemical bondings. In contrast, prediction of the structure of supramolecules, how they behave, or even whether or not they can exist is difficult, because, assuming the character of the constituent molecules is predictable, the intermolecular interactions are not fully understood. Studies on the intermolecular interactions of benzene and other aromatic hydrocarbons were intensively conducted during the 1990s and early 2000s and reviewed several times [1-7]; on the other hand, those of heteroaromatic molecules have been less investigated in spite of their importance in biochemistry, material chemistry, physical chemistry, and structural chemistry. Compared to benzene and other aromatic hydrocarbons, heteroaromatic molecules are expected to exhibit different behavior because the intrinsic  $\pi$ -excessive and  $\pi$ -deficient characters would affect  $X/\pi$  interactions considerably and the unsymmetrical molecular structure would give an additional contribution in a dipole-dipole and dipole-induced dipole manner. This article outlines the basic principles and recent advances on intermolecular interactions of heteroaromatic  $\pi$  molecules (X/ $\pi$  interactions), which include energetically favorable configurations, the magnitude and origins of interaction energies, and the deviation from those of aromatic hydrocarbons. The intermolecular interactions mentioned in this article are depicted in Fig. 1.

The  $\pi$  moieties stacked in a face-to-face manner cause attractive interaction, which is referred to as  $\pi/\pi$  interaction [1]. The typical  $\pi/\pi$  interaction energy is 2–3 kcal mol<sup>-1</sup> for benzene dimer. Since  $\pi/\pi$  interactions originate principally from dispersion forces [2], the magnitude of the interaction energy is likely to vary significantly for heteroaromatic molecules depending on their  $\pi$ -excessive (pyrrole, furan, and thiophene) and  $\pi$ -deficient (pyrrole, imidazole, and triazine) characters. Moreover, dipole–dipole and/or dipole–induced dipole interactions would emerge due to the less symmetrical molecular structure. On the other hand, when  $\pi$  moieties are placed in an edge-to-face manner, attractive interaction between the C–H group and  $\pi$  moiety is caused, called  $CH/\pi$  interaction [3]. In  $CH/\pi$  interactions, charge transfer and dispersion forces play important roles. Interaction energies of  $CH/\pi$  interactions are known to be comparable to those of  $\pi/\pi$  interactions in benzene dimers.

Interactions of cationic species with  $\pi$  electrons are called *cation*/ $\pi$  interactions [4, 8]. The interaction energy is considerably larger, going up to several tens of

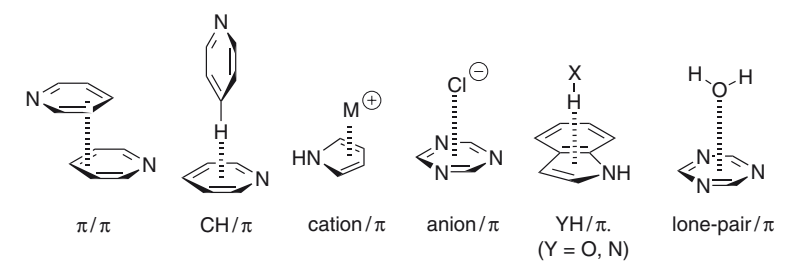


Fig. 1 Intermolecular interactions of heteroaromatic molecules

kilocalories per mole. As cation/ $\pi$  interactions appear to originate from electrostatic forces between the positive charge of the cation and the negative character of the  $\pi$  electrons, it would be larger for  $\pi$ -excessive heteroaromatic molecules. In contrast, interactions between anion and  $\pi$  electrons are referred to as  $anion/\pi$  interactions [5]. Since benzene is a  $\pi$ -excessive moiety substantially, anion/ $\pi$  interaction is unimportant in most benzene derivatives except those bearing two or more electron-withdrawing substituents, such as hexafluorobenzene. On the other hand, there exist intrinsically  $\pi$ -deficient heteroaromatic molecules, for which anion/ $\pi$  interactions would be very important.

 $OH/\pi$  and  $NH/\pi$  interactions are called "weak hydrogen bonds" [6], where polarized  $\delta$ + moieties and  $\pi$  electrons attractively interact. Although the interaction energies are rather small, a few kilocalories per mole or less, they appear frequently and often play a significant role, especially in biochemical compounds [7].

The  $\pi$  electrons can interact even with lone-pair electrons in an attractive manner, which is called *lone-pair*/ $\pi$  interactions [9]. The existence of lone-pair/ $\pi$  interactions was recently confirmed. Since those interactions are attractive only for electron-deficient  $\pi$  moieties, they are supposed to be exclusively important for  $\pi$ -deficient heteroaromatic molecules, as is the case for anion/ $\pi$  interactions.

Results of a simple keyword search (on 21st April 2008) on SciFinder Scholar (Thomson Scientific) of those interactions are shown in Table 1. It is emphasized that the numbers are not proportional to the importance of each interaction and that this order may change. In this article, each interaction in this attention-based ranking is explained.

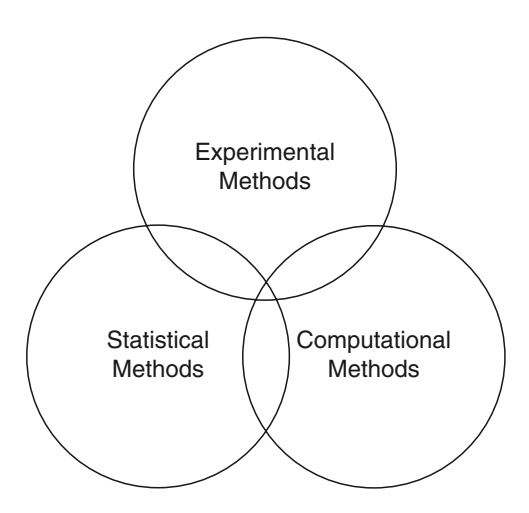
There are three principal methods for studying intermolecular interactions: experimental methods, statistical methods, and theoretical methods (Fig. 2).

In experimental methods, information on geometries and interaction energies in molecular complexes is obtained. Experiments are generally performed for molecular complexes in the gas phase, where influences from other molecules and molecular complexes are excluded. Electron diffraction study of benzene is a typical example, which revealed that benzene dimer preferred a T-shaped configuration over the  $\pi$  stack configuration [10]. In contrast, to the best of our knowledge, there are no similar studies on heteroaromatic compounds.

**Table 1** Frequency of appearance of each interaction searched by SciFinder Schloar

Interaction	Frequency
π/π	37,170
Cation/π	1363
CH/π	600
Anion/π	215
$OH/\pi$	198
$NH/\pi$	101
Lone-pair/π	50

Fig. 2 Three methods for studying intermolecular interactions



Statistical methods use database analysis, where the Cambridge structural database (CSD) and Brookhaven protein databank (PDB) are typically used. One may worry about various intra- and intermolecular influences on geometrical parameters registered in the databases, but they are virtually canceled out in the course of averaging a large amount of data. Indeed, mean values obtained by statistical methods are generally in good agreement with experimental and/or theoretical results. However, when the amount of data is small, the statistical methods are usually inapplicable because influences from individual situations cannot be canceled out.

Even though there is neither an appropriate method for experimental study nor a sufficient amount of data in the databases, theoretical methods are always applicable. By theoretical methods, information can be obtained not only on favorable configurations and energies in the molecular complexes but also on the origin of the intermolecular interactions. When the theoretical methods are conducted, the consistency with experimental results as well as validity of the employed procedures should be carefully examined. Results of theoretical studies may vary considerably depending on the choice of calculation methods and basis function sets. HF/6-31G\* calculations largely give rough, or even essentially incorrect results [11]. Density functional theory (DFT) calculations are widely applicable (e.g., for cation/ $\pi$  interactions), although estimation of electron correlations is insufficient. The most reliable and frequently used methods are the combination of *n*th order Møller–Plesset (MPn) methods or coupled-cluster (CC) methods with diffusion basis sets, wherein electron correlations are explicitly taken into account. The MP2 (n=2) and MP4 (n=4) methods as the former, and CCSD and CCSD(T) methods as the latter are widely used. These methods are absolutely necessary for investigation of  $\pi/\pi$  interactions, where dispersion forces play a significant role. In addition, since basis set superposition error (BSSE) is a concern in weakly bound dimer, BSSE should be eliminated via the counterpoise correction of Bernardi and Boys [12].

### 2 $\pi/\pi$ and CH/ $\pi$ Interactions

## 2.1 Geometry and Interaction Energy of Two Aromatic Molecules

Interactions between two aromatic moieties are classified into three categories (Fig. 3):

- a. Parallel-displaced (offset-stacked) configuration (Fig. 3a)
- b. Face-to-face sandwich configuration (Fig. 3b)
- c. T-shaped configuration (Fig. 3c)

Intermolecular interactions in (a) and (b) are called  $\pi/\pi$  interaction and that in (c) is called CH/ $\pi$  interaction. The interaction energies of each configuration are also exhibited in Fig. 3. The shift of the centroids of the aromatic rings depicted in Fig. 3 is called "offset". When the offset is equal to zero (see Fig. 3b), it is generally disadvantageous in energy due to  $\pi$  electron repulsions; thus, most frequently only (a) and (c) are compared. In this article, both (a) and (b) are referred to as  $\pi$  stack configuration, and (c) as T-shaped configuration.

Intermolecular interactions of benzene dimer have been investigated theoretically. While (c) was solely observed in the gas-phase experiment, according to Tsuzuki et al. [13] and Sinnokrot et al. [14], there is no significant difference between calculated interaction energies of (a) and (c), the interaction energies commonly being -2.5 kcal mol<sup>-1</sup> (the negative value represents attractive force). The values shown in Fig.3 are interaction energies in the gas phase, while the interaction is weakened to -1.5 kcal mol<sup>-1</sup> in solution [15]. Interaction energies of (b) are smaller than those of (a) by 1 kcal mol<sup>-1</sup>. The  $\pi/\pi$  interactions are thought to originate principally from dispersion forces; on the other hand, Hunter and Sanders explained them in terms of attractive interactions between  $\pi$  electrons (negative) and the  $\sigma$  skeleton (positive) [16].

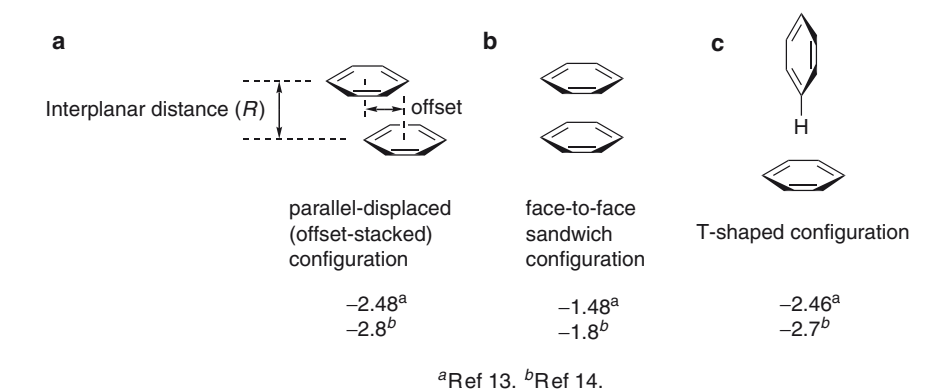


Fig. 3 Typical configurations of benzene dimers. a Parallel-displaced (offset-stacked) configuration; b face-to-face sandwich configuration; c T-shaped configuration. Interaction energies are in kcal  $mol^{-1}$  [13, 14]

## 2.2 Theoretical Studies on $\pi/\pi$ and $CH/\pi$ Interactions of $\pi$ -Deficient Heteroaromatic Molecules

The  $\pi/\pi$  interaction of the benzene-pyridine complex was theoretically investigated by Waller et al. by using hybrid DFT methods [17]. The interaction energy was estimated to be -2.89 kcal mol<sup>-1</sup> with an interplanar distance of 3.665 Å (optimized), being 0.58 kcal mol<sup>-1</sup> larger than that of benzene dimer (-2.31 kcal mol<sup>-1</sup>) obtained by the same calculation methods (see Fig. 4). Mignon et al. [18] and Tsuzuki et al. [19] also calculated the  $\pi/\pi$  interaction energies of benzene-pyridine to be -2.78 kcal mol<sup>-1</sup> (MP2 methods) and -3.04 kcal mol<sup>-1</sup> (CCSD(T) methods), respectively. Regardless of calculation method, the  $\pi/\pi$  interaction energies of the benzene–pyridine complex are ca. 0.5 kcal mol<sup>-1</sup> larger than that of benzene dimer. Similar to benzene dimer, the origin of  $\pi/\pi$  interaction of benzene-pyridine is principally dispersion force, and electrostatic force also plays a significant role. Tsuzuki et al. also calculated the interaction energies of benzene–pyridinium and benzene-N-methylpyridinium by using CCSD(T) methods to be -14.77 kcal mol<sup>-1</sup> (T-shaped; see Fig. 5) and -9.36 kcal mol<sup>-1</sup> ( $\pi$  stack), respectively [19]. These interactions are claimed to be classified as neither  $\pi/\pi$  nor CH/ $\pi$  interactions but as cation/ $\pi$  interactions, because electrostatic and inductive forces play a significant role therein (see Sect. 3).

The  $\pi/\pi$  interaction energies of benzene-1,3,5-triazine were estimated by Ugozzoli et al. [20]. Although there are several configurations giving local energy minima, the global minimum is at antiparallel-displaced configuration with interplanar distance of 3.3 Å and offset of 1.2 Å. The interaction energy is –5.29 kcal mol<sup>-1</sup> (MP2 methods), significantly larger than that of benzene dimer. The increase of interaction energy can be attributed to the  $\pi$ -deficient character of the 1,3,5-triazine moiety, although the dispersion force might be overestimated (vide infra).

Interaction energies of several configurationally fixed pyridine dimers were calculated by Mishra et al. using MP2/6-311++ $G^{**}$  methods [21]. As shown in Fig.4,  $\pi$  stack dimers are energetically more favorable than T-shaped ones. Although the origin of the interaction energy is principally dispersion force, the dipole–dipole interaction appears to contribute significantly (dipole moment of pyridine is 2.22 D1), because the interaction energies are different between parallel-displaced and antiparallel-displaced configurations. Mishra and coworkers also performed calculations of pyridine trimers, where the interaction energy was the largest when three pyridine moieties were  $\pi$ -stacked in an antiparallel-displaced manner. Interestingly, the interaction energy was estimated to be -8.04 kcal mol<sup>-1</sup>, being close to the experimental value of vaporization energy of pyridine (8.48 kcal mol<sup>-1</sup>). Piacenza et al. calculated the interaction energies of pyridine dimer by using DFT-D and SCS-MP2 methods [22] with geometrical optimization. The global minimum was again found for the antiparallel-displaced configuration, where pyridine moieties are somewhat tilted (Fig. 6a). It was also found that configurations bearing two CH/N and CH/ $\pi$  interactions (Figs. 6d, e) as well as CH/N interaction dimer (Fig. 6f) are comparable in the interaction energy of  $\pi$  stack dimers.

 $<sup>^{1}</sup>$ D (Debye) is equal to  $3.336 \times 10^{-30}$  C m<sup>2</sup>.

Compound	Methods	Interaction Energy / kcal mol <sup>-1</sup>	R/Å	Reference
R	CCSD(T)/basis set limit (AIMI model) <sup>a</sup> CCSD(T)/basis set limit Hybrid DFT <sup>b</sup> /6-311++G** MP2/6-31G*(0.25)	-2.48 -2.78 -2.31 -1.83	3.5 <sup>c</sup> 3.4 <sup>d</sup> 3.76 <sup>d</sup> 3.8 <sup>c</sup>	13 14 17 23
R	CCSD(T)/basis set limit (AIMI model) <sup>a</sup> CCSD(T)/basis set limit Hybrid DFT <sup>b</sup> /6-311++G** MP2/6-31G*(0.25)	-2.46 -2.74 -2.31 -1.83	5.0 <sup>c</sup> 5.0 <sup>d</sup> 3.76 <sup>d</sup> 3.8 <sup>c</sup>	13 14 17 23
R	Hybrid DFT <sup>b</sup> /6-311++G** MP2/6-31G*(0.25) estd CCSD(T)/basis set limit //MP2/6-311G*	-2.89 -2.78 -3.04	3.67 <sup>d</sup> 3.52 <sup>d</sup> N. A.	17 18 19
N R N	MP2/6-311++G** DFT-D/auc-cc-pVTZ SCS-MP2/aug-cc-VTZ MP2/6-31G*(0.25)	-3.97 -3.1 -3.8 -1.84	3.6 <sup>c</sup> 3.49 <sup>d</sup> 3.49 <sup>d</sup> 3.8 <sup>c</sup>	21 22 22 23
N R N	MP2/6-311++G** MP2/6-31G*(0.25)	-2.39 -1.84	3.6° 3.8°	21 23
N R	DFT-D/auc-cc-pVTZ SCS-MP2/aug-cc-VTZ	-2.3 -2.8	3.52 <sup>d</sup> 3.52 <sup>d</sup>	22 22
N R N	MP2/6-311++G**	-1.91	3.4 <sup>c</sup>	21
N N N	MP2/6-31G*(0.25) MP2/aug-cc-VDZ CCSD(T)/aug-cc-VDZ	-3.92 -3.87 -2.64	3.6° 3.6° 3.6°	23 24 24
N N R N	MP2/aug-cc-VDZ CCSD(T)/aug-cc-VDZ	-3.77 -2.79	3.4 <sup>c</sup> 3.4 <sup>c</sup>	24 24

<sup>&</sup>lt;sup>a</sup>In AIMI (aromatic intermolecular interaction) model, CCSD(T) interaction energy at the basis set limits is obtained as the sum of MP2 interaction energy and CCSD(T) correction term (which is nearly constant) for fixed geometry of benzene dimer. The molecular geometry of benzene is optimized at the MP2/6-31G\* level. <sup>b</sup> The hybrid functional includes a mixture of half the exact (HF) exchange with half of the the uniform electron gas exchange, plus Lee, Yang, and Parr's expression for the correlation energy. <sup>c</sup> Fixed. <sup>d</sup>Optimized.

**Fig. 4**  $\pi/\pi$  and CH/ $\pi$  interaction energies (kcal mol<sup>-1</sup>) and interplanar distances (Å) of dimers of benzene, pyridine, pyrimidine, 1,3,5-triazine, and benzene–pyridine calculated using different methods [13, 14, 17–19, 21–24]

Fig. 5 Change of  $\pi/\pi$  interaction energies by protonation in benzene–pyridine complex [19]

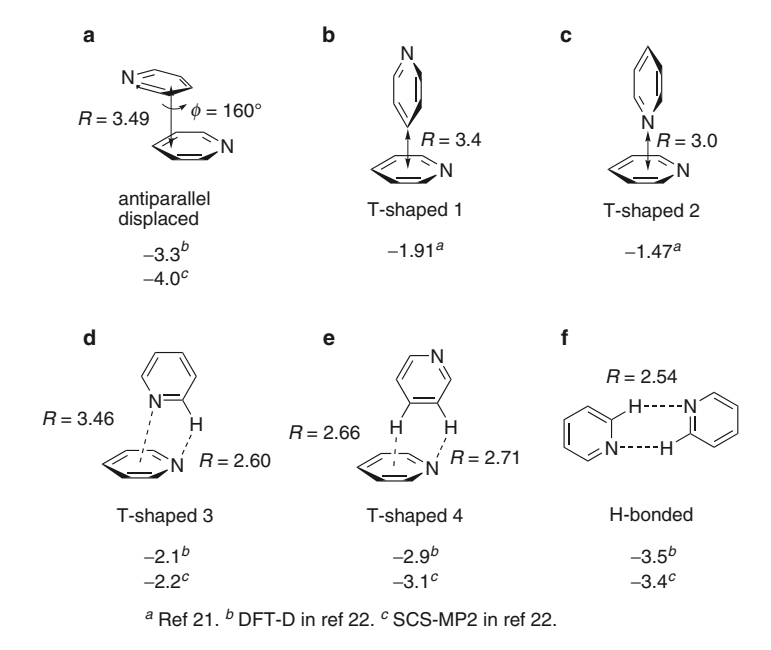


**Fig. 6** Interaction energies (kcal mol<sup>-1</sup>) and interplanar distances (Å) of various pyridine dimers (a-f) [21,22]. See also **Fig. 4** 

Lin et al. calculated  $\pi/\pi$  interaction energies of dimers of pyrimidine, pyridine, and benzene [23]. Because of the fixation of the geometrical parameters, the interaction energies shown in Fig.4 should not be of the potential minima. The order of the magnitude of interaction energies is, however, important, where  $\pi/\pi$  interaction energy of the pyrimidine dimer is considerably larger than that of pyridine and benzene dimers due to the  $\pi$ -deficient character (see also  $\pi/\pi$  interaction energy of furan dimer in Sect. 2.3).

Larger  $\pi/\pi$  interaction energies of  $\pi$ -deficient heteroaromatic dimers were also reported for 1,3,5-triazine and pyrimidine. Although the interaction energies varied considerably depending on the choice of the method, they are anyhow larger than interaction energy of benzene dimer calculated by the same method. MP2 calculation

predicted that the interaction energy of 1,3,5-triazine dimer is larger than that of pyrimidine dimer, while CCSD(T) gave the opposite results [2, 24]. By evaluating compensation of errors, the former method was claimed to be more reliable. Conclusively,  $\pi/\pi$  interaction energies of  $\pi$ -deficient heteroaromatic dimers are estimated generally to be 0.6–3 kcal mol<sup>-1</sup> larger than that of benzene dimer. This is attributable to a decrease of the intermolecular  $\pi$  electron repulsions. Although the origin of the  $\pi/\pi$  interactions is mainly dispersion force, dipole–dipole and dipole–induced dipole interactions may contribute partially.

## 2.3 Theoretical Studies on $\pi/\pi$ and $CH/\pi$ Interactions of $\pi$ -Excessive Heteroaromatic Molecules

While  $\pi$ -deficient heteroaromatic molecules have larger  $\pi/\pi$  interaction energies than benzene dimer, interactions of  $\pi$ -excessive heteroaromatic molecules are generally weak or even repulsive. Results of calculations on  $\pi/\pi$  and CH/ $\pi$  interactions of pyrrole, furan, and thiophene dimers are summarized in Fig. 7.

Šponer et al. [2, 24] reported the  $\pi/\pi$  interaction of pyrrole dimer to be repulsive (MP2 methods) or slightly attractive (CCSD(T) methods). As mentioned above, the former is more reliable. The repulsive (or weakly attractive) interaction may arise from larger  $\pi$  electron repulsions than for benzene dimer. Regardless of the calculation methods, the antiparallel-displaced configuration is preferable to the parallel-displaced one, presumably due to the dipole–dipole interaction.

Calculations of  $\pi/\pi$  interaction energy of parallel-displaced furan dimers were conducted by Lin et al. [23] and Hopkins et al. [25]. Lin et al. estimated it to be -0.80 kcal mol<sup>-1</sup> (MP2/6-31G\*(0.25) methods with fixed geometry), which was 1 kcal mol<sup>-1</sup> smaller than that of benzene dimer obtained by the same methods (see Fig. 7). On the other hand, Hopkins et al. obtained different values, -2.58 and -2.38 kcal mol<sup>-1</sup>, by means of CCSD(T)/6-31G\*(0.25)//MP2/aug-cc-VDZ and CCSD(TQ)/6-31G\*(0.25)//MP2/aug-cc-VDZ methods, respectively, with optimization of all geometrical parameters [25]. By evaluating the validity of the calculation methods, -2.38 kcal mol<sup>-1</sup> appears to be closest to the actual value. In contrast to pyrrole and thiophene (vide infra) dimers, the  $\pi/\pi$  interaction energy of parallel-displaced furan dimers is close to state-of-the-art  $\pi/\pi$  interaction energies of benzene dimer (see Fig. 4)

Interaction energies of thiophene dimer in  $\pi$  stack and T-shaped configurations were calculated by Tsuzuki et al. to be -1.71 and -3.12 kcal mol<sup>-1</sup>, respectively [26]. The preference of T-shaped configuration of thiophene dimer is in marked contrast to benzene dimer, where interaction energies of  $\pi$  stack (-2.48 kcal mol<sup>-1</sup>) and T-shaped (-2.46 kcal mol<sup>-1</sup>) configurations at the same calculation level are nearly equal. The energy decomposition analysis showed that, as both dispersion force and electrostatic repulsion are larger in the  $\pi$  stack thiophene dimer than in benzene dimer due to the  $\pi$  excessive character, they are canceled out to give the small interaction energy as a result. On the other hand, the larger interaction energy in the T-shaped thiophene dimer arises principally from larger dispersion and

Compound Methods		Interaction Energy / kcal mol <sup>-1</sup>	R/A	Reference
NH R	MP2/aug-cc-VDZ CCSD(T)/aug-cc-VDZ	+0.63 -0.09	3.6 <sup>a</sup> 3.8 <sup>a</sup>	24 24
HN R	MP2/aug-cc-VDZ CCSD(T)/aug-cc-VDZ	+0.97 +1.23	3.6 <sup>a</sup> 3.8 <sup>a</sup>	24 24
O R	MP2/6-31G*(0.25) CCSD(T)/6-31G*(0.25) //MP2/aug-cc-VDZ CCSD(TQ)/6-31G*(0.25) //MP2/aug-cc-VDZ	-0.80 -2.58 -2.38	4.0 <sup>a</sup> N. A. N. A.	23 25 25
S	CCSD(T)/basis set limit (AIMI model) <sup>c</sup>	-1.71	3.3ª	26
S	MP2/6-31+G**	-1.74	3.79 <sup>b</sup>	27
s H	CCSD(T)/basis set limit (AIMI model)	° –3.12	3.3ª	25

<sup>&</sup>lt;sup>a</sup> Fixed. <sup>b</sup>Optimized. <sup>c</sup>See Fig.4.

Fig. 7  $\pi/\pi$  and CH/ $\pi$  interaction energies (kcal mol<sup>-1</sup>) and interplanar distances (Å) of pyrrole, furan, and thiophene dimers calculated using different methods [24–27]

electrostatic forces than those in benzene dimer. Unlike pyridine dimer, coplanar arrangement (see Fig. 6f) of thiophene dimer is weakly bound with the interaction energy of less than 1 kcal mol<sup>-1</sup>, indicating that sulfur atoms of the thiophene ring do not behave as good CH/S bond acceptors. The difference in interaction energy of antiparallel- and parallel-displaced configurations is very small. This may be attributed to the small magnitude of the dipole moment of the thiophene molecule (0.52 D) [27], which is incapable of significant contribution to the total interaction energy. Rodríguez-Ropero et al. studied  $\pi/\pi$  interactions not only of thiophene dimer but also of its trimer and tetramers by using MP2 methods [28]. For the dimer, the interaction energy, -1.74 kcal mol<sup>-1</sup>, is very close to Tsuzuki's value [26], although two thiophene moieties are not in an anti-parallel geometry but torsioned by 60°. The interaction energy of the trimer  $(-3.76 \text{ kcal mol}^{-1})$  is larger than twice that of the dimer by  $0.28 \text{ kcal mol}^{-1}$ . This may be referred to as the cooperation effect in the  $\pi$  stack of aromatic moieties. More significant cooperation effect is found for the tetramer, the interaction energy of which  $(-5.77 \text{ kcal mol}^{-1})$ 

is larger than three times that of the dimer by 0.55 kcal mol<sup>-1</sup>. In view of future applications as a molecular device, the  $\pi$  stack structure of thiophene oligomers was investigated by Hutchinson et al. [29]. Studies on charged thiophene oligomers were conducted by Scherlis et al. [30]

In summary,  $\pi/\pi$  interaction energies of dimers of  $\pi$ -excessive heteroaromatic molecules (pyrrole and thiophene, except for furan) are commonly smaller than that of benzene dimer. This is in remarkable contrast to  $\pi$ -deficient heteroaromatic dimers, the  $\pi/\pi$  interaction energies of which are essentially larger than that of benzene dimer. Contribution of dipole–dipole and dipole–induced dipole interactions are not very important, because the origin of  $\pi/\pi$  interactions is principally dispersion force. On the other hand,  $CH/\pi$  interaction energies are revealed to be larger for both  $\pi$ -excessive heteroaromatic dimer (thiophene) and  $\pi$ -excessive heteroaromatic dimer (pyridine) than for benzene dimer. This is an unexpected result because charge transfer and dispersion forces, which are the principal origin of  $CH/\pi$  interactions, are supposed to enhance for  $\pi$ -excessive heteroaromatic dimers but to diminish for  $\pi$ -deficient heteroaromatic ones. It should be noted that the calculations were performed by different methods. As the interaction energies may vary depending on the choice of calculation method, comparison of results obtained by an identical method is desirable.

## 2.4 Substituent Effects in $\pi/\pi$ and CH/ $\pi$ Interactions

The magnitude of  $\pi/\pi$  interaction energy varies depending on nature of the substituents on the benzene ring. Sinnokrot et al. reported that  $\pi/\pi$  interaction energies of benzene dimer are increased by substitution of any group [31]. The interaction energies are more significantly increased when an electron-withdrawing group is substituted. For example, the interaction energy of benzene-benzonitrile (-2.79 kcal mol<sup>-1</sup>) calculated by estd CCSD(T)/aug-cc-pVTZ methods is 1.19 kcal mol<sup>-1</sup> larger than that of benzene dimer (-1.60 kcal mol<sup>-1</sup>), while that of benzene-phenol (-1.85 kcal/mol) is only 0.25 kcal mol<sup>-1</sup> larger than that of benzene dimer. The increase of interaction energies by substitution of electron-withdrawing groups can be rationalized in terms of the reduction of  $\pi$  electron repulsions. On the other hand, as both  $\pi$  electron repulsion and dispersion forces (attractive) are increased by substitution of electron-donating groups, their influences should be mostly canceled out so as to increase the interaction energies slightly. Similarly, substituent effects on  $\pi/\pi$  interaction energy in water were reported by Rashkin et al. [32]

Largely,  $\pi/\pi$  interaction energies of benzene–pyrimidine and benzene–imidazole complexes are also increased by substitution on the benzene moiety, as shown in Fig. 8 [33]. MP2 calculations revealed that the magnitude of the interaction energies increases significantly when electron-withdrawing groups are substituted. In contrast, the interaction energy is increased only slightly (in phenol–pyrimidine) or deceased (in phenol–imidazole) by substitution of electron-donating groups. The different behavior of pyrimidine and imidazole may be due to the respective  $\pi$ -deficient and  $\pi$ -excessive characters. It is noteworthy that, while the interaction energies are

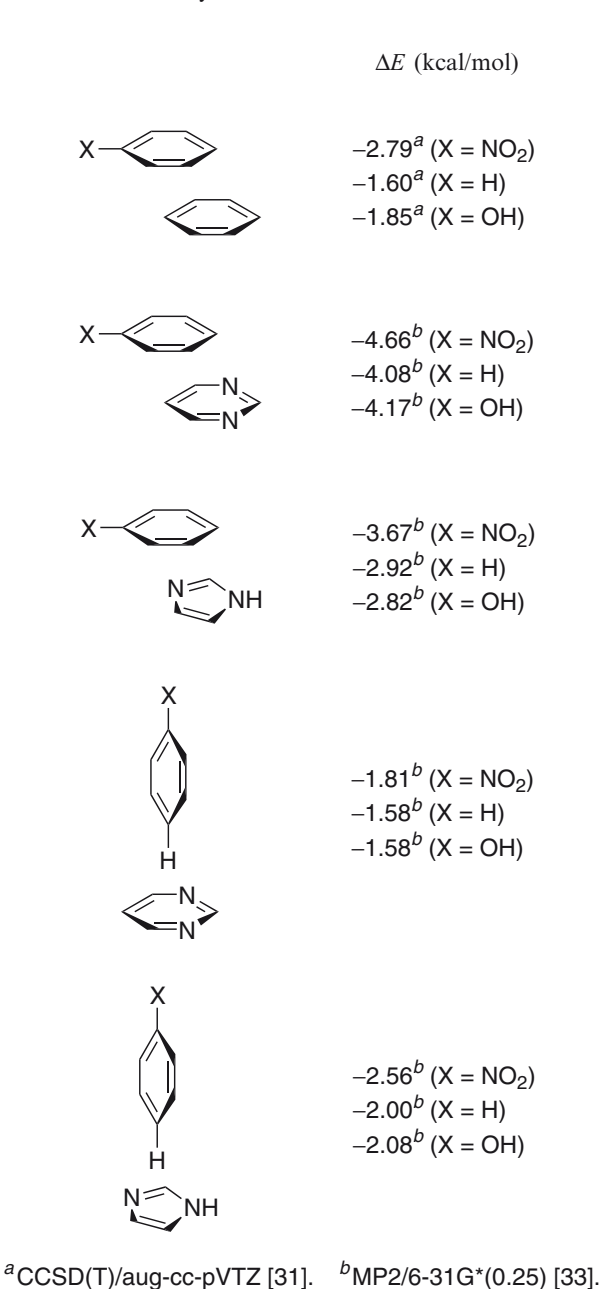


Fig. 8  $\pi/\pi$  and CH/ $\pi$  interaction energies (kcal mol<sup>-1</sup>) of substituted benzene with benzene, pyrimidine, and imidazole [31, 33]

larger in substituted benzene-heteroaromatic molecules than in substituted benzene-benzene in general, deviation from the non-substituted molecular complex by substitution of the functional group is smaller in the former. Substituents on the

benzene ring will also increase CH/ $\pi$  interaction energies (Fig. 8) of benzene–pyrimidine and benzene–imidazole complexes [33]. Similarly to  $\pi/\pi$  interactions, the influences of electron-withdrawing groups are relatively large, and those of electron-donating groups are essentially small.

Substituent effects on  $\pi/\pi$  interaction were experimentally studied by Gungs et al. [34]. They performed variable-temperature NMR analysis of triptycene derivative 1 (see Fig. 9), where, since the  $\pi$  stack is present in *syn* conformer while absent in *anti* conformer, *syn/anti* ratios give rise to estimation of the magnitude of intramolecular  $\pi/\pi$  interactions ( $\Delta G$ ). Unlike benzonitrile-benzene derivatives [Y = CH, Z = C(CN)], substituent effects among X = Me, H, and F were considerably smaller in pyridine-benzene derivatives (Y = CH, Z = N) and pyrimidine-benzene derivatives (Y = Z = N). On the other hand, the  $\pi/\pi$  interaction energies of pyridine-benzene derivatives and pyrimidine-benzene derivatives were essentially larger than those of benzene-benzene derivatives. These findings are in good agreement with the theoretical results mentioned above.

$\Delta G$ / kcal mol <sup>-1</sup>				
(X)	(Y, Z)			
	N, N	CH, N	СН, СН	CH, C(CN)
Me	-0.64	-0.53	-0.03	-0.46
Н	-0.62	-0.44	-0.03	-0.69
F	-0.64	-0.40	-0.13	-0.82

**Fig. 9** *Above:* Schematic representation of *syn-anti* equilibrium of **1**. The  $\pi/\pi$  interaction is represented by the *broken line. Below:* Gibbs free energies ( $\Delta G$ ) at T = 298 K were estimated by <sup>1</sup>H NMR spectra in CDCl<sub>3</sub>. The errors are within 0.3 kcal mol<sup>-1</sup> [34]

## 2.5 Statistical and Experimental Studies on $\pi/\pi$ and $CH/\pi$ Interactions

Statistical studies using CSD on  $\pi/\pi$  and YH/ $\pi$  interactions (Y = O, N, C) of isoxazole, imidazole, and indole, which belong to important heteroaromatic molecules in the life sciences, were conducted by Malathy Sony et al. [35]. Examination of angular dependency of CH/ $\pi$  contacts indicate that, due to the  $\pi$ -excessive character, those three heteroaromatic molecules have stronger CH/ $\pi$  interactions than substituted benzenes in crystalline. Compared to benzene–benzene and indole–benzene, indole–indole substantially prefers the  $\pi$  stack configuration to the T-shaped one. This is not due to an effect of the nitrogen atom but to the  $10\pi$  electron system, which would give rise to a stronger dispersion force than the  $6\pi$  system of benzene. The  $\pi$  stack preference of indole dimers may arise partly from the packing demand, because the  $\pi$  stack configuration is advantageous in view of decreased void space and increased packing coefficient. This is supported by the fact that a similar  $\pi$  stack preference of aromatic moieties is also observed in the structural database of proteins.

Janiak also found that pyridines and quinolines that are coordinated to metal ions statistically prefer  $\pi$  stack configurations [36]. Importantly, although T-shaped configurations of indole dimers are rarely found [35], they are absent in metal-coordinated pyridine dimers and quinoline dimers. The mean geometrical parameters of metal-coordinated pyridine dimers are shown in Fig.10. The enhanced preference for  $\pi$  stack configurations of metal-coordinated pyridines and quinolines should originate from the decreased  $\pi$  electron density by coordination of metal cations.

Since the origin of  $\pi/\pi$  interaction is principally dispersion force, the magnitude of the interaction energy should be enhanced for molecules bearing the extended  $\pi$  system. Indeed, the  $\pi/\pi$  interaction energy of naphthalene dimer is estimated to be -5.69 kcal mol<sup>-1</sup> by CCSD(T) methods [37], whereas that of benzene dimer is -2.48 kcal mol<sup>-1</sup> [13]. Also, MP2 calculations [38] revealed that the  $\pi/\pi$  interaction energy of anthracene dimers is as large as -7.61 kcal mol<sup>-1</sup>, while that of naphthalene dimer is -3.74 kcal mol<sup>-1</sup>. The strong  $\pi/\pi$  interaction of anthracene dimers was employed to construct host scaffold in crystalline-state host–guest complexes [39, 40]. For fused heteroaromatic molecules,  $\pi/\pi$  interaction energies are also expected to be larger, but studies on such molecules are rare except for DNA/RNA bases (adenine, thymine, guanine, cytosine, and uracil) [41].

Association constants (K) of quinoline were experimentally determined by Latypov et al. at 298 K in chloroform [42]. The K was observed to change significantly

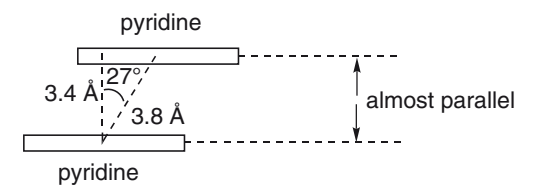


**Fig. 10** Mean geometry of metal-coordinated pyridine dimer [36]

depending on concentration; K was  $8.8 \times 10^3$  L mol<sup>-1</sup> at lower concentrations and 45 L mol<sup>-1</sup> at higher concentrations. Itahara et al. studied formation of intramolecular  $\pi$  stack in oligomethylene-linked (n=3,4,5,6,8) adenine dimer (2), benzimidazole dimer (3), and adenine–benzimidazole (4) [43]. In aqueous solutions, heteroaromatic moieties were observed to associate in an intramolecular manner in 2 and 4 while no association was found in 3. The results were explained in terms of difference in the dipole moments of adenine and benzimidazole moieties. As shown, although the origin of the  $\pi/\pi$  interaction is attributed mainly to the dispersion force, dipole–dipole interactions may play a significant role in association behavior.

Bis(4-pyridyl) and bis(4-pyridyl-N-oxide) moieties are often used to construct supramolecular motifs, being referred to as tecton [44]. The  $\pi/\pi$  interactions are more important than cation/ $\pi$  interactions and hydrogen bonds therein because of the large interaction energy, which arises not only from the intrinsic  $\pi$ -deficient character of pyridine but also its coordination to the metal ions. The crystal structure of [Ag(azpy)(NO<sub>3</sub>)]·H<sub>2</sub>O·CH<sub>3</sub>OH (azpy = trans-4,4'-azopyridine) [45] is shown in Fig. 11 as a typical example of supramolecular crystals consisting of a  $\pi$  stack of pyridyl moieties, where azpy moieties are bridged by silver(I) ion to form a one-dimensional chain, and pyridyl moieties are arranged in a face-to-face manner with an interplanar distance of 3.53 Å.

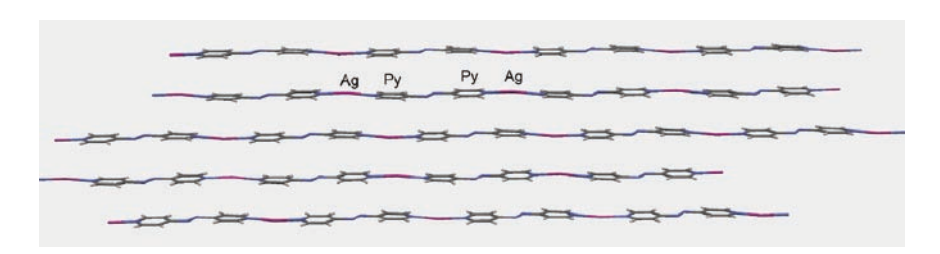


Fig. 11 Crystal structure of [Ag(azpy)(NO<sub>2</sub>)]·H<sub>2</sub>O·CH<sub>2</sub>OH [45]

## 3 Cation/ $\pi$ Interactions

Attractive interactions between  $\pi$  electrons and cations have been known for a long time. For example, in the  $\pi$  prismand [46] and deltaphane [47] those interactions play significant roles. Systematic studies on those *cation*/ $\pi$  *interactions* was begun by Dougherty [4, 8] near the end of the 1990s. Afterwards, a large number of theoretical and experimental studies were conducted to disclose the full nature of the cation/ $\pi$  interactions.

Cation/ $\pi$  interactions are generally larger in energy than those of other X/ $\pi$  interactions. For example, the association enthalpy of Na<sup>+</sup> and benzene was experimentally determined to be  $-22.1 \pm 1.4$  kcal mol<sup>-1</sup> (0 °C) [48], which is substantially larger than the calculated  $\pi/\pi$  interaction energy of benzene dimer (-2.48 kcal mol<sup>-1</sup>) [13].

The magnitude, favorable geometry, and origin of cation/ $\pi$  interactions are highly dependent on the character of the cation and  $\pi$  moiety. According to theoretical studies by Kim et al. [49], cation/ $\pi$  interactions of either Li<sup>+</sup>, Na<sup>+</sup>, K<sup>+</sup>, Ag<sup>+</sup>, or NH<sub>4</sub><sup>+</sup> with  $\pi$  moieties (ethylene, benzene, and pyrrole) are categorized into three groups with respect to the origin of the interaction energy:

- 1. In the case of small metal cations (Li<sup>+</sup>, Na<sup>+</sup>), inductive force is principal and electrostatic force follows
- 2. In the case of large metal cations (K<sup>+</sup>, Ag<sup>+</sup>), both inductive and electrostatic forces are important and dispersion force is negligible
- 3. In the case of organic cation (NH<sub>4</sub><sup>+</sup>), both inductive and dispersion forces are important

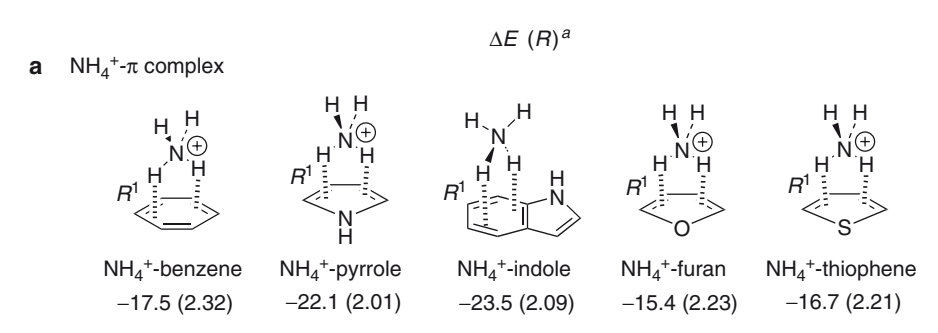
The interaction energies estimated by using MP2/6-31+G\* methods are shown in Fig.12, which are in good agreement with both experimental [48] and other theoretical results (MP2/6-311G\*\*) [50]. The different behavior of benzene and pyrrole complexes is also revealed as follows:

	Δ <b>E</b> (R	$\Delta E\left(R\right)^{a}$		
	M <sup>⊕</sup>	M <sup>⊕</sup> HN ↓ R		
M = Li <sup>+</sup>	31.95 (1.91)	36.30 (1.95)		
Na <sup>+</sup>	20.23 (2.40)	23.87 (2.46)		
K <sup>+</sup>	14.59 (2.90)	17.36 (2.88)		
$NH_4^+$	14.17 (2.99)	17.96 (3.00)		
$C(NH_2)_3^+$	10.81 (3.98)	14.38 (3.96)		
N(CH <sub>3</sub> ) <sub>4</sub> <sup>+</sup>	6.90 (4.25)	8.75 (4.19)		

Fig. 12 Interaction energies ( $\Delta E$  in kcal mol<sup>-1</sup>) and the perpendicular distance (R in Å) from the controld of the  $\pi$  moiety to the cation [49]

1. In benzene complexes, the cation is placed on the top of the centroid of the ring, while in pyrrole complexes it is rather far from the nitrogen atom. The different behavior may by rationalized in terms of electrostatic repulsion between the cation and positively polarized nitrogen atom.

- 2. While the distances (*R*) are essentially identical between pyrrole-K<sup>+</sup> and benzene-K<sup>+</sup>, they are rather different between pyrrole-Li<sup>+</sup> and benzene-Li<sup>+</sup> and between pyrrole-Na<sup>+</sup> and benzene-Na<sup>+</sup>. This is again due to electrostatic repulsion of the positive charge of the cation and pyrrole nitrogen, which is more significant in Li<sup>+</sup> and Na<sup>+</sup> because of their small ion radii.
- 3. Although both benzene and pyrrole are  $6\pi$  molecules, the interaction energies are always larger in the latter because the higher  $\pi$  electron density in pyrrole enhances inductive and electrostatic forces, which are the principal origin of cation/ $\pi$  interactions.



**b** heterocyclic-NH<sub>4</sub><sup>+</sup> hydrogen bond complex

c protonated heterocyclic-NH<sub>3</sub> hydrogen bond complex

$$R^2$$
 $H$ 
 $N-H$ 
 $NH_3$ -pyridinium
 $-42.5$  (2.74)

 $R^2$ 
 $H$ 
 $NH_3$ -imidazolium
 $R^2$ 
 $NH_3$ -imidazolium
 $R^2$ 
 $R^$ 

Fig. 13 Interaction energies and optimized geometries of  $NH_4^+$  complexes of benzene, pyrrole, indole, furan, and thiophene (**a**, **b**), and  $NH_3$  complexes of pyridinium and imidazolium (**c**). Interaction energies are in kcal mol<sup>-1</sup>.  $R^1$  and  $R^2$  represent the perpendicular distances between the H of  $NH_4^+$  and the aromatic plane (**a**, **b**) and the  $N\cdots$ H distance (**c**), respectively, and are in Å (*in parenthesis*) [51]

Geometries and interaction energies of NH, complexes of various heteroaromatic molecules including pyrrole, imidazole, pyridine, indole, furan, and thiophene, together with benzene, were studied by Zhu et al. using B3LYP methods (Fig. 13) [51]. The optimized geometry can be classified into three categories: (a)  $NH_{*}^{+}-\pi$  complex, (b) heterocycle–NH<sub>4</sub> hydrogen bond complex, and (c) N-protonated heterocycle–NH<sub>3</sub> hydrogen bond complex. For basic molecules such as pyridine and imidazole, geometry (c) is the most favorable, while for pyrrole, which bears no lone pair, (a) is energetically favored. In the case of furan and thiophene, both (a) and (b) are observable. In type-(a) complexes, large interaction energies are commonly observed irrespective of the  $\pi$  moiety. Similar results were obtained in theoretical studies on the complexes of Al<sup>+</sup> and benzene, pyridine, furan, and pyrrole [52]. In geometrically optimized pyrrole–NH, complex, the N+–H bond directs toward the C-C bond of the pyrrole moiety, probably for the same reason as mentioned for pyrrole-metal cation complexes. Similar structural features are observed in furan-NH, and thiophene-NH<sub>4</sub><sup>+</sup>. It may be noted that NH<sub>4</sub><sup>+</sup> interacts with the benzo moiety preferentially over pyrrolo in the cation/ $\pi$  complex of indole and NH<sub>4</sub><sup>+</sup>.

The NICS(1) calculations revealed that cation/ $\pi$  interactions hardly affect aromaticity [53]. This may be related to the finding that geometrical parameters in the molecule, such as bond distances and angles, are not essentially changed by formation of cation/ $\pi$  interactions [51].

Due to their large interaction energies, cation/ $\pi$  interactions are capable of affecting the structure, reactivity, and properties of supramolecules significantly. The lariat crown ether (Fig. 14) synthesized by De Wall et al. [54] and Gokel et al. [55] captures K<sup>+</sup> efficiently with the aid of cation/ $\pi$  interaction of indole rings in the lariat moiety. Single-crystal X-ray study of the complex revealed that the distance between K<sup>+</sup> and the centroid of pyrrole moiety was 3.45 Å.

Cation/ $\pi$  interactions play a significant role in the properties of several bioorganic molecules, such as the neurotransmitter ACh, serotonin (5-HT), and  $\gamma$ -aminobutyric acid (GABA), etc. [56] They also contribute to construction of the higher-order structure of proteins. PDB database analysis successfully revealed that when Lys or Arg (which have cationic side-chains) are located close to Phe, Tyr, and Trp, the protein structure undergoes distortion due to cation/ $\pi$  interactions [57]. More frequently, experimental as well as theoretical investigations on model compounds are

Fig. 14 Schematic representation of inclusion behavior of lariat crown ether with  $K^+$  with the aid of cation/ $\pi$  interaction [54, 55]

conducted for large biomolecules because of their complicated structural motives. Ruan et al. investigated cation/ $\pi$  interaction energies of cations (Na<sup>+</sup> and K<sup>+</sup>) and aromatic amines (Phe, Tyr, and Trp) both experimentally (threshold collision-induced dissociation, TCID) and theoretically (B3LYP methods). The interaction energies observed in TCID studies of Na<sup>+</sup> complexes were found to increase in the order Phe (49.2) < Tyr (50.1) < Trp (51.9), which shows good correlation with the polarizability of the amino acids (Phe, 18.09 Å<sup>2</sup>; Tyr, 18.81 Å<sup>2</sup>; Trp, 21.96 Å<sup>2</sup>). This behavior is in good agreement with the theory of the origin of cation/ $\pi$  interactions, which explains the significant contribution of inductive force to the total energy [58].

## 4 Anion/ $\pi$ Interactions

Ruan et al. classified complexes consisting of anion and aromatic molecule into four types (Fig. 15a-d) [59]:

- a. Non-covalently bonded complex (anion/ $\pi$  complex)
- b. Weakly-covalently bonded  $\pi$  complex
- c. Covalently bonded  $\sigma$  complex
- d. Complex linked by CH/X- interaction

The first three (a, b, c) may be distinguished not only by geometries but also by the magnitude of charge transfer (CT) interaction between the anion and aromatic  $\pi$  moiety. Since (b), (c), and (d) should be regarded as the reaction intermediates and hydrogen-bonded complex, respectively, intermolecular interaction in (a) is referred to as anion/ $\pi$  interaction in this article. Hence, anion complexes of calixpyrroles reported by Sessler et al. [60] are not mentioned here because they are comprised of NH/F- or NH/RO- interactions and thus should be categorized as (d). Examples of (d)-type complexes are reviewed by Beer et al. [61]

Anion/ $\pi$  interactions [5] are especially important for heteroaromatic molecules. Since benzene itself is essentially  $\pi$ -electron-rich, having large negative quadruple moment  $Q_{zz}$  (-8.48 B² anion/ $\pi$  interaction becomes important only when electron-withdrawing groups are multiply substituted. Hexafluorobenzene is a typical example, having a large positive  $Q_{zz}$  (+9.05 B) (see Fig. 16). In contrast, there exist intrinsically  $\pi$ -deficient heteroaromatic compounds, such as 1,3,5-triazine ( $Q_{zz}$  = +0.90 B) and 1,2,4,5-tetrazine ( $Q_{zz}$  = +3.22 B), which can participate in anion/ $\pi$  interactions without electron-withdrawing substituents [62].

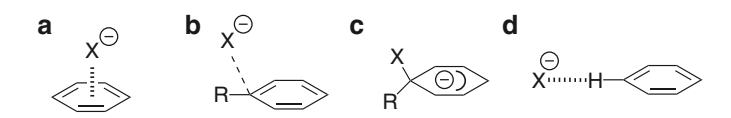
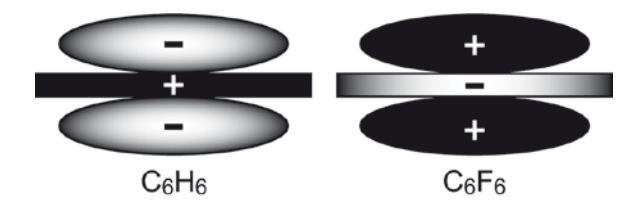


Fig. 15 Four categories (a-b) of complexes consisting of anion (X<sup>-</sup>) and aromatic molecule [59]

 $<sup>^{2}</sup>$  B (Buckingham) is equal to  $3.336 \times 10^{-40}$  C m<sup>2</sup>.



**Fig. 16** Schematic representation of quadrupole moments of benzene (*left*) and hexafluorobenzene (*right*) [63]

**Fig. 17** Left: Complexes consisting of 1,3,5-triazine and Cl<sup>-</sup> connecting by either anion/π interaction (a) or hydrogen bond (b). Energies are in kcal mol<sup>-1</sup> and interplanar distances are in Å (in parenthesis). Right: Optimized structure of host–guest complex that includes F<sup>-</sup> by means of anion/π (and CH/F<sup>-</sup>) interactions [65, 67]

The anion/ $\pi$  interactions of hexafluorobenzene with  $H_2O$ , HCN, or HF were theoretically studied by Quiñonero et al. [63]. They found that hexafluorobenzene can form stable complexes with HO<sup>-</sup>, Cl<sup>-</sup>, Br<sup>-</sup>, and CO<sub>3</sub><sup>2-</sup>, the interaction energies ranging from -10 to -27 kcal mol<sup>-1</sup>. In all the complexes, the anion species are located on the top of the centroid of the benzene ring. Similar short contacts are frequently found in CSD. Geometrical analysis of perfluorophenyl groups and neighboring electrically negative atoms, such as halogen, oxygen, sulfur, and nitrogen atoms, revealed that those atoms had a propensity to locate on the top of the centroid of the perfluorophenyl ring with a distance of 3.4–3.8 Å. Similarly to cation/ $\pi$  interactions, electrostatic and polarization forces are important in anion/ $\pi$  interactions [5].

Anion/ $\pi$  interactions of heteroaromatic molecules have been mainly studied for six-membered rings containing nitrogen atoms, especially 1,3,5-triazine [64]. Mascal calculated anion/ $\pi$  interaction energies of 1,3,5-triazine and 2,4,6-trifluoro-1,3,5-triazine with Cl<sup>-</sup>, F<sup>-</sup>, and N<sub>3</sub><sup>-</sup> by means of MP2 methods [65]. The energy minimum (local) of 1,3,5-triazine–Cl<sup>-</sup> complex is found when the Cl<sup>-</sup> ion is located on the top of the centroid of triazine ring with a distance of 3.2 Å, the anion/ $\pi$  interaction energy being –4.8 kcal mol<sup>-1</sup> (Fig.17a). The global energy minimum of 1,3,5-triazine–Cl<sup>-</sup> complex, however, is not that shown in Fig.17a but the hydrogen-bonded

complex shown in Fig.17b, the interaction energy of which is -7.4 kcal mol<sup>-1</sup>. Introduction of electron-withdrawing substituents on the aromatic moiety will increase the interaction energies; the anion/ $\pi$  energy of 2,4,6-trifluoro-1,3,5-triazine–Cl<sup>-</sup>complex is -14.8 kcal mol<sup>-1</sup>. The magnitude of the interaction energy varies significantly according to the environment: in the case of 1,3,5-triazine–Cl<sup>-</sup> complex, the anion/ $\pi$  energy is -8.5 kcal in the gas phase, -0.4 kcal mol<sup>-1</sup> in hexane, and +3.2 kcal mol<sup>-1</sup> in water. The strong attractive force and geometrical preference of anion/ $\pi$  interactions appear to be favorable for constructing supramolecular complexes. Indeed, Mascal et al. [66] and Zuo et al. [67] reported cyclophane-type host molecules (6) that can accommodate fluoride anion as a guest component by means of anion/ $\pi$  (and CH/F<sup>-</sup>) interactions (Fig.17).

Theoretical investigations on anion/ $\pi$  interactions were also performed by Quiñonero et al. [68]. By using RI-MP2 and DF-DFT [68], the interaction energies were estimated to be -5.3 kcal mol<sup>-1</sup> with the distance between anion and the centroid of the ring being 3.22 Å (RI-MP2), and -3.5 kcal mol<sup>-1</sup> with a distance of 3.59 Å (DF-DFT). Kim et al. calculated anion/ $\pi$  interaction energies (MP2) of 1,3,5-triazine and Cl<sup>-</sup>, CN<sup>-</sup>, and CO<sub>3</sub><sup>2-</sup> to be -5.39, -7.15, and -16.48 kcal mol<sup>-1</sup>, respectively [69]. They emphasized that both electrostatic and inductive forces contribute significantly in anion/ $\pi$  interactions. In comparison to cation/ $\pi$  interactions, dispersion force is relatively important, especially in complexes of CN<sup>-</sup> and CO<sub>3</sub><sup>2-</sup>. An important contribution of inductive forces to anion/ $\pi$  interactions is also proved by the fact that the anion/ $\pi$  interaction energies of 1,3,5-triazine–halogen anion complexes are larger than those expected on the basis of permanent quadruple moment of 1,3,5-triazine. The deviation from the expected interaction energy can be explained in terms of polarization of the  $\pi$  moiety induced by the anion [65].

Theoretical studies revealed that, like cation/ $\pi$  interactions, anion/ $\pi$  interactions do not affect aromaticity [53].

Anion/ $\pi$  interactions in complexes of cyanuric acid and its sulfur analogs with halogen anions were examined both theoretically and experimentally in an intramolecular manner (Fig.18) [70]. MO calculations at MP2 levels revealed that the interaction energies decreased in the order F<sup>-</sup> (-25.1 to -26.9 kcal mol<sup>-1</sup>) > Cl<sup>-</sup> (-14.7 to -15.6 kcal mol<sup>-1</sup>) > Br<sup>-</sup> (-13.7 to -14.4 kcal mol<sup>-1</sup>) and did not vary when the oxygen atom of cyanuric acid was replaced by sulfur. The X-ray structure

Fig. 18 Schematic presentation of  $anion/\pi$  interaction in cyanuric acid derivative 7, which is observed in both the theoretically optimized structure and the X-ray structure [70]

showed that 7 was indeed involved in anion/ $\pi$  interactions and that the observed complex was structurally in good agreement with the theoretically predicted one.

The presence of anion/ $\pi$  interactions can be detected spectroscopically in solution. Rosokha et al. reported that when a bromide salt was added to a solution of tetracyanopyrazine (TCP), a new absorption band appeared. The spectral change was attributed to the formation of CT complex, the stoichiometric ratio of which was 1:1. X-ray structures of CT complexes were also studied, where anion/ $\pi$  interaction existed between TCP and halogen anion [71].

CSD analysis revealed preferred affinity of heteroaromatic compounds containing nitrogen atoms for anions. Ahuja et al. reported that short intermolecular contacts of nitrogen-containing heteroaromatic moieties (pyridine, phenanthroline, and terpyridine) and anions ( $NO_3^{2-}$ ,  $CIO_4^{-}$ ,  $BF_4^{-}$ , and  $PF_6^{-}$ ) were frequently observed in crystalline [72]. A typical example is  $Fe(bipy)_3(CIO_4)_3$  (**8**), in which the oxygen atom of the  $CIO_4^{-}$  ion is located on the top of the centroid of the pyridine ring, as shown in Fig.19 [73]. The anion/ $\pi$  interaction perhaps results from the coordination of pyridine to  $Fe^{3+}$  ion, or, at least, should be enhanced by the coordination. This is supported by the fact that, while pyridine itself cannot form a stable complex with  $CI^{-}$  anion (that is,  $\Delta E > 0$ ), once pyridine coordinates to  $Ag^{+}$  it will form the anion/ $\pi$  complex with large  $\Delta E$  (-18.4 kcal mol $^{-1}$ , estimated by RI-MP2 calculation) [74].

Anion/ $\pi$  interactions appear less frequently than cation/ $\pi$  ones. This is not because the interaction energy is small but because anion/ $\pi$  interaction is attractive only when  $\pi$ -deficient aromatic compounds are concerned. Actually, the interaction energies are comparable between anion/ $\pi$  and cation/ $\pi$  interactions. In view of the design of supramolecules, anion/ $\pi$  interactions are as important as cation/ $\pi$  interactions. In line with this, Demeshko et al. reported supramolecules constructed by anion/ $\pi$  interactions between 1,3,5-triazine and Cl<sup>-</sup> anion [75]. Anion/ $\pi$  interactions are found in coordination polymer consisting of pyridine rings, where, in addition to normal anion/ $\pi$  interactions, sandwich structures such as anion/ $\pi$ /anion and  $\pi$ /anion/anion are also included [76]. Sandwich structure in an anion/ $\pi$ /anion manner is also seen in the X-ray structure of zinc-2,4,6-tris(di-2-picorylamino)-1,3,5-triazine

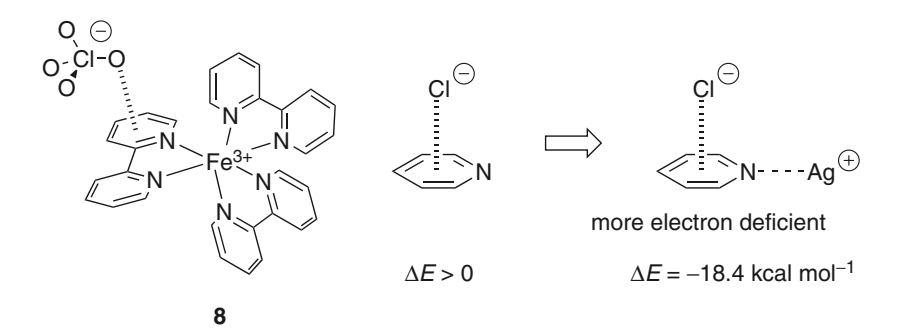


**Fig. 19** *Left*: Schematic representation of anion/ $\pi$  interaction between  $ClO_4^-$  and pyridine ring observed in X-ray structure of  $Fe(bipy)_3(ClO_4)_3$  (8). *Right*: Change of the interaction energy before and after coordination of pyridine to  $Ag^+$  [73, 74]

complex [77]. Anion/ $\pi$  interactions also play a significant role in determining the crystal structure of silver complexes of 3,6-bis(2'-pyridyl)-1,2,4,5-tetrazine and 3,6-bis(2'-pyridyl)-1,2,4,5-tetrazine, where 1,2,4,5-tetrazine moieties interact with AsF<sub>6</sub>-, PF<sub>6</sub>-, or SbF<sub>6</sub>- [78, 79], and bis(pyridinium) salt, and pyrimidinium moieties interact with BF<sub>4</sub>- or NO<sub>3</sub>- [80]. In the X-ray structure shown in Fig. 20, compound **9** accommodates Cl<sup>-</sup> by means of multiple anion/ $\pi$  interactions [81]. Similarly to the aforementioned Fe(bipy)<sub>3</sub>(ClO<sub>4</sub>)<sub>3</sub> and pyridine–AgCl complex (Fig.19), anion/ $\pi$  interaction is probably enhanced by the coordination of pyridine nitrogen to copper ions.

Even  $\pi$ -deficient aromatic molecules can participate in cation/ $\pi$  interactions, and  $\pi$ -excessive ones in anion/ $\pi$  interactions. Garau et al. showed that 1,3,5-triazine, a

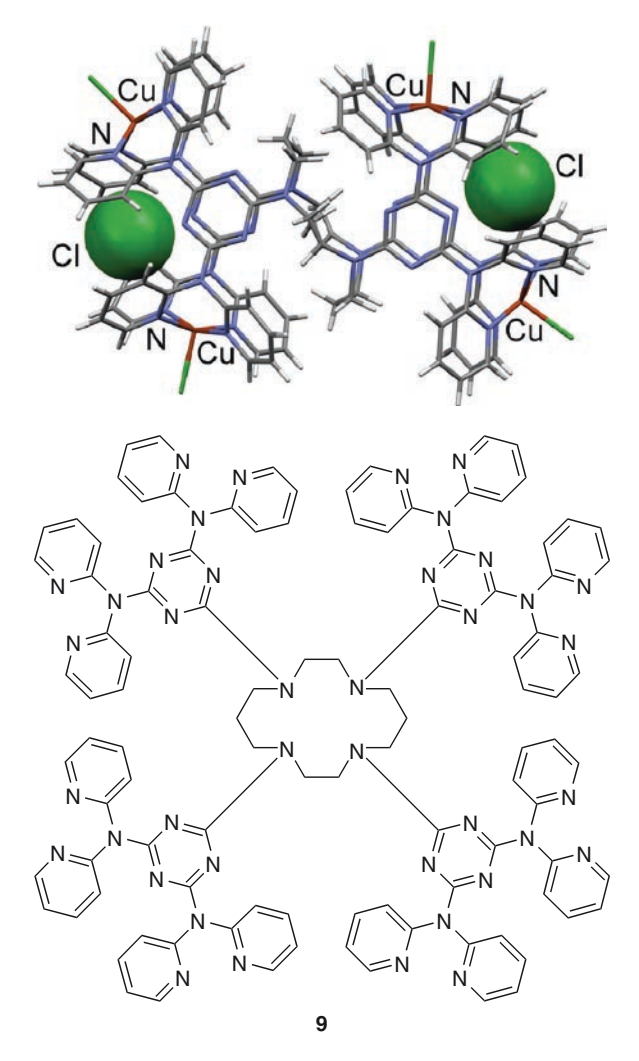


**Fig. 20** *Above*: Ball-and-stick representation of  $[Cu_4(9)Cl_4](Cl_4)(H_2O)_{13}$ . *Below*: Structure of compound **9** [81]

typical molecule participating in anion/ $\pi$  interactions, can interact with cations in an attractive manner [82]. While the anion/ $\pi$  interaction energy of 1,3,5-triazine and Cl<sup>-</sup> was estimated to be -5.3 kcal mol<sup>-1</sup> by RI-MP2 methods with the distance of 3.22 Å [68], 1,3,5-triazine can interact with Na<sup>+</sup> in a cation/ $\pi$  manner with interaction energy of -2.6 kcal mol<sup>-1</sup> and distance of 2.63 Å. One may think it curious that 1,3,5-triazine can participate in cation/ $\pi$  interactions. However, by remembering that inductive forces contribute significantly to the total interaction energies in both cation/ $\pi$  [49, 58, 65] and anion/ $\pi$  interactions [69], it may be facilely understood that not only anions but also cations can induce polarization of the  $\pi$  moiety to cause attractive cation/ $\pi$  and anion/ $\pi$  interactions.

## 5 OH/ $\pi$ and NH/ $\pi$ Interactions

OH/ $\pi$  and NH/ $\pi$  interactions, as well as CH/ $\pi$  interactions, are regarded as "weak hydrogen bonds" [6, 7], the interaction energy of which is one to a few kilocalories per mole. In spite of their weakness, these interactions can play an important role in organic and bioorganic chemistry. For example, all porphyrins included in proteins registered in PDB are involved in either CH/ $\pi$  or NH/ $\pi$  interactions, which often stabilize configurations of porphyrin and protein [83].

Apparently, OH/ $\pi$ , NH/ $\pi$ , and CH/ $\pi$  interactions should be attractive forces between positively polarized ( $\delta$ +) hydrogen atoms and negatively polarized ( $\delta$ -) oxygen, nitrogen, and carbon atoms, while they likely have different characters because the CH group is a "soft" acid while OH and NH groups are "hard" acids. Tsuzuki investigated similar and different features of YH/ $\pi$  (Y = O, N, C) interactions by means of CCSD(T) calculation [84]. The Y···H distance, total YH/ $\pi$  interaction energy ( $E_{total}$ ), and contribution of electrostatic ( $E_{es}$ ), repulsive ( $E_{rep}$ ), and correlation forces ( $E_{corr}$ ) in optimized geometry of methane–benzene, ammonia–benzene, and water–benzene are shown in Fig. 21. Results of the calculations can be summarized as follows:

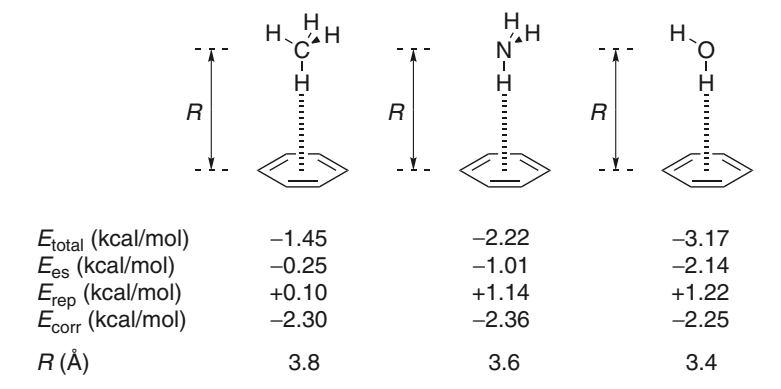
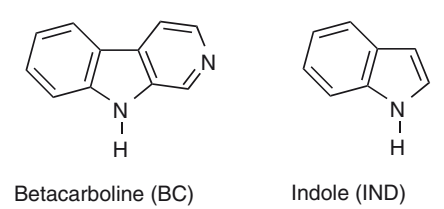


Fig. 21 Y···H distance, total YH/ $\pi$  interaction energy ( $E_{\text{total}}$ ), and contribution of electrostatic ( $E_{\text{es}}$ ), repulsive ( $E_{\text{rep}}$ ), and correlation forces ( $E_{\text{corr}}$ ) of optimized geometry of methane-benzene (left), ammonia-benzene (left), and water-benzene (right) [84]

N. Hayashi et al.

- 1. The interaction energies increase in the order  $CH/\pi < NH/\pi < OH/\pi$
- 2. In contrast, Y···H distances decrease in the order  $CH/\pi < NH/\pi < OH/\pi$ , where  $H···\pi$  distances are virtually constant
- 3. The origin of the interaction is principally dispersion force irrespective of Y
- 4. In contrast, electrostatic forces highly depend on Y
- 5. Contribution of CT is small, thus YH/ $\pi$  interactions behave as a long-distance forces

Muñoz et al. studied the relationship between  $\pi$  acceptor characters and the magnitude of NH/ $\pi$  interactions by measuring IR spectra of betacarboline (BC) [85] and indole (IND) [86] interacting with benzene, naphthalene, phenanthrene, toluene, m-xylene, and mesitylene. When benzene was added into CCl<sub>4</sub> solution of BC and IND, hypsochromic shifts of the NH vibration peak were observed. Changes when the other  $\pi$  molecules were added may be categorized into two types. The first is inertness of the peak position shift of the N-H vibration with increased association constant (K), which was observed when naphthalene and phenanthrene were used instead of benzene. The virtually constant N-H peak position shifts are indicative of the same magnitude of NH/ $\pi$  interactions of BC-benzene, BC-naphthalene, and BC-phenanthrene, and the increase of K results from the increased number of the acceptor sites (that is, benzene ring). The second is further hypsochromic shift of the peak positions of N-H vibration, which was observed when toluene, m-xylene, and mesitylene were employed. This indicates that the increase of  $\pi$  electron density by electron-donating methyl groups strengthens  $NH/\pi$  interactions. In contrast, when pyridine, quinoline, or phenanthridine was added, the expected NH/ $\pi$  interaction was not observed but only the hydrogen bond between NH(BC) and N(pyridine, quinoline, phenanthridine).



Theoretical studies (MP2 methods) predicted that  $OH/\pi$  interaction energies of aromatic compounds with water increase in the order benzene (-2.1 kcal mol<sup>-1</sup>) < phenol (-2.3 kcal mol<sup>-1</sup>) < indole (-3.5 kcal mol<sup>-1</sup>) [87]. Interestingly, this order is in good agreement with the order of the possibility that those moieties are involved in  $OH/\pi$  interactions in proteins: 6% for phenyl group of Phe (phenylalanine), 8% for hydroxyphenyl group of Tyr (tyrosine), and 18% for indolyl group of Trp (tryptophan) [88].

There is an issue of site-selectivity of the YH/ $\pi$  interaction in fused heteroaromatic molecules. As mentioned previously (Fig.13), the N<sup>+</sup>-H group prefers to interact not with pyrrole but with the benzene moiety of indole [51]. Similar selectivity was observed in CH/ $\pi$  interactions of ethylene-3-methylindole (MP2/

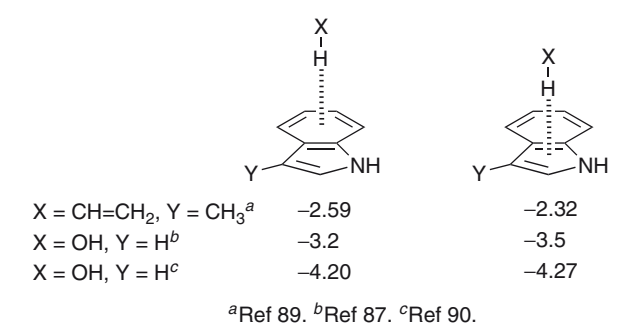


Fig. 22 CH/ $\pi$  and OH/ $\pi$  interaction energies (kcal mol<sup>-1</sup>) with benzene (*left*) and pyrrole moiety (*right*) in ethylene–3-indole (CH/ $\pi$ ) and water–indole (OH/ $\pi$ ) [87, 89, 90]

cc-pVTZ calculations) [89]. In contrast, in the case of water–indole, interaction energies with the pyrrole moiety are slightly larger than those with the benzene moiety [87, 90]. The origin of the selectivity is not clear. The interaction energies are summarized in Fig. 22.

CSD analysis revealed that, although the interaction energies are larger, OH/ $\pi$  and NH/ $\pi$  interactions do not appear as frequently as CH/ $\pi$  interactions in crystalline [35]. This is because, while the CH group is only capable of participating in CH/ $\pi$  interactions, OH and NH groups can not only be involved in OH/ $\pi$  and NH/ $\pi$  interactions but also in traditional hydrogen bonds. Due to the larger interaction energy, OH and NH groups preferably form traditional hydrogen bonding. Thus, OH/ $\pi$  and NH/ $\pi$  interactions are less frequently encountered than expected from the interaction energies.

#### 6 Lone-Pair/π Interactions

Recently, a novel class of  $X/\pi$  interactions, lone-pair/ $\pi$  (or  $n/\pi$ ) interactions, has attracted attention [9]. Here, lone-pairs interact with  $\pi$ -deficient aromatic moieties in an attractive manner. Like anion/ $\pi$  interactions, they are essentially important for heteroaromatic chemistry because, unlike aromatic hydrocarbons, some heteroaromatic molecules are intrinsically  $\pi$ -deficient.

In lone-pair/ $\pi$  interactions, the HOMO of the molecule bearing the lone-pair and LUMO of that bearing the  $\pi$  moiety are concerned, and their gap substantially affects the interaction energy. Reyes et al. proposed using "molecular electronegativity," which is defined as  $[-HOMO(lone\ pair) - LUMO(\pi^*)]/2$ , as a measure to predict which of  $CH/\pi$  and lone-pair/ $\pi$  are most energetically favorable. They found that when the molecular electronegativity is smaller than 0.15, the  $CH/\pi$  configuration should be preferred, while, when it is larger than 0.15, the lone-pair/ $\pi$  is energetically favorable in water-organic molecule complexes [91]. Figure 23 shows the molecular electronegativity of 1,3,5-triazine, benzene, azacoronene, and coronene, the optimized

N. Hayashi et al.

Fig. 23 Optimized configurations and interaction energies of complexes of 1,3,5-triazine, benzene, azacoronene, and coronene with water, and "molecular electronegativity" values of each aromatic component [91]

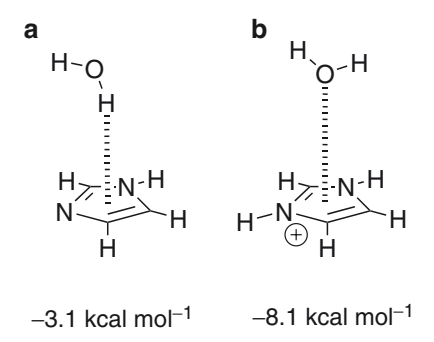


**Fig. 24** Preferred geometries of imidazole–water (*left*) and imidazolium–water (*right*) complexes. Interaction energies are estimated by MP2 calculations [87]

configuration of their complexes with water, and the interaction energies calculated by LMP2 methods. While benzene and coronene, which have small molecular electronegativities, favor  $OH/\pi$  interactions, both 1,3,5-triazine and azacoronene, which have large molecular electronegativities, preferentially participate in lone-pair/ $\pi$  interactions. The interaction energies are similar in benzene–water and coronene–water, whereas those of 1,3,5-triazine–water and azacoronene are considerably different.

As mentioned in Sect. 4, anion/ $\pi$  interaction energies will be significantly enhanced when the aromatic moiety coordinates to cationic species (see the interaction energies of Cl<sup>-</sup>-pyridine complexes in Fig.19) [74]. Similarly, protonation to the nitrogen atom of the heteroaromatic molecule can enhance the magnitude of the lone-pair/ $\pi$  interaction energy. Scheiner et al. found that the lone-pair/ $\pi$  interaction energy of a water-imidazole complex will increase by protonation of the imidazole moiety. Figure 24 shows the global energy minima of the imidazole-water complex, where they interact in an OH/ $\pi$  manner, indicating that the lone-pair/ $\pi$  interaction energy is less than -3.1 kcal mol<sup>-1</sup>. Thus, the increase of lone-pair/ $\pi$  interaction energy by protonation should be larger than 5.0 kcal mol<sup>-1</sup> [87].

Comparison of lone-pair/ $\pi$  interactions of borazine-boran and borazine-ammmonia were conducted by Kawahara et al. using MP2 methods [92]. As expected, benzene interacts attractively with the vacant p orbital of boran due to its  $\pi$ -excessive character, while it repels the lone-pair of ammonia. In contrast, hexafluorobenzene, a  $\pi$ -deficient molecule, interacts both with ammonia and boran attractively. Borazine is also revealed to be amphiphilic; it can interact both with ammonia and boran in an attractive manner, although the interaction energies are considerably different. The interaction energies are shown in Fig. 25.

There are several examples of supramolecular structures where lone-pair/ $\pi$  interactions play a significant role. Lu et al. reported a supramolecular crystal constructed by a combination of lone-pair/ $\pi$  interactions between a chloro group and 1,3,5-triazine, between ethereal oxygen and 1,3,5-triazine, and the CH/ $\pi$  interaction between phenyl groups (Fig. 26) [93]. Sarkhel et al. found the crystal structure of a RNA

Fig. 25 Lone-pair/ $\pi$  interaction energies (kcal mol<sup>-1</sup>) of  $\pi$  molecules (benzene, hexafluorobenzene, and borazine) and lone-pair molecules (ammonia and boran). Note that interaction energy between benzene and ammonia is not that of NH/ $\pi$  interaction [92]

	H $H$ $H$	F F F	H H N B N H B N B H
NH <sub>3</sub>	+1.25	-2.01	-0.45
вн3	-3.22	-3.16	-3.68

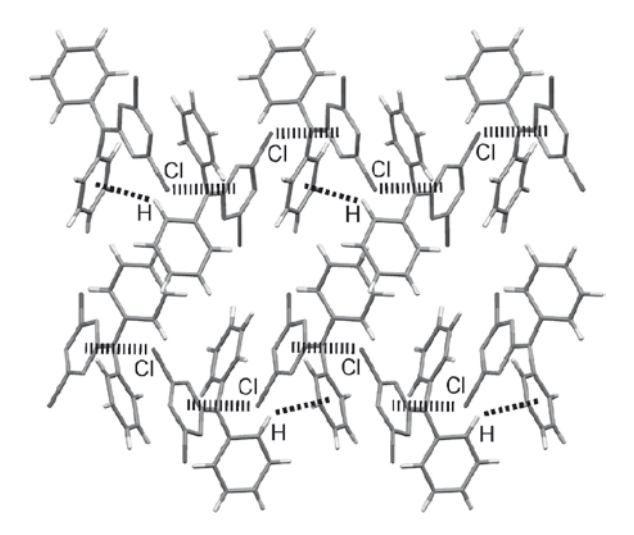


**Fig. 26** X-ray structure of 2,4-chloro-6-diphenylamino-1,3,5-triazine. Lone-pair(Cl)/ $\pi$  and CH/ $\pi$  interactions are represented by *thick* and *thin broken lines*, respectively, while lone-pair(O)/ $\pi$  interactions are not shown [93]

N. Hayashi et al.

pseudo-knot where water molecules and RNA bases are stacked with the aid of lone-pair/ $\pi$  and OH/ $\pi$  interactions [94]. These results indicate that lone-pair/ $\pi$  interaction energies should be large enough to regulate the supramolecular structure, especially when  $\pi$ -deficient heteroaromatic compounds are concerned. It is noted that short contacts of lone-pair and  $\pi$  moiety may not necessarily be regarded as lone-pair/ $\pi$  interactions, since they sometimes locate closely just due to the packing demand [9].

# 7 Interplay of $\pi/\pi$ Interaction and Hydrogen Bonding

One of the most important interactions, other than  $X/\pi$  interactions, in heteroaromatic chemistry is the hydrogen bond [95]. Although both nitrogen and oxygen atoms of heteroaromatic rings can serve as a hydrogen bond acceptor, CSD studies revealed that oxygen atoms participate in hydrogen bonding less frequently than expected (Fig. 27)[96, 97]. Nobeli et al. found [97] that, while 64 out of 126 pyridines and 84 out of 115 of pyrimidines were involved in hydrogen bonding to OH groups connecting to  $sp^3$  carbon atoms, 149 out of 823 tetrahydrofurans and only one out of 71 furans participated in hydrogen bonding to such OH groups. By theoretical calculation, the hydrogen-bonding energy of pyridine–methanol (–6.7 kcal mol<sup>-1</sup>) is about twice as large as that of furan–methanol (–3.7 kcal mol<sup>-1</sup>). This is because the electrostatic potential around the pyridine nitrogen is substantially different from that of furan oxygen, giving the different proton-accepting abilities.

The N–H groups in heteroaromatic rings can also behave as hydrogen bond donors. Interaction energies of NH/O and NH/N hydrogen bonds are about 4–6 kcal mol<sup>-1</sup>, which are a few kilocalories per mole larger than those of "weak hydrogen bonds," such as OH/ $\pi$ , NH/ $\pi$ , and CH/ $\pi$  interactions. Although "canonical hydrogen bonds" are no more referred to in this article, the interplay of hydrogen bonding and  $\pi/\pi$  interactions is alternatively shown, which has attracted much attention in relation to the structural chemistry of DNA. Guo et al. calculated heats of formation of (multiple) hydrogen-bonded dimer (A in Fig. 28) and  $\pi$  stack dimer (D) of compound 10, and of the hydrogen-bonded  $\pi$  stack dimer (B and E) by using hybrid DFT calculations. They found that B was an exothermic process of –0.3 to –1.6 kcal mol<sup>-1</sup>, while D was endothermic of +0.4 to +7.9 kcal mol<sup>-1</sup> [98]. The results indicate that  $\pi$ -stacking energy should be increased by the formation of hydrogen bonds, because hydrogen bonds will enhanced CT interaction forces.

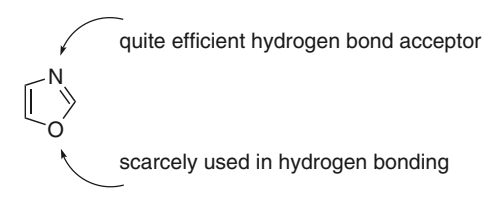


Fig. 27 Participation of nitrogen and oxygen atoms in hydrogen bonding

**Fig. 28** Stepwise construction of  $\pi$ -stacked dimer from monomer **10** either via hydrogen-bonded dimer (*A*, *B*) or  $\pi$ -stacked monomer (*D*, *E*) [98]

	<b></b>	х—			<	X H CZ	
		$X = NO_2$	X = H	$X = CH_3$	$X = NO_2$	X = H	$X = CH_3$
$MEP^a$	-0.0880	-0.0883	-0.0978	-0.0983	-0.0815	-0.0897	-0.0908
$\Delta q^a$		-0.0118	-0.0314	-0.0341	+0.0396	+0.0207	+0.0155

 $<sup>^{</sup>a}\Delta q$  (a.u.) and MEP (a.u.) represent charge transfer to the pyrimidine and molecular electrostatic potential minimum around the pyrimidine nitrogen atoms, respectively.

Fig. 29 Properties of pyrimidine and pyrimidine-substituted benzene complexes in the paralleldisplaced and T-shaped configurations [27]

In contrast, the influence of  $\pi/\pi$  interactions on hydrogen bonding was investigated by Mignon et al. They calculated MEPs (molecular electrostatic potentials) of pyridine [18], pyrimidine, and imidazole [33] (MEP may be used as a measure of strength of hydrogen bonding or basicity) and found that MEPs of those molecules will be increased by formation of  $\pi$  stack with benzene. The changes in basicity highly depend on the magnitude of CT with benzene, because CT interactions give rise to an increase of  $\pi$  electron density around the nitrogen atom of the heteroaromatic rings (thus, MEP values are negatively increased). Substitution of electron-withdrawing groups on the benzene moiety would diminish the magnitude of CT ( $\Delta q$ ), suppressing increase of basicity of the heteroaromatic moiety, while electron-donating substituents have little effect. Values of  $\Delta q$  and MEP calculated by MP2 methods are shown in Fig. 29. In T-shaped complexes, the electron flow is inverted (that is, the heteroaromatic ring becomes an electron-donating moiety). But, when an electron-withdrawing

N. Hayashi et al.

group is substituted onto the benzene,  $\Delta q$  will increase to negatively decrease MEP, so that basicity will be weakened again. Conclusively, substitution of an electron-withdrawing group will decrease basicity of the heteroaromatic moiety, whether the configuration of the complex is  $\pi$  stack or T-shaped.

Mignon et al. also investigated influences of  $\pi$  stacking on the hydrogen-bonding acceptability of DNA/RNA bases, such as adenine, cytosine, uracil, and guanine [99], and found that, while hydrogen bond acceptabilities of those DNA/RNA bases are diminished by formation of  $\pi$  stacking in the optimized structures, they are enhanced in the actual structures. The former is due to repulsion of hydrogen-bond accepting sites, since they are electrostatically negative; on the other hand, in the latter, they are fixed to locate closely within the double-helix structure of DNA/RNA, thus being able to form hydrogen bonds cooperatively.

## **8 Concluding Remarks**

In this article, the nature, geometry, and energy of  $X/\pi$  interactions involving heteroaromatic molecules, such as  $\pi/\pi$  interactions, CH/ $\pi$  interactions, cation/ $\pi$  interactions, anion/ $\pi$  interactions, YH/ $\pi$  (Y = O and N) interactions, and lone-pair/ $\pi$  interactions, have been reviewed and compared to those of aromatic hydrocarbons. Strong interactions, e.g., cation/ $\pi$  interactions, have been widely used to construct supramolecules and in crystal engineering. Weak interactions are also important subjects of investigation. Although they cannot determine the structure by themselves, weak interactions appear quite frequently and are capable of affecting the structure and properties of molecules and molecular complexes.

Studies on those interactions have been facilitated by recent progress in computational chemistry based on the development and generalization of new calculation methods (especially DFT methods) as well as evolution of computer hardware. As mentioned, a large number of findings have accumulated in the last 10 years, yet there are still many issues remaining. For example, precise calculation of intermolecular interactions is restricted to small molecules due to the limitations of computer resources at present. But, in the future, it is expected that further evolution of computer hardware as well as development of new calculation methods should enable us to calculate interactions for large molecules. Accumulation of experimental data on fundamental phenomena and compounds is also expected. Experimental studies on non-substituted heteroaromatic compounds have been very rare, in comparison to those on benzene and other hydrocarbons.

Another reason for the significant development of studies on intermolecular interactions of heteroaromatic molecules was to explain the intriguing properties and characters of heteroaromatic molecules and supramolecules and to make guidelines for their design. A typical example is the supramolecular crystal developed by Imahori, where porphyrins form a  $\pi$  stack by self-organization and, together with arrangement of fullerenes, provide an essential structure for a highly efficient solar

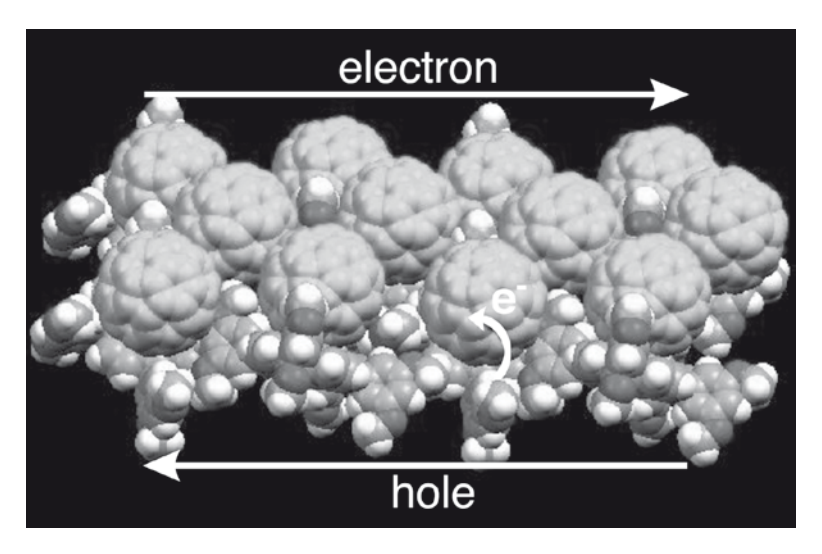


Fig. 30 Self-organization structure consisting of  $\pi$  stack of porphyrin moieties. Electron and hole may move along the depicted *arrows*. Direction of charge transfer is represented by the *curved arrow*. Courtesy of Profs. Umeyama and Imahori at Kyoto University, Kyoto, Japan [100, 101]

cell [100, 101] (see Fig. 30). Knowledge of intermolecular interactions will facilitate design of such interesting and useful molecular complexes.

#### References

- 1. Hunter CA, Lawson KR, Perkins J, Urch CJ (2001) J Chem Soc Perkin Trans 2:651
- 2. Hobza P, Šponer J (1999) Chem Rev 99:3247
- 3. Nishio M (1998) The  $CH/\pi$  interaction-evidence, nature, and consequences. Wiley-VCH, New York
- 4. Ma JC, Dougherty DA (1997) Chem Rev 97:1303
- 5. Schottel BL, Chifotides HT, Dunbar KR (2008) Chem Soc Rev 37:68
- 6. Desiraju GR, Steiner T (1999) The weak hydrogen bond in structural chemistry and biology. Oxford University Press, Oxford
- 7. Alkorta I, Rozas I, Elguero J (1998) Chem Soc Rev 27:163
- 8. Dougherty DA (1996) Science 271:163
- 9. Egli N, Sarkhel S (2007) Acc Chem Res 40:197
- Janda KC, Hemminger JC, Winn JS, Novick SE, Harris SJ, Klemperer W (1975) J Chem Phys 63:1419
- 11. Stone AJ (1997) The theory of intermolecular forces. Oxford University Press, Oxford
- 12. Bernardi F, Boys SF (1970) Mol Phys 19:553
- 13. Tsuzuki S, Honada K, Uchimaru T, Mikami M, Tanabe T (2002) J Am Chem Soc 124:104
- 14. Sinnokrot MO, Valeev EF, Sherrill CD (2002) J Am Chem Soc 124:10887
- 15. Jennings WB, Farrell BM, Malone JF (2001) Acc Chem Res 34:885
- 16. Hunter CA, Sanders JKM (1990) J Am Chem Soc 112:5525

N. Hayashi et al.

17. Waller MP, Robertazzi AR, Platts JA, Hibbs DE, Williams PA (2006) J Comp Chem 27:491

- 18. Mignon P, Loverix S, De Proft F, Geerlings P (2004) J Phys Chem A 108:6038
- 19. Tsuzuki S, Mikami M, Yamada S (2007) J Am Chem Soc 129:8658
- 20. Ugozzoli F, Massera C (2005) CrystEngComm 7:121
- 21. Mishra BK, Sathyamurthy N (2005) J Phys Chem A 109:6
- 22. Piacenza M, Grimme S (2005) ChemPhysChem 6:1554
- Lin I-C, von Lilienfeld OA, Coutinho-Neto MD, Tavernelli I, Rothlisberger U (2007) J Phys Chem B 111:14346
- 24. Šponer J, Hobza P (1997) Chem Phys Lett 267:263
- 25. Hopkins BW, Tschumper GS (2004) J Phys Chem A 108:2941
- 26. Tsuzuki S, Honda K, Azumi R (2002) J Am Chem Soc 124:12200
- 27. Thomas JB, Roth WR, Verkade JG (1972) J Am Chem Soc 94:8854
- 28. Rodríguez-Ropero F, Casanovas J, Alemán C (2007) J Comp Chem 29:69
- 29. Hutchinson GR, Ratner MA, Marks TJ (2005) J Am Chem Soc 127:16866
- 30. Sherlis DA, Marzari N (2004) J Phys Chem B 108:17791
- 31. Sinnokrot MO, Sherrill CD (2003) J Phys Chem A 107:8377
- 32. Rashkin MJ, Waters ML (2002) J Am Chem Soc 124:1860
- 33. Mignon P, Loverix S, Geerlings P (2005) Chem Phys Lett 401:40
- 34. Gungs BW, Wekusa F, Barnes CL (2008) J Org Chem 73:1803
- 35. Malathy Sony SM, Ponnuswamy MN (2006) Cryst Growth Des 6:736
- 36. Janiak C (2001) J Chem Soc Dalton Trans, 3885
- 37. Tsuzuki S, Uchimaru T, Matsuura K, Mikami M, Tanabe K (2000) Chem Phys Lett 319:547
- 38. Gonzalez C, Lim EC (2000) J Phys Chem A 104:2953
- 39. Hayashi N, Mori T, Yamaguchi K, Tsukamoto N, Matsumoto K (2003) Heterocycles 61:357
- 40. Hayashi N, Yamaguchi K, Matsumoto K (2001) Supramol. Chem. 13:45
- 41. Pejov L (2001) Chem Phys Lett 339:269
- 42. Latypov S, Fakhfakh MA, Jullian JC, Franck X, Hocquemiller R, Figadère B (2005) *Bull Chem Soc Jpn* 78:1296
- 43. Itahara T, Imaizumi K (2007) J Phys Chem B 111:2025
- 44. Roesky HW, Andruh M (2003) Coord Chem Rev 236:91
- 45. He C, Zhang BG, Duan CY, Li JH, Meng QJ (2000) Eur J Inorg Chem 2549
- 46. Vögtle F, Kessener (1984) Chem Ber 117:2538
- 47. Kang HC, Hanson AW, Eaton B, Boekelheide V (1985) J Am Chem Soc 107:1979
- 48. Amicangelo JC, Armentrout PB (2000) J Phys Chem A 104:11420
- 49. Kim D, Hu S, Tarakeshwar P, Kim KS, Lisy JM (2003) J Phys Chem A 107:1228
- 50. Tsuzuki S, Yoshida M, Uchimaru T, Mikami M (2001) J Phys Chem A 105:769
- 51. Zhu WL, Tan XJ, Puah CM, Gu JD, Jiang HL, Chen KX, Felder CE, Silman I, Sussman JL (2000) *J Phys Chem A* 104:9573
- 52. Stöckigt D (1997) J Phys Chem A 101:3800
- 53. Rodríguez-Otero J, Cabaleiro-Lago EM, Peña-Gallego A (2008) Chem Phys Lett 452:49
- 54. De Wall SL, Meadows ES, Barbour LJ, Gokel, GW (1999) J Am Chem Soc 121:5613
- 55. Gokel GW, Barbour LJ, Ferdani R, Hu J (2002) Acc Chem Res 35:878
- 56. Dougherty DA (2008) J Org Chem 73:3667
- 57. Gallivan JP, Dougherty DA (1999) Proc Natl Acad Sci USA 96:9459
- 58. Ruan C, Rodgers MT (2004) J Am Chem Soc 126:14600
- 59. Berryman OB, Bryantsev VS, Stay DP, Johnson DW, Hay BP (2007) J Am Chem Soc 129:48
- 60. Sessler JL, Gale PA, Genge JW (1998) Chem Eur J 4:1095
- 61. Beer PD, Gale PA (2001) Angew Chem Int Ed 40:486
- 62. Garau C, Quiñonero D, Frontera A, Ballester P, Costa A, Deyà PM (2003) Org Lett 5:2227
- Quiñonero D, Garau C, Rotger C, Frontera A, Ballester P, Costa A, Deyà PM (2002) Angew Chem Int Ed 41:3389
- 64. Gamez P, Mooibroek TJ, Teat SJ, Reedijk J (2007) Acc Chem Res 40:435
- 65. Mascal M, Armstrong A, Bartberger MD (2002) J Am Chem Soc 124:6274

- 66. Mascal M (2006) Angew Chem Int Ed 45:2890
- 67. Zuo C-S, Quan J-M, Wu Y-D (2007) Org Lett 9:4219
- Quiñonero D, Garau C, Frontera A, Ballester P, Costa A, Deyà PM (2005) J Phys Chem A 109:4632
- 69. Kim D, Tarakeshwar P, Kim KS (2004) J Phys Chem A 108:1250
- Frontera A, Saczewski F, Gdaniec, M, Dziemidowicz-Borys E, Kurland A, Deyà PM, Quiñonero D, Garau C (2005) Chem Eur J 11:6560
- 71. Rosokha YS, Lindeman SV, Rosokha SV, Kochi JK (2004) Angew Chem Int Ed 43:4650
- 72. Ahuja R, Samuelson AG (2003) CrystEngComm 5:395
- 73. Figgis BN, Skelton BW, White AH (1978) Aust J Chem 31:57
- 74. Quiñonero D, Frontera A, Deyà PM (2008) ChemPhysChem 9:397
- 75. Demeshko S, Dechert S, Meyer F (2004) J Am Chem Soc 126:4508
- 76. Black CA, Hanton LR, Spicer MD (2007) Inorg Chem 46:3669
- Maheswari PU, Modec B, Pevec A, Kozlev ar B, Massera C, Gamez, P, Reedijk J (2006) Inorg Chem 45:6637
- 78. Shottel B, Bacsa J, Dunbar KR (2005) Chem Commun, 46
- Shottel BL, Chifotides HT, Shatruk M, Chouai A, Pérez LM, Bacsa J, Dunbar KR (2006) J Am Chem Soc 128:5895
- 80. Garcia-Raso A, Albertí FM, Fiol, JJ, Tasada A, Barreló-Oliver M, Molins E, Escudero D, Frontera A, Quiñonero D, Deyà PM (2007) Eur J Org Chem 5821
- de Hoog P, Gamez P, Mutikainen I, Turpeinen U, Reedijk J (2004) Angew Chem Int Ed 43:5815
- Garau C, Frontera A, Quiñonero D, Ballester P, Costa A, Deyà PM (2004) J Phys Chem A 108:9423
- 83. Stojanovi SĐ, Medakni VB, Predovi G, Beljanski M, Zari , SD (2007) *J Biol Inorg Chem* 12:1063
- 84. Tsuzuki S, Honda K, Uchimaru T, Mikami M, Tanabe K (2000) J Am Chem Soc 122:11450
- Muñoz MA, Sama O, Galán M, Guardado P, Carmona C, Balón M (1999) J Phys Chem B 103:8794
- 86. Muñoz MA, Feccero R, Carmona C, Balón M (2004) Spectrochim Acta A 60:193
- 87. Scheiner S, Kar T, Pattanayak J (2002) J Am Chem Soc 124:13257
- 88. Steiner T, Koellner G (2001) J Mol Biol 305:535
- 89. Macias AT, Mackerell AD Jr (2005) J Comput Chem 26:1452
- Mons M, Dimicoli I, Tardivel B, Piuzzi F, Brenner V, Millié P (1999) J Phys Chem A 103:9958
- 91. Reyes A, Fomina L, Rumsh L, Fomine S (2005) Int J Quantum Chem 104:335
- 92. Kawahara S, Tsuzuki S, Uchimaru T (2005) Chem Eur J 11:4458
- 93. Lu Z, Games P, Mutikainen I, Turpeinen U, Reedijk J (2007) Cryst Growth Des 7:1669
- 94. Sarkhel S, Rich A, Egli M (2003) J Am Chem Soc 125:8998
- 95. Jeffery GA (1997) An introduction to hydrogen bonding. Oxford University Press, Oxford
- 96. Böhm H-J, Klebe G, Brode S, Hesse U (1996) Chem Eur J 2:1509
- 97. Nobeli I, Price SL, Lommerse JPM, Taylor R (1997) J Comp Chem 18:2060
- 98. Guo D, Sijbesma RP, Zuihof H (2004) Org Lett 6:3667
- 99. Mignon P, Loverix S, Steyaert J, Geerlings P (2005) Nucleic Acids Res 33:1779
- 100. Kang S, Umeyama T, Ueda M, Matano Y, Hotta H, Yoshida K, Isoda S, Shiro M, Imahori H (2006) Adv Mater 18:2549
- 101. Imahori H, Ueda M, Kan S, Hayashi H, Hayashi S, Kaji H, Seki S, Saeki A, Tagawa S, Umeyama T, Matano Y, Yoshida K, Isoda S, Shiro M, Tkachenko NV, Lemmetyinen H (2007) Chem Eur J 13:10182

Top Heterocycl Chem (2009) 18: 37-74

DOI: 10.1007/7081\_2008\_9

© Springer-Verlag Berlin Heidelberg 2008 Published online: 4 November 2008

# Supramolecular Host–Guest Chemistry of Heterocyclic V-Shaped Molecules

#### Roger Bishop

**Abstract** The host–guest inclusion properties of heterocyclic molecules that utilise  $C_2$ -symmetric V-shaped building blocks in their construction are reviewed. Such compounds are classified here according to the molecular structures of these building blocks. Salient features of the crystal structures of the resulting inclusion compounds are described and the f unctions of their key supramolecular synthons are analysed. Concepts underpinning the deliberate design and synthesis of new host molecules of this type are explained and then put into practice.

**Keywords** Host–guest, Inclusion, Intermolecular forces, Supramolecular synthons, V-shaped molecules

#### **Contents**

1	Introduction			
	1.1	Scope of the Review	38	
	1.2	Hosts and Guests	38	
	1.3	Symmetry Requirements	39	
		V-Shaped Building Blocks	39	
	1.5	Some Synthetic Approaches	40	
2	Kaga	Kagan's Ether Derived Systems		
3	Tröger's Base Derived Systems		42	
4	·			
	4.1	Synthetic Design	46	
		Aromatic Wings	47	
	4.3	The V-Shaped Linker	48	
		Substituent Groups	49	
		Chirally Pure or Racemic Hosts?	49	

School of Chemistry, Dalton Building, The University of New South Wales, UNSW Sydney NSW 2052. Australia

e-mail: r.bishop@unsw.edu.au

R. Bishop

5	Bicyclo[3.3.0]octane-Derived Systems		
	5.1	Synthesis	50
	5.2	Host-Guest Behaviour	52
6	Bicy	clo[3.3.1]nonane Derived Systems	56
	6.1	Synthesis	56
	6.2	Host-Guest Behaviour	60
7	9-He	9-Heterobicyclo[3.3.1]nonane Derived Systems	
		Synthesis	
	7.2	Host-Guest Behaviour	67
8	Cond	clusions	71
Re	ferend	es	72

#### **Abbreviations**

EE edge-edge
EF edge-face
OFF offset face-face
PHD pi-halogen dimer

#### 1 Introduction

## 1.1 Scope of the Review

Much research has been published on small molecules that subtend a concave surface capable of interacting with other molecules. A wide range of terms such as tweezer, clip, jaw, pincer, cleft, V-shape, and concave has been used to describe such systems. While tweezer [1, 2] and concave [3] are precise terms, many of the others are less well defined and can often be interchanged. The concepts utilised in making tweezers can be expanded into the construction of molecular capsules, but such design is outside the scope of this article. For brevity this account will be restricted to heterocyclic systems that use  $C_2$ -symmetric V-shaped building blocks in their molecular construction and which also function as host molecules.

#### 1.2 Hosts and Guests

The majority of inclusion compounds [4, 5, 6] can be sub-divided conveniently into three distinct types. In the first of these, the host molecule contains some type of receptor structure which co-ordinates with, or otherwise traps, the guest. Familiar classes of host molecules belonging to this category are the crown ethers, cryptands, cyclodextrins and spherands. In these compounds the host and guest species are very clearly differentiated.

Alternatively, guest inclusion may result from molecules that pack inefficiently just by themselves. In such cases, the inclusion of guests can yield a more dense and lower energy crystal lattice. The resulting materials are termed clathrates or lattice inclusion compounds, and there is usually a clear distinction between the host and guest components. Familiar host molecules of this type are urea, water (the gas hydrates), helical tubuland diols, the MacNicol hexahosts, and Toda's wheel and axle compounds.

In the final group, two or more components are hydrogen bonded together to form a co-crystalline solid. These are well-defined and stoichiometric multi-component compounds, but the distinction between host and guest has now become entirely lost. Materials such as formic acid–hydrogen fluoride, *p*-nitrophenol–diacetamide, and melanine–cyanuric acid, are examples of this third group. An extensive account of the structural chemistry of all three types of molecular inclusion compounds has recently been published [7].

## 1.3 Symmetry Requirements

The role of symmetry is crucial to the design of organic inclusion hosts [8, 9]. It is well known that certain classes, such as  $C_2$ -symmetry, favour inclusion behaviour over others , but the reasons for this are not entirely clear. A certain degree of symmetry certainly assists in propagation of the initial seed nucleus into a full crystal, whereas higher symmetry may provide efficient packing without the need for guest inclusion. Chiral molecules with only the  $C_2$ -symmetry element are slightly twisted and more cumbersome in either their racemic or their chirally-pure forms. It is probably this balance between symmetry and awkwardness that results in  $C_2$ -symmetric molecules being so highly represented as inclusion hosts. Of course, many other factors are involved in ensuring that a particular molecule will function as a host and these will be discussed later.

# 1.4 V-Shaped Building Blocks

There are several simple molecular frameworks that can provide V-shaped building blocks for the construction of host molecules. The examples discussed here are Kagan's ether 1, Tröger's base 2, bicyclo[3.3.1]nonane 3, its 9-thia 4 and 9-oxa 5

<sup>&</sup>lt;sup>1</sup>In this article, the molecular structure of only one enantiomer of a chiral molecule will be drawn, and the terms *syn* and *anti* will refer to the relative geometry of neighbouring bridges present in multicyclic structures.

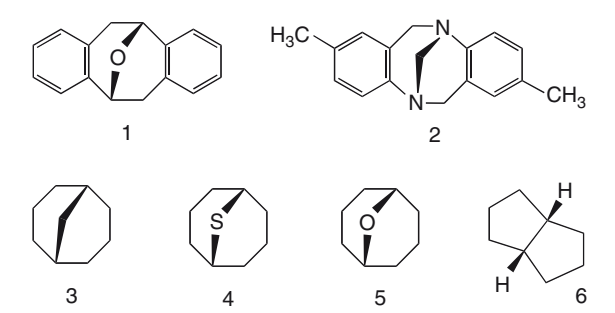


Fig. 1 Examples of V-shaped building blocks that can be used in the synthesis of inclusion host systems featuring  $C_2$ -symmetry

analogues, and bicyclo[3.3.0]octane **6** (Fig. 1). These units constitute a central linking core that imparts  $C_2$ - (or pseudo- $C_2$ -) symmetry to the host molecule and also permits limited conformational flexibility. A certain degree of flapping and/or twisting is possible within these frameworks, such that the host molecule may modify its shape slightly when confronted with potential guests of differing steric or supramolecular demand.

# 1.5 Some Synthetic Approaches

Pre-formed V-shaped molecules can often be converted into new derivatives through direct reaction. However, many processes are also available for incorporation of a V-shaped core into part of a much larger molecule. Ideally, of course, the method chosen should be simple to carry out and widely applicable. Intramolecular Friedel-Crafts reactions are generally employed to generate molecules based on Kagan's ether and also dibenzobicyclo[3.3.1]nonane derivatives [10, 11]. Primary aromatic amine-aldehyde condensation reactions are used to afford Tröger's base analogues [12]. Other approaches include the Diels-Alder reaction (especially using diarylisobenzofuran [13] or diaryltetrazines [14]), the Fischer indole cyclisation [15], and the Issidorides-Haddadin condensation between a ketone and benzofurazan oxide [16]. However, the most widely applied method in this area has been the Friedländer reaction [17], through its popularisation by Thummel [18–20], Marchand [21], Mehta [13] and other workers. Part of the original work on this reaction utilised amine hydrochloride salts at high temperature, thereby misleading some modern chemists into the belief that vigorous conditions were obligatory. In fact, as reconfirmed by Thummel, many high yielding Friedländer condensations proceed easily in solution at room temperature.

## 2 Kagan's Ether Derived Systems

Kagan's ether 1 is generally prepared in its racemic form and shows no inclusion properties. It has a V-shaped  $C_2$ -symmetric structure with an angle between the normals to the aromatic planes of around 93°. Its inherent potential has, however, led to the synthesis of more complex analogues, such as **7–10** (Fig. 2), successfully designed to act as chiral molecular tweezers [22]. Examples of some of the resulting inclusion compounds are described below.

Fig. 2 Examples of molecular tweezer molecules constructed using Kagan's ether building blocks

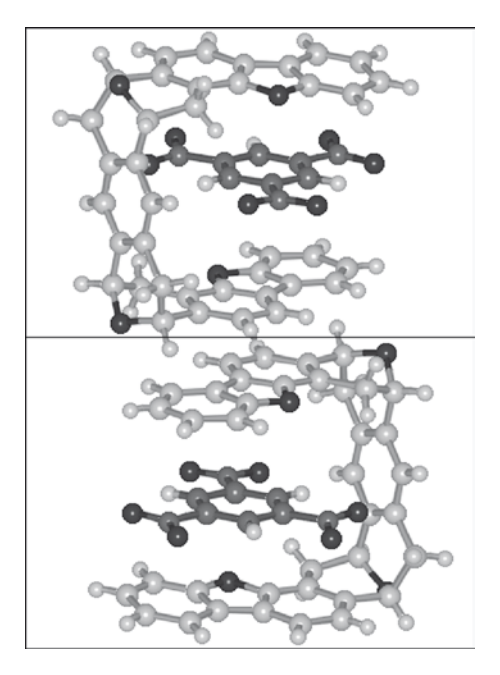


Fig. 3 Partial crystal structure of compound (8).(1,3,5-trinitrobenzene) showing the mode of guest enclosure within the cleft of the molecular tweezer [24]

The *syn*-derivative **7** yields the lattice inclusion compound (**7**)<sub>2</sub>.(ethyl acetate) in which offset stacks of the host molecules produce channels containing the disordered guests. The basic unit comprises the guest molecule enclosed by two offset molecules of **7**. This host also forms a compound with molecular iodine [23].

The longer tweezer **8** has a deeper cleft with its two arms ideally distanced to accommodate an aromatic guest [24]. The inclusion compound (**8**).(1,3,5-trinitrobenzene) is consequently produced (Fig. 3) with the guest molecule securely trapped within the cavity.

Similarly, the naphthalene-substituted compound **9**, also with a deeper cleft than **7**, forms compounds with guests such as maleic anhydride, 4-chloronitrobenzene, and 1,3,5-trinitrobenzene [22]. Kagan's ether can be incorporated into more involved tweezers, one of the more radical designs being the salicylaldehyde-based system **10** [25].

# 3 Tröger's Base Derived Systems

Tröger's base 2 is generally obtained as the racemic material through the acid catalysed condensation of formaldehyde with p-toluidine. Despite being first reported in 1887, its correct structure was not determined till nearly 50 years later [26]. This

Fig. 4 Examples of ionic Tröger's base derivatives that exhibit inclusion host properties

compound is notable for being the first chiral amine that could be resolved due to its high nitrogen inversion energy barrier [27]. Although the parent structure itself is not a host, its concave face, chirality, and simple access have made it a popular target for modification and also for the investigation of carbocyclic analogues [28–30].

Quaternary Tröger's base salts such as 11 and 12 (Fig. 4) exhibit inclusion behaviour with a range of guest molecules [31–34]. In the crystal structure of  $(11)_2$ . (dioxane) (R = R<sub>1</sub> = Me; X = I), shown in Fig. 5 [32], the guest molecules and iodide ions lie above and below building blocks generated from two units of 11. Inclusion behaviour also extends to the ethano-bridged homologue 13, as illustrated in Fig. 6 [35]. Wilcox has taken a more systematic approach by incorporation of the Tröger's base moiety into the water-soluble macrocyclic receptor 14 which complexes acidic aromatic guests [36].

Inclusion properties can be imparted to some covalent Tröger's base derivatives by increasing their molecular size and complexity (Fig. 7), the tetraester cleft compound 15 being the first reported example [37]. Molecules of 15 are arranged as parallel stacks with two ethanol guests enclosed by each cleft and adjacent molecules of 15 (Fig. 8). The simpler diphenyl Tröger's base analogue 16 includes dioxane

**Fig. 5** The crystal structure of  $(11)_2$ . (dioxane) (where  $R = R_1 = Me$ ; X = I), showing the guest molecules located in the centre and the iodide ions at the edges of this diagram [32]

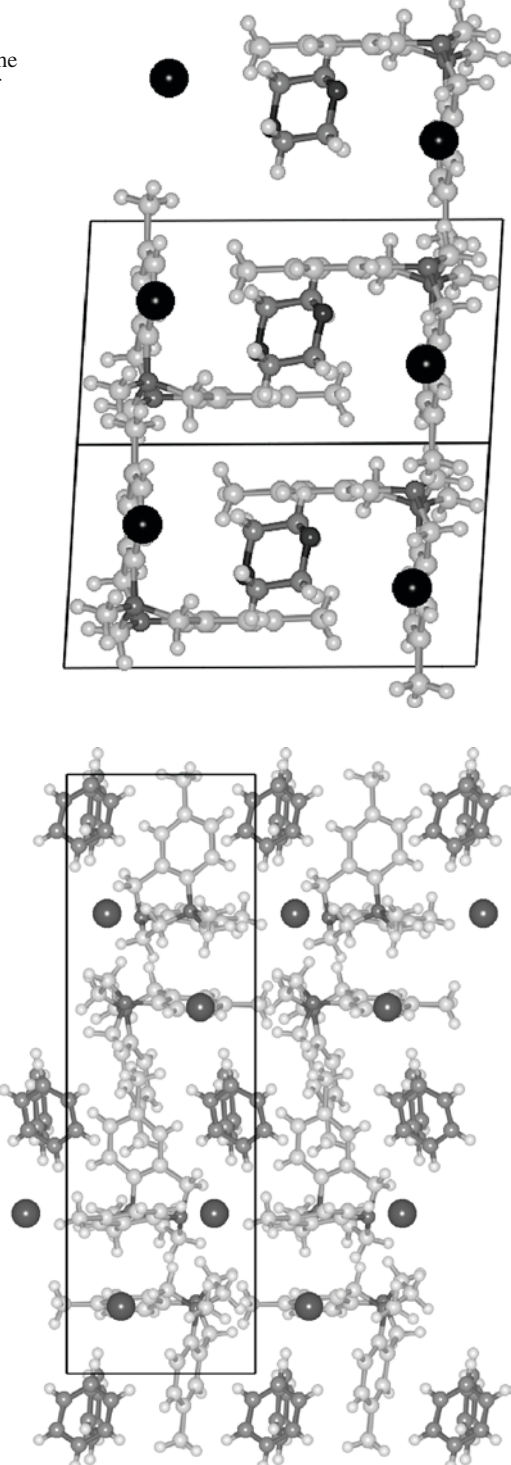


Fig. 6 The crystal structure of chirally pure (+)-(13).(benzene), showing the guest molecules and iodide ions occupying alternate horizontal zones in the solid [35]

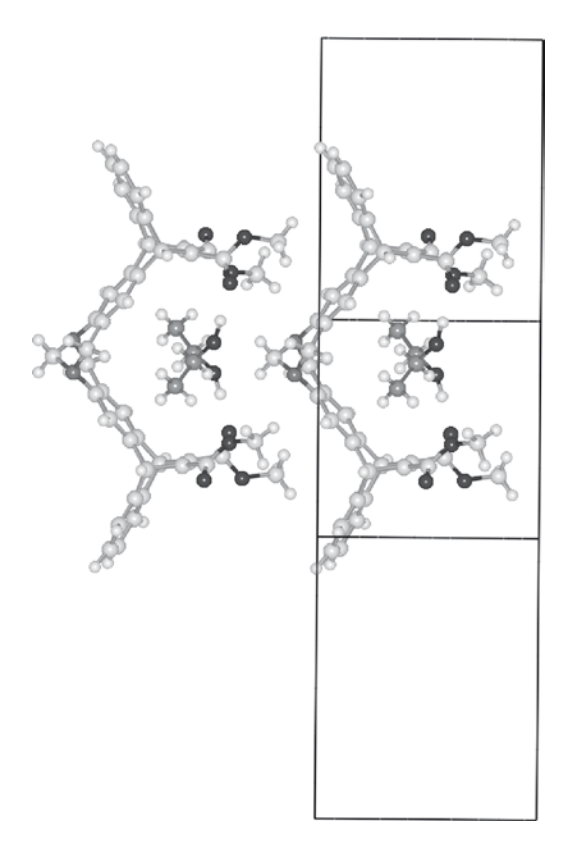
Fig. 7 Structures of some of the larger covalent Tröger's base derivatives 15–18 that form inclusion compounds

[33]. Although the *anti*-isomer of the bis(Tröger's base) **17** has a non-cleft shape it nonetheless includes ethanol guest molecules in its crystal structure. Perversely, the corresponding *syn*-isomer, with a molecular cleft geometry, does not include guests [38, 39].

The linear symmetrically-fused tris-derivatives **18** have been reported recently by Wärnmark and colleagues [40]. The *syn,syn*-, and to a lesser extent the *syn,anti*-isomers contain substantial concave pockets, whereas the *anti,anti*-isomer does not. Inclusion properties have been demonstrated for the first two isomers.

Bis(porphyrin)-fused Tröger's base derivatives have been synthesised and studied by Crossley. These molecules have very large concavities with the metal atoms providing two internal and two external binding sites that are ideal for the binding of difunctional carboxylic acids. For example, the concavity of a tin(IV) host can be spanned neatly by means of succinate ion [41].

**Fig. 8** Part of the crystal structure of (**15**).(ethanol)<sub>2</sub> showing how the guests occupy cages formed by a host cleft and the neighbouring molecules of **15** [37]



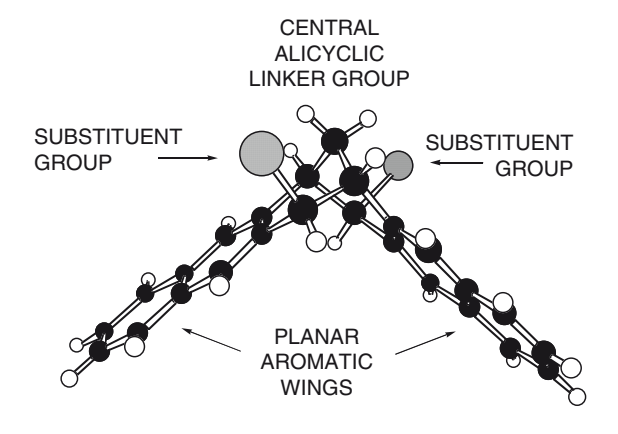
# 4 A Modular Design Approach

# 4.1 Synthetic Design

From these examples, it is seen that V-shaped building blocks can indeed be used to synthesise host molecules that will enclose guests within cleft-like cavities. A number of the inclusion compounds formed by hosts based on Kagan's ether and Tröger's base sub-units, however, did not have that topology. Whereas carefully designed tweezer hosts certainly work, the observed lattice inclusion compounds actually comprise a diverse range of arrangements. Molecules of the V-shaped type have immense potential as new lattice inclusion hosts but a more reasoned strategy is required. Consequently, we have developed a synthetic approach to ensure that new hosts can be prepared very simply [42]. Since these molecules lack hydrogen bonding groups, their availability also allows systematic investigation of the weaker and less familiar supramolecular synthons [43, 44] involved in their solid state chemistry.

Our design uses three modular construction units, all of which play important roles in the function of the host (Fig. 9). First, two aromatic wings provide planar

Fig. 9 Diagrammatic representation of a modular design for the synthesis of new lattice inclusion hosts based around a V-shaped core



surfaces that can interact with guests or other host molecules. The most common interactions expected are the well-known aryl edge-face (EF) interactions [45] and aryl offset face-face (OFF) interactions [46]. Second, these wings are connected to a central alicyclic V-shaped core, chosen to impart  $C_2$ - (or pseudo- $C_2$ -) symmetry to the host molecule and to permit limited conformational flexibility. Third, substituent groups prevent the wing interactions extending too effectively throughout the entire crystal. The spoiler-effect of these substituents creates a molecule that packs poorly by itself. Hence, a lower crystal lattice energy value often results by means of guest incorporation. These design features are discussed below in greater detail. The wings, V-shaped groups, and substituents use modular units that can be replaced by alternatives. Hence our design leads not just to one host compound but, instead, to related families of new lattice inclusion hosts. If the molecular building blocks are available compounds, then the preparation of these hosts is often just a two-step synthesis.

# 4.2 Aromatic Wings

The EF and OFF interactions are two of the most common supramolecular synthons that act as non-covalent links between molecules. These aryl interactions are influenced both by the C:H ratio and the size of the planar surface area in any given case [47–49]. Such aromatic hydrocarbons pack efficiently through repetition of the EF and/or OFF motifs to generate crystals with no need to include guest molecules. It is for this reason that our host design incorporates substituent groups that prevent this happening. As hinted at by the Kagan's ether (Sect. 2) and Tröger's base (Sect. 3) results, there is a minimum wing surface area (or related concave surface area) necessary for guest inclusion to take place. Furthermore, the use of heteroaromatic wings will permit additional edge-edge (EE) packing in many instances.

## 4.3 The V-Shaped Linker

The aliphatic V-shaped linker group performs three important roles. First, it functions as a spacer that physically separates the two aromatic wings and their associated regions of supramolecular activity. Use of bicyclo[3.3.0]octane-2,6-dione, bicyclo[3.3.1]nonane-2,6-dione, or 9-heterobicyclo[3.3.1]nonane-2,6-diones allows both aromatic wings to be conjoined in a one-flask condensation reaction and produces a high yield of a  $C_2$ -symmetric adduct. If the symmetric bicyclo[3.3.0] octane-3,7-dione or bicyclo[3.3.1]nonane-3,7-dione molecules are employed instead, then regioselective Friedländer condensations occur that result in the same outcome. Consequently, compounds with  $C_2$ -symmetry (or pseudo  $C_2$ -symmetry) are obtained in the solid state (Sect. 1.3). Finally, these central linker groups permit a certain amount of conformational mobility. Too much would be an undesirable property, but these linkers let the molecule twist and/or expand-contract in response to the presence of different potential guest molecules. This also permits competition between different types, and combinations, of intermolecular attractive forces.

A measure of this flexible response to differing environments is the value of the fold angle (see Fig. 10) recorded from X-ray crystal determination. Fold angles for diquinolines with bicyclo[3.3.0]octane or bicyclo[3.3.1]nonane linkers normally lie

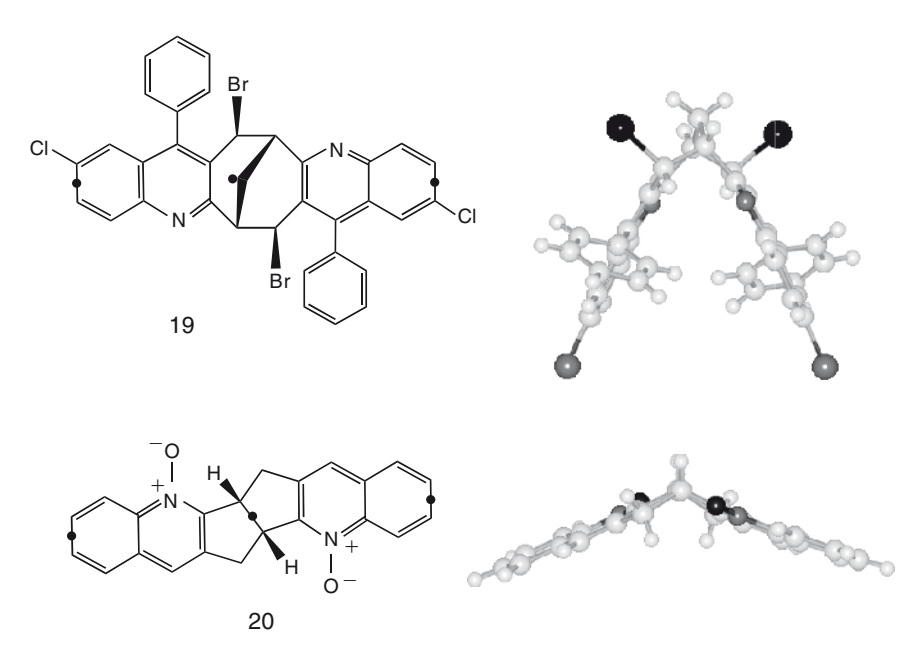


Fig. 10 Molecules showing the minimum (19;  $67.0^{\circ}$ ) and maximum (20;  $141.4^{\circ}$ ) experimental fold angles recorded by us in the solid state. These angles are measured between the points indicated by the *solid circles* [50, 51]

between 80° and 115° but, occasionally, extreme values are encountered. For example, the fold angles for four lattice inclusion compounds of **19** are consistent over 86.2–90.2°, but the remarkable value of 67.0° in the apohost **19** crystal structure is the lowest that we have observed [50]. In this case, generation of an A-shaped molecular conformation leads to compact layers and generation of an efficient network of intermolecular halogen... $\pi$  and aryl EF attractions. In contrast, the compound **20** shows a large angular expansion to 141.4° due to the involvement of both its aromatic wings in EE packing motifs [51]. These examples illustrate how the conformational mobility of the linker group is available to allow modification of the crystal packing when necessary.

## 4.4 Substituent Groups

The substituent groups on the molecular framework are crucial for creation of inclusion behaviour. Their presence ensures that favourable interactions between the aromatic wings are attenuated such that they do not dominate the host packing. They also ensure that the pure substrate has a slightly awkward shape. Hence, guest molecules are incorporated in preference to the hosts packing inefficiently on their own. Although this requirement may appear counter-intuitive, it is actually an obligatory requirement in the deliberate design of new lattice inclusion hosts of this type. The substituents may also provide local hot spots that encourage additional intermolecular host–host and/or host–guest motifs to form in the inclusion structure. Halogen substituents, for example, may participate in halogen…halogen [52, 53],  $\pi$ …halogen [54, 55], and/or  $\pi$ …halogen dimer (PHD) [56] motifs.

These substituents can be simple non-hydrogen atoms or can be more complex functional groups. They may be introduced directly by using appropriately substituted building blocks at the condensation stage, or be introduced by subsequent reaction. Electrophilic aromatic substitution reactions of the wings, and radical benzylic bromination of the central linker, have both been used widely by us. The latter process has been found to be a highly regio- and stereo-selective process that proceeds in excellent yield. Almost without exception, the unsubstituted substrates show no host behaviour whereas the substituted compounds are excellent hosts. However, if the number of phenyl substituents is increased beyond a certain point (Sect. 6.2), then inclusion properties may be observed without the need for further substituents.

# 4.5 Chirally Pure or Racemic Hosts?

Bicyclo[3.3.0]octane-2,6-dione, bicyclo[3.3.1]nonane-2,6-dione, and the 9-hetero-bicyclo[3.3.1]nonane-2,6-diones are usually prepared as the racemic material. Consequently, their use as V-shaped linkers in host synthesis will yield racemic

compounds. Resolution of the diones is, however, possible. Hence chirally pure samples of the diheteroaromatic molecules can be synthesised if required. The choice of a chirally pure, or a racemic, host depends entirely on the particular example. For some types of host molecule it is critical to use the homochiral compound, but in other cases inclusion only occurs when the racemic mixture is used. The latter circumstance is preferable in the sense that synthesis of the racemic material is normally quicker and cheaper. However, if the experimental aim was the resolution of racemic guest molecules, then this approach would be generally disadvantageous.

It turns out that the racemic diheteroaromatic compounds discussed here are vastly more effective hosts than their single enantiomer forms. The reason for this is easy to understand from the analyses of the crystal structures of their inclusion compounds, wherein many centrosymmetric packing motifs are encountered. Of course, these interactions cannot exist in the resolved case, and thus the single enantiomer compounds often pack most unhappily as a consequence.

## 5 Bicyclo[3.3.0]octane-Derived Systems

## 5.1 Synthesis

Heteroaromatic rings may be easily attached to a bicyclo[3.3.0] octane core by means of the Friedländer condensation reaction [17], thereby also imposing  $C_2$ -symmetry on the resulting heterocyclic adduct. Five host molecules (24–26, 28, 30) have been prepared using this simple approach: four of them in overall two-step processes and one in a three-step sequence (Fig. 11).

Thus, condensation of two equivalents of 2-aminobenzaldehyde **21** and one equivalent of bicyclo[3.3.0]octane-2,6-dione **22** gave the diquinoline adduct **23** in 75% yield [57, 58]. The substituent groups (see Sect. 4.4) can then be added by two alternative methods. Free radical benzylic bromination yields the dibromide **24** in a highly regio- and stereo-selective process [59], or alternative electrophilic aromatic substitution gives the tetrabromide **25** [60, 61]. The latter compound undergoes benzylic bromination to produce the third host, hexabromide **26** [62].

Illustrating the modular nature of the host design, 5-chloro-2-aminobenzaldehyde **27** can be used (instead of **21**) as the 2-aminocarbonyl component of the Friedländer condensation, thereby allowing preparation of the tetrahalo host **28** [63, 64]. Bicyclo[3.3.0]octane-3,7-octane **29** can be employed as the carbonyl component (instead of its isomer **22**) and this ultimately leads to the dibromodiquinoline **30** (isomeric with **24**). The Friedländer reaction of **21** and **29** could, in principle, yield two diquinoline condensation products dependent on the enolisation direction of the ketone groups of the latter starting material. However, only the condensation geometry illustrated is observed in practice [65], because double bonds occupying the 2 and 6 positions of the bicyclo[3.3.0]octane ring system are less strained than

i NaOH,  $H_2O$ , MeOH. ii NBS,  $CCl_4$ . iii  $Br_2 Ag_2SO_4$ ,  $H_2SO_4$ .

Fig. 11 Synthesis of five inclusion hosts 24-26, 28, 30 constructed around a bicyclo[3.3.0]octane core [57-65]

for the alternative 2 and 7 positional isomer. This situation is also the case for the analogous bicyclo[3.3.1]nonane derivatives discussed in Sect. 6.1.

#### 5.2 Host-Guest Behaviour

Host-host and host-guest interactions dominate the inclusion compounds formed by **24** such that this dibromide behaves in a consistent manner with all of its guests [57, 58]. Two molecules of **24** wrap around one guest molecule to produce a penanular repeat unit with a rectangular cross-section. These building blocks then associate into layers by means of OFF interactions (Fig. 12). Adjacent layers can stack directly on top each other so that the guests occupy parallel tubes, or the layers may be laterally displaced thus confining the guests within cage-like enclosures. In all these inclusion compounds, multiple C-H...N interactions connect the layers in an EE manner (Fig. 13). These are of two distinct types: cyclic motifs containing two separate C-H...N interactions (see Sect. 6.2) and bifurcated motifs with the two C-H...N associations linked through a common nitrogen atom (see Sect. 7.2).

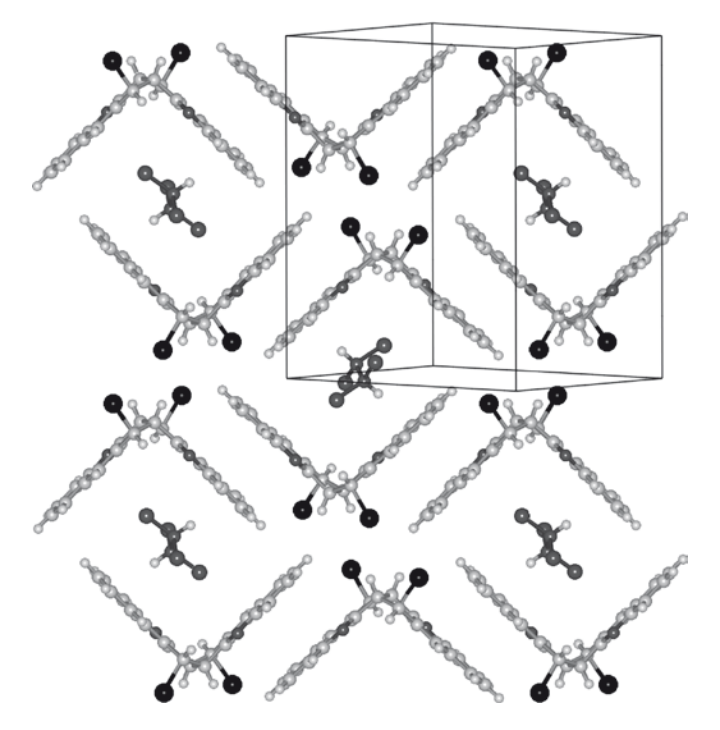
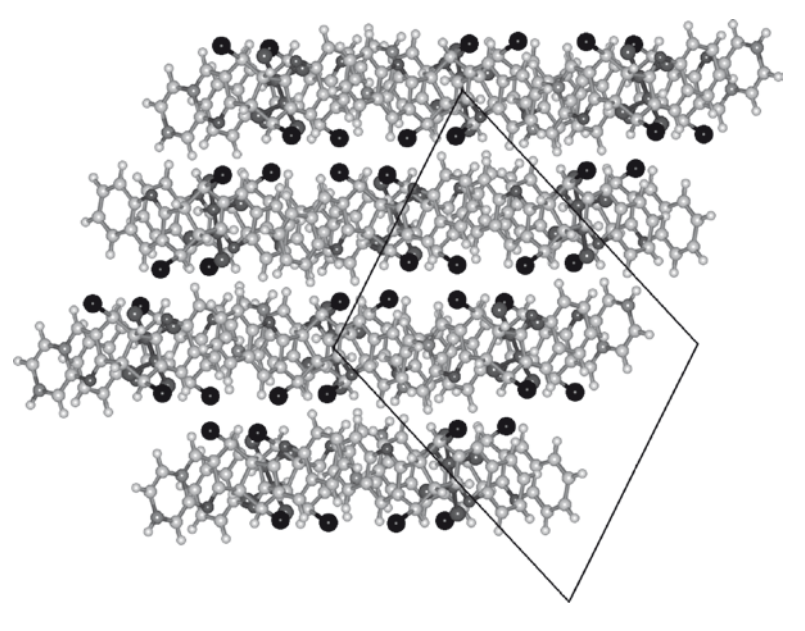


Fig. 12 Part of one layer of molecular pens in the crystal structure of compound (24)<sub>2</sub>.(1,1,2,2-tet-rachloroethane), showing one guest enclosed within each molecular pen [58]



**Fig. 13** Edge-on view of four layers of molecular pens in the compound (**24**)<sub>2</sub>.(1,1,2,2-tetrachloroethane) [58]

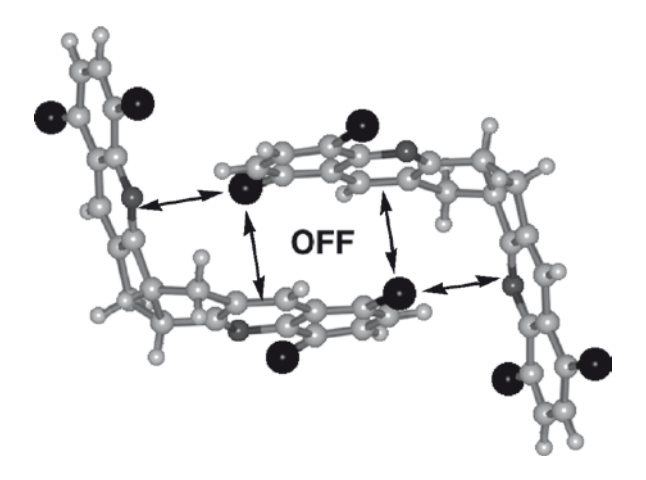


Fig. 14 The  $\pi$ -halogen dimer (PHD) unit of 25 present in the inclusion compound (25).(CCl<sub>4</sub>). Arrows indicate the four  $\pi$ -halogen interactions present in the unit and guest molecules are omitted [60]

The tetrabromide **25** behaves differently, but again very consistently, in all of its inclusion structures [60, 61]. These crystals contain  $\pi$ -halogen dimer (PHD) units [56]. In this motif, two molecules of opposite handedness associate by means of an *endo*-facial OFF interaction but with, in addition, two of the electron-rich halogen atoms positioned over the four electron deficient pyridine rings (Fig. 14). The PHD

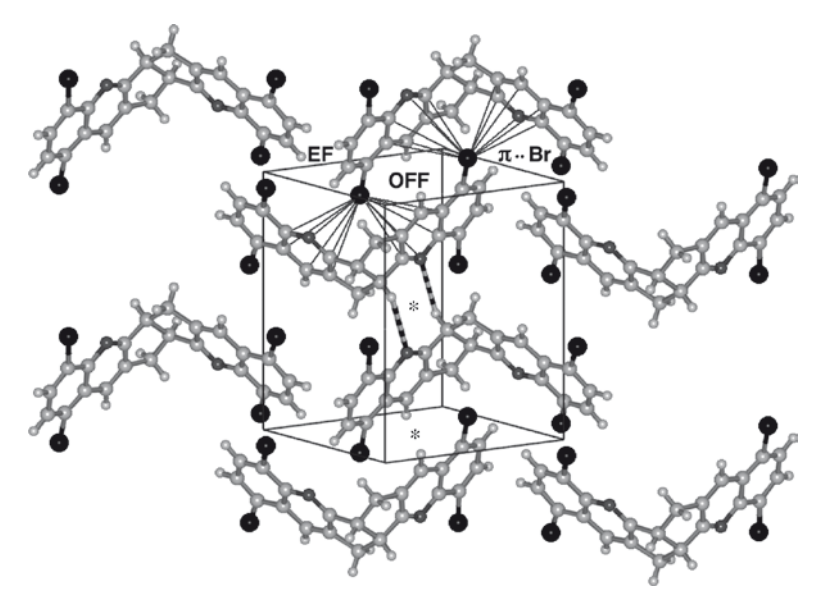


Fig. 15 Layers of host molecules in (25).(CCl<sub>4</sub>) showing (top centre) a PHD unit, and (centre) a C-H...N dimer. Guest molecules are omitted for clarity. The asterisks indicate inversion centres in this structure [60]

units of **25** can stack as a staircase structure (see Sect. 6.2) using additional OFF interactions, with the guest molecules occupying interstitial spaces between the parallel staircases. Alternatively, as illustrated in Fig. 15, the PHD units can associate with themselves, and further molecules of **25**, as layer structures. In this case the guests are positioned between these layers.

Hexabromide **26** is remarkable for its property of only including small aromatic hydrocarbon guests. Its apohost structure (Fig. 16) consists of layers of molecules of **26**. The intra-layer associations comprise OFF and EF motifs, while the interlayer attractions are Br...Br interactions. Inclusion of an aromatic guest such as *p*-xylene occurs within the layers, thereby increasing the extent of directional intralayer OFF and EF attractions, with concomitant reduction of the number of less directional inter-layer Br...Br contacts (Fig. 17) [62].

Notional replacement of two H by two Cl atoms in compound 24 would give the tetrahalide 28. This minor structural alteration is found to result in major supramolecular change, however, and the inclusion ability of 28 is greatly diminished. One molecular pen, and one staircase compound, are the only confirmed inclusion compounds [63], but the apohost forms an extraordinary interlocking molecular multi-grid lattice that assembles using only weak non-directional forces. This is in marked contrast to the properties of the majority of molecular grid compounds [64]. Work on the dibromide 30 is only in its early stages, but the results obtained so far suggest that its properties are similar to its positional isomer 24 [65].

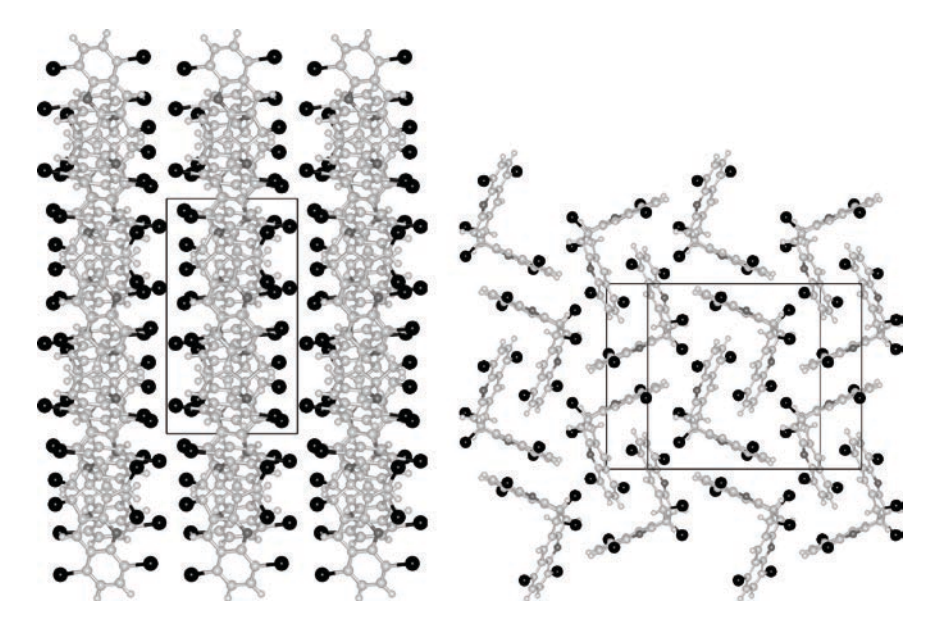
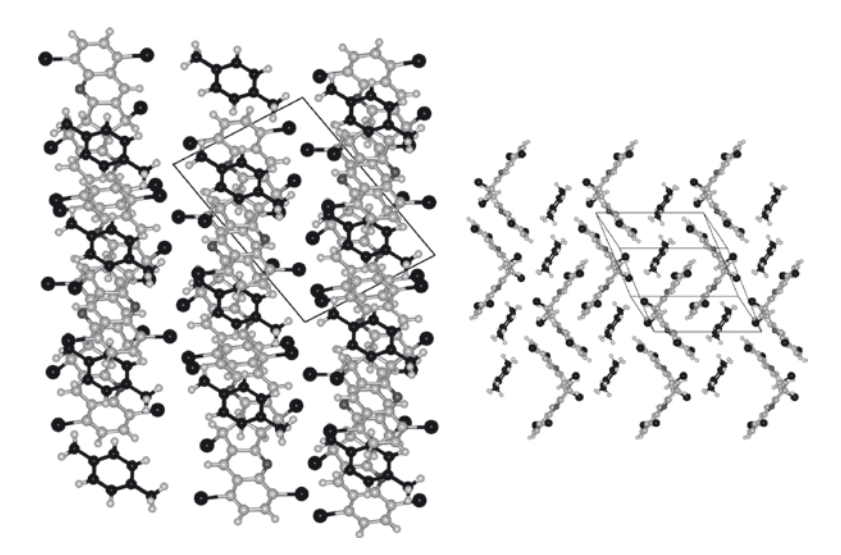


Fig. 16 Two views of the layer structure present in the apohost 26 crystal structure. Note the high density of Br...Br interactions present [62]



**Fig. 17** Two views of the layer structure present in (26).(*p*-xylene). Note the reduced density of Br...Br inter-layer attractions and the concomitant increase in intra-layer aromatic interactions [62]

## 6 Bicyclo[3.3.1]nonane Derived Systems

## 6.1 Synthesis

The bicyclo[3.3.1]nonane ring system has proved popular in a wide range of chemical investigations. Many simple derivatives, particularly hydroxy substituted examples, have interesting inclusion properties [66]. Not being heterocyclic, however, these lie outside the scope of the present article. Figure 18 shows two heterocyclic derivatives built around a bicyclo[3.3.1]nonane core. The derivatives **31** were obtained by Fischer indole reaction methodology and these form inclusion compounds [15, 67]. The extended system **32** illustrates how the bicyclic ring system can be converted into an effective ligand by the addition of dipyridyl functionalities. Zinc(II) macrocycles were studied in this instance [68].

We have synthesised, predominantly by use of the Friedländer condensation, a total of 13 host molecules, namely **19**, **35–42**, **44**, **48**, **50** and **54**, that contain the V-shaped bicyclo[3.3.1]nonane core. Bicyclo[3.3.1]nonane-2,6-dione **33** is a readily available material that was used to obtain the seven hosts shown in Fig. 19. It reacts efficiently with 2-aminobenzaldehyde **21** in the ratio 2:1 to afford the diquinoline derivative **34**. Regio- and stereo-selective benzylic bromination [59] then yields the dibromide **35**, which gives the corresponding dichloro compound **36** by means of halogen exchange [69, 70]. Alternatively, the tetrabromide **37** and tetraiodide **38** are produced from **34** by electrophilic aromatic substitution [71–73]. The tetraphenyl

Fig. 18 Examples of heteroatom-functionalised bicyclo[3.3.1]nonane derivatives. The *black spheres* indicate the zinc(II) coordination sites available for the structure 32

i NaOH, H $_2$ O, MeOH. ii NBS, CCI $_4$ . iii Br $_2$ , Ag $_2$ SO $_4$ , H $_2$ SO $_4$ . iv I $_2$ , Ag $_2$ SO $_4$ , H $_2$ SO $_4$ . v PhB(OH) $_2$ , Pd(PPh $_3$ ) $_4$ . vi HNO $_3$ , H $_2$ SO $_4$ .

**Fig. 19** Synthesis of seven diquinoline hosts **35–41** involving use of bicyclo[3.3.1]nonane-2,6-dione **33** in their construction [69–75]

derivative **39** was obtained by Suzuki-Miyaura reaction of the tetrabromide **37** [74], while the dinitro compounds **40**, **41** were prepared by nitration of **34** [75].

Employment of different 2-aminocarbonyl components (27, 43 or 45) in the Friedländer condensation, followed by benzylic bromination, afforded the next

three hosts 42 [76, 77], 44 [78], and 19 [50, 79]. As seen in Fig. 20, minor alterations in the condensation reaction conditions are required in different cases. Typically these involve the choice of acid or base catalysis, the alcohol solvent, and reaction time or temperature. The literature report of compound 31 observed that it was remarkably insoluble for a substance of such low molecular mass due, in part, to its strong hydrogen bonding [15]. Low solubility is also shared by many of the diquinoline compounds described here, but the reasons for this behaviour are less clear. The best yields are obtained when the double Friedländer product precipitates from solution as it is formed, and this outcome is controlled by variation of the above reaction parameters. The precise experimental conditions have been published in all cases.

i NaOH, EtOH. ii NBS, CCI4. iii HCI, EtOH. iv HCI, MeOH.

**Fig. 20** Syntheses of three substituted diquinoline hosts **42**, **44** and **19** that employ alternative 2-aminocarbonyl reagents in the Friedländer condensation [50, 76–79]

A switch to the isomeric linking reagent bicyclo[3.3.1]nonane-3,7-dione **46**, with the aminocarbonyl reagents **21** or **49** (Fig. 21), allowed preparation of the hosts **48** [80, 81] and **50** [82]. Once again, only the  $C_2$ -symmetric condensation adducts **47** and **50** are produced when this alternative achiral diketone is used (see Sect. 5.1).

Finally, a different approach was utilised for the synthesis of the diquinoxaline host **54** (Fig. 22) [83]. Here, the Issidorides–Haddadin reaction [16] was used to combine benzofurazan oxide **51** with bicyclo[3.3.1]nonane-2,6-dione **33**. The resulting tetrakis(*N*-oxide) **52** was then reduced to the diquinoxaline derivative **53** using sodium dithionite, and finally the benzylic bromination process gave the target compound **54**. In our work we have mainly compared the supramolecular behaviour of diquinoline hosts produced using the Friedländer reaction. It should be emphasised, however, that alternative condensation methods (such as the Issidorides–Haddadin reaction) will permit the synthesis of many additional heteroaromatic hosts.

NH<sub>2</sub> + 0 
$$\frac{1}{87\%}$$
 47  $\frac{1}{11}$  75%

Br
NO<sub>2</sub> NH<sub>2</sub> A6  $\frac{1}{87\%}$  A8

A8

NO<sub>2</sub> NH<sub>2</sub> NO<sub>2</sub> NO<sub>2</sub> NO<sub>2</sub> NO<sub>2</sub> NO<sub>2</sub> NO<sub>2</sub>

i NaOH, H2O, MeOH. ii NBS, CCl4. iii HCl, EtOH.

Fig. 21 Synthesis of the hosts 48 and 50 prepared using bicyclo[3.3.1]nonane-3,7-dione 46 to generate the central linker group in the condensation process [80–82]

i MeOH, NH<sub>3</sub>. ii Na<sub>2</sub>S<sub>2</sub>O<sub>4</sub>, HCl, DMF, H<sub>2</sub>O. iii NBS, CCl<sub>4</sub>.

Fig. 22 Use of the Issidorides–Haddadin reaction to prepare the diquinoxaline derivatives 52 and 53, and thence the V-shaped host molecule 54 [83]

#### 6.2 Host-Guest Behaviour

The bicyclo[3.3.1]nonane derivative 31 (R = H) forms the inclusion compound  $(31)_2$ .(DMF)<sub>5</sub>, which comprises a layer structure built up from molecular pens linked by OFF interactions [15]. Unlike 24, and the other diquinoline crystal structures described in this article, these pens are sufficiently large to each enclose two guest molecules (Fig. 23). Additional disordered DMF molecules occupy channels in the structure.

The dihalo diquinolines **35** and **36** exhibit the unusual property of only forming inclusion compounds with small polyhalocarbon guest molecules [69, 70]. Other potential guests of similar size and shape, but containing alternative functionality, are excluded. In the structure (**35**).(chloroform), two host molecules associate by means of a robust motif involving two identical aryl C-H...N interactions. This type of edge-edge (EE) supramolecular synthon is not possible for aromatic hydrocarbons but proves to be commonplace among many classes of heteroaromatic substances [69]. In (**35**).(chloroform), the second nitrogen atoms of this dimer each hydrogen bond to a guest creating the centrosymmetric building block illustrated in Fig. 24. These units are then arranged as a sandwich structure containing alternating layer zones of hydrocarbon and halogen functionality (Fig. 25). In the latter regions, the host *exo*-bromine atoms and guest chlorine atoms form a network of multiple halogen...halogen interactions, thus explaining the novel guest selectivity of these particular hosts.

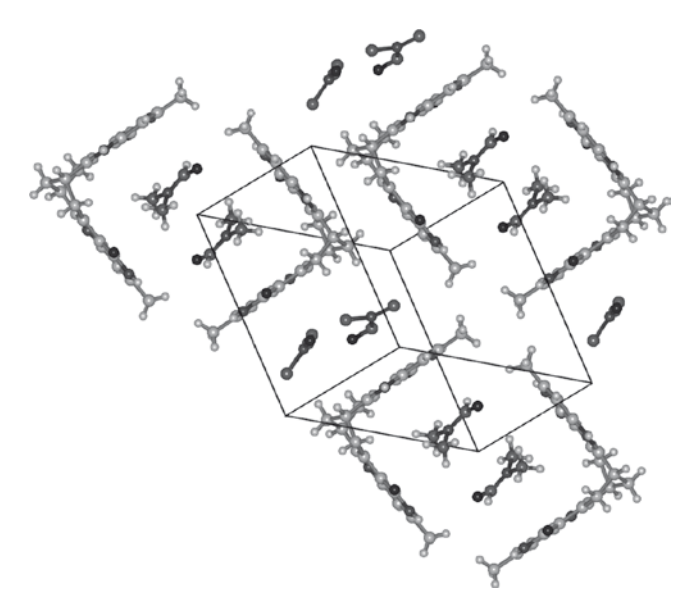


Fig. 23 Part of a layer of molecular pens in crystalline (31;  $R = H)_2$ .(DMF)<sub>5</sub> and showing the location of both crystallographic types of DMF guest molecules [15]

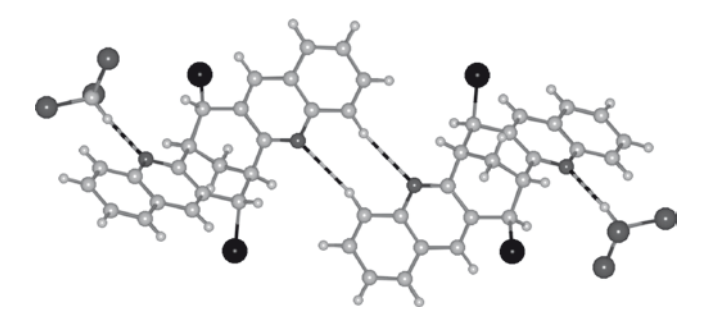


Fig. 24 The centrosymmetric building block present in solid (35).(chloroform), showing the aryl edge-edge C-H...N dimer motif (D = 3.65 Å) and the C-H...N hydrogen bonded guests (D = 3.37 Å) [69]

The hosts **37** and **38** behave entirely differently [71–73]. In all their inclusion compounds, hosts of opposite handedness form PHD units (Sect. 5.2) [56] that stack by means of OFF interactions into staircase structures. These staircases then pack parallel to each other with the guest molecules occupying sites between them. A number of variations of the staircase structure are encountered, depending on the identity of the guest and on the number of crystallographically independent host molecules present in the solid. The most common type is represented here by (**37**)<sub>4</sub>. (trifluoromethylbenzene) which contains two independent hosts A,B and their

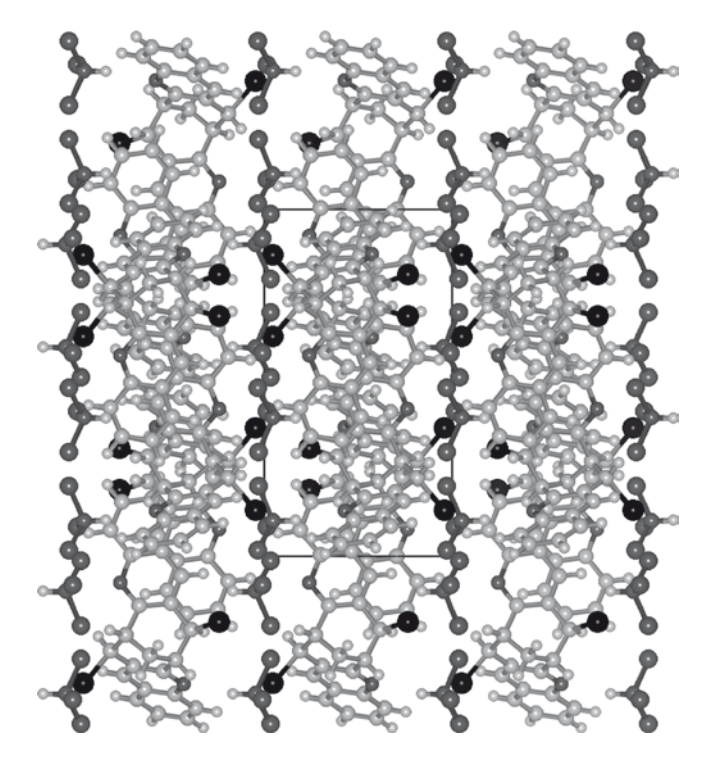


Fig. 25 The layer structure present in (35).(chloroform) showing the alternating zones of hydrocarbon and halogen (Cl *grey* and Br *black*) [69]

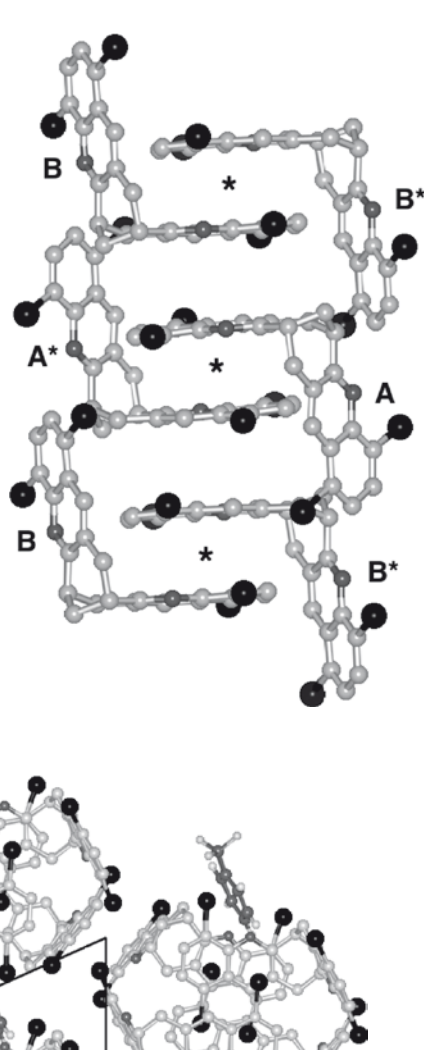
enantiomers A\*,B\*. The PHD units, A/A\* and B/B\*, stack alternately along each staircase (Fig. 26). Adjacent staircases associate by means of OFF interactions with the guests occupying channels along the staircase direction (Fig. 27).

Addition of a sufficient number of aromatic rings, as in the tetraphenyl derivative **39**, confers inclusion properties without the need for further substitution (such as halogen or nitro groups) [74]. This host molecule represents a structural cross-over from the behaviour of the other hosts described here into the Weber multi-ring aryl hydrocarbon family [84, 85]. The inclusion compounds of **39** utilise an (EF)<sub>6</sub> brick building block repeat in their crystal structures (Fig. 28). A related, but different, (EF)<sub>6</sub> unit is described below for the hosts **44** and **60**.

Both the  $C_2$ -symmetric dinitro derivatives **40**, **41** act as inclusion hosts and afford a range of structurally very different inclusion structures. Counter-intuitively, the nitro groups here do not play a major role as supramolecular synthons; rather they act as spoiler groups that do not favour facile molecular packing and thereby encourage guest inclusion in the lattice [75].

We have found that minor changes in molecular structure frequently result in major unpredictable alterations in supramolecular behaviour. For example, the

Fig. 26 Part of one molecular staircase in solid  $(37)_4$  ( $CF_3$ - $C_6H_5$ ) with the hydrogen atoms removed for clarity. The A/A\* and B/B\* PHD units stack by means of OFF interactions. Inversion centres are indicated by *asterisks* and the guest molecules are omitted [72]



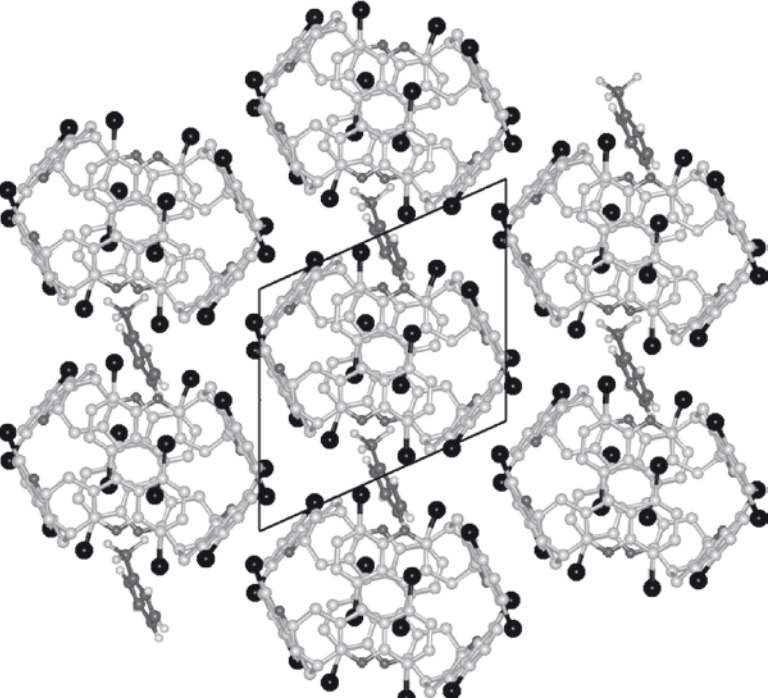


Fig. 27 Projection of the structure  $(37)_4$  (CF<sub>3</sub>-C<sub>6</sub>H<sub>5</sub>), showing top views of seven adjacent parallel staircases. The trifluoromethylbenzene guests occupy interstitial sites and only one guest disorder component is shown for clarity [72]

64 R. Bishop

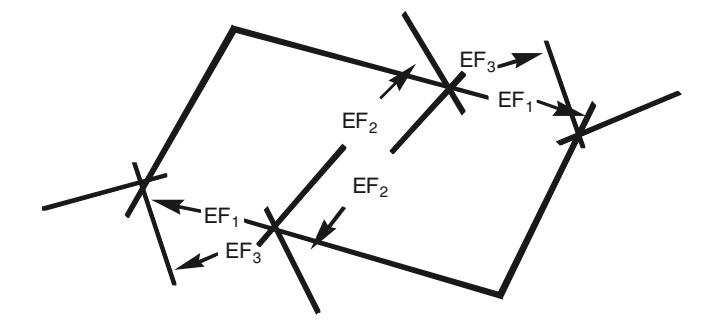
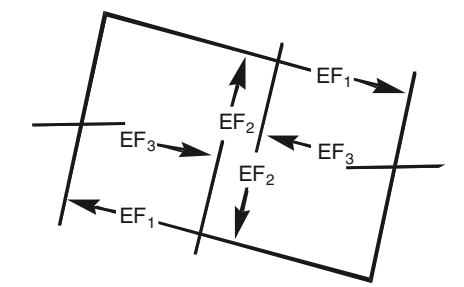


Fig. 28 Diagrammatic representation of the centrosymmetric (EF)<sub>6</sub> building block utilised in the crystal structures of the lattice inclusion compounds of 39, such as (39).(chloroform) [74]



**Fig. 29** The centrosymmetric (EF)<sub>6</sub> building block utilised in the inclusion crystal structures of **44** (and also compound **60**) [78]

nominal replacement of two H atoms in 35 by two Cl atoms to give 42, results in quite different inclusion properties. In this instance, the EE C-H...N dimers frequently formed by 35 are absent in the compounds of 42. There is concomitant change from only halocarbon guests to inclusion of a broader range of guest functionalities and corresponding packing modes [76, 77]. These effects are very difficult to rationalise at our current level of understanding of supramolecular chemistry.

Other host modifications are easier to interpret. The dibromo host **35** employs both OFF and EF interactions in its inclusion structures, but this situation changes dramatically with the dibromo diphenyl compound **44** where the additional phenyl substituents have the effect of suppressing OFF behaviour [78]. Instead, two molecules of **44** with opposite handedness associate as a centrosymmetric dimer employing three different EF interactions (Fig. 29). These dimeric (EF)<sub>6</sub> bricks (which are different in detail to those present in **39**) pack into layers with the guests occupying inter-brick spaces. Differences in the translation and/or orientation of the bricks allow incorporation of guests of differing sizes and shapes (Fig. 30). This supramolecular behaviour using molecular dimers (bricks) and host–guest interactions (mortar) reveals close analogies with human building methods. Interestingly, the apohost **44** still assembles using brick units. This absence of host–guest interactions (no mortar used) corresponds to the dry stone construction technique.

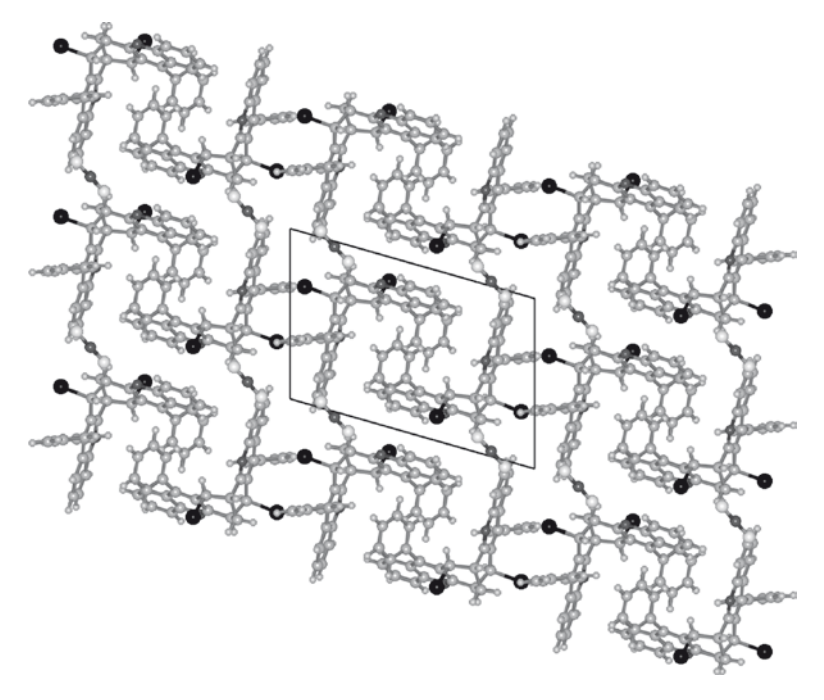


**Fig. 30** Part of the crystal structure of (44).(carbon disulphide) showing the (EF)<sub>6</sub> repeat units (*bricks*). The guest molecules (*mortar*) are located at the corners of the dimers (*bricks*) [78]

The host molecule **19** contains two chlorine atoms in addition to the substituents already present in **44**. This time, however, the resulting behavioural differences are easily understood. The presence of the Cl atoms would change  $EF_1$  in Fig. 29 into a  $Cl...\pi$  interaction about 1 Å longer than the original interaction. Although  $EF_2$  would be unaffected,  $EF_3$  could no longer operate due to its two interacting components being forced apart. Thus, new packing modes must be expected for the inclusion compounds of **19**. It turns out that this host, like the earlier **35**, demonstrates a strong preference for the inclusion of polyhalomethane guests [50, 79]. Its means of doing so, however, are varied and different from the earlier compound. This dichloro host is notable for allowing the concomitant formation of two different inclusion compounds from *d*-chloroform solution, namely (**19**).(CDCl<sub>2</sub>) and (**19**).(CDCl<sub>3</sub>).

The compound **35** described earlier was found to utilise the aryl EE C-H...N dimer (both as single units and in chains) in several of its inclusion crystals. Host **48** is a structural isomer where the N atom is now located closer to the bromine substituent. This small positional change results in significantly decreased solubility in both the corresponding bicyclo[3.3.0]octane and bicyclo[3.3.1]nonane series of diquinolines. In its tetrahydrofuran, dichloromethane and chloroform compounds, each host molecule of **48** subtends two identical C-H...N dimers giving rise to weakly hydrogen bonded chains (Fig. 31). However, in the compound (**48**), (benzene)<sub>3</sub>

R. Bishop

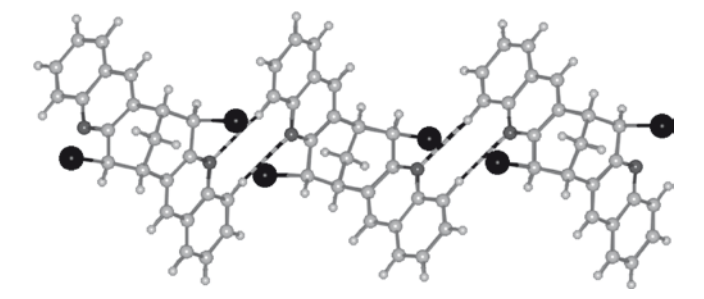


Fig. 31 Part of a chain of host molecules, linked by centrosymmetric C-H...N dimer interactions (d = 2.76, D = 3.75 Å), in the compound (48).(tetrahydrofuran), [80]

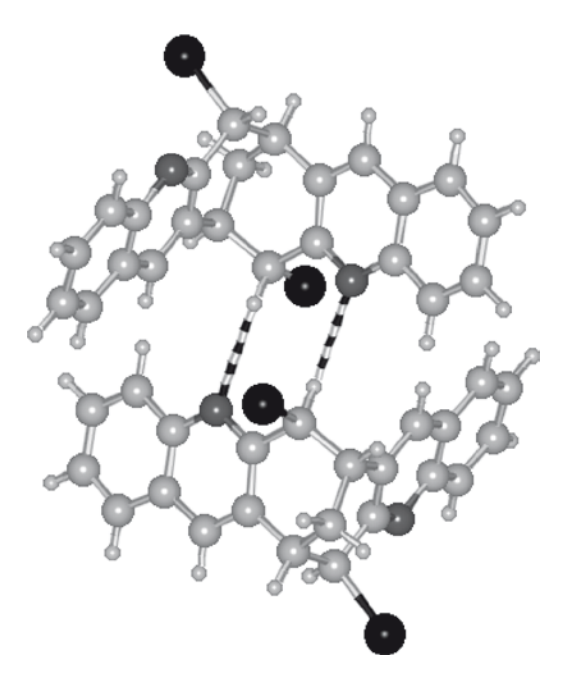


Fig. 32 The centrosymmetric BrC-H...N dimer present in solid  $(48)_2$ . (benzene)<sub>3</sub>. This new type of dimer contains C-H...N distances of d = 2.67 and D = 3.51 Å, respectively [80]

an alternative motif was recorded, namely the centrosymmetric BrC-H...N dimer illustrated in Fig. 32 [80, 81].

The dinitro host **50** can be prepared in just one step from the components **49** and **46** and is found to behave very differently from the earlier dinitro compounds **40** and **41**. In **50**, the nitro groups are no longer just spoiler groups and now are proactively involved in formation of its inclusion compounds [82].

The diquinoxaline derivative **54** utilises a cyclic EE host–host motif that is intermediate in structure between those illustrated in Figs. 31 and 32. In other words, this arrangement comprises a combination of one aryl C-H...N and one BrC-H...N interaction (Fig. 33). The different heteroaromatic wings of this compound in no way inhibit the inclusion properties of this different type of host [83].

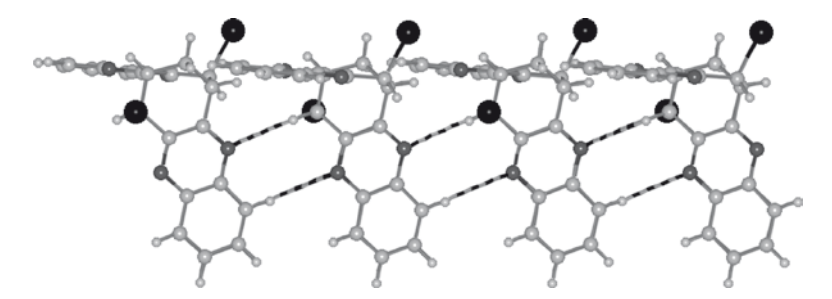


Fig. 33 The cyclic EE motif present in crystalline  $(54)_2$ .(1,1,2,2-tetrachloroethane) that utilises both aryl C-H...N and BrC-H...N interactions. Guest molecules are omitted for clarity [83]

# 7 9-Heterobicyclo[3.3.1]nonane Derived Systems

# 7.1 Synthesis

9-Heterobicyclo[3.3.1]nonane derivatives have also been used as modules in the Friedländer reaction and they have afforded the five potential diquinoline host molecules **57**, **59**, **60**, **63** and **64** shown in Fig. 34. Unexpectedly, one of these compounds, namely **63**, proved to be a non-host for reasons explained below. Therefore our current prediction rate for designed heteroaromatic lattice inclusion hosts is 22 out of 23 cases (96%), an unprecedented rate of success.

Condensation of two equivalents of 2-aminobenzaldehyde **21** and one equivalent of 9-thiabicyclo[3.3.1]nonane-2,6-dione **55** affords the diquinoline derivative **56** in good yield, and then benzylic bromination yielded the anticipated host **57** [86]. Alternative aminocarbonyl modules can also be used successfully. The halogenated aminobenzaldehyde **58** gave host **59** in a one-step synthesis [87], and use of the aminobenzophenone **43** led to the dibromo diphenyl host **60** [88].

9-Oxabicyclo[3.3.1]nonane-2,6-dione **61** is also effective in the Friedländer reaction, yielding the heterocycle **62** which can be elaborated into both of the brominated diquinolines **63** [89] and **64** [90].

## 7.2 Host-Guest Behaviour

The inclusion behaviour of the dibromo thiadiquinoline 57 shows some similarities to its methylene analogue 35, but it traps a wider functional range of guests, for example now also including aromatic compounds. Compound (57).(benzene) contains infinite EF chains of benzene molecules, which are equivalent to part of the structure in pure solid benzene. In this inclusion compound, however, there are additional host–guest EF and OFF interactions present as shown in Fig. 35 [86].

68 R. Bishop

i NaOH, H $_2$ O, MeOH. ii NBS, CCl $_4$ . iii HCl, EtOH. iv NaOH, H $_2$ O, EtOH. v NBS, C $_6$ H $_5$ -CF $_3$ . vi Br $_2$ , Ag $_2$ SO $_4$ , H $_2$ SO $_4$ .

**Fig. 34** Use of 9-heterobicyclo[3.3.1]nonane-2,6-dione building blocks in the synthesis of V-shaped heteroaromatic host molecules [86–90]

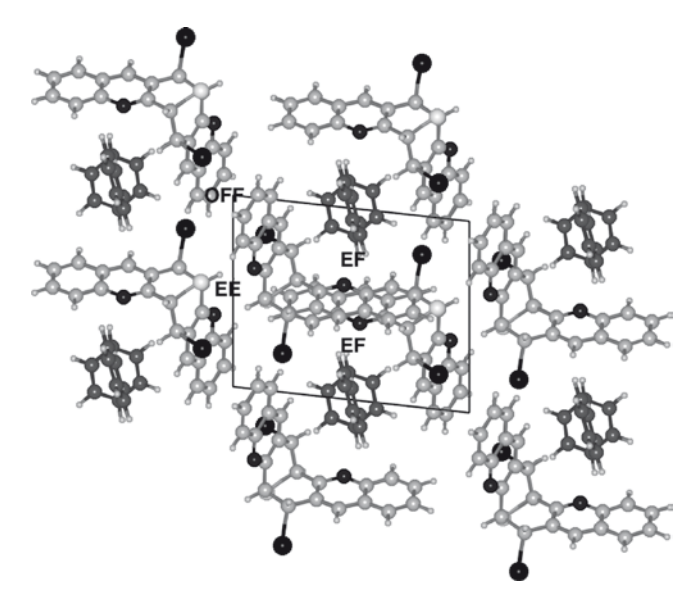
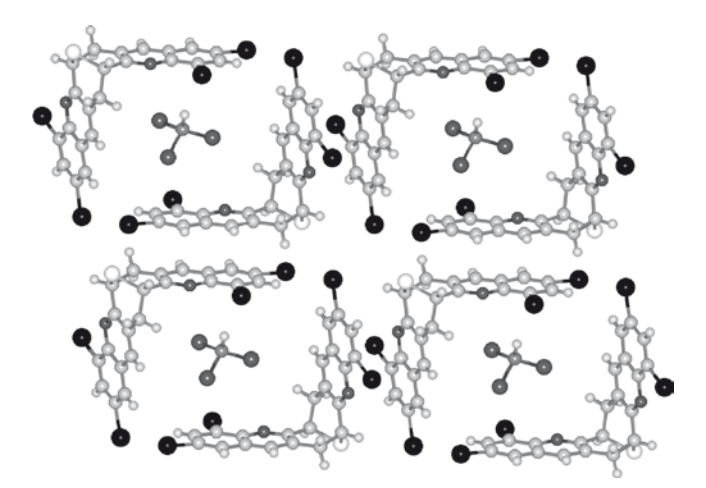


Fig. 35 Part of the crystal structure of the inclusion compound (57).(benzene) with the aryl interactions indicated [86]



**Fig. 36** Crystal structure of (**59**)<sub>2</sub>.(chloroform) showing one disorder component only of the guest contained in the molecular pens [87]

The tetrabromo thiadiquinoline compound **59** tends to enclose its guests within molecular pens, as illustrated in Fig. 36 for (**59**)<sub>2</sub>.(chloroform). The different peripheral substitution pattern of this host leads to the involvement of previously unrecorded types of weak aryl EE host–host packing motifs [87].

70 R. Bishop

The inclusion structures of host **60** once again involve dimeric building blocks comprising a centrosymmetric arrangement of three independent EF motifs. These (EF)<sub>6</sub> units are isostructural with those observed for its methylene analogue **44** (see Fig. 29). Host **60** demonstrates Janus-like character, in the sense that about half of its inclusion crystal structures are isostructural with those of **44**, but the other half are different. This behaviour is difficult to rationalise since the S atom does not play an overt supramolecular role in the latter crystal structures [88].

In marked contrast to all our other predictions, the oxa-bridged diquinoline **63** does not form inclusion compounds, despite the behaviour of its very close structural relatives **35**, **36** and **57**. The reason for this unexpected behaviour was revealed on investigation of its crystal structure [89]. This showed the presence of an especially favourable ether–1,3-*peri* aromatic hydrogen interaction between neighbouring molecules of **63** (Fig. 37). This bifurcated motif had not been previously identified but we found that it was moderately common in the Cambridge Structural Database [91]. The C-H...O values for compounds **62** (d = 2.57, 2.66 Å) and **63** (d = 2.57, 2.69 Å) are the shortest values on record and clearly over-rule other tendencies for **63** to act as a lattice inclusion host. It is notable that the corresponding thia-interaction was absent in the inclusion crystal structures of **57**, but that bifurcated aza-interactions were observed between host layers in molecular pen inclusion structures.

In contrast, the tetrabromo oxa-bridged compound **64**, where the ether–1,3-*peri* interaction is impossible, formed staircase inclusion compounds close in structure to those of its methylene analogues **37** and **38** (Fig. 38) [90].

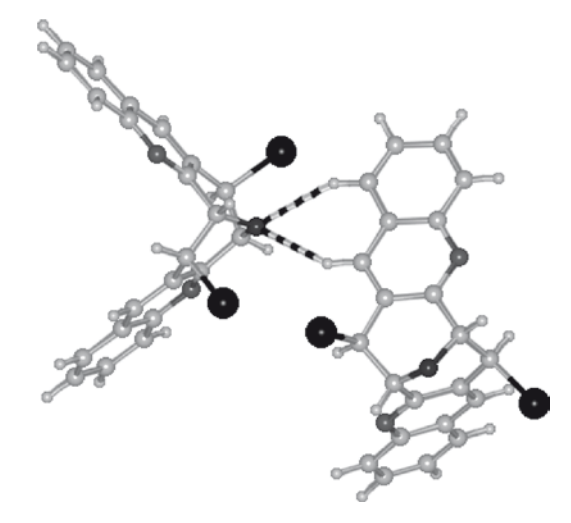
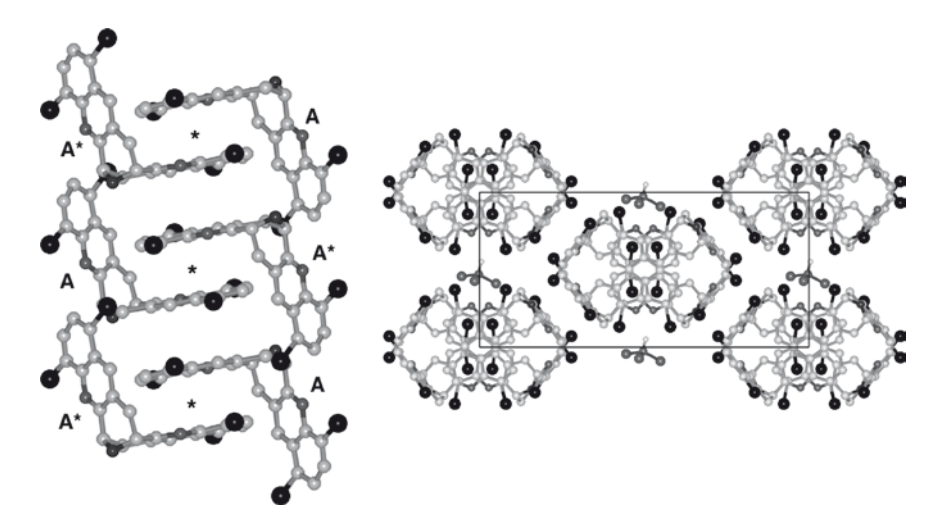


Fig. 37 Part of the crystal structure of the dibromo oxa-bridged diquinoline 63, showing the intermolecular ether–1,3-peri aromatic hydrogen interaction (dashed lines) [89]



**Fig. 38** Two views of the staircase structure present in (64)<sub>2</sub>.(chloroform). *Left*: side view of one staircase showing the stacked PHD units (hydrogen atoms omitted). *Right*: projection view of several parallel staircases showing the included guest molecules [90]

# 8 Conclusions

This review has identified and described several core units that can be incorporated into larger molecular structures and which thereby impart both V-shapes and  $C_2$  symmetry. Careful design can produce tweezer molecules that grasp guest molecules between their extremities. Very many other V-shaped molecules, however, exhibit lattice inclusion properties. Although the guests can occupy the concavity itself, for example in molecular pen structures, this is often not the case at all. If the V-shaped concavity is not provided with supramolecular anchor points then the guests are free to occupy alternative sites within the crystal lattice.

Evidence has been provided to show that new lattice inclusion hosts of this type can now be designed reliably. For aromatic systems there is a minimum surface area requirement. This is approximately four aromatic or heteroaromatic rings, either independent of each other or fused together. The potential host molecules must also pack awkwardly by themselves. This is achieved by the presence of peripheral substituents (spoiler groups). There remains considerable scope for the synthesis of new inclusion hosts based on Kagan's ether and Tröger's base cores if these design principles are applied to them in the future.

Host molecules without strong hydrogen bonding groups provide excellent templates for the systematic study of weaker supramolecular synthons. Our understanding of such lesser-known interactions, and the extent to which they can be usefully applied in self-assembly, is still at a relatively rudimentary level. The synthetic approach described, however, is one effective means of correcting this situation.

72 R. Bishop

**Acknowledgements** I wish to thank Solhe Alshahateet, Jason Ashmore, Chris Marjo and Noman Rahman for their synthetic work, and Don Craig and Marcia Scudder for the crystallographic determinations, described in this article. Financial support of our research was provided by the Australian Research Council and the University of New South Wales. I also gratefully thank Dr. Scudder for generating the crystal structure diagrams used to illustrate this article.

# References

- 1. Chen C-W. Whitlock HW Jr (1978) J Am Chem Soc 100:4921–4922
- 2. Zimmerman SC (1993) Top Curr Chem 165:71–102
- 3. Liebig T, Abbass M, Lüning U (2007) Eur J Org Chem 972-980
- Atwood JL, Davies JED, MacNicol DD (eds) (1984) Inclusion compounds, vols. 1–3, Academic. London
- 5. MacNicol DD, Toda F, Bishop R (eds) (1996) Comprehensive supramolecular chemistry, vol. 6. Solid-state supramolecular chemistry: crystal engineering. Pergamon, Oxford
- Atwood JL, Davies JED, MacNicol DD (eds) (1984) Inclusion compounds, vol. 4–5. Oxford University Press, Oxford
- Herbstein FH (2005) Crystalline molecular complexes and compounds, vols. 1 and 2. Oxford Science, Oxford
- Goldberg I (1991). In: Atwood JL, Davies, JED, MacNicol DD (eds) Inclusion compounds, vol. 4. Oxford University Press, Oxford, chap 10, pp 406–447
- 9. MacNicol DD, Downing GA (1996) Symmetry in the evolution of host design. In: MacNicol DD, Toda F, Bishop R (eds) Comprehensive supramolecular chemistry, vol. 6. Solid-state supramolecular chemistry: crystal engineering, Pergamon, Oxford, chap 14, pp 421–464
- Tatemitsu H, Ogura F, Nakagawa Y, Nakagawa N, Naemura K, Nakazaki M (1975) Bull Chem Soc Jpn 48:2473–2483
- Lee CKY, Groneman JL, Turner P, Rendina PLM, Harding MM (2006) Tetrahedron 62:4870–4878
- 12. Mas T, Pardo C, Salort F, Elguero J, Torres MR (2004) Eur J Org Chem 1097-1104
- Mehta G, Prabhakar C, Padmaja N, Ramakumar S, Viswamitra MA (1989) Tetrahedron Lett 30:6895–6898
- Bartsch RA, Eley MD, Marchand AP, Shukla R, Kumar KA, Reddy GM (1996) Tetrahedron 52:8979–8988
- Stoncius S, Butkus E, Zilinskas A, Larsson AK, Öhrström L, Berg U, Wärnmark K (2004)
   J Org Chem 69:5196–5203
- 16. Issidorides CH, Haddadin MJ (1966) J Org Chem 31:4067-4068
- 17. Cheng C-C, Yan S-J (1982) Org React 28:37-201
- 18. Thummel RP, Jahng Y (1985) J Org Chem 50:2407-2412
- 19. Thummel RP, Lim J-L (1987) Tetrahedron Lett 28:3319–3322
- 20. Thummel RP (1992) Synlett 1-12
- Marchand AP, Annapurna P, Flippen-Anderson JL, Gilardi R, George C (1988) Tetrahedron Lett 29:6681–6684
- 22. Harmata M (2004) Acc Chem Res 37:862-873
- 23. Harmata M, Barnes CL (1990) Tetrahedron Lett 31:1825-1828
- 24. Harmata M, Barnes CL (1990) J Am Chem Soc 112:5655-5657
- 25. Harmata M, Wu Y, Kahraman M, Welch CJ (2001) Synth Commun 31:3345-3359
- 26. Bag BG (1995) Curr Sci 68:279-288
- 27. Prelog V, Wieland P (1944) Helv Chim Acta 27:1127-1134
- 28. Kimber MC, Try AC, Painter L, Harding MM, Turner P (2000) J Org Chem 65:3042-3046
- 29. Turner JJ, Harding MM (2005) Supramol Chem 17:369-375
- 30. Friberg A, Olsson C, Ek F, Berg U, Frejd T (2007) Tetrahedron Asymmetry 18:885-891

- 31. Harmata M, Kahraman M (2000) Tetrahedron Asymmetry 11:2875–2879
- 32. Weber E, Müller U, Worsch D, Vögtle F, Will G, Kirfel A (1985) *J Chem Soc Chem Commun* 1578–1580
- 33. Bond DR, Scott JL (1991) J Chem Soc, Perkin Trans 2:47–51
- 34. Wilen SH, Qi JZ, Williard PG (1991) J Org Chem 56:485-487
- Lenev DA, Golovanov DG, Lyssenko KA, Kostyanovsky RG (2006) Tetrahedron Asymmetry 17:2191–2194
- 36. Wilcox CS, Cowart MD (1986) Tetrahedron Lett 27:5563-5566
- 37. Wilcox CS, Greer LM, Lynch V (1987) J Am Chem Soc 109:1865-1867
- 38. Pardo C, Sesmilo E, Gutiérrez-Puebla E, Monge A, Elguero J, Fruchier A (2001) J Org Chem 66:1607–1611
- 39. Mas T, Pardo C, Elguero J (2004) Arkivoc iv:86-93
- Artacho J, Nilsson P, Bergquist K-E, Wendt OF, Wärnmark K (2006) Chem Eur J 12:2692–2701
- 41. Brotherhood PR, Wu RA-S, Turner P, Crossley MJ (2007) Chem Commun 225-227
- Bishop R (2006) Crystal engineering of halogenated heteroaromatic clathrate systems. In: Tiekink ERT, Vittal JJ (eds) Frontiers in crystal engineering. Wiley, Chichester, chap 5, pp 91–116
- 43. Desiraju GR, Steiner T (1999) The weak hydrogen bond in structural chemistry and biology. Oxford Science, Oxford
- 44. Desiraju GR (1995) Angew Chem Int Ed Engl 34:2311-2327
- 45. Suezawa H, Yoshida T, Hirota M, Takahashi H, Umezawa Y, Honda K, Tsuboyama S, Nishio M (2001) *J Chem Soc, Perkin Trans* 2:2053–2058
- 46. Hunter CA, Sanders JKM (1990) J Am Chem Soc 112:5525-5534
- 47. Gavezzotti A, Desiraju GR (1988) Acta Cryst B44:427-434
- 48. Desiraju GR, Gavezzotti A (1989) J Chem Soc Chem Commun 621-623
- 49. Dunitz JD, Gavezzotti A (1999) Acc Chem Res 32:677-684
- 50. Ashmore J, Bishop R, Craig DC, Scudder ML (2006) CrystEngComm 8:923-930
- 51. Nguyen VT, Rahman ANMM, Bishop R, Craig DC, Scudder ML (1999) Aust J Chem 52:1047–1053
- 52. Sarma JARP, Desiraju GR (1986) Acc Chem Res 19:222–228
- 53. Price SL, Stone AJ, Lucas J, Rowland RS, Thornley A (1994) J Am Chem Soc 116:4910–4918
- 54. Prasanna MD, Guru Row TN (2000) Cryst Eng 3:135-154
- 55. Jetti KR, Nangia A, Xue F, Mak TCW (2001) Chem Commun 919-920
- Bishop R, Scudder ML, Craig DC, Rahman ANMM, Alshahateet SF (2005) Mol Cryst Liq Cryst 440:173–186
- 57. Rahman ANMM, Bishop R, Craig DC, Scudder ML (1999) Chem Commun 2389-2390
- 58. Rahman ANMM, Bishop R, Craig DC, Scudder ML (2003) Eur J Org Chem 79-81
- 59. Marjo CE, Bishop R, Craig DC, Scudder ML (2004) Mendeleev Commun 278–279
- 60. Rahman ANMM, Bishop R, Craig DC, Scudder ML (2002) CrystEngComm 4:510-513
- 61. Rahman ANMM, Bishop R, Craig DC, Scudder ML (2004) Org Biomol Chem 2:175–182
- 62. Rahman ANMM, Bishop R, Craig DC, Scudder ML (2003) Org Biomol Chem 1:1435-1441
- 63. Rahman ANMM, Bishop R, Craig DC, Scudder ML (2002) J Supramol Chem 2:409-414
- Alshahateet SF, Rahman ANMM, Bishop R, Craig DC, Scudder ML (2002) CrystEngComm 4:585–590
- 65. Al Djaidi DS (2006) Ph.D. thesis, University of New South Wales
- 66. Kim S, Bishop R, Craig DC, Scudder ML (2002) J Org Chem 67:3221–3230
- 67. Stoncius S, Orentas E, Butkus E, Öhrström L, Wendt OF, Wärnmark K (2006) *J Am Chem Soc* 128:8272–8285
- 68. Anderberg PI, Turner JJ, Evans KJ, Hutchins LM, Harding MM (2004) *Dalton Trans* 1708–1714
- 69. Marjo CE, Scudder ML, Craig DC, Bishop R (1997) J Chem Soc Perkin Trans 2:2099-2104
- 70. Bishop R, Marjo CE, Scudder ML (1998) Mol Cryst Liq Cryst 313:217–222

74 R. Bishop

71. Marjo CE, Rahman ANMM, Bishop R, Scudder ML, Craig DC (2001) *Tetrahedron* 57:6289–6293

- 72. Rahman ANMM, Bishop R, Craig DC, Marjo CE, Scudder ML (2002) Cryst Growth Des 2:421–426
- 73. Rahman ANMM, Bishop R, Craig DC, Scudder ML (2003) CrystEngComm 5:422-428
- 74. Ashmore J, Bishop R, Craig DC, Scudder ML (2008) CrystEngComm 10:131-137
- 75. Ashmore J, Bishop R, Craig DC, Scudder ML (2008) CrystEngComm 10: 839-845
- 76. Ashmore J, Bishop R, Craig DC, Scudder ML (2002) CrystEngComm 4:194–198
- 77. Ashmore J, Bishop R, Craig DC, Scudder ML (2007) Cryst Growth Des 7:47-55
- 78. Ashmore J, Bishop R, Craig DC, Scudder ML (2004) CrystEngComm 6:618-622
- 79. Ashmore J, Bishop R, Craig DC, Scudder ML (2003) Mendeleev Commun 144–146
- 80. Alshahateet SF, Bishop R, Craig DC, Scudder ML (2001) CrystEngComm 3:225–229
- 81. Alshahateet SF, Bishop R, Craig DC, Scudder ML (2004) Cryst Growth Des 4:837–844
- 82. Alshahateet SF, Ong TT, Bishop R, Kooli F, Messali M (2006) Cryst Growth Des 6:1676-1683
- 83. Marjo CE, Bishop R, Craig DC, Scudder ML (2001) Eur J Org Chem 863-873
- 84. Weber E (1996). In: MacNicol DD, Toda F, Bishop R (eds) Comprehensive supramolecular chemistry, vol. 6. Solid-state supramolecular chemistry: crystal engineering. Pergamon, Oxford, chap 17, pp 535–592
- 85. Müller T, Seichten W, Weber E (2006) New J Chem 30:751-758
- 86. Alshahateet SF, Bishop R, Craig DC, Scudder ML (2001) CrystEngComm 3:264–269
- 87. Alshahateet SF, Bishop R, Scudder ML, Hu CY, Lau EHE, Kooli F, Judeh ZMA, Chow PS, Tan RBH (2005) CrystEngComm 7:139–142
- 88. Alshahateet SF, Bishop R, Craig DC, Kooli F, Scudder ML (2008) CrystEngComm 10:297–305
- 89. Alshahateet SF, Bishop R, Craig DC, Scudder ML (2001) CrystEngComm 3:107-110
- 90. Alshahateet SF, Bishop R, Craig DC, Scudder ML (2003) CrystEngComm 5:417-421
- 91. Allen FH, Davies JE, Galloy JJ, Johnson O, Kennard O, Macrae CF, Mitchell EM, Mitchell GF, Smith JM, Watson DG (1991) *J Chem Inf Comput Sci* 31:187–204

Top Heterocycl Chem (2009) 18: 75-102

DOI: 10.1007/7081\_2009\_2

© Springer-Verlag Berlin Heidelberg 2009

Published online: 27 March 2009

# Inclusion and Optical Resolution of Guest Molecules by Selected Synthetic Dihydroxy- and Trihydroxy-Host Compounds Containing Heterocyclic Scaffolds

Mino R. Caira and Koichi Tanaka

**Abstract** This review focuses on structural aspects of inclusion complexation between selected host molecules that contain - OH sensor groups appended to, or associated with, heterocyclic moieties, and both non-chiral and chiral guests. Among the host compounds discussed, those derived from tartaric acid feature prominently as they have been extensively explored, especially in the context of optical resolution of racemic guests. Of the various techniques employed in the study of the derived solid-state inclusion complexes, single crystal X-ray studies have contributed significantly to an understanding of the roles of hydrogen bonding, van der Waals, C-H··· $\pi$  and  $\pi$ - $\pi$  interactions in complex stabilization. For the host molecules described, the literature surveyed accordingly provides many case studies that feature X-ray analysis as a primary tool for investigating the mechanistic aspects of inclusion phenomena such as optical resolution and enantioselective photoreactivity.

**Keywords** Diols, Inclusion compounds, Optical resolution, Solid-state photoreactions, TADDOLs, Triphenolics, X-ray analysis

M.R. Caira

Centre for Supramolecular Chemistry Research, Department of Chemistry, University of Cape Town, Rondebosch 7701, South Africa e-mail: Mino.Caira@uct.ac.za

K. Tanaka

Department of Chemistry and Materials Engineering, Faculty of Chemistry, Materials and Bioengineering and High Technology Research Center, Kansai University, Suita, Osaka, 564-8680, Japan

#### Contents

1	Introduction		76	
	1.1	Scope of the Review	76	
	1.2	General Design Strategy of Host Molecules Based on Heterocyclic		
		Frameworks and Appended Hydroxyl Sensor Groups	78	
	1.3	Survey of Preparative Methods and Representative Examples	79	
2	Inclusion Chemistry		81	
	2.1	Methodology and Characterization of the Products of Inclusion	81	
	2.2	Chiral Resolution by Inclusion Crystallization with Optically		
		Active Heterocyclic Hosts Derived from Tartaric Acid	82	
	2.3	Enantioselective Photoreactions in the Solid State	95	
	2.4	Inclusion Ability of N,N',N"-Trihydroxyisocyanuric Acid and		
		Macrocyclic Triphenolic Host Molecules	99	
3	Con	Concluding Remarks: Status of the Research and Future Directions		
Re	feren	ces	101	

### **Abbreviations**

ATR	Attenuated total reflection
CD	Circular dichroism
DSC	Differential scanning calorimetry
EIC	Enantioselective inclusion complexation
GC	Gas chromatography
HPLC	High performance liquid chromatography
OSN	Organic solvent nanofiltration
PXRD	Powder X-ray diffraction
SSNMR	Solid-state nuclear magnetic resonance
TADDOL	$\alpha,\alpha,\alpha',\alpha'$ -Tetraaryl-1,3-dioxolane-4,5-dimethanol
TGA	Thermogravimetric analysis

#### 1 Introduction

#### Scope of the Review 1.1

In contrast to classical resolution of acidic or basic racemates, which relies on the crystallization of diastereomeric salts with an optically active compound of natural origin, optical resolution by selective inclusion using designed synthetic host molecules can be applied to a much wider range of substrates, which accounts for the ongoing interest and intensive research activity in this niche area of supramolecular chemistry. Guest inclusion in the solid-state is also exploited for carrying out enantioselective photoreactions that might proceed with difficulty, or be unachievable by other means. These topics are addressed in this short review with reference to a limited variety of host compounds and with a focus on solid-state structural aspects.

While a wide variety of host compounds containing diol functions exists (e.g. 1–3, Scheme 1) [1], those in which the diol unit is appended to heterocyclic moieties

Scheme 1 Structures of representative diol hosts and the synthesis of the TADDOL host 4 [4]

constitute a much smaller class. The chiral  $\alpha,\alpha,\alpha',\alpha'$ -tetraaryl-1,3-dioxolane-4,5-dimethanols (TADDOLs, e.g. 4) fall into this category.

Owing to their widespread exploitation and ongoing successful applications in inclusion chemistry [2], this review focuses primarily on these compounds and their use in enantioselective inclusion of organic guest molecules as well as enantioselective photoreactions occurring in the solid-state. Selected studies published between ~2000 and the present are featured here in order not only to illustrate the diversity of applications in the inclusion of organic guest molecules, but more specifically to highlight the nature of the host-guest interactions that are responsible for the observed phenomena. In addition to the diol hosts described above, some material is presented on host compounds containing trihydroxy functions (namely triphenolics) and heterocyclic moieties, these being much less common and explored to a much lesser extent.

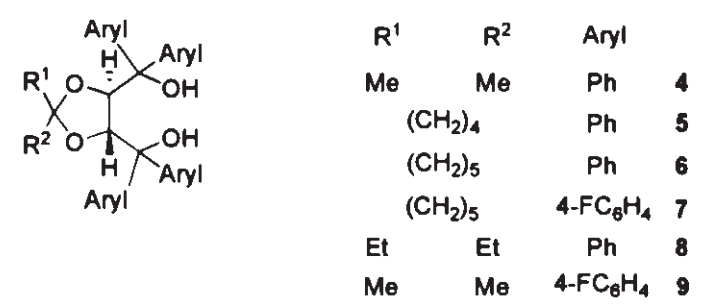
Spectroscopic methods employed in the characterization of solid inclusion complexes are limited in their ability to provide details of host-guest interaction at the molecular level; in many cases, X-ray analysis of single crystals (providing with high accuracy and precision the intimate details of host-guest hydrogen bonding, C-H··· $\pi$  and  $\pi$ - $\pi$  interactions, as well as the topologies of crystal cavities accommodating included guest molecules) is necessary to complement the data gleaned by other techniques. For most of the selected studies, therefore, the use of X-ray diffraction in the identification of key interactions responsible for selective guest inclusion and photoreactions is highlighted.

# 1.2 General Design Strategy of Host Molecules Based on Heterocyclic Frameworks and Appended Hydroxyl Sensor Groups

Chiral host compounds such as 1,6-di(o-chlorophenyl)-1,6-diphenylhexa-2-diyne-1, 6-diol 1, 2,2'-dihydroxy-1,1'-binaphthyl 2, and 2,2'-dihydroxy-9,9'-spirobifluorene 3 (Scheme 1) were designed with a view to incorporating hydroxyl groups into rigid frameworks so that the former could hydrogen bond with a guest molecule and the latter, comprising bulky groups, could effectively surround the guest molecule, to yield a stable crystal of the inclusion complex [1]. Ample evidence for the predicted inclusion ability of such hosts was obtained from X-ray studies of the inclusion compounds of 1–3. Since, however, an optical resolution step is required in the synthesis of these host molecules, advantage could be gained by designing a host on the same principles as outlined above, but using instead a naturally occurring compound as the chiral source. Tartaric acid had long been identified as a chiral building block for synthesis [3] and in 1988, Toda and Tanaka reported the design of a new chiral host, trans-4,5-bis(hydroxy-diphenylmethyl)-2,2-dimethyl-1,3-dioxacyclopentane 4, based on the above principles and using diethyl tartrate in its synthesis, as shown in Scheme 1 [4]. Several other analogues of 4 were generated in this period and their guest inclusion potentials were evaluated.

The ability of the host 4 and its analogues to enclathrate a wide range of guests including alcohols, dipolar aprotic molecules, amides, heterocycles, aromatic hydrocarbons and amines, was subsequently demonstrated. X-ray analysis of representative inclusion compounds confirmed the notion that hydrogen bonding between the host and guest molecules, coupled with secondary interactions involving the bulky phenyl groups, stabilise the crystal structures. Early X-ray studies included inter alia those of crystalline inclusion compounds of 4 with a series of achiral amine guests [5] and two chiral bicyclic enone guests [6]. The utility of host 4 in the optical resolution of the latter class of guests had been convincingly demonstrated, optically active isomers being isolated in 100% ee by inclusion complexation. This host compound is currently but one of the commonly used TADDOLs, several of which are shown in Scheme 2.

The comprehensive review of TADDOLs, their derivatives and analogues [2] referenced earlier, appeared in 2001 and contains nearly 500 references. A detailed



**Scheme 2** Representative TADDOL hosts [2]

discussion of the structural features of these molecules, based to a large extent on the results of a significant number of accumulated crystal structures, is provided in that work. A virtually invariable feature of such hosts in their inclusion compounds is the formation of an intramolecular hydrogen bond of the type -O-H···O-H, between the hydroxyl groups, thereby adding rigidity to the molecule, and leaving one of them free to act as a donor in hydrogen bonding to a guest molecule (Fig. 1). The representative structures discussed below generally include this motif but deviations from this pattern that feature in inclusion compounds studied more recently are also described.

# 1.3 Survey of Preparative Methods and Representative Examples

A common procedure for the preparation of inclusion compounds of the type discussed here is to co-dissolve two equivalents of the racemic material (guest) and one equivalent of the chiral host (e.g. a TADDOL) in a pure solvent or a solvent mixture and allow crystallization to proceed spontaneously. The crystals of the inclusion compound, containing one of the enantiomers of the guest exclusively (or a mixture enriched in one enantiomer), are subsequently heated under vacuum under controlled conditions, whereupon the pure/enriched guest is released and isolated.

The choice of solvent may be a crucial factor in this process. For example, in a report on the resolution of  $(\pm)$ -( $\alpha$ -cyclopropylethanol) by inclusion complexation with a chiral TADDOL **H** [7], it was reported that a one-step crystallization from diethyl ether-hexane solution yielded the complex  $2\mathbf{H}\cdot(\alpha$ -cyclopropyl-ethanol) with an enantiomeric enrichment of 75%, whereas no resolution was observed after crystallization of the same inclusion complex from benzene-hexane. In attempts to effect the same resolution using host analogues, it was similarly found that different degrees of guest resolution were achieved depending on whether diethyl ether-hexane or THF-hexane was employed as the medium. These examples indicate that the solvent/solvent mixture

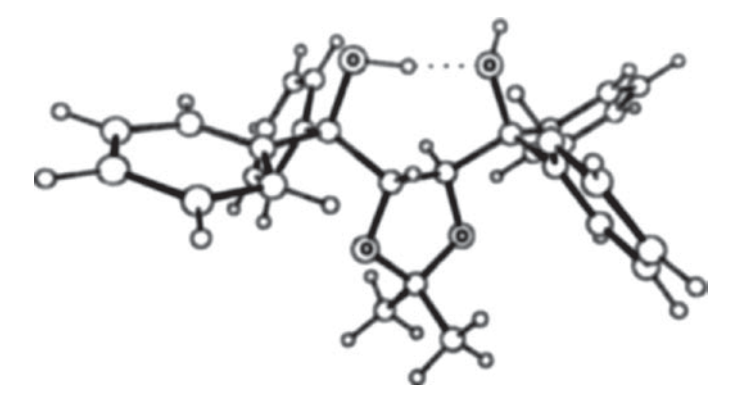


**Fig. 1** Host molecule **4** as it occurs in the inclusion complex with (–)-(*R*)-6-methylbicyclo(4.4.0) dec-1-en-3-one [6]. Oxygen atoms are labelled and the intramolecular hydrogen bond is shown as a *dotted line* 

employed in the process of enantioselective inclusion is by no means 'inert' and that optimisation of its composition forms an essential part of the experimental protocol, just as it does in the case of classical resolution by diastereomeric salt formation. It should be noted that, in addition to capturing a guest molecule in enantioselective fashion, a given chiral host may also include solvent molecules from the crystallization medium. For example, in the resolution of racemic phenyl-methylphospholene oxide with a chiral TADDOL host ( $\mathbf{H}$ ) using a 1:5 acetone-pentane mixture, the inclusion crystal formed was found to have the composition  $\mathbf{H} \cdot (-)$ -(phenyl-methylphospholene oxide)-acetone [8]. As described in Sect. 2.2, X-ray analysis reveals the role that such included solvent molecules may play in complex crystals.

For preparative resolution of racemic guests, a single inclusion recrystallization step may yield enantiomeric purities greater than 98%. However, in some cases multi-step crystallization may be necessary to achieve the desired degree of enantiomeric purity. In the case of  $(\pm)$ - $(\alpha$ -cyclopropylethanol) [7], two-step inclusion crystallization from diethyl ether-hexane solution followed by thermal desolvation of the inclusion crystals at 60–90 °C yielded the guest alcohol having optical purities of 97–98% ee with the series of hosts employed. The latter were recovered in 95–96% yields, ready to be employed in new separation cycles.

An alternative procedure is to carry out the enantioselective process under heterogeneous conditions, by adding a stirred suspension of the chiral host in, e.g. water, to the racemate. Subsequently, the mixture is filtered and recovery of the pure guest under vacuum completes the process. Other variations are described in the review cited above [2]. One of these involves 'distillatory separation of racemates' in which the residue obtained by evaporating the solvent used in the enantioselective enclathration step is successively distilled at low temperature to eliminate the guest enantiomer that is not included in the crystal, and at elevated temperature under vacuum to release the included enantiomer from the enantio-enriched solid complex [9, 10].

The requirement that the guest in the solid complex be relatively volatile for isolation by distillation is not always met, and even when it is, distillation may still present technological challenges in large scale operations. To address this, a novel process that involves a combination of enantioselective inclusion complexation (EIC) and organic solvent nanofiltration (OSN) has been developed [11]. The fivestep process entails (a) enantioselective resolution, (b) elution of the non-included guest enantiomer from the solution phase, (c) decomplexation to release the included guest from the inclusion compound, (d) elution of the included guest, and (e) host precipitation. Crucially, nanofiltration of the suspension is employed first in step (b), where the non-included enantiomer permeates the membrane while the enantioenriched solid inclusion complex is retained. In step (c) liberation of the included enantiomer is effected by the addition of a decomplexation solvent. Nanofiltration is again employed in step (d), the guest permeating the membrane while the soluble host is retained. Finally, in step (e) the host is precipitated using the resolution solvent and diafiltration is employed to remove the decomplexation solvent. Advantages of the process include its operation at ambient temperature and reuse/recycling of the host compound. The potential for extending the scope of EIC from the laboratory scale to pilot or industrial scale separations using this approach was highlighted.

# 2 Inclusion Chemistry

# 2.1 Methodology and Characterization of the Products of Inclusion

Typical studies of enantioselective inclusion using chiral hosts include accounts of the resolution procedures employed, enantiomeric purities obtained, and both chemical and structural characterization of the reported inclusion complexes. A very broad overview of the methodology used follows here and examples which illustrate specific applications are given in subsequent sections.

Included guests are usually characterised by chiral HPLC, chiral GC and CD measurements. For chemical characterisation of inclusion complexes, host-guest stoichiometries are usually determined by any one, or a combination of, elemental analysis,  $^{\rm l}$ H-NMR spectroscopy and (in the case of volatile guests) thermogravimetric analysis (TGA). Complementary differential scanning calorimetry (DSC) yields useful information on the temperature range and enthalpy change for loss of the guest on heating, reflecting the thermal stability of the inclusion complex. IR spectroscopy has proven useful both in detecting shifts in  $\nu_{\rm OH}$  of TADDOL hosts that indicate host-guest interactions via hydrogen bonding as well as distinguishing different conformations of included guest molecules.

Although the well-known technique of single crystal X-ray analysis is widely and routinely practised, some remarks on its application to enantioselective inclusion complexation are appropriate. As indicated in the Introduction, this technique yields a significant amount of accurate and precise information on host-guest interactions in the solid-state and such an analysis is consequently highly desirable for a crystal of an inclusion compound to support conclusions drawn from other techniques. From the X-ray analysis, the nature of the enclathration of a chiral guest molecule within the host matrix can be described in terms of interactions gauged from intermolecular geometrical parameters for hydrogen bonds, C-H··· $\pi$ ,  $\pi$ ··· $\pi$  and other interactions, as well as the topology of the cavity that accommodates the guest molecule. All of these structural features determine the stability of the crystalline inclusion compound, and a correlation between these features and, e.g. TGA and DSC data, can often be found. 'Mapping' of the guest cavity in crystals of inclusion compounds is frequently carried out in studies of enantioselective inclusion processes to gain an understanding of the reasons for the specificity of enantiomeric uptake in the solid inclusion complex. For enantioselective photoreactions, analogous mapping is performed to deduce the feasibility of molecular motion during reaction and hence to rationalise the stereochemical outcome.

When heavy-atoms are present in the crystal of the inclusion compound, determination of the absolute configuration of the included enantiomer can generally be deduced using standard crystallographic procedures based on anomalous dispersion effects. In the absence of heavy-atoms, absolute configuration determination is compromised. In either case, however, the absolute configuration of the guest can be unequivocally deduced provided that the chirality of the starting host material is known.

Some inclusion compounds contain a mixture of guest enantiomers. Their co-existence can usually be easily detected in electron-density maps and their proportions evaluated in the X-ray analysis by allowing their site-occupancies to refine in the least-squares process.

Powder X-ray diffraction (PXRD) remains an extremely useful and rapid method of solid phase characterization and can be used in the first instance to identify a new crystalline phase representing a probable inclusion compound, since the latter will have a distinctly different PXRD pattern from those of the host or guest (if the latter is a solid at ambient temperature). It is particularly useful for identifying solid-state isostructurality of chemically different compounds and its judicious use could, in some instances, obviate the need for full three-dimensional structural analysis.

Research in the area of solid-state NMR (SSNMR) is motivated by the general challenge of the increasing need for stereochemical characterization in diverse fields, and especially in pharmaceutical production. A recent paper described the use of SSNMR as a tool for the investigation of enantioselective inclusion complexation [12]. Here, using model compounds (including a TADDOL as a host), it was demonstrated that SSNMR could distinguish the uncomplexed host from the host-guest complex.

# 2.2 Chiral Resolution by Inclusion Crystallization with Optically Active Heterocyclic Hosts Derived from Tartaric Acid

Before considering recent documented cases of enantioselectivity in inclusion complex formation, it should be noted that achiral molecules may also form inclusion compounds with the diol hosts described. In some cases, inclusion of such molecules may lead to their being trapped in unexpected conformations or tautomeric forms, as illustrated in the following examples.

An interesting case of the former relates to conformers of chloro- and bromocyclohexane which are not easily isolated in a pure state due to the dynamic equilibrium that exists between their respective equatorial and axial conformers. These species were isolated for the first time as equatorial conformers exclusively within solid inclusion complexes, namely those with the host *rac-*7 (Scheme 2) [13]. The inclusion complexes were obtained in the form of colourless crystals from solutions of the TADDOL host 7 in the respective liquid guests and were initially examined using IR spectroscopy in attenuated total reflection (ATR) mode. In the spectrum of the complex 7-chlorocyclohexane, a very strong band at 726 cm<sup>-1</sup>, attributable to equatorial C-Cl stretching appeared, accompanied by a weak absorption at 684 cm<sup>-1</sup> which could be assigned either to axial C-Cl stretching or a vibration associated with host 7. For the analogous complex 7-bromocyclohexane, similarly unequivocal results were obtained. To obtain an unambiguous result, the X-ray structure of 7-chlorocyclohexane was determined. This showed clearly the presence of only the equatorial conformer of the guest in the inclusion crystal,

as illustrated in Fig. 2 (left), which includes the crystallographic asymmetric unit. In the host molecule 7, the intramolecular -O-H···OH hydrogen bond previously described is again present, but in the inclusion complex the second hydroxyl group does not participate in hydrogen bonding to the guest. This is unusual for inclusion complexes of host 7 but can be seen to be due to the preferred formation of a very stable, centrosymmetric hydrogen bonded dimeric host unit (Fig. 2, right), in which there are four homodromic H-bonds. This presumably occurs since the racemic host is used here and the guest does not possess a suitably strong H-bond acceptor atom such as O or N.

The complex 7-chlorocyclohexane is thus unusual in that, save for omnipresent van der Waals interactions, there are no discernible interactions such as H-bonding or C-H··· $\pi$  between the host and guest molecules; the latter therefore simply act as filler molecules in stabilising the crystal structure, with the important feature, however, that they are exclusively present in the equatorial conformation. Evidently the host dimers pack in such a way as to provide cavities with a topology that better accommodates the equatorial conformer than the axial one. Analogous results were reported for the complex 7-bromocyclohexane, which, not surprisingly, is isostructural with 7-chlorocyclohexane. This is readily apparent from the close similarity of the computed PXRD patterns of the two crystals.

In a more recent study by the same group, the first isolation of the axial conformers of chloro- and bromocyclohexane by solid-state inclusion was reported [14]. This was achieved using the host 9,9'-bianthryl and is very significant owing to the lower stability of the axial conformers. This study led to an interesting observation in the case of the included chlorocyclohexane guest, namely the presence of a weak 1,3-diaxial Cl···H interaction, indicated by a distance of 2.90 Å, nominally

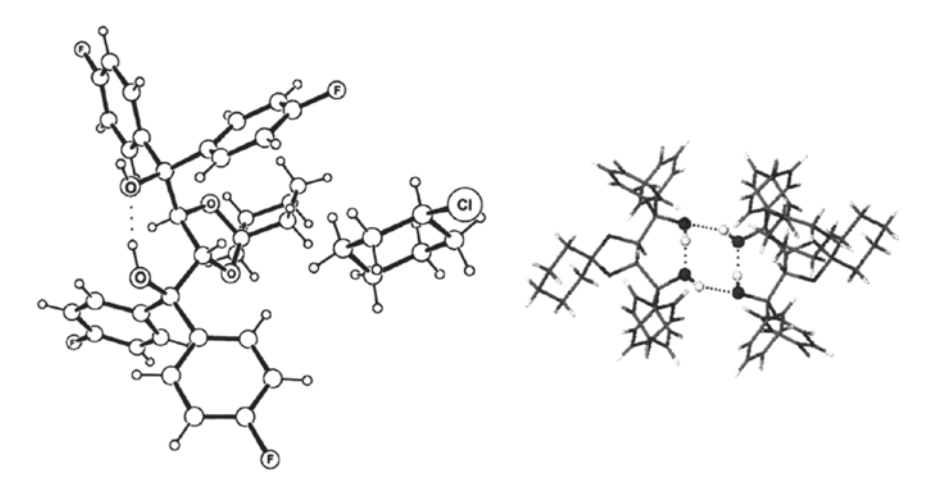


**Fig. 2** The equatorial conformer of chlorocyclohexane trapped in the inclusion complex with a TADDOL host (*left*) and the structure of a centrosymmetric hydrogen bonded host dimer in the inclusion crystal (*right*) [13]

shorter than the sum of the van der Waals radii of Cl and H (2.95 Å). As the authors pointed out, this conflicts with the commonly accepted notion that 1,3-diaxial interactions in the chair form of a cyclohexane ring are repulsive and that they should therefore have a destabilising effect. In order to confirm that such an interaction is not specific to the axial conformer of cyclohexane, they prepared the inclusion complex between *cis*-1,2-dichlorocyclohexane and the TADDOL host *rac*-7 (Scheme 2). The structure of the asymmetric unit in this crystal is shown in Fig. 3. As in 7-chlorocyclohexane, the host molecule again forms a centrosymmetric H-bonded dimer (not shown). Similar close Cl···H 1,3-diaxial contacts of 2.94 (a) and 2.93 Å (b) were found, supporting the conclusion that such interactions may be considered general for cyclohexane ring systems.

In an earlier, closely related study by the same group, the (R, R)-(-)-trans-diequatorial isomer of trans-1,2-dichlorocyclohexane was isolated for the first time as the guest in its inclusion complex (2:1 host-guest ratio) with the optically active host (R, R)-(-)-5 (Scheme 2) [15]. Analysis of the chiral crystal cavity surrounding the guest molecule led to the conclusion that its topology was consistent with the di-equatorial isomer exclusively, as was the 3 Å distance between the Cl atoms in the guest molecule.

Keto-enol tautomerism has also been the subject of investigation in the context of inclusion compound formation. Pure acetylacetone (10) had been found to occur as a dynamic or static mixture of the two enol forms 11 and 12 (Fig. 4, top) in its crystal structure determined at 110 K [16]. This interpretation was based on accurately deter-

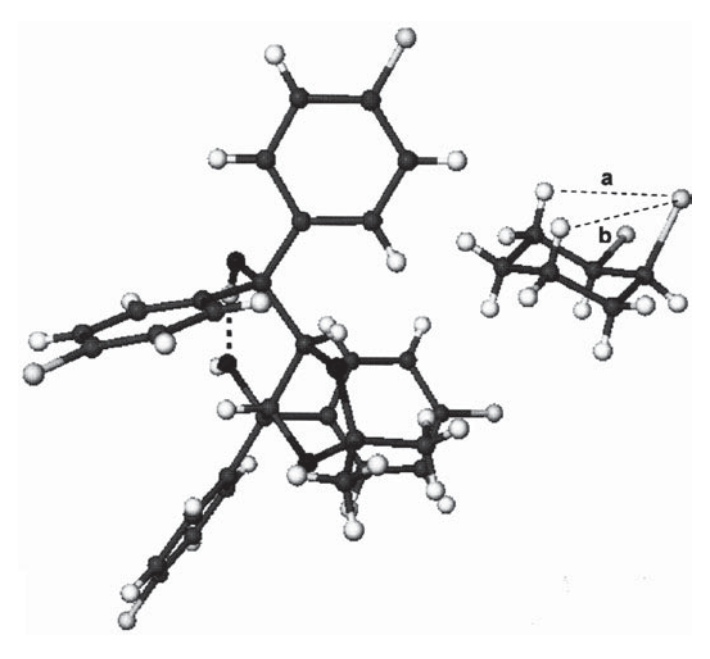


Fig. 3 The structure of the asymmetric unit in the inclusion complex between *cis*-1,2-dichlorocyclohexane and the TADDOL host *rac-*7 [14]

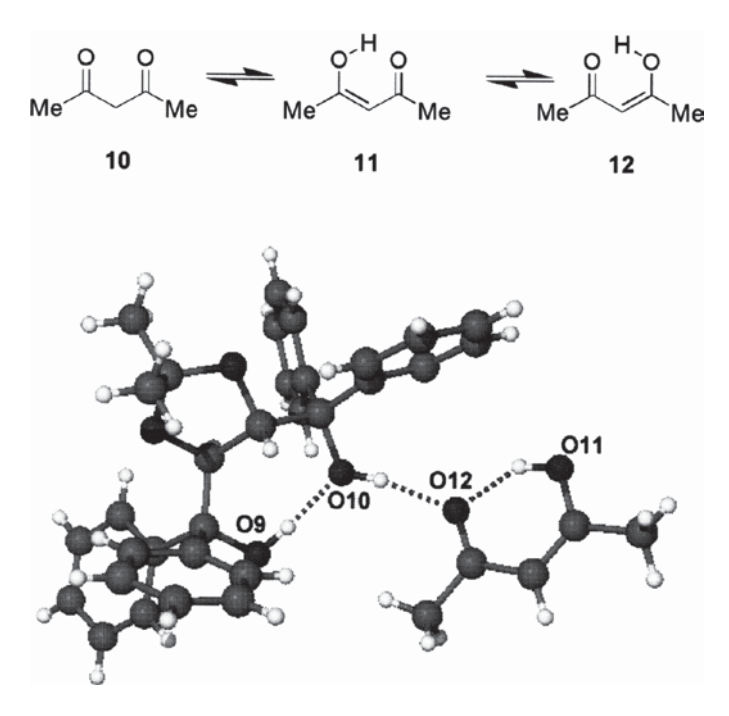


Fig. 4 Keto-enol tautomerism in acetylacetone (top) and the pure enol form included in its complex with the host (R, R)-(-)-4 [17]

mined carbon-oxygen and central carbon-carbon distances, whose values in the crystal are the averages of standard C-O, C=O and C-C, C=C distances respectively. In a recent study of the 1:1 inclusion complex between acetylacetone and host (*R*, *R*)-(–)-4 (Scheme 2), the guest molecule was found to be included as the pure enol form exclusively [17]. The crystallographic asymmetric unit comprises two 1:1 complex units, only one representative unit being shown in Fig. 4 (bottom) for simplicity since, as concerns guest tautomerism, the structural results for the two are equivalent.

The familiar host intramolecular hydrogen bond O9-H···O10 is present in this crystal. The second hydroxyl group of the host molecule donates a hydrogen bond O10-H···O12 to the carbonyl oxygen atom of the guest while the latter is also an acceptor in the intramolecular hydrogen bond O11-H···O12 donated by the hydroxyl oxygen atom O11. Carbon-oxygen and carbon-carbon distances unequivocally indicate that the guest is in the enol form. For example, C-O12 and C-O11 are 1.258(3) and 1.321(3) Å respectively and similar corresponding values are found for the guest of the second complex in the asymmetric unit. The authors attributed the presence of the enol form in the crystal to the formation of hydrogen bond O10-H···O12, whose effect is to reduce the basicity of atom O12 and the mobility of the central H-atom in acetylacetone, thereby stabilising the resonance form containing an asymmetric intramolecular H-bond. In the crystal of pure acetylacetone, on the other hand [16], the presence of a strong resonance-assisted

intramolecular H-bond lowers the barrier for proton transfer between the two oxygen atoms, with the result that the electron-density is a superposition of enol forms 11 and 12. The situation in the complex of Fig. 4 described by Toda et al. [17] is not unique and these authors provide references to other inclusion complexes in which acetylacetone has been isolated in the enol tautomeric form.

One of the manifestations of chirality is that arising from hindered rotation of functional groups. Scheme 3 shows model structures displaying chirality of this type. For compounds in this class, reports of successful enantiomeric separation using diol hosts have appeared [18, 19].

Scheme 3 Chirality in *N*-nitrosopiperidines (13, 14) and in thio-/selenoamides (15, 16) [18, 19]

For the N-nitrosopiperidine shown and its analogues, restricted rotation around the nitrogen-nitrogen bond due to its partial double-bond character gives rise to enantiomers 13 and 14, for which there is a fairly high energy barrier of 23–25 kcal mol<sup>-1</sup> for their interconversion. Isolation of the stereoisomers should therefore be possible at ambient temperature. The authors of this work reported successful resolution of simple N-nitrosopiperidines by enantioselective inclusion using cholic and deoxycholic acid as host molecules, but for larger analogues, no inclusion compounds formed, a result attributed to the relatively small size of the channels in the crystals of the bile acids. Instead, reaction of several larger nitrosamine molecules with TADDOL hosts **4–6** (Scheme 2) in 1:1 molar ratio in toluene-hexane mixtures yielded inclusion complexes with varying degrees of enantioselectivity. For the majority of the guests investigated, X-ray analysis revealed that in their inclusion complexes, the nitroso group was found to be disordered over two positions with a range of site-occupancies, thus indicating different extents of enantio-enrichment. However, in one case, the host 4 and the nitrosamine 17 yielded an inclusion crystal (Fig. 5) whose X-ray analysis indicated the probable presence of only one guest enantiomer in the inclusion crystal, selectivity being provided by the chiral crystalline host arrangement and the hydrogen bond linking the host to the nitroso oxygen atom [18].

A further significant result was reported, namely the conversion of the entire quantity of the racemic guest employed in the inclusion experiment to the single enantiomer shown in Fig. 5, thus providing an interesting example of a complete asymmetric

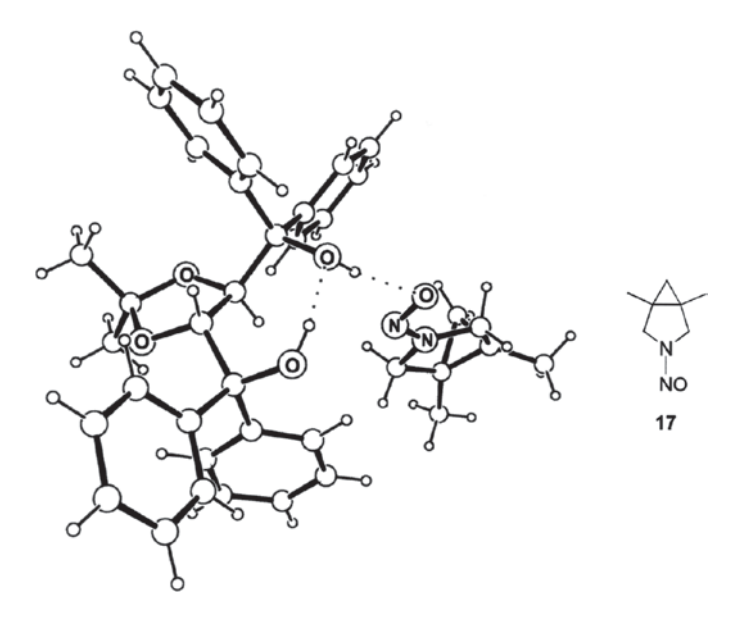


**Fig. 5** Crystal asymmetric unit showing enantioselective inclusion by host **4** of the nitrosamine **17** (*left*) whose chemical structure is shown (*right*) [18]

transformation. The authors reported this as a general result for the guests studied since the yields of the resolutions generally exceeded 50%. Another aspect of this revealing study related to a novel method of isolation of the enclathrated nitrosamines, namely via competitive complexation of the host diols with piperazine. For the nitrosamine inclusion compounds with host 5 (Scheme 2), addition of piperazine in diethyl ether at 0°C led to formation of an insoluble inclusion complex 5-(piperazine)<sub>2</sub> and liberation of the nitrosamine guest molecules which enabled their subsequent isolation.

Chirality in the thioformamides and selenoformamides (15, 16 Scheme 3) arises from hindered rotation around the C-N bond. In an analogous study by the same group [19], parallel results to those for the nitrosamines were obtained in the resolution of these amides into their enantiomers using TADDOL host compounds. The authors concluded that this approach is 'a reliable and effective method of optical resolution of configurationally labile compounds'. X-ray analyses again played a pivotal role in the assignment of absolute configurations to the enclathrated guest molecules.

Thermodynamically controlled deracemization of  $\alpha$ -substituted cyclohexanones based on inclusion chemistry with TADDOL hosts has been reported [20, 21]. An example of this process is the conversion of racemic 2-benzylcyclohexanone to the R-isomer of 74% ee in quantitative yield using the host (R,R)-(-)-6 (Scheme 2) in basic suspension media. This has been discussed in detail in the above references, but in short, the process involves a two-phase system comprising the solid phase of

the chiral host  $\mathbf{H}$  and the liquid phase (aqueous basic methanol) in which the racemic guest  $\mathbf{G}$  is solvated and equilibration of the enantiomers occurs. In the solid phase, diastereomeric complexes  $\mathbf{H} \cdot (R) - \mathbf{G}$  and  $\mathbf{H} \cdot (S) - \mathbf{G}$  are generated, formation of the thermodynamically more stable one resulting in guest enantiomeric enrichment and subsequent recovery of the corresponding stereoisomer in high yield. The nature of the chiral molecular recognition step in this process was probed by single crystal X-ray analysis of the representative inclusion complex  $\mathbf{6} \cdot (R)$ -2-cyclohexanone [22], whose crystal packing diagram projected down the a-axis is shown in Fig. 6. The compound crystallises in the space group  $P2_1$  with two independent 1:1 host-guest complex units in the asymmetric unit (labelled  $\mathbf{H1}$ ,  $\mathbf{G1}$  and  $\mathbf{H2}$ ,  $\mathbf{G2}$ ). A modelling study of the guest compound (R)-2-cyclohexanone showed that the theoretically most stable conformation resembled those of the two independent guest molecules in the crystal, but slight differences in the orientations of the phenyl groups occur when the molecules are accommodated by the chiral cavities provided by the host assembly, i.e. crystallization is accompanied by an induced host-guest fit.

The intramolecular host -O-H···OH hydrogen bonding typical of TADDOLs occurs once again in **6**, the 'free' hydroxyl group acting as donor in a hydrogen bond to the carbonyl oxygen of the guest molecule (representative dotted lines, Fig. 6). A very detailed analysis of the packing in the crystal by the authors, including a mapping of the host cavities, led to the conclusion that the particularly elegant combination of van der Waals interactions between hydrophobic groups and hydrogen bonding observed is responsible for stabilising the crystal structure.

In addition, failure to isolate the inclusion complex between  $\mathbf{6}$  and (S)-2-cyclohexanone after repeated attempts provided evidence for the higher stability of the complex  $\mathbf{6} \cdot (R)$ -2-cyclohexanone, thus supporting the model of a thermodynamically controlled deracemization process for the selective enclathration observed.

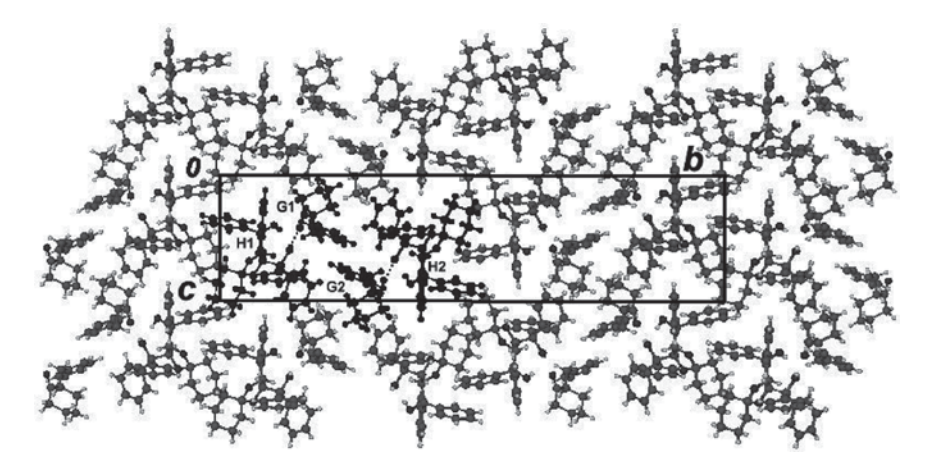
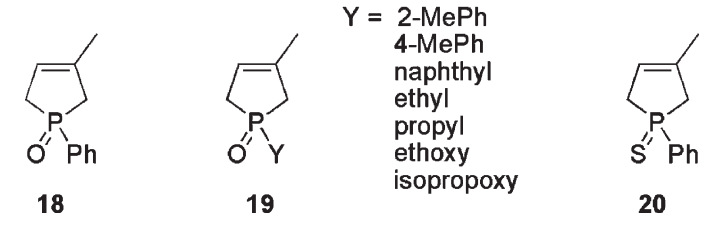


Fig. 6 [100] Projection of the molecular packing in the crystal of the inclusion complex  $6 \cdot (R)$ -2-cyclohexanone [22]

The versatility of chiral phosphine oxides in various chemical applications, including transition metal complex chemistry and homogeneous catalysis, places a continual demand on new methodologies for efficient isolation of these species by resolution techniques. One method of resolution, for example, is through diastereomeric salt formation with resolving agents such as (+)-mandelic acid bromocamphorsulphonic acid, and (-)-dibenzoyltartaric acid. The synthetic versatility of 3-methyl-3-phospholene 1-oxides (Scheme 4) recently prompted Novák et al. [8] to devise a practical procedure for the resolution of 18 using the chiral TADDOL host compound (-)-4 (Scheme 2).



Scheme 4 Phosphorus-containing compounds resolved by TADDOL hosts [8, 23]

A complete flowchart for this process was provided, showing the isolation of the preferentially included guest enantiomer (-)-18 in 96.5% ee and 43% yield, as well as that of (+)-18 recovered from the mother liquors of 99% ee in 27% yield. Preliminary data for analogous resolution of 19 (Y = ethoxy) with (-)-3 were also provided, this work representing the first examples of the enantiomeric separation of a cyclic phosphine oxide or a phosphinate via enantioselective inclusion complex formation.

The absolute configuration of the guest (-)-18 was established as (S) from the X-ray structure of the inclusion complex. Not surprisingly, molecular recognition is based on host(O-H)···O=P(guest) hydrogen bonding but interestingly, the inclusion complex unit also contains an acetone molecule, which the authors describe as not only acting as a co-solvent but whose presence is essential in promoting a closely packed crystal. This indicates another aspect of the potential importance of the solvent medium in enantioselective inclusion complex crystallization.

In an extension of the above study, the same group more recently resolved the series of racemic 1-aryl, 1-alkyl, and 1-alkoxy-3-methyl-3-phospholene 1-oxides 19 as well as 1-phenyl-3-methyl-3-phospholene 1-sulfide 20 (Scheme 4) using analogous procedures [23]. The method was assessed as having general value for such phospholene chalcogenides, yielding their optically active forms in  $\geq$ 95% ee after two recrystallization steps in eight cases of the nine studied. X-ray analysis of representative structures again highlighted host(O-H)···O=P(guest) hydrogen bonding as a primary interaction in the inclusion crystal, in these cases complemented by a series of weaker C-H···O hydrogen bonds and C-H··· $\pi$  interactions.

An outline of a novel chiral separation process that uses a combination of enantioselective inclusion complexation and organic solvent nanofiltration [11] was

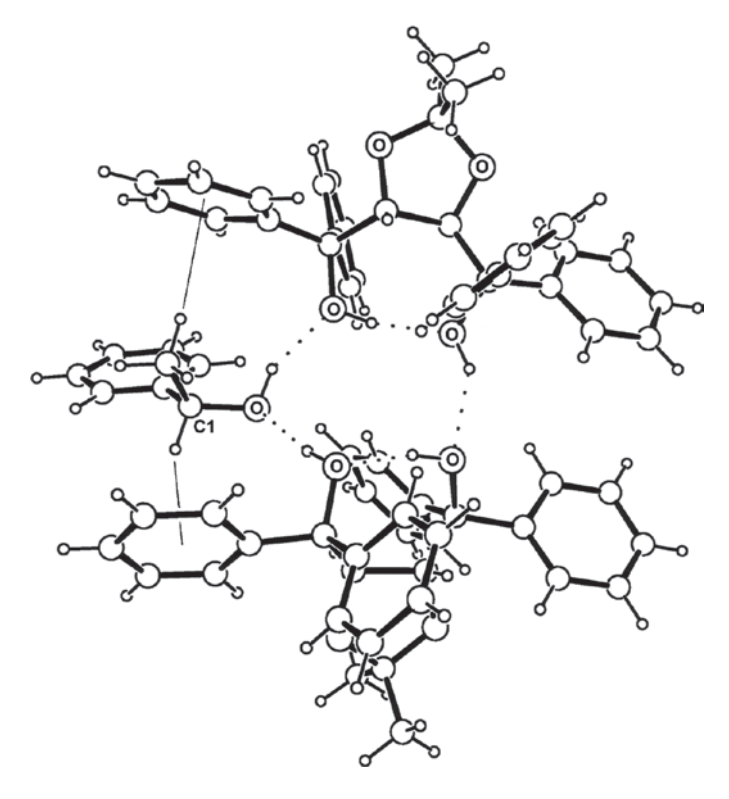


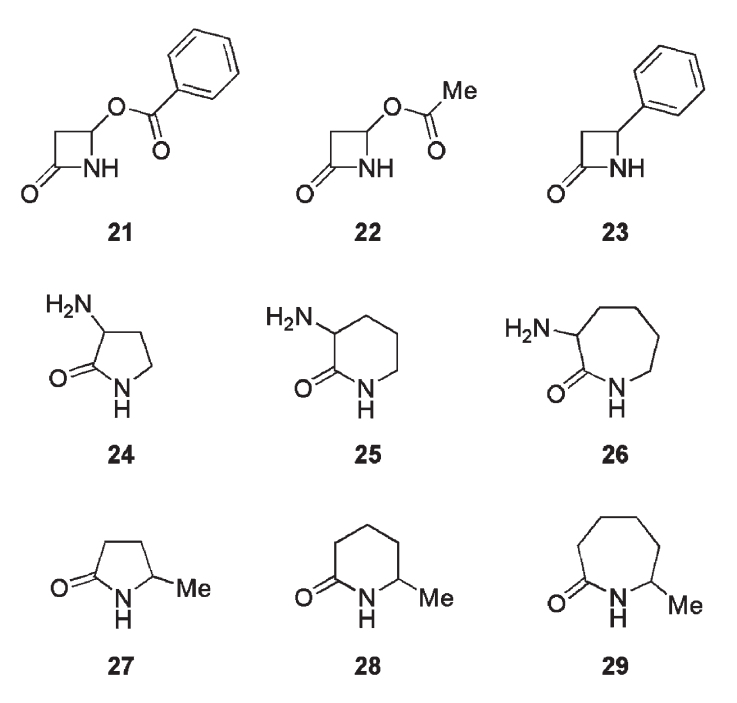
Fig. 7 The 2:1 crystal asymmetric unit in the inclusion complex 24·(S)-1-phenylethanol [11]

presented in the Introduction. This methodology was tested using racemic 1-phenylethanol as model compound. The latter was rapidly resolved with chiral TADDOL host 4 (Scheme 2) through selective formation of the inclusion complex 24·(S)-1-phenylethanol, initially identified as a crystalline product by PXRD and subsequently obtained as single crystals by recrystallization of the crude complex from a 1:2 (v/v) toluene-hexane mixture. The 2:1 crystal asymmetric unit is shown in Fig. 7. A cyclic arrangement of five O-H···O hydrogen bonds is formed, two of them being intramolecular (involving the host molecules) while three of them are intermolecular H-bonds (host-host and two host-guest). As the authors point out, this arrangement can be considered as an interruption of the 'square' of cyclic hydrogen bonds that characterises the free host motif in its crystal structure (or in fact of the host dimers illustrated in, e.g., Fig. 2 shown earlier), with the guest hydroxyl group inserting itself into, and enlarging, the H-bond cycle [11]. Given that a change in chirality at the guest atom C1, i.e. exchanging the hydride and methyl moieties, should not disrupt the hydrogen bonding pattern observed, the authors deduced that the observed selective inclusion of the (S)-enantiomer must hinge on interactions that these moieties engage in with their immediate surroundings.

Inspection of the close contacts revealed that both moieties are involved in  $C-H\cdots\pi$  interactions to neighbouring host phenyl rings (thin lines in Fig. 7). The

unfavourable contacts that would result from exchanging the methyl and H atoms would require a different relative orientation of the two host molecules which might then compromise the stability of the H-bond cycle, the latter appearing to be the energetic factor favouring formation of the inclusion complex. This provides a rationale for the selective inclusion of the (S)-enantiomer of the guest.

Racemic lactams, which generally present challenges for resolution by classical methods, have recently been successfully resolved using TADDOL hosts. Scheme 5 shows the structures of the relevant  $\beta$ -lactams 21–23 [24],  $\alpha$ -aminolactams 24–26 [25], and  $\alpha'$ -methyllactams 27–29 [25]. Compounds 21–23 were resolved using optically active host 6 (Scheme 2), the inclusion complex crystallizing with the guest (S)-(–)-21 yielding the highest enantioselectivity of 98% ee. IR spectroscopy was useful in detecting inclusion complex formation: for the complex, the  $v_{OH}$  peak appeared at 3,137 cm<sup>-1</sup> whereas the free host showed peaks at 3,530 and 3,340 cm<sup>-1</sup>, while the  $v_{C=O}$  peak of the racemic guest (±)-21 appearing at 1,788 cm<sup>-1</sup> was shifted to lower frequency and split into two peaks at 1,762 and 1,727 cm<sup>-1</sup>.



Scheme 5  $\beta$ -lactams 21–23 [24],  $\alpha$ -aminolactams 24–26 [25], and  $\alpha'$ -methyllactams 27–29 [25] recently investigated for inclusion by TADDOL hosts

The value of 8% ee for the resolution of 22 was very low compared with those for 21 and 23, suggesting that the presence of the phenyl group is important for enantioselectivity. X-ray analysis of  $6\cdot(S)$ -(-)-21 was undertaken to identify possible factors contributing to its apparent stability. Part of a hydrogen bonded spiral generated by a twofold screw axis in the crystal is shown in Fig. 8 which indicates

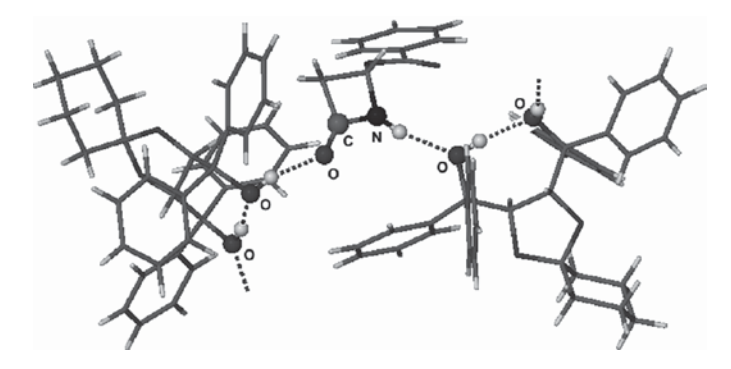


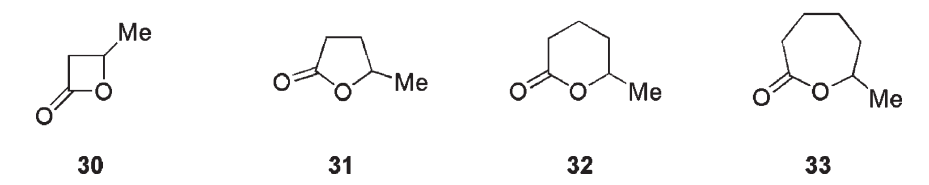
Fig. 8 Host-guest hydrogen bonding in the inclusion complex  $6\cdot(S)$ -(-)-21 [24]

that the amide function of the guest is anchored to two host molecules via one  $guest(N-H)\cdots O(host)$  and one  $host(O-H)\cdots (O=C)guest$  hydrogen bond.

Careful inspection of the region surrounding the guest phenyl ring did not reveal any particularly strong intermolecular contacts that could be used to rationalise the selective inclusion of the (S)-enantiomer. In this case, therefore, it was concluded that while host-guest molecular recognition is driven by strong hydrogen bond formation (N-H···O, O-H···O), enantioselectivity appears to be determined primarily by shape selection afforded by chiral cavities of appropriate topology in the surrounding host structure.

Enantioselective inclusion of the racemic compounds 24–29 using host molecules (R,R)-(-)-4 and (R,R)-(-)-6 (Scheme 2) was studied in an analogous manner [25]. The highest enantioselectivities (all with >99% ee) were obtained via inclusion crystallization of host (R,R)-(-)-4 with (S)-(-)-26, host (R,R)-(-)-6 with (S)-(-)-26, and (R,R)-(-)-6 with (S)-(-)-25. The racemic guest 24 did not form inclusion complexes with either host compound, and in the series of methyl substituted lactams 27–29, resolution with both hosts succeeded only for compound 28, that with host (R,R)-(-)-4 being superior but achieving guest resolution of only 69% ee. It was thus deduced that the presence of the amino group on the lactam plays a prominent role in chiral recognition. X-ray analysis of the 1:2 inclusion complex crystal (R,R)-(-)- $4\cdot(S)$ -(-)-26 was duly undertaken to probe the molecular interactions responsible for enantioselectivity. As regards the host molecule, the general pattern of hydrogen bonds was that commonly observed in its inclusion compounds. It was, however, recognised that in this 1:1 system, there is an excess of hydrogen bond donors over acceptors and that a consequence of this is formation of an intramolecular hydrogen bond N-H-O between the guest amino group and its carbonyl group, the former also accepting a hydrogen bond O-H···N from a hydroxyl group of the host molecule. These and other structural features were used as a basis for rationalising both the efficient chiral recognition as well as stabilisation of the inclusion crystal in the solvent medium, namely toluene [25].

The importance of optically active lactones as natural products and as useful building blocks in the synthesis of biologically active substances, including biodegradable polymers, prompted a recent study of the optical resolution of the homologous series of medium-size lactones 30–33 (Scheme 6) using host compounds (R,R)-(–)-4, and (R,R)-(–)-5 and (R,R)-(–)-6 [26]. Of all possible host-guest combinations, only that between host (R,R)-(–)-4 and racemic guest 33 did not produce an inclusion complex. For all the other combinations, inclusion crystals with varying host-guest ratios (1:1, 2:1, 3:1 and 3:2, determined by  $^1H$  NMR spectroscopy) were isolated and the ee values (range 11–99% ee) were generally determined using HPLC. Thermogravimetry was also employed to determine the guest release temperatures as a measure of complex stability.



Scheme 6 A homologous series of lactones investigated for inclusion by TADDOL hosts [26]

A particularly novel and intriguing feature discovered for this series of guests was the occurrence of 'odd-even effects' on the chiral recognition in their enantioselective inclusion with the optically active hosts listed. For example, whereas the host (R,R)-(-)-5 preferentially included the (S)-enantiomer of the four-membered ring lactone 30 as well as the (S)-enantiomer of the six-membered ring lactone 32, it included the (R)-enantiomers of the five- and seven-membered ring lactones 31 and 33 respectively. Several of the inclusion compounds, available as high-quality single crystals, were analysed by X-ray diffraction to confirm the absolute configurations of the included guests and to rationalise the observed enantioselectivities. This can be illustrated with reference to the 2:1 inclusion complex (R,R)-(-)-4 with guest 31. For the single crystal that was selected for X-ray analysis, a twofold disorder of the guest carbon atom at the asymmetric centre was observed, thus indicating the simultaneous presence of both enantiomers in the crystal. Refinement of their site-occupancies resulted in a value of 0.73 for the (S)-enantiomer (and therefore 0.27 for the (R)-enantiomer), corresponding to an estimated ee of 46% for the selected crystal, in fair agreement with the value determined for the crystal batch using HPLC (38%). The X-ray structure of the asymmetric unit, comprising two host molecules and one guest molecule, is shown in Fig. 9. In the inclusion crystal, the three molecules are connected via a continuous chain of O-H···O hydrogen bonds that involve the four host hydroxyl groups, with the chain terminating in one (host)O-H···O=C(guest) H-bond. The two components of the guest disorder are indicated, the chiral carbon atom with major occupancy being labelled (S-) and that with minor occupancy labelled (R-). Both of the tertiary H atoms on the disordered chiral carbon centres (C\*) engage in C\*-H··· $\pi$  interactions with neighbouring host phenyl groups, but that for the (S)-enantiomer is geometrically more favourable, providing a reason for the observed enantioselectivity.

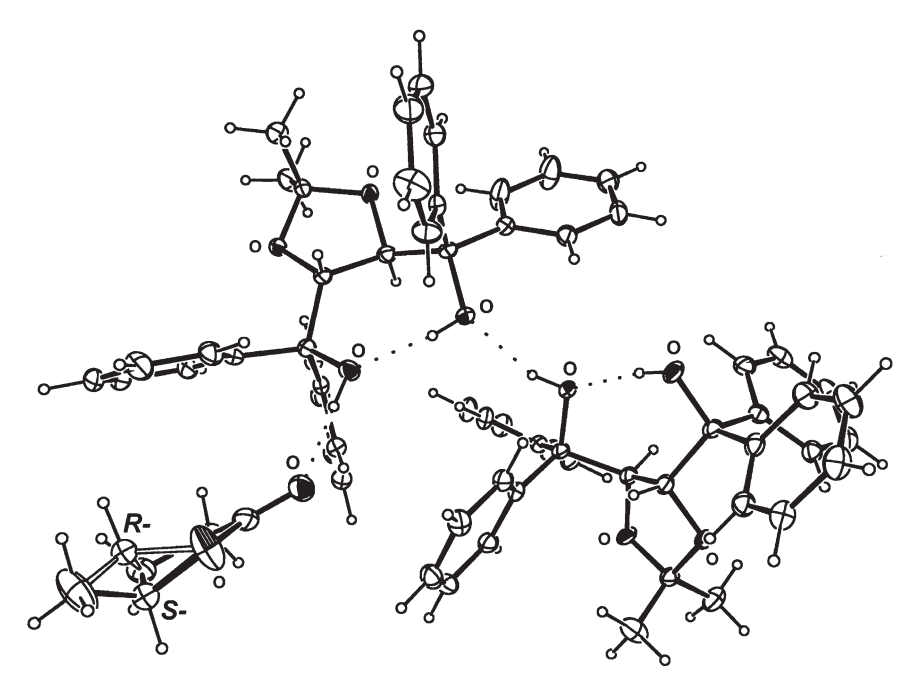


Fig. 9 The crystal asymmetric unit in the 2:1 inclusion complex (R,R)-(-)-4 with guest 31. Disorder at the guest chiral centre is indicated [26]

For the 1:1 inclusion complex formed between host (R,R)-(-)-4 and guest 32, no guest disorder was actually observed in the crystal selected for X-ray analysis, the guest being present as the (R)-enantiomer exclusively, Again, a geometrically very favourable C\*-H··· $\pi$ (host phenyl) interaction for this enantiomer was identified as a stabilising factor in its preferential inclusion.

X-ray analyses of the 1:1 inclusion complexes of the host (R,R)-(-)-5 with the guests 30, 31 and 32 were also reported in this study and yielded further interesting insights into the modes of guest inclusion in this series. For the first two complexes, isostructurality was detected, i.e. these crystals have very similar unit cell dimensions, a common space group  $(P2_12_12_1)$  and host atoms occupying virtually identical positions in their respective crystals, as evident from Fig. 10, in which these two structures (left, centre) are projected down common directions. The respective guest molecules in the two isostructural crystals pack in analogous layers (running vertically in Fig. 10). Despite these gross similarities, the microenvironments surrounding the chiral centres in guest molecules 30 and 31 are such that they have opposite configurations ( $(S_{-})$ ) and  $(R_{-})$  respectively), a result that can be reconciled with the detailed intermolecular interactions observed in the crystals. As is evident from Fig. 10, the cavities that accommodate the guest molecules are sufficiently 'elastic' to enclathrate guest molecules 30 and 31, which differ by a methylene group. However, when the sterically more bulky guest molecule 32 forms an inclusion compound with the same host, the same crystal structure apparently cannot be maintained and

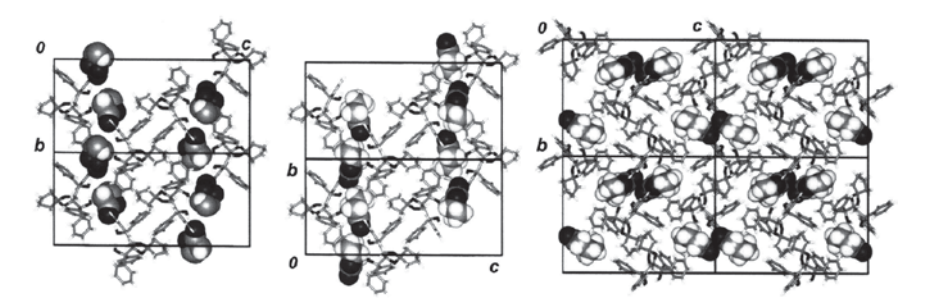


Fig. 10 Crystal packing diagrams illustrating enclathration of the guests 30 (left), 31 (centre) and 32 (right) by the host compound (R,R)-(--)-5 [26]

an entirely new one arises (Fig. 10, right). In all of the inclusion complexes in this series, host-guest recognition is mediated primarily by strong host(O-H)···O=C(guest) hydrogen bonding and 'fine-tuned' by softer interactions including C-H···O hydrogen bonds and C-H··· $\pi$  interactions [26].

Various examples of attempts to rationalise selective inclusion of guest enantiomers by representative chiral hosts based on heterocyclic frameworks have been cited above. These highlighted the fact that detailed observations from X-ray crystal structures can often provide the necessary clues for understanding the stereochemical outcomes observed. However, such reconciliation is not always possible. The multiple and varied combinations of intermolecular interactions that occur in inclusion crystals following their formation via solvent media are subtle and may lead to enantioselective results that are beyond such simplistic reasoning. Predicting the enantioselectivity of a given chiral host when it reacts with a racemic host also remains a difficult task, reflecting one aspect of the general ongoing challenge of theoretically based crystal structure prediction addressed by solid-state scientists.

## 2.3 Enantioselective Photoreactions in the Solid State

As a result of molecular movement that is possible within the solid phase, chemical reactions in the solid-state are manifold and often proceed more efficiently and selectively than they do in solution, if the latter are even possible. An extensive review of solid-state reactions covering the period ~1980–2000 describes a vast range of thermal and photoreactions that have been performed in the absence of solvent [27]. In the case of photoreactions, these include processes as diverse as dimerisations, polymerisations, cyclisations, isomerisations, solvolyses, photodecarbonylations, photoadditions and enantioselective photoreactions. In the latter class, three categories were highlighted in the cited review, namely photoreactions directly involving chiral substrate molecules, those involving achiral substrates within chiral inclusion crystals, and those involving achiral molecules within their chiral crystals.

Here, a few more recent studies of enantioselective solid-state photoreactions are described that specifically involve the TADDOL-type diol hosts discussed in earlier sections. Again, the emphasis is on the contribution of X-ray studies to the understanding of the mechanisms of these processes.

A significant study of intramolecular rotation and photocyclisation of an anilide in its inclusion crystal was carried out by monitoring the process as a partial single-crystal to single-crystal transformation [28]. The overall reaction, shown in Scheme 7, represents photoirradiation of *N*-methyl-*N*-{(*E*)-methylmethacryloyl}anilide **34** in the form of its inclusion complex with the chiral TADDOL host (–)-**4**, to give the cyclised product **35**. Photoirradiation was carried out with high-pressure Hg lamps. Examination of the X-ray structure of the inclusion crystal (–)-**4**·**34** revealed the molecular conformation adopted by the included guest **34**, showing that the initial helical orientation of the methylmethacryl moiety is not stereochemically well disposed for achieving the overall reaction. This necessitates significant intramolecular rotation of the moiety to precede the cyclisation process. Photoirradiation of single crystals was therefore carried out, with X-ray diffraction being used to monitor the process.

Scheme 7 Photoirradiation of the anilide 34 in the form of its inclusion complex with the chiral TADDOL host (-)-4, yielding the cyclised product 35 [28]

Diffraction intensity decreased with time and after 143 h of photoirradiation, X-ray intensities were recorded and the structure of the disordered product determined. This contained the cyclised product (–)-35 with occupancy 26%.

From a careful study of the product and the reaction cavity in the inclusion crystal, it was possible to deduce that the intramolecular rotation required to effect cyclisation was thermally induced by the photoirradiation. It was proposed that following flattening of the helical side-chain and formation of the six-membered ring, conrotation of H atoms at positions 1 and 6, and a suprafacial 1,5-hydrogen shift occur, yielding the product (–)-35. An essential feature of the proposed mechanism is expansion of the reaction cavity resulting from photoirradiation, which then permits a 180° rotation around a carbon-carbon bond of the guest side-chain in the solid-state. The unit cell volumes of the crystals before and after photoirradiation were reported as 940.2(2) and 952.2(5) ų respectively. The pivotal role of the host molecules in this process was identified as one of maintaining the crystal lattice during the photoreaction.

Analogous mechanistic studies were reported for the enantioselective photocyclisation of acrylanilides **36–38** and *N*-ethyl-*N*-methylbenzoylformamide **39** (Scheme 8) in inclusion crystals with TADDOL hosts (R,R)-(-)-[trans]-2,3-bis  $(\alpha$ -hydroxydiphenylmethyl)-1,4-dioaxaspiro-[4,4]nonane and -[4,5]decane [29].

Scheme 8 Acrylanilides 36–38 and *N*-ethyl-*N*-methylbenzoylformamide 39 undergoing enantioselective photocyclisation in inclusion crystals with TADDOL hosts [29]

The X-ray analyses of the inclusion crystals confirmed that the high stereo- and enantioselectivities of the photocyclisations observed in this series are due to the detailed natures of the chiral crystalline environments provided by the respective host compounds.

Novel TADDOL host compounds **40a** and **40b** derived from tartaric acid were respectively employed in studies of the enantioselective photoreaction of 4-isopropyltropolone methyl ether [30] and the enantioselective photocyclisation of 1-alkyl-2-pyridones to  $\beta$ -lactams (Scheme 9) [31]. In both cases, X-ray analysis of representative inclusion crystals was pursued in order to understand the selectivities involved in these reactions.

Scheme 9 Enantioselective photoreaction of 4-isopropyltropolone methyl ether [30] (top) and the enantioselective photocyclisation of 1-alkyl-2-pyridones to  $\beta$ -lactams [31] (bottom)

The X-ray structure of the 1:1 complex between host **40b** and **41b** (R = n-Bu) revealed strong intermolecular hydrogen bonding ( $O \cdot \cdot \cdot O$  2.671(8) Å) between the carbonyl oxygen atom of the pyridone guest molecule and an oxygen atom of a hydroxyl group of the host molecule. A feature of the host molecule, manifested in this complex, is its ability to accommodate planar ring systems of guest molecules. The guest pyridone ring is accordingly inserted between host aromatic rings, overlapping efficiently with one of them, while the n-butyl chain plays an anchoring role in spatial orientation of the guest. The resulting restrictions in guest molecular movement could thus be used to rationalise the proposed detailed photoreaction pathway occurring when two guest pyridone carbon atoms change their configurations from  $sp^2$  to  $sp^3$  with consequent repulsion between the attached H atoms and the host phenyl ring. During photoreaction, the pyridine carbon atoms must thus move away from the host phenyl ring to generate the observed product.

Photodimerization of coumarins has been the subject of several investigations that have been supported by complementary X-ray studies. For example, the enantioselective [2+2] photodimerization reactions of coumarin and thiocoumarin in their inclusion compounds with TADDOL-type hosts as well as diols related to 1 (Scheme 1), featuring single-crystal to single-crystal transformations, were reported in 2000 [32]. More recently, it was shown that the enantioselective [2+2] photodimerization reaction of coumarin also proceeds in homogeneous solution [33]. This instance of an enantioselective photoreaction occurring in solution in the presence of host compounds is relatively rare.

Recent studies employing the catalytic properties of TADDOL-type molecules in enantioselective processes include the asymmetric synthesis of rocaglamides (natural products containing a cyclopent[b]tetrahydrobenzofuran skeleton) [34] and metal-free catalysis for the promotion of highly diastereo- and enantioselective Mukaiyama aldol reactions [35]. In the latter study, it was hypothesised that the high enantioselectivity observed in certain reactions of this type in the presence of TADDOL hosts could be accounted for by the intermediacy of a highly ordered transition state between the former and the aldehyde reactant. Successful isolation of a crystalline inclusion complex between host rac-44 and *p*-anisaldehyde 45 (Scheme 10) and its subsequent X-ray structure determination revealed

Scheme 10 TADDOL host rac-44 and *p*-anisaldehyde 45 which form an inclusion crystal [35]

Ar =1-naphthyl, R = Me

the usual presence of an intramolecular OH···O hydrogen bond in the host molecule, and more pertinent to the above hypothesis, an intermolecular H-bond between the 'free' host hydroxyl group and the carbonyl oxygen atom of p-anisaldehyde.

This structural result lends strong support to the authors' premise [35] that activation of the carbonyl group can occur through a single-point hydrogen bond to the catalyst molecule. One of their conclusions from the reported studies, namely that TADDOL "may well be a 'privileged scaffold' for asymmetric catalysis mediated by hydrogen bonding", is very significant.

# 2.4 Inclusion Ability of N,N',N"-Trihydroxyisocyanuric Acid and Macrocyclic Triphenolic Host Molecules

As mentioned in the Introduction, host molecules based on heterocyclic frameworks that contain three hydroxyl/phenolic sensor groups are encountered much less frequently than those with two. This section is not intended to be comprehensive but merely highlights two types of compound falling into this category that the present authors have recently investigated for their potential as selective hosts. The first is N,N',N"-trihydroxyisocyanuric acid 46 (Fig. 11). Despite the presence of multiple hydrogen bond donor and acceptor functions in this molecule, the authors found no previous reports on its behaviour as a host molecule in inclusion chemistry. Solutions of 46 in several neat solvents yielded crystals of their respective inclusion compounds, namely 46.3(N,N-dimethylformamide), 46.N,N-dimethylacetamide, 46·1.5(4-methylpyridine), 46·1.5(2-hydroxypyridine), and 46·2H<sub>2</sub>O [36]. The first of these, containing DMF as guest, was shown by NMR spectroscopy to have the 1:3 host-guest composition indicated above, but thermogravimetry between ambient temperature and ~150 °C (which involved more prolonged exposure of the inclusion crystals to the atmosphere prior to analysis) indicated a stoichiometry of 1:2. This suggested higher lability of one of the three included guest molecules. The X-ray

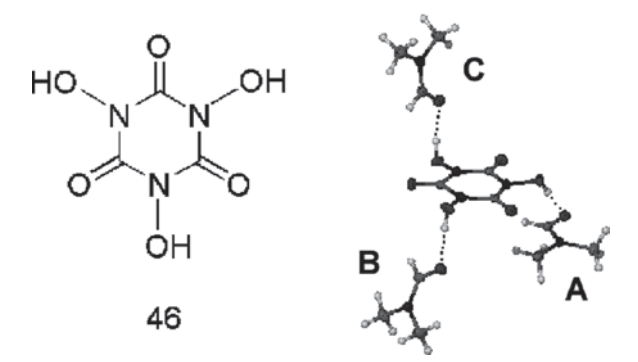


Fig. 11 Chemical structure of the triphenolic host 46 (*left*) and the X-ray structure of the 1:3 H-G asymmetric unit in the crystal of its inclusion complex with the guest DMF [36]

100 M. Caira and K. Tanaka

structure (Fig. 11) showed that each hydroxyl group of **46** is a donor in a hydrogen bond to the carbonyl oxygen atom of a DMF molecule. However, the uniformity of the hydrogen bond strengths reflected in the O···O distances (2.553(2)–2.566(2) Å) could not explain the tendency for apparent stepwise guest loss from the crystal.

Examination of crystal packing diagrams revealed that host molecules are bounded by two distinct sets of layers, one of these (parallel to the crystal 001 planes) containing B and C guest molecules (Fig. 11), while the other (parallel to 010) contains A and C guest molecules. The observed pattern of desolvation was thus finally attributed to the non-uniform distribution of the guest molecules within topologically distinct layers, which presumably would affect the relative rates of diffusion of guest molecules out of the inclusion crystal.

The second type of triphenolic host molecule featured briefly here is exemplified by the compounds 47 and 48 (Scheme 11). The synthesis and X-ray structure of the hexaamine triphenolic macrocycle 47 was reported a decade ago [37]. This compound crystallises in the space group R3 with Z = 3, requiring threefold molecular symmetry. In its unsolvated/uncomplexed state, there is intramolecular hydrogen bonding (O-H···N, N-H···O and N-H···N) that stabilises the macrocyclic conformation. The more rigid oxidised analogues 48 (hexaimine triphenolic Schiff base macrocycles) should be less versatile than 47 as host molecules. The affinity for lanthanide ions by the host 48 (R = Me) has been demonstrated recently and the X-ray structure of the europium complex was reported [38]. These macrocyclic compounds are potential chiral host molecules that could also find application in the separation of solvent mixtures or the resolution of racemic organic guests. Studies to investigate the inclusion ability of analogues of 48 are underway in our laboratory and there is certainly preliminary evidence of solvent inclusion within the cavities of some of these molecules. Given the lack of structural data for such hosts and their inclusion complexes in the literature, X-ray analysis will be an important supportive technique in this study.

Scheme 11 Representative marocyclic host compounds containing three -OH sensor groups [37]

# 3 Concluding Remarks: Status of the Research and Future Directions

The success of enantioselective inclusion complexation (EIC) has been demonstrated exhaustively by researchers specialising in this field and the examples provided in the foregoing sections support this opinion. On the other hand, to maintain a balanced view, one is aware of the fact that not all researchers engaged in enantiomeric separation are equally optimistic about the scope of the EIC approach [39]. However, as noted earlier, with such novel developments as EIC-organic solvent nanofiltration, the scope of EIC can be extended to the resolution of non-volatile racemates and even to large-scale applications [11]. Certainly, the occurrence of enantioselective photoreactions in the solid state that do not have counterparts in solution places EIC in an unchallenged position as a method for producing novel products and research in this area is consequently likely to proceed at an accelerated pace in the future. The chiral hydrogen-bond donor role of TADDOLs in EIC is also likely to become more prominent following the recent optimistic comments by McGilvra et al. [35] suggesting that their further investigation should lead to 'exciting new developments in asymmetric catalysis'.

In virtually all of the selected studies described above, X-ray analysis has featured as an important supportive technique. Thus, developments in this field (including, e.g., the increasing rate of diffraction data capture made possible by the use of synchrotron radiation and the increasing numbers of crystal structure determinations from powder diffraction data) should ensure that X-ray analysis maintains its status as a primary contributor in the investigation of EIC and solid-state photoreaction studies.

**Acknowledgements** MRC thanks the University of Cape Town and the National Research Foundation for research support. Any opinion, findings and conclusions or recommendations expressed in this material are those of the authors and therefore the NRF does not accept any liability in regard thereto.

#### References

- Toda F (1996) Diol, bisphenol, and diamide host compounds. In: McNicol D D, Toda F, Bishop R (eds) Comprehensive supramolecular chemistry, chap 15, vol 6. Oxford, Pergamon, pp 465–516
- 2. Seebach D, Beck AK, Heckel A (2001) Angew Chem Int Ed 40:92-138
- 3. Seebach D, Hungerbühler E (1980) In: Scheffold E (ed) Modern synthetic methods, vol 2. Salle, Saüerlander, pp 91-171
- 4. Toda F, Tanaka K (1988) Tetrahedron Lett 29:551-554
- 5. Weber E, Dörpinghaus N, Goldberg I (1988) J Chem Soc Chem Comm 1566-1568
- 6. Nassimbeni LR, Niven ML, Tanaka K, Toda F (1991) J Chem Crystallogr 21:451-457
- Vinogradov MG, Kurilov DV, Chel'tsova GV, Ferapontov VA, Heise GL (2003) Mendeleev Commun 13:124–125
- 8. Novák T, Schindler J, Ujj V, Czugler M, Fogassy E, Keglevich G (2006) Tetrahedron Asymmetry 17:2599–2602

102 M. Caira and K. Tanaka

- 9. Kaupp G (1994) Angew Chem Int Ed Engl 33:728-729
- 10. Toda F, Takumi H (1996) Enantiomer 1:29-33
- 11. Ghazali NF, Ferreira FC, White AJP, Livingston AG (2006) Tetrahedron Asymmetry 17: 1846–1852
- 12. Gajda J, Jeziorna A, Ciesielski W, Potrzebowski WM, Prezdo WW, Potrzebowski MJ (2007) Solid State Nucl Magn Reson 31:153–161
- 13. Hirano S, Toyota S, Toda F (2004) Chem Commun 2354-2355
- 14. Hirano S, Toyota S, Kato M, Toda F (2005) Chem Commun 3646–3648
- 15. Kato M, Tanaka K, Toda F (2001) Supramol Chem 13:175-180
- 16. Boese R, Antipin MY, Blaeser D, Lyssenko KA (1998) J Phys Chem B 102:8654
- 17. Urbanczyk-Lipkowska Z, Yoshizawa K, Toyota S, Toda F (2003) CrystEngComm 5:114–116
- Olszewska T, Milewska MJ, Gdaniec M, Małuszyńska H, Połoński T (2001) J Org Chem 66:501–506
- Olszewska T, Pyszno A, Milewska MJ, Gdaniec M, Połoński T (2005) Tetrahedron Asymmetry 16:3711–3717
- 20. Tsunoda T, Kaku H, Nagaku M, Okuyama E (1997) Tetrahedron Lett 38:7759–7760
- Kaku H, Ozako S, Kawamura S, Takatsu S, Ishii M, Tsunoda T (2001) Heterocycles 55:847–850
- 22. Kaku H, Takaoka S, Tsunoda T (2002) Tetrahedron 58:3401–3407
- Novák T, Ujj V, Schindler J, Czugler M, Kubinyi M, Mayer ZA, Fogassy E, Keglevich G (2007) Tetrahedron Asymmetry 18:2965–2972
- 24. Tanaka K, Takenaka H, Caira MR (2006) Tetrahedron Asymmetry 17:2216-2219
- Urbanczyk-Lipkowska Z, Fukuda N, Tanaka K (2007) Tetrahedron Asymmetry 18:1254–1256
- 26. Tanaka K, Kukichi D, Caira MR (2006) Tetrahedron Asymmetry 17:1678-1683
- 27. Tanaka K, Toda F (2000) Chem Rev 100:1025-1074
- 28. Hosomi H, Ohba S, Tanaka K, Toda F (2000) J Am Chem Soc 122:1818–1819
- 29. Ohba S, Hosomi H, Tanaka K, Miyamoto H, Toda F (2000) Bull Chem Soc Jpn 73:2075
- 30. Tanaka K, Nagahiro R, Urbanczyk-Lipkowska Z (2001) Org Lett 3:1567–1569
- 31. Tanaka K, Fujiwara, Urbanczyk-Lipkowska Z (2002) Org Lett 4:3255–3257
- 32. Tanaka K, Mochizuki E, Yasui N, Kai Y, Miyahara I, Hirotsu K, Toda F (2000) Tetrahedron 56:6853–6865
- 33. Tanaka K, Fujiwara T (2005) Org Lett 7:1501–1503
- 34. Gerard B, Sangji S, O'Leary D, Porco JA Jr (2006) J Am Chem Soc 128:7754–7755
- 35. McGilvra JD, Unni AK, Modi K, Rawal VH (2006) Angew Chem Int Ed 45:6130-6133
- 36. Caira MR, Fujiwara T, Tanaka K (2006) Anal Sci 22:x69-x70
- 37. Korupoju SR, Zacharias PS (1998) Chem Commun 1267–1268
- 38. Paluch M, Lisowski J, Lis T (2006) Dalton Trans 381-388
- Müller S, Afraz MC, de Gelder R, Ariaans GJA, Kaptein B, Broxterman QB, Briggink A (2005) Eur J Org Chem 1082–1096

Top Heterocycl Chem (2009) 18: 103-118

DOI: 10.1007/7081\_2008\_16

© Springer-Verlag Berlin Heidelberg 2009

Published online: 14 March 2009

# Supramolecular Structures and Nanoassemblies of Oligothiophenes and Tetrathiafulvalenes

#### Masahiko Iyoda, Tohru Nishinaga, and Masayoshi Takase

Abstract Supramolecular nanostructures derived from self-assembling oligothiophenes and tetrathiafulvalenes are reviewed. The two representative sulfur-containing  $\pi$ -electron systems have been extensively studied for their application in material sciences and have been shown to exhibit their excellent characteristics in conductive and optical properties. In the last decade, several researchers have developed these versatile  $\pi$ -electron systems as soft materials by means of substituents that cause weak intermolecular interactions. As the result, unique nanostructures such as fibers and particles endowed with characteristic conductive and optical properties have been demonstrated. These techniques may offer a bottom-up approach to construct future organic and molecular electronics.

**Keywords** Molecular electronics, Nanostructure, Oligothiophenes, Tetrathiafulvalenes, Self-assembly

#### Contents

1	Introduction		
2	Oligothiophenes		
	2.1	Substituents for Self-Assembling Oligothiophenes	104
	2.2	Organogels	105
	2.3	Fibers, Nanocapsules, and Nanoparticles	107
	2.4	Expanded Oligothiophenes	109
3	Tetrathiafulvalene		
	3.1	New Conductive Materials	111
	3.2	TTF Fibers with Hydrogen-Bonding Sites	111
	3.3	Fibers of TTF-Crown Ether Composites	113
	3.4	Fibers of Simple TTF-Esters	114
	3.5	TTF and its Oligomers Without Hydrogen-Bonding Sites	115
4		mary and Outlook	116
Re	ferenc	res	116

M. Iyoda (M), T. Nishinaga, and M. Takase

Department of Chemistry, Graduate School of Science and Engineering,

Tokyo Metropolitan University, Hachioji, Tokyo 192-0397, Japan

e-mail: iyoda@tmu.ac.jp

#### 1 Introduction

Self-assembly of organic  $\pi$ -conjugated systems into complex, organized supramolecular structures via rather weak intermolecular interactions is a promising way to realize functional molecular materials [1–3]. Recently, many intermolecular interactions such as hydrogen bonding [4–6], metal coordination [7–11], charge transfer (CT) interaction [12, 13], and  $\pi$ - $\pi$  stacking [14] have been utilized to construct desired supramolecular architectures such as fibers, ribbons, tapes, nanotubes, and nanoparticles [1, 15–19]. It is known that typical  $\pi$ -donors such as oligothiophenes and tetrathiafulvalenes (TTFs) easily form a face-to-face stacked structure by the use of  $\pi$ - $\pi$  stacking and dipole-dipole interactions [20, 21]. The stacking interactions of oligothiophenes and TTFs in the oxidized state are energetically more favorable owing to an additional electronic exchange interaction [22, 23]. Thus, organic conductors and superconductors based on oligothiophenes and TTFs are constructed using cooperative dipole-dipole,  $\pi$ - $\pi$  stacking, and exchange interactions [24, 25].

Research on the supramolecular architectures of oligothiophenes, TTFs, and TTF oligomers started in 1994 [26] and developed during the past decade. In this chapter, therefore, supramolecular structures and nanoassemblies constructed by oligothiophenes, TTFs, and TTF oligomers are summarized from the viewpoint of new functional materials.

#### 2 Oligothiophenes

Oligothiophenes have been the most well-studied  $\pi$ -conjugated oligomers owing to their excellent characteristics in organic electronics in addition to the versatility in chemical modification of the thiophene ring. By taking advantages of these features, construction of supramolecular fibers, capsules, and particles involving an oligothiophene core have been demonstrated in the last decade. In this section, the supramolecular nanostructures consisting of oligothiophenes are reviewed. Some of these soft materials have been shown to exhibit functions derived from the characteristic  $\pi$ -systems.

## 2.1 Substituents for Self-Assembling Oligothiophenes

It is well known that utilization of weak interactions such as ionic interaction, hydrogen bond, van der Waals force (or London dispersion force), and  $\pi$ – $\pi$  interaction (special case of dispersion force) is essential for constructing supramolecular systems. For molecular design of the self-assembling oligothiohenes that form nanostructures [27–39], substituent units of amide, urea, long alkyl and ethylene glycol chains, and the cholesteryl group have been chosen (Fig. 1). In the case of the amide and urea groups, intermolecular hydrogen bonds play a critical role for the self-assembly,

Fig. 1 Substituent groups for self-assembling oligothiophenes

while van der Waals force is important for the other groups. In addition to  $\pi$ – $\pi$  interactions between the oligothiophene cores, the combined weak forces by these substituents cause supramolecular architectures of fibers, particles, and capsules.

#### 2.2 Organogels

To construct organogels endowed with unique optical, electronic, and electrochemical functions, several oligothiophene-based organogelators have been successfully designed. They are thiophene and bithiophene 1 having substituents of the combination of urea and long alkyl chain [27], terthiophene 2 having *N*-octadecylamide [28], dendron rod-coil type quaterthiophene 3 [29], and quater-, quinque-, and sexithiophenes 4 having a cholesterylamide group [30] (Fig. 2).

The conditions of gelation for these compounds are summarized in Table 1. For these gels and xerogels, fibrous wires or ribbons were formed as usually observed in other gel systems. These aggregates are entangled, which make clusters of solvent molecules immobilized to result in the formation of gels. As concerns the structure of the fibrous aggregates of the bis-urea compounds 1, the breadth and length of fibers are 2-10 and 20-100  $\mu m$ , respectively. From IR spectroscopic analysis and X-ray powder diffraction, the fibers were shown to have a lamellar structure in which intermolecular hydrogen bonds by urea groups are present [27]. In another experiment, the maximum length of fiber 1 was shown to reach up to 500  $\mu m$  upon evaporation from 1-octanol solution on the SiO<sub>2</sub> surface at 70 °C [31].

In the case of 2, the presence of amide group as well as side octyl chain is essential for the gelation. IR and NMR measurements also revealed that the intermolecular hydrogen bonds operated in the gels, while the octyl groups are necessary for enhancing the solubility in common organic solvents [28]. Thus, compound 2a and 2b with

Fig. 2 Oligothiophene-based organogelators

Table 1 Gelation conditions of oligothiophenes 1-4

Compound	Solvent	Method	Concentrations
1	1,2-Dichloroethane	Heating (50–100 °C) → cooling	_a
2c	Ethanol	Heating $\rightarrow$ cooling (25 °C, 30–160 min)	4.2 g dm <sup>-3</sup>
2c	n-Butanol	Heating $\rightarrow$ cooling (25 °C, 30–160 min)	5.3 g dm <sup>-3</sup>
2d	n-Heptane	Heating $\rightarrow$ cooling (25 °C, 30–160 min)	5.3 g dm <sup>-3</sup>
2d	n-Tetradecane	Heating $\rightarrow$ cooling (25 °C, 30–160 min)	3.6 g dm <sup>-3</sup>
2e	n-Heptane	Heating $\rightarrow$ cooling (25 °C, 30–160 min)	5.3 g dm <sup>-3</sup>
2e	n-Tetradecane	Heating $\rightarrow$ cooling (25 °C, 30–160 min)	3.6 g dm <sup>-3</sup>
3	Toluene:THF (30:1)	Heating (110 °C) $\rightarrow$ cooling (rt)	1 wt%
4a	Benzene	Heating $\rightarrow$ cooling (25 °C, 2 h)	2.0 g dm <sup>-3</sup>
4a	Chloroform	Heating $\rightarrow$ cooling (25 °C, 2 h)	2.1 g dm <sup>-3</sup>
4a	1-Octanol	Heating $\rightarrow$ cooling (25 °C, 2 h)	2.0 g dm <sup>-3</sup>
4a	DMSO	Heating $\rightarrow$ cooling (25 °C, 2 h)	15 g dm <sup>-3</sup>
4b	Benzene	Heating $\rightarrow$ cooling (25 °C, 2 h)	2.5 g dm <sup>-3</sup>
4b	Anisole	Heating $\rightarrow$ cooling (25 °C, 2 h)	1.7 g dm <sup>-3</sup>
4b	THF	Heating $\rightarrow$ cooling (25 °C, 2 h)	5.0 g dm <sup>-3</sup>
4b	Cyclohexane	Heating $\rightarrow$ cooling (25 °C, 2 h)	10 g dm <sup>-3</sup>
4c	Diphenyl ether	Heating $\rightarrow$ cooling (25 °C, 2 h)	2.0 g dm <sup>-3</sup>
4c	Benzonitrile	Heating $\rightarrow$ cooling (25 °C, 2 h)	3.3 g dm <sup>-3</sup>
<u>4c</u>	Pyridine	Heating $\rightarrow$ cooling (25 °C, 2 h)	6.7 g dm <sup>-3</sup>

<sup>&</sup>lt;sup>a</sup>Not reported

shorter alkyl group on nitrogen of amide did not form gels, indicating that the van der Waals interactions of long alkyl chains are important. Interestingly, **2c** with moderate length of the alkyl chain was shown to form gels only in polar solvents of alcohol, whereas **2d–e** with long alkyl chains form gels only in apolar solvents of alkanes.

On the other hand, the fibrous aggregates of **3** and **4** show a high aspect ratio. For **3**, a uniform diameter of 9.3 nm was observed in the fiber, which is consistent with the fully extended length of two molecules [29], while unimolecular helical aggregates were observed by means of AFM in the case of **4a** [30]. The left-handed helical sense in aggregates of **4a** is biased, and the pitch of the helical structure is about 76–100 nm, which is estimated to be constructed by 200–270 molecules.

For these soft materials, the unique functions derived from the oligothiophene core have been demonstrated. In the case of 1, conductive properties were studied with the pulse-radiolysis time-resolved microwave conductivity technique. From the measurements, the sum of the mobilities of the positive and negative charge carriers  $\Sigma \mu_{min}$  was determined to be  $1 \times 10^{-3}$  cm<sup>2</sup> V<sup>-1</sup> s<sup>-1</sup> for 1a and  $5 \times 10^{-3}$  cm<sup>2</sup> V<sup>-1</sup> s<sup>-1</sup> for 1b [27]. The mobilities are much higher than the values obtained by the same technique for a cyclohexyl end-capped bithiophene ( $4 \times 10^{-4}$  cm<sup>2</sup> V<sup>-1</sup>) and unsubstituted quaterthiophene ( $1 \times 10^{-3}$  cm<sup>2</sup> V<sup>-1</sup>) [32], clearly indicating that the 1-stacked structure of the aggregates of 1 enhanced the mobility.

Similar enhancement of conductivity was also observed in **3**. The iodine-doped film cast from the self-assembled state (see Table 1) indicated conductivities of  $7.9 \times 10^{-5}$  S cm<sup>-1</sup>, whereas the film cast from THF in which self-assembly did not occur showed only  $8.0 \times 10^{-8}$  S cm<sup>-1</sup>. In addition, the parallel alignment of the aggregated nanofiber of **3** was accomplished by means of alternating current electronic field where the aggregates become charged and oscillate due to electrophoresis and shear forces operate to align parallel to the electric field lines [29].

On the other hand, **4** showed reversible thermochromism through the sol–gel phase transitions. Upon the formation of gels at room temperature, the longest absorption maxima corresponding to the  $\pi$ – $\pi$ \* transition of oligothiophene moieties were shifted hypsochromically, suggesting the formation of H-aggregate in the gels. Also sol–gel phase transition by redox stimuli was demonstrated for **4c**. When **4c** gel in TCE was oxidized with FeCl<sub>3</sub>, the red gel turned into a dark-brown solution, which turned back to the red gel by adding ascorbic acid as reducing reagent [30].

## 2.3 Fibers, Nanocapsules, and Nanoparticles

Similar fiber formation as observed in the gels described above was also demonstrated for sexithiophene 5 having penta(ethylene glycol) chains at both ends [33, 34], oligothiophene dendrimers 6 [35], and septithiophene and its fullerene dyad 7 [36] (Fig. 3), although gel formation from these molecules has not been reported. On graphite surfaces, both 5 and 6 form nanowire, where the interaction between the molecules and the graphite surface appears to play a significant role. Also, both oligothiophene 7a and its dyad 7b form fiber-like nanostructures on ITO/PEDOT–PSS substrates.

5a (R = H)
b (R = CH<sub>3</sub>, SS enantiomer)
c (R = CH<sub>3</sub>, RR enantiomer)
$$C_{e}H_{13}$$

Fig. 3 Oligothiophenes forming nanostructures

On the surface of a silicon wafer, **5** also forms fibril nanowire. Interestingly, the fibers of **5b** present a left-handed helical structure [33], whereas achiral analog **5a** does not form chiral fibrils under the same conditions [34]. From these results, one may suppose that the helical structure stems from the chiral side chain of **5b** with (*R*, *R*)-configuration. Unexpectedly, however, the fibers of **5c** with (*S*, *S*)-configuration also form only left-handed helical structures, even though the CD spectra of the solid state assemblies of **5b** and **5c** on a silica glass substrate show a mirror image [34]. Thus, it is concluded that the hydrophilicity of the silicon surface plays a definitive role in the expression of chirality in the fiber.

When a solution of dendrimer **6** was casted on mica surface, globular aggregates were observed by atomic force microscope [35]. The size of the aggregates varied due to the different degrees of intermolecular  $\pi$ – $\pi$  interactions of hydrophobic **6** on a hydrophilic mica surface. However, the inner structure of the aggregates is not certain from the measurements. On the other hand, self-assembly of **5b** in 2-propanol [37] or in butanol [38] also leads to spherical nanostructures. The average diameters of the capsules from 2-propanol are 55 nm at 20 °C and 125 nm at 60 °C. A similar

Fig. 4 Quaterthiophene forming vesicle

size is also reported for the capsule from butanol, but the size become much smaller (20 nm) after depositing a diluted ( $2 \times 10^{-5}$  M) solution. The assemblies are hollow spheres, which were shown to be deformed by a magnetic field due to a large anisotropy in the diamagnetic susceptibility resulting from the sexithiophene moiety [37]. Similar oligothiophene-based vesicles in water have also been reported using quaterthiophene 8 (Fig. 4) [39].

In the case of 7, thermal annealing on ITO/PEDOT-PSS substrates enhanced the structural order, and fibrous nanostructures were observed with AFM. By taking advantage of the self-assembling properties of dyad 7b, the photovoltaic characteristics of devices fabricated with 7b were compared with those fabricated with a mixture of 7a and fullerene derivative in which the formation of nanostructures was hampered by the fullerene. The dyad device showed better power conversion efficiency (0.15%) and external quantum efficiencies (31% at 440 nm) than those (0.09, 12% at 420 nm) of the mixture device [36].

## 2.4 Expanded Oligothiophenes

Similar nanostructures have also been constructed from expanded oligithiophenes, such as oligomers and polymers of oligothiophenes with indenofluorene and fluorene [40] and giant macrocycles composed of thiophene, ethylene, and acetylene building units [41–43] (also, unpublished results from this laboratory). Giant macrocycles **9a–e** are regarded as an infinite π-conjugated system with an inner cavity [44–46], and hence giant macrocycles have attracted recent attention from the viewpoint of single-molecule electronics and unique nanostructures corresponding to the ring size (Fig. 5). Fully conjugated giant macrocycles **9a–e** with 1.8–6.0 nm inner cavity and 3.3–7.5 nm outside molecular diameters were synthesized by McMurry coupling reaction of the linear 5-mer-dialdehyde [41, 42]. Similar McMurry coupling of the linear 6-mer-dialdehyde produced the corresponding 12-, 18-, 24-, and 30-mers [43].

Interestingly, the morphology of giant macrocycles **9a–e** depends on the ring size. Thus, the 10-mer **9a** afforded single crystals, whereas 15- and 20-mers self-aggregate in the solid state to form fibrous materials that are ca. 200 nm thick and more than 1 mm long. In contrast to single crystal and fiber formation of **9a–c**, larger macrocycles **9d,e** form nanoparticles with a size of 300–800 nm (Fig. 6).

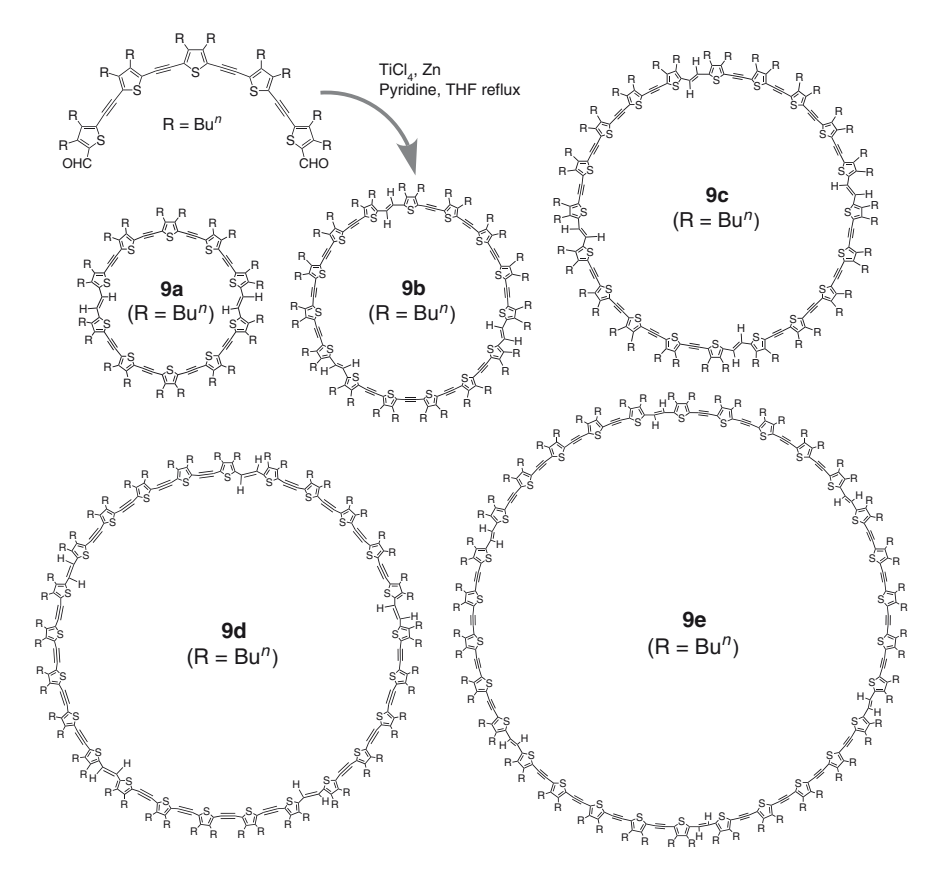


Fig. 5 McMurry coupling for expanded oligothiphenes 9a-e

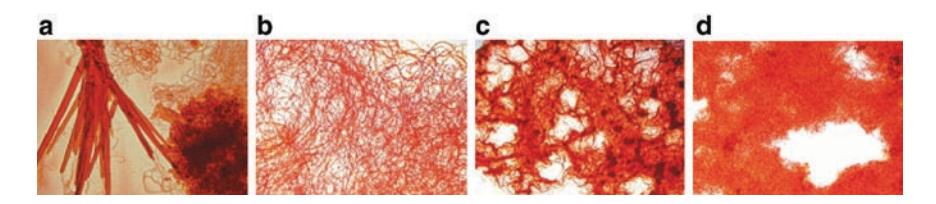


Fig. 6 Microscopic images of 9a (a), 9b (b), 9c (c), and 9d (d) with 1000× magnification [48]

#### 3 Tetrathiafulvalene

Among sulfur-containing heterocycles, tetrathiaflyalene (TTF) and its analogs have been intensively studied due to their unique  $\pi$ -donor properties [47–53]. It is well known that, though TTF has 14  $\pi$ -electrons, it is categorized as a non-aromatic

Fig. 7 Sequential oxidation and reduction of TTF

compound according to Hückel's rule owing to the lack of cyclic conjugation [54, 55]. In contrast, the radical cation and dication species are aromatic as a result of the  $6\pi$ -electrons of the 1,3-dithiolium cation. They are thermally stable and can be reduced back to the neutral species reversibly (Fig. 7). More importantly, although dimeric TTF/TTF is weakly stable through  $\pi$ - $\pi$  stacking and S···S interaction, the dimeric TTF/TTF<sup>+</sup> is strongly stabilized to produce a mixed-valence form, and therefore allow electric conductivity [56, 57]. Furthermore, two cation-radicals TTF<sup>2+</sup>/TTF<sup>2+</sup> attractively form  $\pi$ -dimer in solution, leading to the formation of a Mott-insulating semi-conductor in the solid state [58, 59].

#### 3.1 New Conductive Materials

On account of the above-mentioned unique properties of TTF, chemical modification and oligomerization of TTF have been carried out in order to explore new building blocks [53, 60, 61]. Especially, since the high electric conductivity in a chloride salt of TTF and the metallic behavior of the charge transfer (CT) complex of TTF and tetracyanoquinodimethane (TCNQ) were discovered, many kinds of TTF and their analogs have been synthesized from the view point of material and physical science [62, 63]. In general, however, conductive molecular complexes are supposed to be studied in a single-crystal state, which would be problematic in processing for material application. To solve this problem, supramolecular chemistry has currently been applied to this area, which brings the development of "soft materials" of TTF. Thus, in this section, we highlight the recent progress of supramolecular architectures of TTFs, especially fibrous structures, and the properties that are expected to be applicable to organic electronics.

## 3.2 TTF Fibers with Hydrogen-Bonding Sites

Amphiphilic molecules having solvophilic and solvophobic sites may form micelles or bilayer membranes in organic solvents. The initial formation of these mesophases sometimes results in the construction of nanostructures such as fibers, ribbons, tapes, and tubes utilizing supramolecular interactions as the driving force. One of the most efficient interactions for constructing one-dimensional supramolecular

fibers from organic molecules is hydrogen bonding between amphiphilic molecules. To the best of our knowledge, the first example of TTF fiber having hydrophobic alkyl groups and hydrogen bonding sites was reported by Jørgensen and Bechgaad in 1994 [26, 64]. Bis-arborol-TTF derivative 10 with long alkyl chains and amide groups formed string-like superstructure (i.e., fibers) from its aqueous solution (Fig. 8). Although no conductivity measurement of their fibers was conducted, this work inspired many researchers to develop other TTF fibers containing hydrogenbonding sites and a long alkyl chain. In 2005, three research groups independently reported their successful studies based on a similar concept, where their TTF derivatives possess either an amide or urea group as a hydrogen-bonding site together with a long alkyl chain. These TTF derivatives were expected to form gels or fibers utilizing mainly hydrogen-bonding interaction, together with weaker van der Waals,  $\pi$ - $\pi$  stacking, and S···S interactions (11 [65], 12 [66], 13 [67], Fig. 8). Among them, for 13 it was demonstrated that the doping of fibers by iodine vapor resulted in the formation of charge transfer states exhibiting semiconductivity of ca. 10<sup>-5</sup> S cm<sup>-1</sup>, which was the first example where electrical conductivities were measured after doping [67].

Very recently, Amabilino et al. reported a more sophisticated system based on **14**. Thus, **14** formed gel from hexane, and its xerogel showed a high conductivity by doping with iodine vapor and successive annealing procedure [68]. Also, they demonstrated that incorporating a small amount (1 wt%) of TTF-capped gold nanoparticle **15-**Au into **14** produced metallic fibers (ca. 10 S cm<sup>-1</sup>) in a doped xerogel without annealing (Fig. 9) [69]. In the latter case, nanoparticles organize the secondary structure of the fibers, which show metallic conductivity after doping.

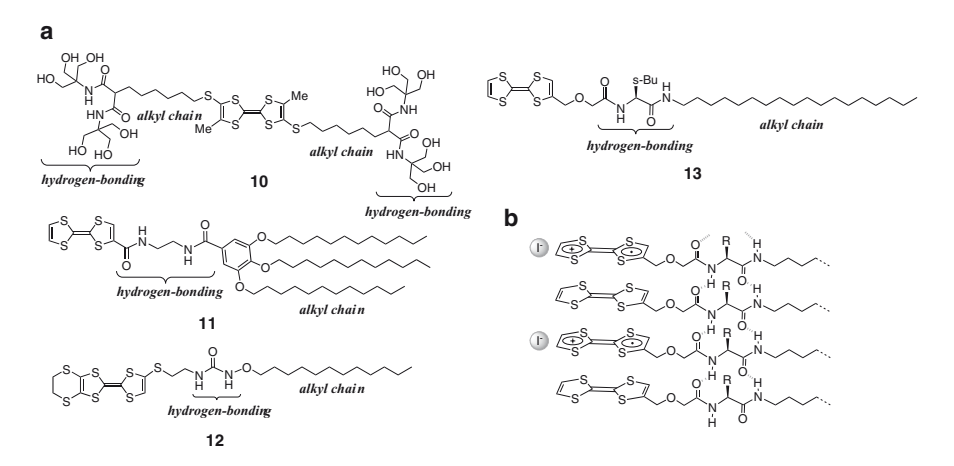


Fig. 8 a Chemical structures of TTF derivatives 10–13 forming hydrogen-bonding fibers. b Segregated-stacking structure of a mixed-valence state of 13 after iodine doping

Fig. 9 Chemical structure of TTF derivative 14 and a schematic drawing of gold nanoparticle 15-Au

Fig. 10 Chemical structures of TTF derivatives 16 and 17 forming non-hydrogen-bonding fibers

## 3.3 Fibers of TTF-Crown Ether Composites

Similar fiber formation was also demonstrated without utilizing hydrogen bonding. Crown ether-appended TTF derivatives **16** and **17** were successfully synthesized and characterized. They were designed based on the amphiphilic strategy, i.e., consisting of hydrophilic crown ether and hydrophobic alkyl chain, together with TTF as  $\pi$ - $\pi$  stacking and S···S interaction moieties (Fig. 10) [70–72]. Employing the Langmuir–Blogett (LB) technique, the CT complex between amphiphilic TTF **16a** and 2,3,5,6-tetrafluoro-7,7,8,8-tetracyano-p-quinodimethane (F<sub>4</sub>-TCNQ) gave orientated fibers on a mica surface. Deposition depended not only on the surface pressure and temperature but also on the metal ions used [71]. Using the similar compound **16b**, nanodot-array structures were also produced in Langmuir–Blogett films, which were simply fabricated by spin-coating technique, and thus controllable by the rotational speed [72]. In the case of **17**, dominating multiple TTF–TTF and TTF–phthalocyanine (Pc) interactions over Pc–Pc interaction resulted in the formation of helical bundles of fibers [73].

#### 3.4 Fibers of Simple TTF-Esters

TTF derivatives with a long alkyl chain self-aggregate into a one-dimensional columnar structure in the solid state and show semiconductive properties (fastener effect) [74]. To utilize this effect in the construction of electroactive nanostructures, we focused on known simple amphiphilic TTF derivatives **18a,b** and **19a,b** (Fig. 11). Although these molecules have already been employed by several groups as synthetic precursors of functional  $\pi$ -systems, no significant properties of **18a,b** and **19a** easily form gels from nonpolar hydrocarbon solvents, we expected self-assembling fiber formation by intuition, and therefore reexamined the nanostructures constructed by these extremely simple TTF derivatives [75–77].

Diesters **18a,b** exhibited gelling ability for hexane with formation of fibrous superstructures (Fig. 12a, b). The fibers of **18b** were estimated to be about 2–5  $\mu$ m in diameter and 1–10 mm in length by SEM and AFM measurements, indicating micron–fiber formation. In contrast, **18a** showed no gelation from common organic

Fig. 11 Chemical structures of TTF-esters 18a,b and 19a-c

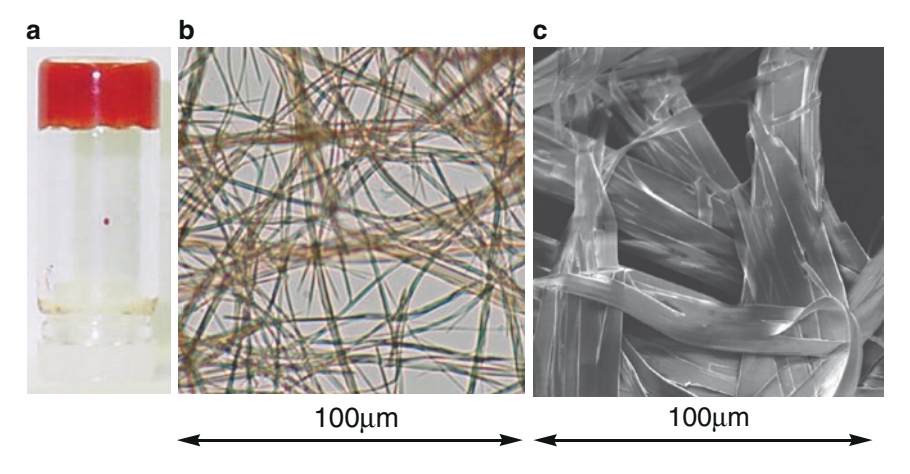


**Fig. 12** a **18b** gel from hexane (10 mg cm<sup>-3</sup>). **b** Optical micrograph of **18b** xerogel. **c** SEM picture of tape-like structure of **18a** in CH<sub>2</sub>CN (2 mg cm<sup>-3</sup>) [78]

solvents, and a yellow fibrous material was formed from acetonitrile. An SEM image of 18a fibers revealed a tape-like morphology with 2–10  $\mu$ m width and 100–1000 nm thickness (Fig. 12c). Carboxylic acid 19a gelated hexane and cyclohexane to form a reddish-orange gel. However, the ammonium salt of 19b showed no gelation or fiber formation from common organic solvents.

#### 3.5 TTF and its Oligomers Without Hydrogen-Bonding Sites

Both dendritic nanostructures composed of oxidized TTF and silver and nanowires composed of oxidized TTF and gold were synthesized [78, 79]. Silver dendritic nanostructures containing TTF were prepared by reduction of AgNO<sub>3</sub> [78], whereas TTF-gold nanowires were prepared by mixing HAuCl<sub>4</sub> and TTF [79]. The average size of TTF-gold nanowires is 90 nm diameter and 15 μm length, the composite being [(TTFCl<sub>0.78</sub>)Au<sub>0.12</sub>]. Thus, the neutral and oxidized TTF align along the one direction to show electric conductivity of ca. 10<sup>-2</sup> S cm<sup>-1</sup>.

With the above approaches for making fibrous structures in mind, we have designed and synthesized cyclic TTF trimer **20a** in which TTF moieties are tethered to each other by di-ethynyl linkage, making an [18]annulene structure (Fig. 13) [75, 80]. Cooperative S···S and  $\pi$ – $\pi$  interactions were expected to enhance stacking ability, which therefore makes an efficient charge-carrier percolation pathway through the stacked supramolecular architecture. In fact, **20a** gave stringy materials from aqueous THF solution. Measurements after doping with iodine vapor showed conductivity as high as  $2.4 \times 10^{-2}$  S cm<sup>-1</sup>. Interestingly, a similar cyclic trimer **20b** possessing six peripheral *n*-hexyl alkyl chains, not electron-withdrawing ester groups, synthesized by Diederich et al., was reluctant to aggregate in apolar aromatic solvents whereas **20a** formed fibers under the same conditions [81]. Similar enhancement of supramolecular organization by ester groups can be seen for the extended  $\pi$  systems [82–85].

Fig. 13 Chemical structures of planar TTF oligomers 20–22

The same approach was also applied to the other system by our group. The starburst TTF trimer **21** [86] and hexamer **22** [87] were synthesized where three or six TTF moieties were connected to the central benzene ring via ethynyl linkage (Fig. 13). In these molecules, multiple TTF moieties can be planarized by a free rotation of ethynyl linkages when it stacks intermolecularly, and hence cooperative S···S and  $\pi$ - $\pi$  interactions are favorable. As to neutral **22**, dark blue fibrous materials were obtained from a CHCl<sub>3</sub>/hexane mixed solution and the X-ray diffraction (XRD) pattern of the crushed wires exhibited a hexagonally ordered columnar structure with a  $\pi$ - $\pi$  stacking distance of 3.53 Å. It should be noted that the wires of chemically oxidized **22**\*·ClO<sub>4</sub>- showed an electric conductivity of 1.1 × 10<sup>-3</sup> S cm<sup>-1</sup>, whereas the drop-cast film obtained from the same material, which gave no evidence of  $\pi$ - $\pi$  stacking and columnar structures from the XRD experiment, showed a much lower conductivity of 3.1 × 10<sup>-5</sup> S cm<sup>-1</sup>. These results imply that supramolecular fibers can be effective materials for realizing molecular electronics, due not only to the size issue but to their high performance.

#### 4 Summary and Outlook

In this chapter, supramolecular nanostructures derived from self-assembling oligothiophenes and TTFs are reviewed. By combining the soft material approach with electro-active sulfur containing  $\pi$ -electron systems, unique nanostructures having characteristic electronic and optical properties can be constructed. These techniques may offer a bottom-up approach to the construction of future organic and molecular electronics.

#### References

- 1. Hoeben FJM, Jonkheijm P, Meijer EW, Schenning APHJ (2005) Chem Rev 105:1491
- 2. Wu J, Pisula W, Müllen K (2005) Chem Rev 105:718
- Vriezema DM, Aragonés MC, Elemans JAAW, Cornelissen JJLM, Rowan AE, Nolte RJM (2005) Chem Rev 105:1445
- Bushey ML, Nguyen T-Q, Zhang W, Horoszewski D, Nuckolls C (2004) Angew Chem Int Ed 43:5446
- 5. Brammer L (2004) Chem Soc Rev 33:476
- 6. Huc I (2004) Eur J Org Chem, p. 17
- Ruben M, Rojo J, Romero-Salguero FJ, Uppadine LH, Lehn J-M (2004) Angew Chem Int Ed 43:3644
- 8. Kitagawa S, Kitaura R, Noro S (2004) Angew Chem Int Ed 43:2334
- 9. Hofmeier H, Schubert US (2004) Chem Soc Rev 33:373
- 10. Würthner F, You C-C, Saha-Möller CR (2004) Chem Soc Rev 33:133
- 11. Oh M, Carpenter GB, Sweigart DA (2004) Acc Chem Res 37:1
- 12. Marsden JA, Miller JJ, Shirtcliff LD, Haley MM (2005) J Am Chem Soc 127:2464
- 13. Pease AR, Jeppesen JO, Stoddart JF, Luo Y, Collier CP, Heath JR (2001) Acc Chem Res 34:433

- 14. Watson MD, Fechtenkotter A, Müllen K (2001) Chem Rev 101:1267
- 15. Shimizu T, Masuda M, Minamikawa H (2005) Chem Rev 105:1401
- Yamamoto Y, Fukushima T, Saeki A, Seki S, Tagawa S, Ishii N, Aida T (2007) J Am Chem Soc 129:9276
- 17. Zhang G, Jin W, Fukushima T, Kosaka A, Ishii N, Aida T (2007) J Am Chem Soc 129:719
- Yamamoto Y, Fukushima T, Suna Y, Ishii N, Saeki A, Seki S, Tagawa S, Taniguchi M, Kawai T, Aida T (2006) Science 314:1761
- 19. Ajayaghosh A, Praveen VK (2007) Acc Chem Res 40:644
- Iyoda M, Hasegawa M, Hara K, Takano J, Ogura E, Kuwatani Y (2004) J Phys IV France 114:455
- 21. Hasegawa M, Kuwatani Y, Iyoda M (2004) J Phys IV France 114:505
- 22. Werz DB, Gleiter R, Rominger F (2002) J Am Chem Soc 124:10638
- 23. Glusker JP (1998) Top Curr Chem 198:1
- 24. Bendikov M, Wudl F, Perepichka DF (2004) Chem Rev 104:4891
- 25. Mori T (2004) Chem Rev 104:4947
- 26. Jørgensen M, Bechgaard K (1994) J Org Chem 59:5877
- Schoonbeek FS, van Esch JH, Wegewijs B, Rep DBA, de Haas MP, Klapwijk TM, Kellogg RM, Feringa BL (1999) Angew Chem Int Ed 38:1393
- 28. Liu P, Shirota Y, Osada Y (2000) Polym Adv Technol 11:512
- 29. Messmore BW, Hulvat JF, Sone ED, Stupp SI (2004) J Am Chem Soc 126:14452
- 30. Kawano S, Fujita N, Shinkai S (2005) Chem Eur J 11:4735
- 31. Rep DBA, Roelfsema R, van Esch JH, Schoonbeek FS, Kellogg RM, Feringa BL, Palstra TTM, Klapwijk, TM (2000) Adv Mater 12:563
- 32. de Haas MP, van der Laan GP, Wegewijs B, de Leeuw DM, Bäuerle P, Rep DBA, Fichou D (1999) Synth Met 101:524
- Schenning APHJ, Kilbinger AFM, Biscarini F, Cavallini M, Cooper HJ, Derrick PJ, Feast WJ, Lazzaroni R, Leclère Ph, McDonell LA, Meijer EW, Meskers SCJ (2002) J Am Chem Soc 124:1269
- Leclère Ph, Surin M, Lazzaroni R, Kilbinger AFM, Henze O, Jonkheijm P, Biscarini F, Cavallini M, Feast WJ, Meijer EW, Schenning APHJ (2004) J Mater Chem 14:1959
- 35. Xia C, Fan X, Locklin J, Advincula RC, Gies A, Nonidez W (2004) J Am Chem Soc 126:8735
- 36. Nishizawa T, Tajima K, Hashimoto K (2007) J Mater Chem 17:2440
- Shklyarevskiy IO, Jonkheijm P, Christianen PCM, Schenning APHJ, Meijer EW, O Henze O, Kilbinger AFM, W. Feast WJ, Guerzo AD, Desvergne J-P, Maan JC (2005) J Am Chem Soc 127:1112
- 38. Henze O, Feast WJ, Gardebian F, Jonkheijm P, Lazzaroni R, Leclère Ph, Meijer EW, Schenning APHJ (2006) J Am Chem Soc 128:5923
- 39. Jiang L, Hughes RC, Sasaki DY (2004) Chem Commun, p 1028
- 40. Grimsdale AC, Müllen K (2005) Angew Chem Int Ed 44:5592
- 41. Nakao K, Nishimura M, Tamachi T, Kuwatani Y, Miyasaka H, Nishinaga T, Iyoda M (2006) J Am Chem Soc 128:16740
- 42. Iyoda M (2007) Heteroatom Chem 18:460
- 43. Williams-Harry M, Bhaskar A, Ramakrishna G, Goodson T, Imamura M, Mawatari A, Nakao K, Enozawa H, Nishinaga T, Iyoda M (2008) J Am Chem Soc 130:3252
- 44. Krömer L, Rios-Carreras I, Fuhrmann G, Musch C, Wunderlin M, Debaerdemaeker T, Mena-Osteritz E, Bäuerle P (2000) Angew Chem Int Ed 39:3481
- 45. Schlüter AD (2005) Top Curr Chem 245:151
- Rahman MJ, Yamakawa J, Matsumoto A, Enozawa H, Nishinaga T, Kamada K, Iyoda M (2008) J Org Chem 73:5542
- 47. Bryce MR (1991) Chem Soc Rev 20:355
- 48. Adam M, Müllen K (1994) Adv Mater 6:439
- 49. Bryce MR (1995) J Mater Chem 5:1481
- 50. Otsubo T, Aso Y, Takimiya K (1996) Adv Mater 8:203

- 51. Bryce MR (2000) J Mater Chem 10:589
- 52. Nielsen MB, Lomholt C, Becher J (2000) Chem Soc Rev 29:153
- 53. Segura JL, Martín N (2001) Angew Chem Int Ed 40:1372
- 54. Narita M, Pittman CU (1976) Synthesis, p 489
- 55. Simonsen KB, Becher J (1997) Synlett, p 1211
- 56. Batail P, ed. (2004) Chem Rev 104:4887
- 57. Nalva HS, ed. (1997) Handbook of organic conductive molecules and polymers, Vol. 1. (1997) John Wiley & Sons, Chichester
- 58. Torrance JB, Scott BA, Welber B, Kaufman FB, Seiden PE (1979) Phys Rev B 19:730
- 59. Iyoda M, Hara K, Kuwatani Y, Nagase S (2000) Org Lett 2:2217
- Iyoda M (2004) In: Yamada J, Sugimoto T (eds) TTF chemistry. Kodansha and Springer, Tokyo, p. 177–204
- 61. Iyoda M, Hasegawa M, Miyake Y (2004) Chem Rev 104:5085
- 62. Wudl F, Smith G, Hufnagel EJ (1970) J Chem Soc Chem Commun, p 1453
- 63. Ferraris J, Cowan DO, Walatka VV, Perlstein JH (1973) J Am Chem Soc 95:948
- 64. Gall TL, Pearson C, Bryce MR, Petty MC, Dahlgaad H, Becher J (2003) Eur J Org Chem 3562
- 65. Kitahara T, Shirakawa M, Kawano S, Beginn U, Fujita N, Shinkai S (2005) J Am Chem Soc 127:14980
- 66. Wang C, Zhang D, Zhu D (2005) J Am Chem Soc 127:16372
- 67. Kitamura T, Nakaso S, Mizoshita N, Tochigi Y, Shimomura T, Moriyama M, Ito K, Kato T (2005) J Am Chem Soc 127:14769
- 68. Puigmartí-Luis J, Laukhin V, delPino ÁP, Vidal-Gancedo J, Rovira C, Laukhin E, Amabilino DB (2007) Angew Chem Int Ed 46:238
- Puigmartí-Luis J, del Pino ÁP, Laukhina E, Esquena J, Laukhin V, Rovira C, Vidal-Gancedo J, Kanaras AG, Nichols RJ, Brust M, Amabilino DB (2008) Angew Chem Int Ed 47:1861
- 70. Kato K, Akutagawa T, Nakamura T (2005) J Synth Org Chem Jpn 63:960
- Akutagawa T, Ohta T, Hasegawa T, Nakamura T, Christensen CA, Becher J (2002) Proc Natl Acad Sci USA 99:5028
- 72. Akutagawa T, Kakiuchi K, Hasegawa T, Noro S, Nakamura T, Hasegawa H, Mashiko S, Becher J (2005) Angew Chem Int Ed 44:7283
- 73. Sly J, Kasák P, Gomar-Nadal E, Rovira C, Górriz L, Thordarson P, Amabilino DB, Rowan AE, Nolte JM (2005) Chem Commun, p 1255
- Inokuchi H, Saito G, Wu P, Seki K, Tang TB, Mori T, Imaeda K, Enoki T, Higuchi Y, Inaka K, Yasuoka N (1986) Chem Lett 15:1263
- 75. Iyoda M, Enozawa H, Hasegawa M (2007) Chem Lett 36:1402
- 76. Kobayashi Y, Hasegawa M, Enozawa H, Iyoda M (2007) Chem Lett 36:720
- 77. Enozawa H, Honna Y, Iyoda M (2007) Chem Lett 36:1434
- 78. Wang X, Itoh H, Naka K, Chujo Y (2003) Langmuir 19:6242
- 79. Naka K, Ando D, Wang X, Chujo Y (2007) Langmuir 23:3450
- 80. Enozawa H, Hasegawa M, Takamatsu D, Fukui K, Iyoda M (2006) Org Lett 8:1917
- 81. Anderson AS, Kilså K, Hassenkam T, Gisselbrecht J-P, Boudon C, Gross M, Nielsen MB, Diederich F (2006) Chem Eur J 12:8451
- 82. Hunter CA, Sanders JKM (1990) J Am Chem Soc 112:5525
- 83. Zhang J, Moore JS (1994) J Am Chem Soc 116:2655
- 84. Ajayagosh A, Praveen VK, Srinivasan S, Varghese R (2007) Adv Mater 19:411
- 85. Feng X, Pisula W, Zhi L, Takase M, Müllen K (2008) Angew Chem Int Ed 47:1703
- 86. Hasegawa M, Takano J, Enozawa H, Kuwatani Y, Iyoda M (2004) Tetrahedron Lett 4109
- 87. Hasegawa M, Enozawa H, Kawabata Y, Iyoda M (2007) J Am Chem Soc 129:3072

Top Heterocycl Chem (2009) 18: 119-154

DOI: 10.1007/7081\_2009\_1

© Springer-Verlag Berlin Heidelberg 2009

Published online: 27 March 2009

# Asymmetric 1,3-Dipolar Cycloaddition Reactions Catalyzed by Heterocycle-Based Metal Complexes

Hiroyuki Suga

**Abstract** Highly enantioselective 1,3-dipolar cycloaddition reactions of several 1,3-dipoles, such as nitrones, nitrile oxides, nitrile imines, diazoalkanes, azomethine imines and carbonyl ylides, catalyzed by heterocyclic supramolecular type of metal complexes consisting of chiral heterocyclic compounds and metal salts were described in terms of their ability of asymmetric induction and enantioface differentiation. The scope and limitations of each cycloaddition reactions were also briefly described. Of the chiral hererocycle-based ligands, chiral bisoxazoline, 2,6-bis(oxazolinyl)pyridine, and related oxazoline ligands are shown to be quite effective in obtaining high levels of asymmtric induction. The combination of the bisoxazoline ligand derived from (1S,2R)-cis-1-amino-2-indanol and metal salts was especially efficient for asymmetric cycloaddition reactions of a number of 1,3-dipoles, such as nitrones, nitrile oxide, nitrile imines, diazoacetates and azomethine imines. The metals utilized for the heterocycle-based complexes show a crucial role for degree of asymmetric induction depending upon the 1,3-dipole used. High levels of enantioselectivity were achieved in 1,3-dipolar cycloaddition reactions of unstable carbonyl ylides with benzyloxyacetaldehyde derivatives,  $\alpha$ -keto esters, 3-(2-alkenoyl)-2-oxazolidinones, and even vinyl ethers, which were catalyzed by Pybox-lanthanoid metal complexes.

**Keywords** 1,3-Dipole, Asymmetric induction, Chiral Lewis acid, Cycloaddition reaction, Metal complex

H. Suga

Department of Chemistry and Material Engineering, Faculty of Engineering, Shinshu University, Wakasato, Nagano, 380-8553, Japan

e-mail: sugahio@shinshu-u.ac.jp

120 H. Suga

7			
			ts

1	Intro	oduction	121			
2	Cycloaddition Reactions of Nitrones					
	2.1	Cycloaddition Reactions of Nitrones with 3-(2-Alkenoyl)-2-oxazolidinones	122			
	2.2	Cycloaddition Reactions of Nitrones with α,β-Unsaturated 2-Acyl Imidazole	127			
	2.3 Exo-selective Cycloaddition Reactions of Nitrones with					
		2-(2-Alkenoyl)-3-pyrazolidinones and 3-(2-Alkenoyl)-2-thiazolidinethiones	127			
	2.4	Cycloaddition Reactions of Nitrones with α'-Hydroxy Enones	130			
	2.5	Cycloaddition Reactions of Nitrones with α,β-Unsaturated Aldehydes	131			
	2.6	Cycloaddition Reactions of Nitrones with Alkylidene Malonates	132			
	2.7	Cycloaddition Reactions of Nitrones with Vinyl Ethers	133			
3	Cycloaddition Reactions of Diazo Compounds					
	3.1	Cycloaddition Reactions of Trimethylsilyldiazomethane	134			
	3.2	Cycloaddition Reactions of Diazoacetate	136			
4	Cycl	loaddition Reactions of Nitrile Oxides	136			
5	Cycl	loaddition Reactions of Nitrile Imines	139			
6	Cycl	loaddition Reactions of Azomethine Imines	139			
7	Cyloaddition Reactions of Carbonyl Ylides					
	7.1	Cycloaddition Reactions of Carbonyl Ylides with Electron-Deficient				
		Carbonyl Dipolarophiles	145			
	7.2	Cycloaddition Reactions of Carbonyl Ylides with Electron-Deficient				
		Olefinic Dipolarophiles	147			
	7.3	Cycloaddition Reactions of Carbonyl Ylides with Electron-Releasing				
		Olefinic Dipolarophiles	149			
8	Conclusion					
Re	feren	ces	151			

### Abbreviations

BINIM	Binaphthyldiimine			
Box	Bisoxazoline			
DBFOX	4,6-Dibenzofuranyl-2,2'-bis(oxazoline)			
DIEA	Diisopropylethylamine			
INDABOX	Bis(3a,8a-dihydro-8H-indeno[1,2d]oxazole			
MS 4 Å	4 Å Molecular sieves			
MS	Molecular sieves			
Pybox	2,6-Bis(oxazolinyl)pyridine			
Rh2[(R)-DBBNP]4	Dirhodium(II) tetrakis[(R)-6,6'-			
	didodecylbinaphtholphosphate]			
Rh2(S-BTPV)4	$Dirhodium (II)\ tetrak is [N-benzene-fused-phthaloyl-(S)-$			
	valinate]			
Rh2[(S)-DOSP]4	Dirhodium(II) tetrakis[(S)-N-(4-dodecylphenylsulfonyl)			
	prolinate]			
Rh2(S-PTTL)4	Dirhodium(II) tetrakis[N-phthaloyl-(S)-tert-leucinate]			
TADDOL	$\alpha, \alpha, \alpha', \alpha'$ -Tetraaryl-1,3-dioxolan-4,5-dimethanole			
Tox	Trisoxazoline			
XABOX	Bis(2-oxazolinyl)xanthene			

#### 1 Introduction

Supramolecules could be defined in the broader sense as the molecules produced by assembly of intermolecular interactions such as hydrogen bonds or coordinate bonds between plural molecules [1–6]. Classically, the metal complexes of porphyrins are included in such molecules and their ability for molecular recognition [7-12] and asymmetric induction using their chiral complexes has been well studied [13–25]. A number of chiral metal catalysts such as chiral Lewis acids have been developed for the efficient asymmetric syntheses of optically active compounds. Most of these catalysts were usually prepared by complexing chiral organic ligands and metal salts under appropriate conditions with coordinate bonds. Although the most active catalysts are probably monomeric species, the initial chiral complexes could exist as more stable aggregated oligomers with intermolecular interactions of coordinate bonds. In the case of chiral Lewis acid catalysts, the catalysts further coordinate to substrates by coordinate bonds to activate the reaction. Therefore, those chiral complexes could also be included in a category of supramolecules in the broader sense. During the past dacade, highly enantioselective 1,3-dipolar cycloaddition reactions catalyzed by chiral Lewis acids have been developed for several 1,3-dipoles (Fig. 1), such as nitrones, nitrile oxides, nitrile imines, diazoalkanes, azomethine imines and carbonyl ylides. Among these chiral Lewis acids used for the asymmetric cycloadditons, heterocyclic supramolecular type of metal complexes consisting of chiral heterocyclic compounds and metal salts have played important roles in asymmtric induction. Of the chiral hererocycle-based ligands, bisoxazolines (Box, Fig. 2) and 2,6-bis(oxazolinyl)pyridines (Pybox, Fig. 3) are probably the most effective chiral ligands in obtaining high levels of asymmtric induction. The aim of this review is to highlight recent studies on asymmetric induction in 1,3-dipolar cycloaddition reactions using these heterocycle-based metal complexes as chiral supramolecular Lewis acids.

## 2 Cycloaddition Reactions of Nitrones

In 1994, the first attempts to apply chiral Lewis acids as asymmetric catalysts for 1,3-dipolar cycloaddition of nitrones were reported by Seerden et al. [26] and Gothelf et al. [27], independently. In the former reaction catalyzed by oxazaborolidines, an electron-rich alkene was involved as a dipolarophile, and the reaction proceeded according to the inverse electron-demand concept, which controlled by the strongest interaction between the dipolarophile HOMO and the 1,3-dipole LUMO, with up to 74% ee. In the later case, electron-deficient 3-(2-alkenoyl)-2-oxazolidinones were used as dipolarophiles, and the chiral TiCl<sub>2</sub>-TADDOL-catalyzed reaction proceeded according to the normal electron-demand concept (1,3-dipole/HOMO-dipolarophile/LUMO) with up to 62% ee.

122 H. Suga

$\stackrel{^{+}}{N} = N - \stackrel{^{-}}{C} R_2$	$\stackrel{+}{N}=N-\stackrel{-}{C}R_2$ $\longrightarrow$ N		Diazoalkane
N=N-NR	<b>←</b>	N≡N−NR	Azide
$\overset{+}{RC} = N - \overset{-}{CR}_2$	<b>←</b>	$RC \equiv \stackrel{+}{N} - \stackrel{-}{C}R_2$	Nitrile ylide
RC=N-NR	<b>←</b>	RC≡N-NR	Nitrile imine
$\overrightarrow{RC} = N - \overrightarrow{O}$	<b></b>	RC≡N-Ō	Nitrile oxide
$R_2$ $\stackrel{+}{C}$ $-N$ $\stackrel{-}{C}R_2$ $R$	<b>←</b> →	$R_2C = \stackrel{+}{N} - \stackrel{-}{C}R_2$	Azomethine ylide
$R_2\overset{+}{\overset{-}{C}}-N\overset{-}{\overset{-}{N}}R$	<b>←</b> →	$R_2C = \stackrel{+}{N} - \stackrel{-}{N}R$	Azomethine imine
$R_2\overset{+}{\overset{-}{C}}-N\overset{-}{\overset{-}{O}}$	<b>←</b>	$R_2C = \stackrel{+}{N} - \stackrel{-}{O}$	Nitrone
$R_2^+$ C-O- $\overline{C}R_2$	<b>←</b>	$R_2C=\overset{+}{O}-\overset{-}{C}R_2$	Carbonyl ylide
$R_2^{+}C^{-}O^{-}O^{-}$	<b>←</b> →	$R_2C=\overset{+}{O}-\overset{-}{O}$	Carbonyl oxide

Fig. 1 1,3-Dipolar compounds

# 2.1 Cycloaddition Reactions of Nitrones with 3-(2-Alkenoyl)-2-oxazolidinones

For heterocycle-based metal complexes as chiral Lewis acids, chiral Box (Fig. 2) magnesium complexes have been used for 1,3-dipolar cycloaddition of nitrones with electron-deficient alkenes. In 1996, Gothelf et al. reported that the reaction of *C,N*-diphenyl and *C*-phenyl *N*-benzyl nitrones with 3-(2-alkenoyl)-oxazolidinones in the presence of Box-Ph-MgI<sub>2</sub> complex (10 mol%) gave *endo*-cycloadducts with good to high diastereoselectivity in an enantioselectivity of up to 82% ee (Scheme 1) [28]. The absolute stereochemistry of the enantioselective 1,3-dipolar cycloaddition of nitrones catalyzed by Box-Ph-MgI<sub>2</sub> complex was shown to be dependent on the presence of molecular sieves (MS). In the presence of powdered molecular sieves 4 Å (MS 4 Å), the reaction proceeds to give the *endo*-cycloadduct in an enantioselectivity of up to 82% ee, whereas the use of H<sub>2</sub>O (20 mol%) as an additive in the absence of MS gave the opposite enantiomer of the *endo*-cycloadduct in

R = Ph: 
$$(S,S)$$
-Box-Ph  
R =  $i$ -Pr:  $(S,S)$ -Box- $i$ -Pr  
R =  $t$ -Bu:  $(S,S)$ -Box- $t$ -Bu

R = R = H  
R, R =  $-(CH_2)_2$ -

(4S,5R)-INDABOX

Fig. 2 Structures of chiral bisoxazolines

$$R^1 = i \cdot Pr$$
,  $R^2 = H$ :  $(S,S) \cdot Pybox \cdot i \cdot Pr$   
 $R^1 = Ph$   $R^2 = H$ :  $(S,S) \cdot Pybox \cdot Ph$   
 $R^1 = Ph$   $R^2 = H$ :  $(S,S) \cdot Pybox \cdot Ph$   
 $R^1 = Ph$   $R^2 = Ph$ :  $(4S,5S) \cdot Pybox \cdot 4,5 \cdot Ph_2$   
 $R^2 = SiBu^t Me_2$ :  $(S,S) \cdot Pybox \cdot TBDPSm$   
 $R^2 = SiBu^t Ph_2$ :  $(S,S) \cdot Pybox \cdot TBDPSm$   
 $R^2 = SiPh_3$ :  $(S,S) \cdot Pybox \cdot TPSm$ 

Fig. 3 Structures of chiral 2,6-bis(oxazolinyl)pyridines

Box-Mgl<sub>2</sub>

$$R^2 = Me, Pr$$
 $R^2 = Me, Pr$ 
 $R^2 = Me, Pr$ 

**Scheme 1** Cycloaddition reactions of nitrones with 3-(2-alkenoyl)-2-oxazolidinones catalyzed by Box-MgI, complex [28, 29]

an enantioselectivity of up to 73% ee [29]. Desimoni et al. also reported that the counterion  $X^-$  for the magnesium salts also affected absolute configuration of selectively obtained *endo*-cycloadduct in Box-Ph-MgX<sub>2</sub> catalyzed reaction of *C,N*-diphenyl nitrone with 3-acryloyl-2-oxazolidinone in addition to the presence of MS (Scheme 2)

124 H. Suga

[30]. The absolute configuration of the cycloadduct of the reaction catalyzed by Box-Ph-Mg(OTf)<sub>2</sub> in the absence of MS was similar to that catalyzed by Box-Ph-Mg(ClO<sub>4</sub>)<sub>2</sub> and opposite to that catalyzed by Box-Ph-MgI<sub>2</sub>. Box-Ph-Mg(ClO<sub>4</sub>)<sub>2</sub> complex gave the opposite absolute configuration of the cycloadduct compared with that obtained with Box-Ph-MgI<sub>2</sub> complex both in the presence and absence of MS. Although the reaction catalyzed by Box-Ph-Mg(OTf)<sub>2</sub> in the presence of MS showed almost no asymmetric induction, the highest enantioselectivity (86% ee) was observed in the absence of MS among a series of Box-Ph-MgX, catalysts.

Box-MgX<sub>2</sub> in CH<sub>2</sub>Cl<sub>2</sub>

$$endo: exo = 56: 44 - 100: 0$$
 $endo: exo = 56: 44 - 100: 0$ 
 $endo: exo = 56: 44 - 100: 0$ 
 $endo: exo = 56: 44 - 100: 0$ 

**Scheme 2** Cycloaddition reactions of nitrones with 3-acryloyl-2-oxazolidinone catalyzed by Box-MgX, complex [29, 30]

Saito et al. reported that the complex consisting of  $Cu(OTf)_2$  and Box derived from (1S,2R)-cis-1-amino-2-indanol (INDABOX) was found to be a more effective catalyst for obtaining higher enantioselectivity in cycloaddition reactions between several C-aryl N-phenyl nitrones and 3-crotonyl-2-oxazolidinone with mostly good to moderate endo-selectivity (Scheme 3) [31]. Enantioselectivities of both endo-and exo-cycloadducts achieved over 93% ee. The INDABOX-Cu(II)-catalyzed reaction of C,N-diphenyl nitrone with 3-acryloyl-2-oxazolidinone showed moderate exo-selectivity (78:22) with high enantioselectivity (96% ee) of exo-adduct.

$$Ar = Ph, 4-CH_3OC_6H_4, 4-CH_3C_6H_4, \\ 4-FC_6H_4, 4-CIC_6H_4, 4-BIC_6H_4, \\ 4-CF_3C_6H_4, 4-NOC_6H_4, 4-NO_2C_6H_4, \\ 2-Naphthyl, 2-Furyl \\ INDABOX-Cu(OTf)_2 \\ gamma \\ endo: exo = 50: 50 - 91: 9 \\ gamma \\ 93\% - > 99\% ee (endo)$$

**Scheme 3** Cycloaddition reactions of nitrones with 3-(2-alkenoyl)-2-oxazolidinones catalyzed by INDABOX-Cu(II) complex [31]

As a part of their development of new metal-catalyzed asymmetric 1,3-dipolar cycloaddition of nitrones, Sanchez-Blanco et al. reported that  $Yb(OTf)_3$  and  $Sc(OTf)_3$  were also effective and selective catalysts for this reaction in 1997 [32]. Application of 2,6-bis[(4S)-isopropyl-2-oxazolin-2-yl]pyridine ((S,S)-Pybox-i-Pr) (Fig. 2) as a chiral ligand for  $Yb(OTf)_3$ -catalyzed reactions of nitrones with 3-(2-alkenoyl)-2-oxazolidinone gave *endo*-cycloadduct with high diastereoselectivity (up to 97:3) and with up to 73% ee (*endo*) (Scheme 4) [32]. In the study on the Pybox ligands (Fig. 3) which were first described by Nishiyama et al. in 1989 [33], Iwasa et al. developed highly effective Pybox-Ni(II) catalyst in 1,3-dipolar cycloaddition reactions between nitrones and 3-(2-alkenoyl)-2-oxazolidinones [34, 35]. In the presence of complexes prepared from sterically tuned Pybox ((S,S)-Pybox-TBSm, (S,S)-Pybox-TBDPSm, (S,S)-Pybox-TIPSm) (Fig. 2) and Ni(ClO<sub>4</sub>)<sub>2</sub>•6H<sub>2</sub>O, 1,3-dipolar cycloaddition reactions of *C*-aryl *N*-phenyl nitrones with 3-(2-alkenoyl)-2-oxazolidinones proceeded smoothly to give the corresponding cycloadducts in 97:3 to >99:1 *endolexo* ratio and 94 to >99% ee for *endo*-adduct (Scheme 5).

$$R^{1} = H, Me$$

$$R^{2} = Me, Pr$$

$$R^{1} = H = H, Me$$

$$R^{2} = Me, Pr$$

$$R^{1} = H = H, Me$$

$$R^{2} = Me, Pr$$

$$R^{1} = H = H = H$$

$$R^{2} = Me, Pr$$

$$R^{2} = Me, Pr$$

$$R^{3} = H = H$$

$$R^{2} = Me, Pr$$

$$R^{3} = H = H$$

$$R^{2} = Me, Pr$$

$$R^{3} = H = H$$

$$R^{2} = Me, Pr$$

$$R^{3} = H = H$$

$$R^{4} = H = H$$

$$R^{2} = Me, Pr$$

$$R^{3} = H = H$$

$$R^{4} = H = H$$

$$R^{2} = Me, Pr$$

$$R^{3} = H$$

$$R^{4} = H$$

$$R^{2} = Me, Pr$$

$$R^{3} = H$$

$$R^{4} = H$$

$$R^{4} = H$$

$$R^{4} = H$$

$$R^{5} =$$

**Scheme 4** Cycloaddition reactions of nitrones with 3-(2-alkenoyl)-2-oxazolidinones catalyzed by Pybox-Yb(III) complex [32]

$$R^{1} = H, \text{ Me, OMe, Br}$$

$$R^{1} = H, \text{ Me, OMe, Br}$$

$$R^{1} = H, \text{ Me, OMe, Br}$$

$$R^{2} = H, \text{ Me}$$

$$R^{2} = H, \text{ Me}$$

$$R^{2} = H, \text{ Me}$$

$$R^{3} = H, \text{ Me, OMe, Br}$$

$$R^{4} = H, \text{ Me, OMe, Br}$$

$$R^{5} = Si(\dot{r} + Pr)_{3} : (S, S) - Pybox - TIPSm$$

**Scheme 5** Cycloaddition reactions of nitrones with 3-(2-alkenoyl)-2-oxazolidinones catalyzed by Pybox-Ni(II) complex [34, 35]

 $R' = SiBu^tPh_2$ : (S,S)-Pybox-TBDPSm

The cycloaddition reactions could be carried out not only in CH<sub>2</sub>Cl<sub>2</sub> but also in alcoholic media such as *t*-BuOH with high *endo*-selectivity (90:10–>99:1) and high enantioselectivity (90–98% ee) [36].

For a new type of heterocycle-based chiral Lewis acid catalyst, Kanemasa et al. reported that 4,6-dibenzofuranyl-2,2'-bis(oxazoline) (DBFOX) was an excellent ligand in combination with a variety of metal salts [37]. The aqua complex derived from the DBFOX/Ph ligand and Ni(ClO<sub>4</sub>)<sub>2</sub>•6H<sub>2</sub>O was applied to asymmetric 1,3-dipolar cycloadditions of a variety of nitrones to 3-(2-alkenoyl)-2-oxazolidinones and the complex acted as an excellent chiral Lewis acid catalyst in the presence of MS 4 Å in terms of both *endo*- and enantioselectivity (Scheme 6) [38]. Maximum enantioselectivities observed were as high as >99% ee, in several cases, and the minimum catalytic loading was 2 mol%.

$$\begin{array}{c} R^2 + O \\ H \\ R^1 \end{array} + \begin{array}{c} O \\ H \\ R^1 \end{array} + \begin{array}{c} O \\ H \\ R^1 \end{array} + \begin{array}{c} O \\ H \\ R^2 \end{array} + \begin{array}$$

R,R-DBFOX/Ph-Ni(ClO<sub>4</sub>)<sub>2</sub>·Ln<sub>3</sub>

**Scheme 6** Cycloaddition reactions of nitrones with 3-crotonoyl-2-oxazolidinone catalyzed by DBFOX-Ni(II) complex [38]

1,3-Dipolar cycloaddition reactions of *C*-aryl *N*-phenyl nitrones with 3-crotonoyl-2-oxazolidinone in the presence of bis(2-oxazolinyl)xanthene ligand (XABOX) and Mn(II) or Mg(II) complex as a chiral Lewis acid catalyst also proceeded smoothly to give the corresponding cycloadducts ranging from 96:4 to >99:1 of *endo:exo* ratio with high enantioselectivity (91–98% ee) of *endo* adduct (Scheme 7) [39].

$$R = H, Me, OMe, Br$$

$$R = H,$$

Scheme 7 Cycloaddition reactions of nitrones with 3-crotonoyl-2-oxazolidinone catalyzed by XABOX-Mn(II) or -Mg(II) complex [39]

# 2.2 Cycloaddition Reactions of Nitrones with α, β-Unsaturated 2-Acyl Imidazole

In the recent development of a number of chiral Lewis acid catalyzed reactions with high enantioselectivity, Evans et al. reported highly enantioselective reactions catalyzed by Pybox-Sc(III) complexes such as addition and annulation reactions of allenylsilanes [40], syn-selective aldol addition reactions of enolesilanes [41, 42], quinone Diels-Alder reactions [43], Friedel-Crafts alkylations [44–47], syn-selective ene reactions [48], vinylsilane additions [49], and Sakurai additions [50]. On the base of the high enantioselectivity of Friedel-Crafts alkylations with  $\alpha,\beta$ -unsaturated 2-acyl imidazoles, Evans et al. studied the asymmetric 1,3-dipolar cycloadition reactions of nitrones with  $\alpha,\beta$ -unsaturated 2-acyl imidazoles using Pybox-rare earth metal triflates as chiral Lewis acid catalysts. From surveys of lanthanoid metal, Pybox ligands, and reaction solvents, cis-(4R,5S)-Pybox-4,5-Ph<sub>2</sub>-Ce(IV) triflate complex in AcOEt was found to be highly efficient in obtaining high levels of asymmetric induction (80–99% ee for endo-cycloadducts) in 1,3-dipolar cycloadditions between N-benzyl, N-methyl, and N-phenyl nitrones and several  $\alpha,\beta$ -unsaturated 2-acyl imidazoles (Scheme 8) [51].

$$R^{1} = \text{Bn, Me, Ph} \qquad R^{3} = \text{Me, Et, } \\ Pr, \\ R^{2} = \text{Ph, 4-MeOC}_{6}H_{4}, \text{ 4-CIC}_{6}H_{4}, \\ 4-\text{MeO}_{2}\text{CC}_{6}H_{4}, \text{ 1-naphthyl,} \\ 2-\text{naphthyl, Et, c-Hex} \qquad Ph \qquad R^{3} = \text{Me, Et, } \\ Ph \qquad N = \text{Ph, CO}_{2}\text{Et} \\ N = \text{Ph, 4-MeO}_{2}\text{CC}_{6}H_{4}, \text{ 1-naphthyl,} \\ N = \text{Ph, CO}_{2}\text{Et} \\ N =$$

Catalyst: cis-(4R,5S)-Pybox-4,5-Ph<sub>2</sub>-Ce(IV) triflate complex

Scheme 8 Cycloaddition reactions of nitrones with  $\alpha,\beta$ -unsaturated 2-acyl imidazoles catalyzed by Pybox-Ce(IV) complex [51]

# 2.3 Exo-selective Cycloaddition Reactions of Nitrones with 2-(2-Alkenoyl)-3-pyrazolidinones and 3-(2-Alkenoyl)-2-thiazolidinethiones

A number of chiral Lewis acids including heterocycle-based metal complexes have been shown to possess high enantioselectivity in the reactions of nitrones with electron-deficient olefins [for recent reviews 52–55] since the first attempts to apply

128 H. Suga

chiral Lewis acids for cycloadditions of nitrones as described above [26, 27]. For the reactions of electron-deficient alkenes, 3-(2-alkenoyl)-2-oxazolidinones have often been employed as bidentate type dipolarophiles to yield, in most cases, the endo-cycloadducts with high enantioselectivity [for recent representative examples 28–36, 38, 39, 51, 56]. To date, however, only a few examples of the *exo*-selective cycloadditions of nitrones with 2-alkenoic acid derivatives in the presence of a chiral Lewis acid have been reported [27, 57-60]. In 2004, Sibi et al. have reported on first highly exo-selective cycloadditions that also possess both high yield and high enantioselectivity with a practical level using the chiral relay in reactions with 2-(2-alkenoyl)-3-pyrazolidinones as the dipolarophiles (Scheme 9) [61]. In contrast to INDABOX-Cu(OTf)<sub>2</sub>-catalyzed cycloaddition reactions with 3-(2-alkenoyl)-2oxazolidinones [31], mostly high exo-selectivity (52:48–96:1) was obtained by using 2-(2-alkenoyl)-1-benzyl-5,5-dimethyl-3-pyrazolidinones as dipolarophiles in combination with INDABOX having cyclopropane at linkage of bisoxazoline as a ligand in the reaction of N-methyl and N-benzyl nitrones. Interestingly, in this case, addition of MS led to a dramatic reversal or reduction in exolendo selectivity, but without compromising the enantioselectivity of the exo isomer. The use of 2-acryloyland 2-(2-ethoxycarbonylpropenoyl)-3-pyrazolidinones indicated decreased exo-selectivity (66:34 and 67:33, respectively). It is also interesting that the reaction of C,N-diphenyl nitrone with 2-crotonoyl-3-pyrazolidinone showed almost no diastereoselectivity (exo:endo = 52:48).

**Scheme 9** Cycloaddition reactions of nitrones with 2-(2-alkenoyl)-3-pyrazolidinones catalyzed by INDABOX-Cu(II) complex [61]

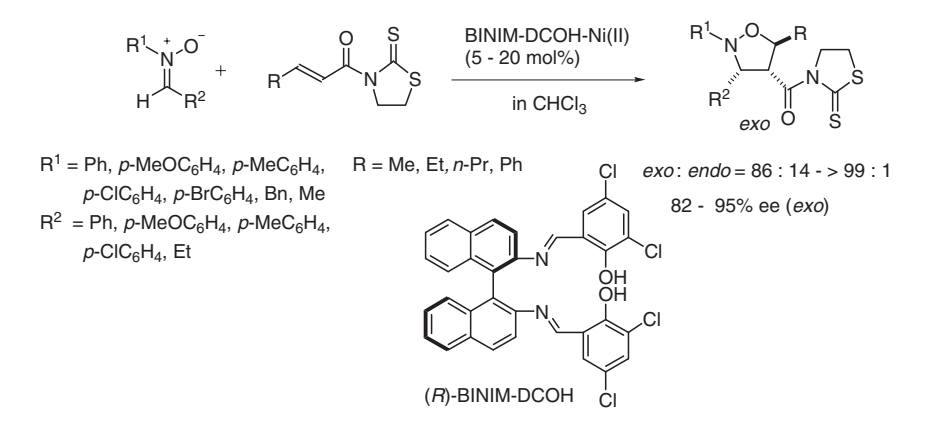
Catalyst: INDABOX-Cu(II) triflate complex

In the investigations to develop novel asymmetric catalysts, Suga et al. have found that the complexes prepared from the binaphthyldiimines (BINIM) (Fig. 4) and Ni(ClO<sub>4</sub>)<sub>2</sub>•6H<sub>2</sub>O as chiral Lewis acids showed good activity and high levels of asymmetric induction in Diels-Alder reactions and Michael type addition reactions [62–64]. Although the highest enantioselectivity in a reaction of *C,N*-diphenyl nitrone with 3-crotonoyl-2-oxazolidinone using BINIM-DC-Ni(II) complex was

 $\begin{array}{lll} & & & & & & & & & & & & & & & & \\ R^1 = \, R^4 = \, CI, \, \, R^2 = \, R^3 = \, H: \, \, (\textit{R}) - BINIM-DC & & & & & & & & \\ R^1 = \, OH, \, \, R^4 = \, H, \, \, R^2 = \, R^3 = \, CI: \, (\textit{R}) - BINIM-DCOH & & & & & & & \\ & & & & & & & & & & \\ & & & & & & & & & & \\ & & & & & & & & & \\ & & & & & & & & \\ & & & & & & & & \\ & & & & & & & \\ & & & & & & & \\ & & & & & & & \\ & & & & & & & \\ & & & & & & & \\ & & & & & & & \\ & & & & & & & \\ & & & & & & \\ & & & & & & \\ & & & & & & \\ & & & & & & \\ & & & & & & \\ & & & & & & \\ & & & & & & \\ & & & & & & \\ & & & & & & \\ & & & & & & \\ & & & & & & \\ & & & & & & \\ & & & & & & \\ & & & & & & \\ & & & & & & \\ & & & & & \\ & & & & & & \\ & & & & & & \\ & & & & & & \\ & & & & & \\ & & & & & & \\ & & & & & & \\ & & & & & & \\ & & & & & & \\ & & & & & & \\ & & & & & \\ & & & & & \\ & & & & & \\ & & & & & \\ & & & & & & \\ & & & & & \\ & & & & & \\ & & & & & \\ & & & & & \\ & & & & & \\ & & & & & \\ & & & & & \\ & & & & \\ & & & & & \\ & & & & \\ & & & & & \\ & & & & \\ & & & & \\ & & & & \\ & & & & \\ & & & & \\ & & & & \\ & & & & \\ & & & & \\ & & & & \\ & & & & \\ & & & \\ & & & & \\ & & & & \\ & & \\ & & & \\ & & \\ & & & \\ & & & \\ & & & \\ & & & \\ & & & \\ & & & \\ & & & \\ & & & \\$ 

Fig. 4 Structures of chiral binaphthyldiimine ligands [66]

limited to 80% ee for *endo*-adduct (*endo:exo* = 82:18) [65], the reaction of *C,N*-diphenyl nitrone with 3-crotonoyl-2-thiazolidinethione using BINIM-DCOH (Fig. 4) as a ligand in conjunction with CHCl<sub>3</sub> as solvent was found to provide the most favorable results in terms of both *exo*-selectivity (>99:1) and enantioselectivity (93% ee) (Scheme 10) [66]. The use of BINIM-4-Me-2QN ligand (Fig. 4) under similar conditions showed also high enantioselectivitity (91% ee) of *exo*-adduct, however, *exo*-selectivity (72:28) was not satisfactorily. The optimized conditions applied to reactions between various nitrones and 3-crotonoyl-2-thiazolidinethione showed that regardless of the electron-donating or -attracting character of the *p*-substituents on the *N*- and *C*-benzene-rings, high *exo*-selectivities (93:7–>99:1) and high enantioselectivities (88–95% ee) were observed in the reactions of several *C,N*-diphenyl nitrones with *p*-substituents (Scheme 10). It should be noted that the reactions of *C,N*-diphenyl nitrone with 3-crotonoyl-2-thiazolidinethione in the



**Scheme 10** Cycloaddition reactions of nitrones with 3-(2-alkenoyl)-2-thiazolidinethiones catalyzed by BINIM-Ni(II) complex [66]

130 H. Suga

Fig. 5 Proposed mechanism for enantioselectivity in nitrone cycloadditions [66]

presence of 5 mol% of the (*R*)-BINIM-DCOH-Ni(II) complex afforded the products in good yields with extremely high *exo*- (99:1) and enantioselectivity (90% ee). The catalytic activities of (*R*)-BINIM-DCOH-Ni(II) catalyst can be extended to *N*-alkyl and *C*,*N*-dialkyl nitrones with good *exo*- (86:14–93:7) and enantioselectivities (82–90% ee). This chiral Ni(II) catalytic system was also applicable to 1,3-dipolar cycloaddition reactions of several nitrones with 3-(2-pentenoyl)-, 3-(2-hexenoyl)-, and 3-cinnamoyl-2-thiazolidinethiones with satisfactory *exo*- (93:7–>99:1) and enantioselectivities (83–93% ee).

Based on the X-ray structural analysis of DBFOX/Ph-Ni(ClO<sub>4</sub>)<sub>2</sub>•3H<sub>2</sub>O reported by Kanemasa et al. [37], the structure of (*R*)-BINIM-DCOH-Ni(II)•2H<sub>2</sub>O was constructed as a hexa-coordinated octahedral complex by the modeling program for mechanistic consideration. After optimization of (*R*)-BINIM-DCOH-Ni(II)•2H<sub>2</sub>O by semiempirical PM3 molecular orbital calculations, the structure of the Ni(II)-3-crotonoyl-2-thiazolidinethione complex, which was constructed by replacing two molecules of water with 3-crotonoyl-2-thiazolidinethione, was also optimized. The model of the complex indicated that the *Si*-face (the lower side view) is much more shielded by a chlorine atom on benzene-ring than the *Re*-face (the top side view) which located within a relatively extensive space (Fig. 5). The space-filling models of the complex showed that *endo* approach of nitrones might be restricted compared with *exo* approach because of steric repulsion between 3,5-dichrolopheny moiety of the Ligand and *N*-substituents (R<sup>1</sup>) on nitrones for *endo* approach (Fig. 6).

# 2.4 Cycloaddition Reactions of Nitrones with α'-Hydroxy Enones

α'-Hydroxy enones could be used as bidentate olefinic dipolarophiles for enantioselective nitrone cycloadditions catalyzed by chiral heterocycle-based metal complexes. Box-t-Bu-Cu(II) complex (10 mol%) was found to be the most successful

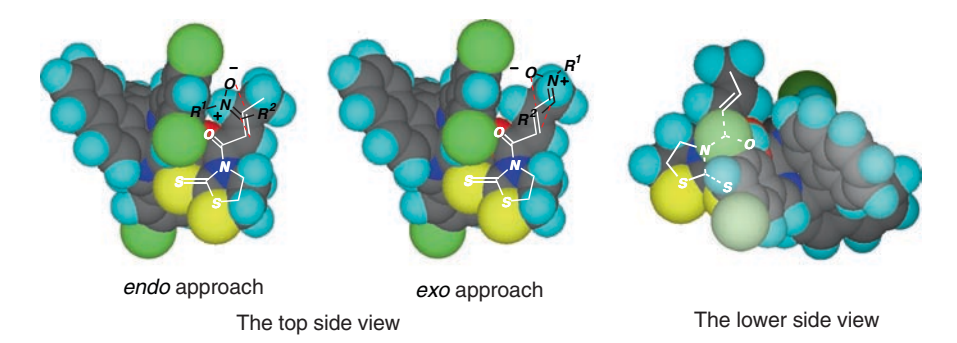


Fig. 6 Optimized structure of (R)-BINIM-DCOH-Ni(II)-3-crotonoyl-2-thiazolidinethione complex [66]

in providing the corresponding cycloadducts with very high stereoselectivity (endo:exo = 76:24–>98:2, 90–>99% ee) and with regioisomeric ratios equal to or greater than 90:10 in the reactions of several *C*-aryl nitrones with  $\alpha'$ -hydroxy enone **1a** (Scheme 11) [67]. This represents that the highest combined regio- and enantioselectivity observed for  $\beta$ -unsubstituted enoyl substrates.  $\beta$ -Substituted  $\alpha'$ -hydroxy enone **1b** also reacted with nitrones under similar conditions to give 3,4,5-trisubstituted isoxazolidines with high diastereo- (about 98:2) and enantioselectivities (>99% ee).

Scheme 11 Cycloaddition reactions of nitrones with  $\alpha'$ -hydroxy enones catalyzed by Box-Cu(II) complex [67]

# 2.5 Cycloaddition Reactions of Nitrones with α,β-Unsaturated Alhehydes

Some chiral Lewis acids can catalyze the nitrone cycloadditions of  $\alpha$ , $\beta$ -unsaturated aldehydes [68–74]. For heterocycle-based metal complex-catalyzed reactions, cycloadditions of *C*,*N*-diphenyl nitrones to a variety of  $\alpha$ , $\beta$ -unsaturated aldehydes

were reported to be effectively catalyzed using the nickel(II), zinc(II), magnesium(II), and cobalt(II) complexes derived from the DBFOX/Ph ligand [73]. The nickel(II) and magnesium(II) complexes in the reactions with  $\alpha$ -alkyl- and  $\alpha$ -arylacrolein, and the zinc(II) complexes in the reactions of C-aryl N-phenyl nitrones with  $\alpha$ -bromoacrolein were more useful (Scheme 12). The highest enantioselectivity up to 99.5% ee was observed in the reaction with  $\alpha$ -bromoacrolein performed at room temperature using especially active catalysts derived from the ZnI<sub>2</sub> complex by replacement of an iodide anion with ClO<sub>4</sub> anion. Furthermore, to solve the aggregation issue of metal complex catalysts, steric protection of the metal center of catalysts by structural modification of chiral ligand was found to be effective in obtaining higher activity in the cases of DBFOX/Ph-transition metal complexes. The second generation of DBFOX/Ph ligands have been successfully applied to the nitrone cycloadditions to a variety of α,β-unsaturated aldehydes with improved exolendo selectivity and enantioselectivity [74]. Excellent enantioselectivities up to 99% ee were demonstrated in the reactions at room temperature with a catalytic loading of 2 mol%.

$$\begin{array}{c} R,R\text{-}DBFOX/Ph-\\ \text{Metal Complex}\\ (10 \text{ mol}\%) \\ \text{in } CH_2Cl_2 \end{array} \begin{array}{c} Ph \\ \text{Ph} \end{array} \begin{array}{c} O \\ \text{Me} \end{array} \begin{array}{c} CHO \\ \text{Ar} \end{array} \begin{array}{c} Ph \\ \text{Br} \end{array} \begin{array}{c} O \\ \text{Ar} \end{array} \begin{array}{c} Ph \\ \text{Br} \end{array} \begin{array}{c} Ar = Ph, \, 4\text{-}MeC_6H4, \\ 4\text{-}BrC_6H_4, \, 4\text{-}NO_2C_6H_4, \\ 2\text{-}Furyl, \, 1\text{-}Naphthyl, } \\ 2\text{-}Naphthyl \end{array} \begin{array}{c} 2\text{-}Rphthyl \end{array} \begin{array}{c} Ar = Ph, \, 4\text{-}MeC_6H4, \\ 4\text{-}BrC_6H_4, \, 4\text{-}NO_2C_6H_4, \\ 2\text{-}Furyl, \, 1\text{-}Naphthyl, } \\ 2\text{-}Naphthyl \end{array} \begin{array}{c} R,R\text{-}DBFOX/Ph-Zn(ClO_4)_2 \\ \text{complex} \\ \text{ds } 90: 10 - > 99: 1 \\ 88 - > 99\% \text{ ee} \end{array} \begin{array}{c} 88 - > 99\% \text{ ee} \end{array} \begin{array}{c} Second \text{ genaration } R,R\text{-}DBFOX/Ph} \\ R,R\text{-}DBFOX/Ph-ZnOTf_2 \\ Complex \\ \text{ds } 95: 5: -> 99: 1 \\ 94 - > 99\% \text{ ee} \end{array}$$

Scheme 12 Cycloaddition reactions of nitrones with  $\alpha,\beta$ -unsaturated aldehydes catalyzed by DBFOX-metal complexes [73, 74]

# 2.6 Cycloaddition Reactions of Nitrones with Alkylidene Malonates

The complex of chiral trisoxazoline (Tox) and  $Co(ClO_4)_2 \cdot 6H_2O$  was found to catalyze the 1,3-dipolar cycloaddition between *C*,*N*-diaryl nitrones with alkylidene malonates with high enantioselectivity (Scheme 13) [75]. The outstanding character of this

$$\begin{array}{c} R_1 + O \\ H + R_2 \end{array} + \begin{array}{c} CO_2R^4 \\ CO_2R^4 \end{array} + \begin{array}{c} R_3 \\ R_2 \end{array} + \begin{array}{c} exo: endo = 90: 10 - > 99: 1 \\ R^2 - CO_2R^4 \end{array} + \begin{array}{c} R_3 \\ R^2 - CO_2R^4 \end{array} + \begin{array}{c} exo: endo = 90: 10 - > 99: 1 \\ R^2 - CO_2R^4 \end{array} + \begin{array}{c} R_3 \\ R^3 - R^3 \\ R^3 - R^3 - R^3 \end{array} + \begin{array}{c} endo: exo = 86: 14 - 95: 5 \\ R^3 - CO_2R^4 \end{array} + \begin{array}{c} R^3 - R^3 -$$

**Scheme 13** Cycloaddition reactions of nitrones with alkylidene malonates catalyzed by Tox-Co(II) complex [75]

reaction is that the *endolexo* selectivity could be controlled effectively by reaction temperature and thus both *cis*- and *trans*-isoxazolidine could be prepared enantioselectively. The reactions at 0 °C gave the isoxazolidines with both high enantioselectivity (89–98% ee) and high *exo*-selectivity (90:10–>99:1). However, when the temperature was lowered from 0 to –40 °C, the same cycloaddition afforded *endo* isomers as the major products (86:14–95:5) with good to high enantioselectivity (71–93% ee). It was also found that the *cis* isomer was smoothly transformed into the *trans* isomer in the presence of Co(II) catalyst at 0 °C. On the basis of this experimental evidence, it was concluded that reaction to form *cis*-isoxazolidine is reversible and subject to kinetic control at –40 °C. In the case of the reaction at 0 °C, the cycloaddition is subject to thermodynamic control, favoring the *trans* isomer.

## 2.7 Cycloaddition Reactions of Nitrones with Vinyl Ethers

The asymmetric inverse-electron demand 1,3-dipolar cycloadditions (1,3-dipole/LUMO-dipolarophile/HOMO) have also been investigated using heterocycle-based metal complexes as chiral Lewis acids. In the presence of Box-t-Bu-Cu(OTf)<sub>2</sub> as the catalyst, the glyoxylate-derived N-benzyl nitrone, which coordinate to the chiral catalyst in a bidentate fashion, reacted smoothly with ethyl vinyl ether at room temperature to give isoxazolidines in good yields and exo-selectivity (up to 84:16) and with high enantioselectivity of up to 93% ee (Scheme 14) [76]. In the reaction with 2-methoxypropene under similar conditions, endo-adduct (endo:exo = 69:31) was preferably obtained with 94% ee. To account for the absolute stereochemistry of the 1,3-dipolar cycloaddition adduct obtained by reaction of the glyoxylate-derived N-benzy nitrone with ethyl vinyl ether catalyzed by the Box-t-Bu-Cu(OTf)<sub>2</sub> catalyst, a pentacoordinated intermediate containing the chiral Box ligand, the

134 H. Suga

**Scheme 14** Cycloaddition reactions of nitrones with vinyl ethers catalyzed by Box-Cu(II) complex [76]

$$\begin{array}{c|c} & & & & & & \\ & & & & & \\ & & & & \\ & & & & \\ & & & \\ & & & \\ & & & \\ & & & \\ & & & \\ & & & \\ & & & \\ & &$$

Fig. 7 Proposed pentacoordinated intermediate for cycloaddition reaction of nitrone with vinyl ether catalyzed by Box-Cu(II) catalyst [76]

nitrone, and ethyl vinyl ether have been proposed (Fig. 7). In the intermediate, the nitrone is coordinated in the equatorial plane and the bisoxazoline in the equatorial and axial positions, leaving the remaining axial position available for the coordination of ethyl vinyl ether. The coordination of ethyl vinyl ether in this axial position allows the alkene fragment to approach the *Re*-face of the nitrone in an *exo*-selective fashion, leading to the formation of the isoxazolidine with the absolute (3*R*,5*S*) stereochemistry as observed by X-ray analysis.

# 3 Cycloaddition Reactions of Diazo Compounds

### 3.1 Cycloaddition Reactions of Trimethylsilyldiazomethane

Kanemasa et al. reported the first successful examples of Lewis acid-catalyzed enantioselective cycloaddition reactions of trimethylsilyldiazomethane using heterocycle-based metal complexes [77]. Mish et al. previously reported the diastereoselective

cycloadditions of trimethylsilyldiazomethane to chiral alkenes and upon treatment with acid chloride/silver triflate after the completion of cycloaddition, 2-pyrazolines were produce by regioselective acyldesilylation [78]. When trimethylsilyldiazomethane was treated with 3-crotonoyl-2-oxazolidinone, acetic anhydride, and MS 4 Å in dichloromethane in the presence of the R,R-DBFOX/Ph-Zn(ClO<sub>4</sub>),•3H<sub>2</sub>O (10 mol%) at -40 °C, the desilylacetylated 2-pyrazoline cycloadduct was found to produce in 87% yield in 99% ee (Scheme 15). The nickel(II) aqua complex (93% ee) and the magnesium complex (up to 82% ee) were a less effective in enantioselectivity than the zinc(II) aqua in the reaction with 3-crotonoyl-2-oxazolidinone. The reaction with 3-acryloyl-2-oxazolidinone catalyzed by the zinc aqua complex (10 mol%) led to a racemic result and both 3-(2-hexenoyl)-2-oxazolidinone (47% ee) and 3-(4-methyl-2-pentenoyl)-2-oxazolidinone (71% ee) were much less enantioselective than the methyl-substituted dipolarophile. In the case of using 3-crotonoyl-4, 4-dimethyl-2-oxazolidinone as a dipolarophile, the R,R-DBFOX/Ph-Mg(ClO<sub>2</sub>)<sub>2</sub> complex was the catalyst of choice to mediate the reaction to give 2-pyrazoline with 97% ee, (Scheme 15) while both the R.R-DBFOX/Ph-zinc(II) and -nickel(II) complexes were totally inactive. Other dipolarophiles having 2-hexenoyl and 4-methyl-2-pentencyl substituents at the nitrogen atom of the 4,4-dimethyl oxazolidinone, showed similarly high enantioselectivities of 98% ee regardless of the α-substituents of dipolar ophiles. It is also interesting to note that two products obtained from 2-oxazolidinone and 4,4-dimethyl-2-oxazolidinone dipolarophiles were found to have the opposite absolute stereochemistry which was determined by X-ray analysis.

TMSCHN<sub>2</sub> + R 
$$\stackrel{\bigcirc}{\longrightarrow}$$
  $\stackrel{\bigcirc}{\longrightarrow}$   $\stackrel{\bigcirc}{\longrightarrow}$ 

**Scheme 15** Cycloaddition reactions of trimethylsilyldiazomethane catalyzed by *R*,*R*-DBFOX/ Ph-metal complexes [77]

### 3.2 Cycloaddition Reactions of Diazoacetate

Sibi et al. have also reported a method for highly enantioselective synthesis of 2-pyrazolines via INDABOX-Mg(II)-catalyzed cycloaddition of diazoesters to 2-(2-alkenoyl)-1-benzyl-5,5-dimethyl-3-pyrazolidinones [79]. Initially formed 1-pylazolines by 1,3-dipolar cycloadditions were isomerized to 2-pyrazolines possessing ester substituent at imino carbon under the reaction conditions. Among Mg(II) salts tested, the best combination of reactivity and enantioselectivity was observed when Mg(NTf<sub>2</sub>)<sub>2</sub>–INDABOX was employed as the chiral Lewis acid (Scheme 16). The methodology allows facile access to enantioenriched pyrazolines (88–99% ee) derived from  $\beta$ -substituted,  $\alpha$ -substituted, and  $\alpha,\beta$ -disubstituted dipolarophiles, the latter two resulting in pyrazolines bearing quaternary *tert*-alkyl amino stereocenters at the 5-position of the pyrazoline.

Catalyst: INDABOX-Mg(NTf2)2 complex

Scheme 16 Cycloaddition reactions of diazoacetate catalyzed by INDABOX-Mg(II) complex [79]

### 4 Cycloaddition Reactions of Nitrile Oxides

Nitrile oxide cycloaddition to olefins is an important synthetic transformation as well as nitrone cycloaddition because the corresponding cycloadducts could be used as building-blocks containing nitrogen and oxygen functionalities by reductive cleavage of the N-O bond. Diastereoselective nitrile oxide cycloadditions have been investigated extensively, and successful methods are at hand, which were utilized for a number of biologically important natural product syntheses. However, the development of enantioselective variants using chiral Lewis acids has been hampered by the use of coordinative amine bases for the generation of the nitrile oxide, by the high donor ability of the oxygen atom of the dipole, and by the propensity of the dipole to dimerize. Recently Sibi et al. have reported on a successful catalytic example (79–99% ee) of the reaction with (2-alkenoyl)-3-pyrazolidinones using INDABOX-Mg(II) complex as a chiral Lewis acid catalyst (Scheme 17) [80]. The reaction of mesityl nitrile oxide, an isolable dipole, with

1-benzyl-2-crotonoyl-5,5-dimethyl-3-pyrazolidinone in the presence of the catalyst (30 mol%) prepared from MgI<sub>2</sub> and INDABOX having cyclopropane at linkage of Box as a ligand showed high regioselectivity (99:1) and excellent enantioselectivity (99% ee). The nature of the magnesium counterion had limited influence, with magnesium perchlorate and triflimide giving results almost as good as with MgI<sub>2</sub>. The combination of the same ligand and Cu(OTf)<sub>2</sub>, which has provided excellent enantioselectivity for various transformations, proved to be ineffective. Lowering the catalytic loading from 30 to 10 to 5 mol% reduced both regionselectivity and enantioselectivity. Reactions with other 2-(alkenoyl)-1-benzyl-5,5-dimethyl-3pyrazolidinones (R<sup>2</sup> = Et, Ph, and CO<sub>2</sub>Et) catalyzed by INDABOX-MgI<sub>2</sub> complex were highly efficient, providing the products in good yields (75-86%) and high regio- (99:1) and enantioselectivity (99% ee). Cycloaddition with several unstable aryl nitrile oxides, which generated from hydroximinoyl chlorides using Amberlyst 21 as the base, gave the corresponding adducts regioselectively (10:1–99:1) in high enantioselectivity (86–99% ee) and reasonable yields (61–75%). Similarly generated aliphatic nitrile oxides also gave the cycloadducts with good selectivities (regioselectivity: 33:1-99:1, 79-92% ee), although the reactions were slower and proceeded in lower yields (44–63%).

$$R^{1}-C \equiv N-O^{-} + R^{2} \qquad \qquad (30 \text{ mol}\%)$$

$$R^{1}=2,4,6-\text{Me}_{3}\text{C}_{6}\text{H}_{2}$$

$$R^{2}=\text{Me, Et, Ph, CO}_{2}\text{Et}$$

$$R^{2}=\text{Me, Et, Ph, CO}_{2}\text{Et}$$

$$R^{1}=\text{Ph, 2-CIC}_{6}\text{H}_{4}, 4-\text{CIC}_{6}\text{H}_{4},$$

$$4-\text{Me}\text{OC}_{6}\text{H}_{4}, t\text{-Bu, } t\text{-Bu}$$

$$Catalyst: \text{INDABOX-Mg(II) complex}$$

**Scheme 17** Cycloaddition reactions of nitrile oxides with 2-(2-alkenoyl)-3-pyrazolidinones catalyzed by INDABOX-Mg(II) complex [80]

Yamamoto et al. also demonstrated that good asymmetric induction (87% ee) observed in the reaction of benzonitrile oxide, which was generated from hydroximinoyl chloride by treatment with triethylamine, with 3-acryloyl-2-imidazolidinone in the presence of 1 equiv. of (S)-Pybox-i-Pr-Mg(II) complex (Scheme 18) [81].

More recently Suga et al. have found that chiral BINIM-Ni(II) complexes were also effective catalysts for asymmetric 1,3-dipolar cycloaddition reactions between 2-acryloyl- and 2-crotonoyl-3-pyrazolidinones, and nitrile oxides which were

**Scheme 18** Cycloaddition reaction of benzonitrile oxide with 3-acryloyl-2-imidazolidinone in the presence of (*S*)-Pybox-*i*-Pr-Mg(II) complex [81]

generated from the corresponding hydroximinoyl chlorides under the infuence of MS 4 Å (Scheme 19) [82]. High to moderate enantionselectivities (76–92% ee) were observed for several nitrile oxides including a straight chain aliphatic nitrile oxide with high regioselectivities (98:2–>99:1) and high to good yields (73–97%) by the catalyst loading of 10 mol%.

$$R = Ph, 4-CIC_{6}H_{4}, \\ t-Bu, i-Bu, n-Bu \\ R = Ph, 4-CIC_{6}H_{4}, \\ t-Bu, n-Bu \\ R = Ph, 4-$$

**Scheme 19** Cycloaddition reactions of nitrile oxides with 2-(2-alkenoyl)-3-pyrazolidinones catalyzed by BINIM-Ni(II) complex [82]

### 5 Cycloaddition Reactions of Nitrile Imines

The INDABOX-Mg(II) complex described in the cycloaddition reactions of nitrile oxides has been found to be an efficient chiral Lewis acid for regioselective and enantioselective cycloadditons of nitrile imines to 3-(2-alkenoyl)-2-oxazolidinones (Scheme 20) [83]. Nitrile imine **2a** was generated from the corresponding hydrazonyl bromide by dehydrohalogenation using diisopropylethylamine as base, and the reaction with 3-crotonoyl-2-oxazolidinone was preformed utilizing the INDABOX ligand in combination with magnesium Lewis acids (Mg(NTf<sub>2</sub>)<sub>2</sub>, MgI<sub>2</sub>, Mg(ClO<sub>4</sub>)<sub>2</sub>) to provide cycloadduct in high yield and excellent enantioselectivity (96–97% ee). Several 3-(2-alkenoyl)-2-oxazolidinones possessing no substituent or a number of substituents R<sup>1</sup> including functionalized groups also allowed to react with nitrile imine **2a** under similar conditions to give cycloadducts in high yields (>90%) and high enantioselectivies (84–99% ee). The hydrazonyl bromide derived from an enolizable aliphatic aldehyde and the derivative of a *p*-methoxyphenyl substituent on nitrogen, which provides a potential handle for nitrogen deprotection, could be used for the reaction with high enantioselectivities (96–99% ee).

Scheme 20 Cycloaddition reactions of nitrile imines catalyzed by INDABOX-Mg(II) complex [83]

### 6 Cycloaddition Reactions of Azomethine Imines

As described above, highly enantioselective 1,3-dipolar cycloaddition reactions catalyzed by chiral Lewis acids have been developed for several 1,3-dipoles. In contrast, catalytic asymmetric [3 + 2] cycloadditions of azomethine imines, which can afford medicinally important pyrazolidines and pyrazolines, have not received as much attention - only a few examples of catalytic asymmetric cycloadditions of azomethine imines and related compounds are available. Shintani et al. reported the highly enantioselective [3 + 2] cycloaddition between azomethine imines and copper acetylides using a chiral phosphaferrocene-oxazoline ligand (Scheme 21) [84, 85]. Kobayashi et al. reported the asymmetric [3 + 2] cycloaddition between hydrazones and electron-rich olefins in the

$$\begin{array}{c} O \\ H \\ H \\ \end{array} \begin{array}{c} O \\ H \\ \end{array}$$

Scheme 21 Enantioselective cycloadditions of azomethine imines with terminal alkynes [84]

presence of a chiral zirconium catalyst; the reaction presumably involves a Zr-associated azomethine imine species (Scheme 22) [86, 87]. Chen et al. reported a related dipole-HOMO/dipolarophile-LUMO controlled cycloaddition reactions using chiral organocatalysts (Scheme 23) [88, 89]. Recently, the first example of chiral Lewis acid-catalyzed asymmetric 1,3-dipolar cycloaddition reactions of azomethine imines with electron-deficient olefins using BINIM-Ni(II) complexes have been reported [90].

Scheme 22 Enantioselective [3 + 2] cycloadditions of hydrazones to olefins [87]

**Scheme 23** Enantioselective cycloadditions of azomethine imines catalyzed by chiral organocatalysts [88]

In the investigation for the reactions of fused azomithine imines with 3-acryloyl-2-oxazolidinone using chiral Lewis acid catalysts, the BINIM-Ni(II) complexes were found to be quite effective not only in obtaining high levels of enantioselectivity, but also in controlling the diastereoselectivity [90]. Catalyzed reactions of azomethine imine 3a with 3-acryloyl-2-oxazolidinone were carried out using chiral catalysts consisting of Ni(ClO<sub>4</sub>)<sub>2</sub>•6H<sub>2</sub>O and chiral BINIM ligands (Fig. 4). The use of BINIM-4Me-2QN as the ligand, in conjunction with CHCl, as the solvent, provided the highest enantioselectivity (97% ee); additionally, this also exhibited good trans-selectivity (Scheme 24). The use of Ni(BF<sub>4</sub>) •6H<sub>2</sub>O instead of Ni(ClO<sub>4</sub>) •6H<sub>2</sub>O for the preparation of the catalyst also resulted in extremely high enantio- (97% ee) and diastereoselectivity (trans:cis = 93:7). Reactions between C-aryl azomethine imines 3b-3g and 3-acryloyl-2-oxazolidinone under the optimized conditions showed high levels of enantio- (90–95% ee) and trans-selectivities (80:20–>99:1); apparently, the reactions are independent of the electronic character of the benzenering substituents. Although the reaction of C-alkyl-azomethine imine 3i resulted in a moderate yield with a slight decrease in enantioselectivity (74% ee), the cycloadditions

$$(R)\text{-BINIM-4Me-2QN-Ni(II)}$$

$$\mathbf{a}: R = \text{Ph, b: } R = \rho\text{-MeOC}_6\text{H}_4, \quad \text{c: } R = \rho\text{-CNC}_6\text{H}_4, \quad \text{e: } R = \rho\text{-CIC}_6\text{H}_4, \quad \text{f: } R = 2\text{-Naphthyl, i: } R = 2\text{-Furyl, j: } R = \text{Cyclohexyl}$$

$$(R)\text{-BINIM-4Me-2QN}$$

Scheme 24 Cycloaddition reactions of azomethine imines 3a-3j with 3-acryloyl-2-oxazolidinone [90]

of naphthyl- **3h** and heteroaryl azomethine imines **3i** afforded extremely high enantioselectivities (95–96% ee).

For mechanistic consideration, the structure of (*R*)-BINIM-4-Me-2QN-Ni(II)-3-acryloyl-2-oxazolidinone complex was optimized by semiempirical PM3 molecular orbital calculations (Fig. 8). As shown in the top view of space-filling models, the *Re*-face of 3-acryloyl-2-oxazolidinone is effectively shielded by the 4-methylquinoline moiety – in contrast, as shown in the lower view, the *Si*-face is located within a relatively extensive space. Accordingly, the shielding of the *Re*-face by the 4-methylquinoline group must also effectively affect the cycloaddition during the transition state. The high enantioselectivity of the cycloaddition reactions of

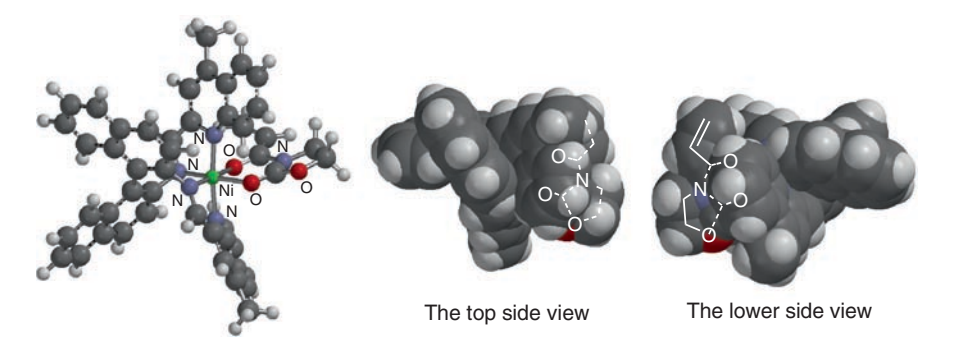


**Fig. 8** Optimized structure of (*R*)-BINIM-4Me-2QN-Ni(II)-3-acryloyl-2-oxazolidinone complex [90]

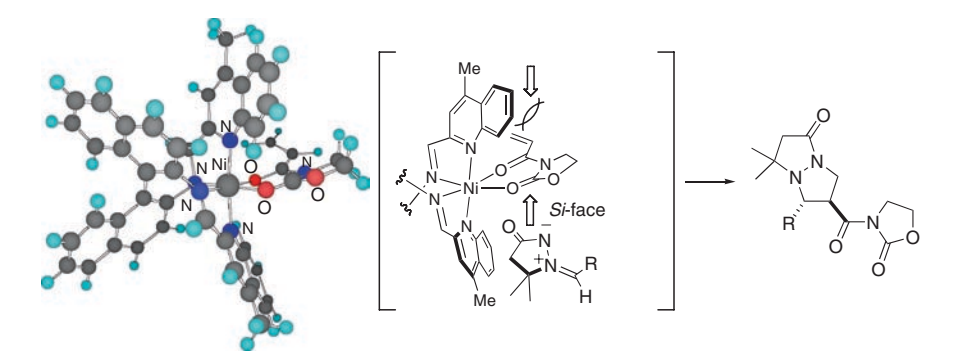


Fig. 9 Proposed mechanism for enantioselectivity in azomethine imine cycloadditions [90]

azomethine imines with 3-acryloyl-2-oxazolidinone can, therefore, be explained by the highly selective *Si*-face approach of the azomethine imines toward the proposed hexa-coordinated Ni(II) complex (Fig. 9).

Quite recently Sibi et al. reported that *cis*- and enantioselective 1,3-dipolar cycloaddition of azomethine imines to 2-acryloyl-1-benzyl-5,5-dimethyl-3-pyrazolidinone was catalyzed by INDABOX-Cu(II) complex as a chiral Lewis acid [91]. The corresponding cycloadducts are isolated with high diastereoselectivities (82:18–96:4 *cis/trans*) and enantioselectivities (78–98% ee) (Scheme 25). Interestingly, the use of chiral Lewis acid complexes prepared from INDABOX and Mg(II), Zn(II), or Ni(II) salts led to *trans*-selective cycloadditions (67:33–96:4 *trans/cis*) of azomethine imine **3a**. The Mg(OTf)<sub>2</sub>- and Zn(OTf)<sub>2</sub>-catalyzed cycloaddition gave the major diastereomer with modest enantioselectivity (47% ee and 59% ee, respectively). However, the Ni(ClO<sub>4</sub>)<sub>2</sub>-catalyzed cycloaddition was highly *trans*-selective (93:7) and gave *trans*-cycloadduct with 85% ee.

Scheme 25 Cycloaddition reactions of azomethine imines 3a–3g, 3k–3l with 2-acryloyl-1-ben-zyl-5,5-dimethyl-3-pyrazolidinone [91]

### 7 Cyloaddition Reactions of Carbonyl Ylides

Tandem Rh(II)-catalyzed carbonyl ylide formation/1,3-dipolar cycloaddition reaction sequence of  $\alpha$ -diazocarbonyl compounds with dipolar philes has been realized as a powerful and efficient methodology for the synthesis of epoxy-bridged complex polycyclic systems [52, 92]. Recently, this method has been applied toward the syntheses of a variety of biologically important natural products such as brevicomin [93], zaragozic acids [94, 95], illudins [96–98], epoxysorbicillinol [99], colchicines [100, 101], aspidophytine [102], and polygalolides [103]. Consequently, it has been a challenge to develop the catalytic enantioselective variant of the methodology in the efficient asymmetric synthesis of medicinally important oxygen-containing polycyclic compounds. Hodgson et al. [104–108] and Kitagaki et al. [109–111] have independently developed a highly enantioselective chiral Rh(II)-catalyzed procedure that feature a chiral Rh(II)-associated carbonyl ylide in the transition state. In 1997, Hodgson et al. reported the first example of asymmetric induction (up to 52% ee) in the carbonyl ylide formation/intramolecular cycloaddition sequence using the chiral Rh prolinate catalyst, Rh<sub>2</sub>[(S)-DOSP]<sub>4</sub>[104]. Subsequently, they reported that high levels of enantioselectivity (up to 90% ee) were obtained when the dirhodium(II) binaphtholphosphate catalyst,  $Rh_{\gamma}[(R)-DBBNP]_{\alpha}$  was used (Scheme 26) [105]. They recently also found high levels of asymmetric induction (up to 92% ee) in the intermolecular cycloadditions of carbonyl ylides with styrene type and strained olefinic diporalophiles (Scheme 27) [106–108]. In 1999, Kitagaki et al. demonstrated the first successful examples of the intermolecular cycloadditions of carbonyl ylides derived from α-diazo ketones with dimethyl acetylenedicarboxylate using  $Rh_2(S-BTPV)_4$  with high enantioselectivity (up to 92% ee) (Scheme 28) [109]. They also reported high levels of enantioselection for the intermolecular cycloadditions of ester-derived carbonyl ylides with DMAD (up to 93% ee) (Scheme 29) [110] and  $\alpha$ -diazo ketone-derived carbonyl ylieds with aromatic aldehydes (up to 92% ee) (Scheme 28) [111]. In contrast to this methodology, Suga et al.

have developed conceptually different approach for catalytic asymmetric induction in carbonyl ylide cycloaddition reactions using heterocycle-based chiral Lewis acids [112–115].

Chiral Rh catalyst (1 mol%)
$$V_2$$
 $V_3$ 
 $V_4$ 
 $V_4$ 
 $V_5$ 
 $V_6$ 
 $V_7$ 
 $V_8$ 
 $V_8$ 

**Scheme 26** Asymmetric intramolecular cycloaddition reactions of carbonyl ylides using chiral Rh catalyst [104, 105]

**Scheme 27** Asymmetric cycloaddition reactions of carbonyl ylides with olefinic dipolarophiles using chiral Rh catalyst [106–108]

**Scheme 28** Asymmetric cycloaddition reactions of carbonyl ylides with acetylenic and carbonyl dipolarophiles using chiral Rh catalyst [109,111]

**Scheme 29** Asymmetric cycloaddition reactions of ester-derived carbonyl ylides using chiral Rh catalyst [110]

# 7.1 Cycloaddition Reactions of Carbonyl Ylides with Electron-Deficient Carbonyl Dipolarophiles

In the Rh(II)-catalyzed reaction of o-methoxycarbonyl- $\alpha$ -diazoacetophenone, a precursor of carbonyl ylide **4**, with benzyloxyacetaldehyde, the presence of complexes (10 mol%) consisting of chiral Pybox ligands (Fig. 2) and rare earth metal

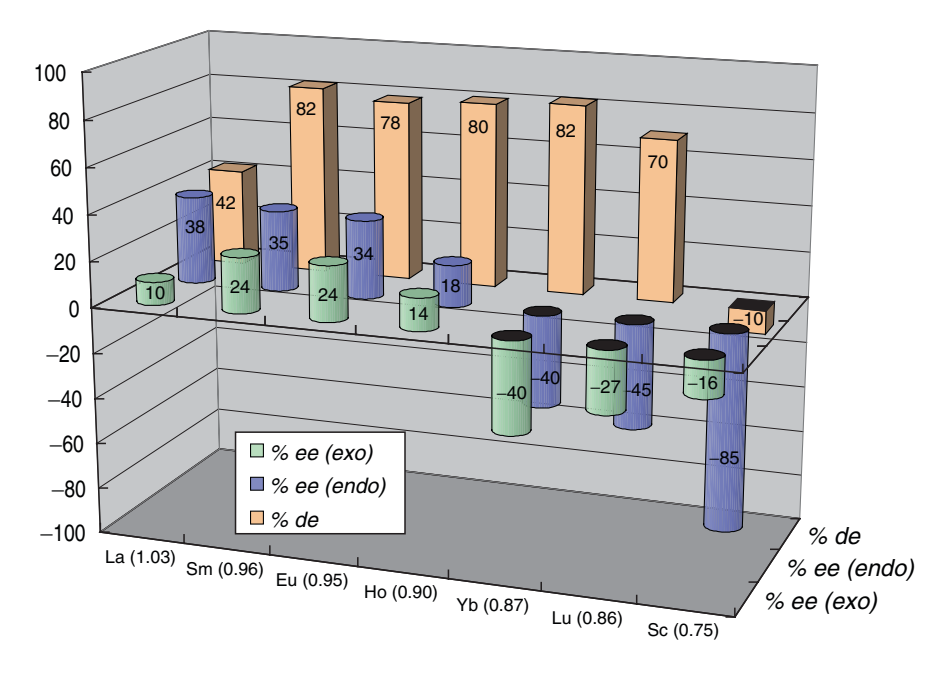


**Fig. 10** Relationship between metals and enantio- and diastereoselectivities in Pybox-*i*-Pr-M(OTf)<sub>3</sub> catalyzed reactions of carbonyl ylide **4** with aldehyde benzyloxyacetaldehyde [113]

triflates was found to show interesting result in terms of enantioselectivity [112, 113]. Although the enantioselectivities were low to moderate, the sense of asymmetric induction of both *endo*- and *exo*-approaches<sup>1</sup> was switched between Ho and Yb by using several lanthanoid triflates in combination with (S,S)-Pybox-i-Pr (Fig. 10). In contrast to these lanthanoid triflates, in the cases in which Sc(OTf)<sub>3</sub> was used in combination with (S,S)-Pybox-i-Pr, promising enantioselectivities (85% ee) of *endo*-cycloadduct were observed (*endo:exo* = 55:45). From the investigation of preparation conditions for the catalyst, preparation in the presence of MS 4 Å (room temperature, 2 h) was found to increase dramatically *endo*-selectivity (88:12) with a high level of asymmetric induction (91% ee) of *endo*-adduct (Scheme 30). The reactions of o-methoxycarbonyl- $\alpha$ -diazoacetophenone with several benzyloxy-acetoaldehyde derivatives under optimized conditions proceeded smoothly with high enantioselectivities (82–93% ee) of *endo*-cycloadducts.

In the (S,S)-Pybox-i-Pr-Sc(III) catalyzed reactions with methyl and benzyl pyruvate, the use of trifluoroacetic acid (TFA) (10 mol%) as an additive was found to improve both diastereo- (exo:endo = 96:4 and 93:7, respectively) and enantioselectivity (84% ee and 94% ee, respectively) (Scheme 31), although the maximum enantiomeric excess of the exo-adduct was only 56% ee when the combination of Sc(OTf), and (S,S)-Pybox-TPSm was used without TFA [112, 113].

<sup>&</sup>lt;sup>1</sup>The *endo-*adduct is defined as the product in which the more important substituent is on the opposite side of the epoxy bridge.

**Scheme 30** Cycloaddition reactions of carbonyl ylide **4** with benzyloxyacetaldehyde derivatives [112, 113]

**Scheme 31** Cycloaddition reactions of carbonyl ylide **4** with  $\alpha$ -keto esters [112, 113]

The (S,S)-Pybox-i-Pr-Sc(III) catalytic system including TFA was applied to the reaction with several benzyl pyruvate derivatives and the other  $\alpha$ -keto esters. High levels of diastereo- (exo:endo=96:4–97:3) and enantioselectivity (92–94% ee) were observed in the reactions with a number of p-substituted benzyl pyruvates. The electronic character of the p-substituents did not influence the selectivity. The asymmetric 1,3-dipolar cycloaddition reactions with several other  $\alpha$ -keto esters were also satisfactory in terms of high enantioselectivities (80–95% ee) of exo-cycloadducts.

# 7.2 Cycloaddition Reactions of Carbonyl Ylides with Electron-Deficient Olefinic Dipolarophiles

In the case of an electron-deficient olefinic dipolarophile, 3-acryloyl-2-oxazolidinone, the catalyst prepared from (*S*,*S*)-Pybox-Ph (Fig. 3) and Yb(OTf)<sub>3</sub> under similar conditions described in Sect. 7.1 showed a promising result in terms of

enantioselectivity (89% ee) of exo-cycloadduct (exo:endo = 54:46) (94% yield). Under the optimized conditions (preparing the complex in THF, lowering the reaction temperature to -25 °C, and slowing addition to 6 h), exo-adduct was obtained diastereoselectively (exo:endo = 80:20-86:14) in high yields (81-94%) with high enantioselectivity (96–97% ee) (Scheme 32) [112, 113]. In contrast to the reaction with 3-acryloyl-2-oxazolidinone, high endo-selectivity was observed in the reaction with 3-crotonoyl-2-oxazolidinone. However, enantioselectivity of endo-adduct was unsatisfactory. After investigating the influence of ester substituents on diazo substrates on enantioselectivity, the reaction of o-[(p-bromobenzyloxy)carbonyl]- $\alpha$ diazoacetophenone (p-bromobenzyl ester) was found to show high enantioselectivity (96% ee) and extremely high endo-selectivity (>99:1) in (4S,5S)-Pybox-4,5-Ph<sub>2</sub>-Yb(III) catalyzed reaction (Scheme 33) [114]. The reactions of o-methoxycarbonyl-α-diazoacetophenone with 3-cinnamoyl and 3-[3-(ethoxycarbonyl) propenoyl]-2-oxazolidinones showed high endo-selectivity with moderate enantioselectivity (72% ee and 78% ee, respectively).

Scheme 32 A cycloaddition reaction of carbonyl ylide 4 with 3-acryloyl-2-oxazolidinone [112, 113]

Scheme 33 Reactions of diazoacetophenones with 3-(2-alkenoyl)-2-oxazolidinones [114]

## 7.3 Cycloaddition Reactions of Carbonyl Ylides with Electron-Releasing Olefinic Dipolarophiles

Asymmetric cycloaddition reactions of carbonyl ylides with electron-deficient dipolarophiles described up to this point could be classified the reaction controlled by the strongest interaction between HOMO of the carbonyl ylides and LUMO of the dipolarophiles. It is known that inverse electron demand type cycloadditions of carbonyl ylides, which controlled by the strongest interaction between the dipolarophile HOMO and the carbonyl ylide LUMO, also occur. The reaction of o-methoxycarbonyl-α-diazoacetophenone with butyl vinyl ether, as an electronrich dipolarophile, also showed asymmetric induction in the presence of complexes of chiral Pyboxs and lanthanoid triflates (Scheme 34) [115]. The effects of the ionic radius of lanthanoid metals [116] on the enantio- and diastereoselectivity were investigated using (4S,5S)-Pybox-Ph, as the ligand and refluxing in CH<sub>2</sub>Cl<sub>2</sub> (Fig. 11). Promising results were obtained for Eu(OTf)<sub>3</sub>, Gd(OTf)<sub>3</sub>, Ho(OTf)<sub>3</sub>, Er(OTf)<sub>3</sub> and Tm(OTf), in terms of enantioselectivity. In regards to the R group on the vinyl ether, a series of reactions in the presence of the (4S,5S)-Pybox-Ph<sub>2</sub>-Eu(III) catalyst under reflux in CH<sub>2</sub>Cl<sub>2</sub> revealed that a bulky substituent such as t-Bu and cyclohexyl yielded higher diastereo- and enantioselectivities – the reaction involving cyclohexyl vinyl ether gave an enantioselectivity of 95% ee. Similarly, catalysts involving Gd(III) and Ho(III) exhibited extremely high enantioselectivity (94% ee and 96% ee, respectively) in their reactions with cyclohexyl vinyl ether.

**Scheme 34** Cycloaddition reactions of carbonyl ylide **4** with vinyl ethers [115]

To investigate the generality of this methodology on other diazo compounds, the reaction between  $\alpha,\alpha'$ -dicarbonyl diazo substrate **5a** (R' = Pr) and butyl vinyl ether was carried out. Although various combinations of the chiral Pybox ligands and lanthanoid triflates as catalysts did not give satisfactory enantioselectivities, chiral (*R*)-BINIM-4Me-2QN-Ni(II) catalyst was found to show high enantioselectivity

<sup>&</sup>lt;sup>2</sup>(4*S*,5*S*)-Pybox-Ph<sub>2</sub>-Eu(OTf)<sub>3</sub> (10 mol%), CH<sub>2</sub>Cl<sub>2</sub>, reflux: 89% yield, 44% ee; (4*S*,5*S*)-Pybox-Ph<sub>3</sub>-Yb(OTf)<sub>3</sub> (10 mol%), CHCl<sub>3</sub>, reflux: 71% yield, 45% ee.

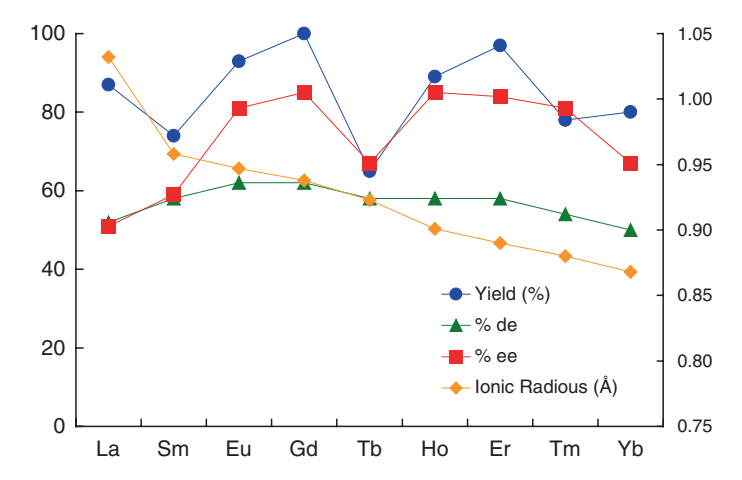


**Fig. 11** Relationship between metal and enantio- and diastereoselectivity in (4*S*,5*S*)-Pybox-Ph,-M(OTf), catalyzed cycloaddition reaction of carbonyl ylide **4** with butyl vinyl ether [115]

(92% ee) with extremely high *endo*-selectivity (>99:1) (Scheme 35) [115]. The BINIM-4Me-2QN-Ni(II) catalyst was also employed for the reactions of several  $\alpha,\alpha'$ -dicarbonyl diazo compounds **5a–5h** with cyclohexyl vinyl ether to give *endo*-cycloadducts exclusively with good to excellent enantioselectivities (77–97% ee).

Scheme 35 Reactions of diazo compounds 5a–5h with vinyl ethers [115]

#### 8 Conclusion

This chapter summarized recent advances in the chemistry of the heterocycle-based metal complexes used in 1,3-dipolar cycloaddition reactions for asymmetric induction and recognition of enantiotopic face as heterocyclic supramolecular type chiral

Lewis acid catalysts. Although there are some limitations to be solved for all of the 1,3-dipoles obtaining high levels of asymmetric induction catalyzed by chiral Lewis acids, a number of heterocycle-based chiral Lewis acids are found to be efficient for highly enantioselective 1,3-dipolar cycloadditions of some 1,3-dipoles. For certain 1,3-dipoles, the use of coordinative amine bases for the generation of the dipole, the high donor ability of the heteroatom of the dipole, and the instability of the dipole may be posed as issues employing chiral Lewis acids compared with similar concerted Diels-Alder reactions with hydrocarbon dienes. It should be note that the chiral heterocycle-based metal complexes are especially effective among a number of chiral Lewis acids developed for other catalytic asymmetric reactions. Of the heterocycle-based ligands, chiral Box, Pybox, and related oxazoline ligands play an important role in the enantioface differentiation of the dipolar cycloadditions. The metals utilized for the heterocycle-based complexes also show a crucial role for degree of asymmetric induction depending upon the 1,3-dipole used. In the reaction of certain 1,3-dipole, the combination of a chiral ligand and a metal salt, which has provided excellent enantioselectivity for cycloadditions of the other 1,3-dipoles, prove to be ineffective in terms of enantioselectivity even with the similar electron-deficient dipolarophiles. Counter ions of metal salts and presence or absence of MS also affect the selectivity. In summary, asymmetric 1,3-dipolar cycloadditions are highly attractive reactions for the synthesis of enantiomerically enriched and biologically active heterocyclic compounds, this field is rapidly evolving and also provides many challenges to develop heterocycle-based metal complexes as novel chiral catalysts for future study.

**Ackowledgments** I wish to thank my coworkers, whose names appear on the cited papers. Financial support for this work by a Grant-in Aid for Scientific Research from the Ministry of Education, Science, Sports and Culture, Japan is gratefully ackowledged.

#### References

- 1. Lehn J-M (1995) Supramolecular chemistry: concepts and perspective. VCH, Weinheim
- Fujita M (2000) Molecular self-assembly organic versus inorganic approaches. Springer, Berlin Heidelberg New York
- 3. Fujita M (1998) Chem Soc Rev 417
- 4. Philip D, Stoddart JF (1996) Angew Chem Int Ed 35:1155
- 5. Conn MM, Rebek J Jr (1997) Chem Rev 97:1647
- 6. Linton B, Hamilton AD (1997) Chem Rev 97:1669
- 7. Mizutani T, Ema T, Tomita T, Kuroda Y, Ogoshi H (1993) J Chem Soc Chem Commun 520
- 8. Mizutani T, Ema T, Tomita T, Kuroda Y, Ogoshi H (1994) J Am Chem Soc 116:4240
- 9. Kurida Y, Kato Y, Higashioji T, Ogoshi H (1993) Angew Chem 105:774
- 10. Konishi K, Yahara K, Toshishige H, Aida T, Inoue S (1994) J Am Chem Soc 116:1337
- 11. Lemaux PL, Bahri H, Simonneaux G (1991) J Chem Soc Chem Commun 1350
- 12. Lemaux PL, Bahri H, Simonneaux G (1994) J Chem Soc Chem Commun 1287
- 13. Collman JP, Zhang X, Lee VJ (1993) Science 261:1404
- 14. Groves JT, Myers RS (1983) J Am Chem Soc 105:5791
- 15. Groves JT, Viski P (1989) J Am Chem Soc 111:8537
- 16. Naruta Y, Tani F, Maruyama K (1989) Chem Lett 1269

- 17. Naruta Y, Tani F, Ishihara N, Maruyama K (1991) J Am Chem Soc 113:1378
- 18. Konishi K, Oda K, Nishida K, Aida T, Inoue S (1992) J Am Chem Soc 114:1313
- 19. Collman JP, Zhang X, Lee VJ, Brauman JI (1992) J Chem Soc Chem Commun 1647
- 20. O'Malley S, Kodadek TJ (1989) J Am Chem Soc 111:9116
- 21. Naruta Y, Tani F, Maruyama K (1990) J Chem Soc Chem Commun 1378
- 22. Chang LC, Konishi K, Aida T, Inoue S (1992) J Chem Soc Chem Commun 254
- 23. Ohkubo K, Sagawa T, Kuwata M, Hata T, Ishida H (1989) J Chem Soc Chem Commun 352
- 24. O'Malley S, Kodadek TJ (1992) Organometallics 11:2299
- 25. Ito A, Konishi K, Aida T (1996) Tetrahedron Lett 37:2585
- Seerden J-PG, Scholte op Reimer AWA, Scheeren HW (1994) Tetrahedron Lett 35:4419
- 27. Gothelf KV, Jøgensen KA (1994) J Org Chem 59:5687
- 28. Gothelf KV, Hazell RG, Jørgensen KA (1996) J Org Chem 61:346
- 29. Gothelf KV, Hazell RG, Jørgensen KA (1998) J Org Chem 63:5483
- 30. Desimoni G, Faita G, Mortoni A, Righetti P (1999) Tetrahedron Lett 40:2001
- 31. Saito T, Yamada T, Miyazaki S, Otani T (2004) Tetrahedron Lett 45:9581
- 32. Sanchez-Blanco AI, Gothelf KV, Jøgensen KA (1997) Tetrahedtron Lett 38:7923
- Nishiyama H, Sakaguchi H, Nakamura T, Horihata M, Kondo M, Itoh K (1989) Organometallics 8:846
- 34. Iwasa S, Tsushina S, Shimada T, Nishiyama H (2001) Tetrahedron Lett 42:6715
- 35. Iwasa S, Tsushima S, Shimada T, Nishiyama H (2002) Tetrahedron 58:227
- 36. Iwasa S, Maeda H, Nishiyama K, Tsushima S, Tsukamoto Y, Nishiyama H (2002) Tetrahedron 58:8281
- 37. Kanemasa S, Oderaotoshi Y, Sakaguchi S, Yamamoto H, Tanaka J, Wada E, Curran DP (1998) J Am Chem Soc 120:3074
- 38. Kanemasa S, Oderaotoshi Y, Tanaka J, Wada E (1998) J Am Chem Soc 120:12355
- 39. Iwasa S, Ishima Y, Widagdo HS, Aokia K, Nishiyama H (2004) Tetrahedron Lett 45:2121
- 40. Evans DA, Sweeney ZK, Rovis T, Tedrow JS (2001) J Am Chem Soc 123:12095
- 41. Evans DA, Masse CE, Wu J (2002) Org Lett 4:3375
- 42. Evans DA, Wu J, Masse CE, MacMillan DWC (2002) Org Lett 4:3379
- 43. Evans DA, Wu J (2003) J Am Chem Soc 125:10162
- 44. Evans DA, Scheidt KA, Fandrick KR, Lam HW, Wu J (2003) J Am Chem Soc 125:10780
- 45. Evans DA, Fandrick KR, Song H-J (2005) J Am Chem Soc 127:8942
- 46. Evans DA, Fandrick KR (2006) Org Lett 8:2249
- 47. Evans DA, Fandrick KR, Song H-J, Scheidt KA, Xu R (2007) J Am Chem Soc 129:10029
- 48. Evans DA, Wu J (2005) J Am Chem Soc 127:8006
- 49. Evans DA, Aye Y (2006) J Am Chem Soc 128:11034
- 50. Evans DA, Aye Y, Wu J (2006) Org Lett 8:2071
- 51. Evans DA, Song H-J, Fandrick KR (2006) Org Lett 8:3351
- 52. Padwa A, Pearson WH (2003) Synthetic application of 1,3-dipolar cycloaddition chemistry toward heterocycles and natural products. Wiley, Hoboken, NJ
- 53. Gothelf KV, Jøgensen KA (2000) Chem Commun 1449
- 54. Gothelf KV, Jøgensen KA (1998) Chem Rev 98:863
- 55. Frederickson M (1997) Tetrahedron 53:403
- 56. Kobayashi S, Kawamura M (1998) J Am Chem Soc 120:5840
- 57. Jensen KB, Gothelf KV, Hazell RG, Jøgensen KA (1997) J Org Chem 62:2471
- 58. Hori K, Kodama H, Ohta T, Furukawa I (1999) J Org Chem 64:5017
- 59. Heckel A, Seebach D (2002) Chem Eur J 8:560
- 60. Desimoni G, Faita G, Mella M, Boiocchi M (2005) Eur J Org Chem 1020
- 61. Sibi MP, Ma Z, Jasperse CP (2004) J Am Chem Soc 126:718
- 62. Suga H, Kakehi A, Mitsuda M (2002) Chem Lett 900
- 63. Suga H, Kakehi A, Mitsuda M (2004) Bull Chem Soc Jpn 77:561
- 64. Suga H, Kitamura T, Kakehi A, Baba T (2004) Chem Commun 1414
- 65. Suga H, Kakehi A, Ito S, Sugimoto H (2003) Bull Chem Soc Jpn 76:327

- 66. Suga H, Nakajima T, Itoh K, Kakehi A (2005) Org Lett 7:1431
- Palomo C, Oiarbide M, Arceo E, García JM, López R, González A, Linden A (2005) Angew Chem Int Ed 44:2
- 68. Viton F, Bernardinelli G, Kündig EP (2002) J Am Chem Soc 124:4968
- 69. Mita T, Ohtsuki N, Ikeno T, Yamada T (2002) Org Lett 4:2457
- Carmona D, Lamata MP, Viguri F, Rodríguez R, Oro LA, Balana AI, Lahoz FJ, Tejero T, Merino P, Franco S, Montesa I (2004) J Am Chem Soc 126:2716
- 71. Kano T, Hashimoto T, Maruoka K (2005) J Am Chem Soc 127:11926
- 72. Jen WS, Wiener JJM, MacMillan DWC (2000) J Am Chem Soc 122:9874
- 73. Shirahase M, Kanemasa S, Oderaotoshi Y (2004) Org Lett 6:675
- 74. Shirahase M, Kanemasa S, Hasegawa H (2004) Tetrahedron Lett 45:4061
- 75. Huang Z-Z, Kang Y-B, Hou J, Ye M-C, Tang Y (2004) Org Lett 6:1677
- 76. Jensen KB, Hazell RG, Jørgensen KA (1999) J Org Chem 64:2353
- 77. Kanemasa S, Kanai T (2000) J Am Chem Soc 122:10710
- 78. Mish MR, Guerra FM, Carreira EM (1997) J Am Chem Soc 119:8379
- 79. Sibi MP, Stanley LM, Soeta T (2007) Org Lett 9:1553
- 80. Sibi MP, Itho K, Jasperse CP (2004) J Am Chem Soc 126:5366
- 81. Yamamoto H, Hayashi S, Kubo M, Harada M, Hasegawa M, Noguchi M, Sumimoto M, Hori K (2007) Eur J Org Chem 2859
- Suga H, Adachi Y, Fujimoto K, Furihata Y, Tsuchida T, Kakehi A, Baba T (2009) J Org Chem 74:1099
- 83. Sibi MP, Stanley LM, Jasperse CP (2005) J Am Chem Soc 127:8276
- 84. Shintani R, Fu GC (2003) J Am Chem Soc 125:10778
- 85. Suárez A, Downey W, Fu GC (2005) J Am Chem Soc 127:11244
- Kobayashi S, Shimizu H, Yamashita Y, Ishitani H, Kobayashi J (2002) J Am Chem Soc 124:13678
- 87. Kobayashi S, Yamashita Y (2004) J Am Chem Soc 126:11279
- 88. Chen W, Yuan X-H, Li R, Du W, Wu Y, Ding L-S, Chen Y-C (2006) Adv Synth Catal 348:1818
- 89. Chen W, Du W, Duan Y-Z, Wu Y, Yang S-Y, Chen Y-C (2007) Angew Chem Int Ed 46:7667
- 90. Suga H, Funyu A, Kakehi A (2007) Org Lett 9:97
- 91. Sibi MP, Rane D, Stanley LM, Soeta T (2008) Org Lett 10:2971
- 92. Padwa A, Weingarten MD (1996) Chem Rev 96:223
- 93. Padwa A, Fryxell GE, Zhi L (1990) J Am Chem Soc 112:3100
- Hodgson DM, Bailey JM, Villalonga-Barber C, Drew MGB, Harrison T (2000) J Chem Soc Perkin Trans 1 3432
- 95. Nakamura S, Hirata Y, Kurosaki T, Anada M, Kataoka O, Kitagaki S Hashimoto S (2003) Angew Chem Int Ed 42:5351
- 96. Padwa A, Sandanayaka VP, Curtis EA (1994) J Am Chem Soc 116:2667
- 97. Kinder FR Jr, Bair KW (1994) J Org Chem 59:6965
- 98. Padwa A, Curtis EA, Sandanayaka VP (1997) J Org Chem 62:1317
- 99. Wood JL, Thompson BD, Yusuff N, Pflum DA, Matthäus MSP (2001) J Am Chem Soc 123:2097
- 100. Graening T, Friedrichsen W, Lex J, Schmalz H-G (2002) Angew Chem Int Ed 41:1524
- 101. Graening T, Bette V, Neudörfl J, Lex J, Schmalz H-G (2005) Org Lett 7:4317
- 102. Mejía-Oneto JM, Padwa A (2006) Org Lett 8:3275
- 103. Nakamura S, Sugano Y, Kikuchi F, Hashimoto S (2006) Angew Chem Int Ed 45:6532
- 104. Hodgson DM, Stupple PA, Johnstone C (1997) Tetrahedron Lett 38:6471
- 105. Hodgson DM, Stupple PA, Johnstone C (1999) Chem Commun 2185
- 106. Hodgson DM, Stupple PA, Pierard FYTM, Labande AH, Johnstone C (2001) Chem Eur J 7:4465
- 107. Hodgson DM, Labande AH, Glen R, Redgrave AJ (2003) Tetrahedron Asymmetry 14:921
- 108. Hodgson DM, Brückl T, Glen R, Labande AH, Selden DA, Dossetter AG, Redgrave AJ (2004) Proc Natl Acad Sci U S A 101:5450

109. Kitagaki S, Anada M, Kataoka O, Matsuno K, Umeda C, Watanabe N, Hashimoto S (1999) J Am Chem Soc 121:1417

- 110. Kitagaki S, Yasugahira M, Anada M, Nakajima M, Hashimoto S (2000) Tetrahedron Lett 41:5931
- 111. Tsutsui H, Shimada N, Abe T, Anada M, Nakajima M, Nakamura S, Nambu H, Hashimoto S (2007) Adv Synth Catal 349:521
- 112. Suga H, Inoue K, Inoue S, Kakehi A (2002) J Am Chem Soc 124:14836
- 113. Suga H, Inoue K, Inoue S, Kakehi A, Shiro M (2005) J Org Chem 70:47
- 114. Suga H, Suzuki T, Inoue K, Kakehi A (2006) Tetrahedron 62:9218
- 115. Suga H, Ishimoto D, Higuchi S, Ohtsuka M, Arikawa T, Tsuchida T, Kakehi A, Baba T (2007) Org Lett 9:4359
- 116. Shannon RD (1976) Acta Crystallogr A 32:751

### Index

A Acetylacetone, 84 Acrylanilides, photocyclisation, 97 Adenine dimer, 16	Brookhaven protein databank (PDB), 5 Building blocks, V-shaped, 39
Adenine dimer, 16 Adenine–benzimidazole, 16	C
2-(2-Alkenoyl)-3-pyrazolidinones, 127	Cambridge structural database (CSD), 5
3-(2-Alkenoyl)-2-thiazolidinethiones, 127	Carbonyl ylides, cycloaddition reactions, 143
Amino acids, 20	electron-deficient carbonyl
Aminobutyric acid (GABA), 19	dipolarophiles, 145
Aminolactams, 91	electron-deficient olefinic
Ammonia-benzene, 25	dipolarophiles, 147
Anion/ $\pi$ interactions, 4, 20	electron-releasing olefinic
Aromatic molecules, interaction energy, 6	dipolarophiles, 149
Aromatic wings, 47	Cation/ $\pi$ interactions, 3, 17
Aryl edge-face (EF) interactions, 47	$CH/\pi$ interactions, 3, 6
Aryl offset face-face (OFF) interactions, 47	substituent effects, 12
Asymmetric induction, 119	2,4-Chloro-6-diphenylamino-1,3,5-triazine, 29
Azacoronene, 27	Clefts, 38
Azomethine imines, cycloaddition reactions, 139	Clips, 38
	Coronene, 27
	Coumarins, photodimerization, 98
В	Couwpled-cluster (CC) methods, 5
Benzene dimers, 3, 6	Crown ethers, 38
Benzene-1,3,5-triazine, 7	Cryptands, 38
Benzene–imidazole complexes, 12	Cyanuric acid, 22
Benzene–pyridine complex, 7	Cycloaddition reaction, 119
Benzimidazole dimer, 16	Cyclodextrins, 38
Betacarboline (BC), 26	Cyclohexanone, 88
Bicyclo[3.3.1]nonane-derived systems, 39, 56	
Bicyclo[3.3.0]octane-derived systems, 40, 50	
Bilayer membranes, 111	D
Binaphthyldiimine ligands, chiral, 129	Database analysis, 1
Bisoxazolines, chiral, 123	DBFOX, 126
Bis(oxazolinyl)pyridines, chiral, 123	Dendrimers, 107
Bis(4-pyridyl), 16	Density functional theory (DFT), 5
Bis(4-pyridyl-N-oxide), 16	1,6-Di(o-chlorophenyl)-1,6-diphenylhexa-2-
Borazine–ammmonia, 29	diyne-1,6-diol, 78
Borazine-boran, 29	Diarylisobenzofuran, 40
Bricks, 64	Diaryltetrazines, 40

156 Index

Diazo compounds, cycloaddition reactions, 134 Diazoacetate, cycloaddition reactions, 136 Dibenzobicyclo[3.3.1]nonane derivatives, 40	4-Isopropyltropolone methyl ether, 97 Issidorides–Haddadin condensation, 40
Dihalo diquinolines, 60 2,2'-Dihydroxy-1,1'-binaphthyl, 78 2,2'-Dihydroxy-9,9'-spirobifluorene, 78 Diols, 75	J Jaws, 38
DNA/RNA bases, 32	K Kagan's ethers, 39, 41
E Edge-edge (EE) packing, 47 Enantioselective inclusion complexation (EIC), 80, 101 Ethylene-3-methylindole, 26	L Lactams, racemic, 91 Lewis acids, chiral, 119, 127 Linker, V-shaped, 48 Lone-pair/π interactions, 27
F Fibers, TTF esters, 114 Fischer indole cyclisation, 40 Formaldehyde/p-toluidine, 42 Formic acid–hydrogen fluoride, 39 Friedländer condensations, 40 Fullerene dyad, 107 Furan dimers, 11	M Melanine–cyanuric acid, 39 Membranes, 111 Metal complex, 119 Methane–benzene, 25 Methyllactams, 91 Molecular pens, 52, 61 Mortar, 64
G Guests, 38	N Nanowires, 107
H Heteroaromatic molecules, π-deficient, 7 π-excessive, 10 9-Heterobicyclo[3.3.1]nonane derived systems, 67 Heterocycles, aromatic, X/π interactions, 1 Hexabromide, 54 Hexafluorobenzene, 20 Hexahosts, 39 Host–guest, 37 behaviour, 52, 60, 67 Hosts, heterocyclic frameworks, appended hydroxyl sensor groups, 78 Hydrogen bonding, 4, 30	Neurotransmitter ACh, 19 NH/ $\pi$ interactions, 4, 25 Nitrile imines, 139 Nitrile oxides, cycloaddition reactions, 136 Nitrones, cycloaddition reactions, 121 enantioselectivity, 130 with, 3-(2-alkenoyl)-2-oxazolidinones, 122 with alkylidene malonates, 132 with vinyl ethers, 133 with $\alpha$ , $\beta$ -unsaturated, 2-acyl imidazole, 127 $\alpha$ '-hydroxy enones, 130 exo-selective cycloaddition reactions, 127 $\alpha$ , $\beta$ -unsaturated aldehydes, 131 p-Nitrophenol-diacetamide, 39 N-Nitrosopiperidine, 86
Imidazolium–water, 28 Inclusion chemistry, 81	

P	Tetracyanopyrazine (TCP), 23
$\pi/\pi$ interactions, 3, 6	Tetracyanoquinodimethane (TCNQ), 111
PHD ( $\pi$ -halogen dimer), 53	Tetrakis(N-oxide), 59
Phenol-imidazole, 12	Tetrathiafulvalenes (TTFs), 104, 110
Phenol–pyrimidine, 12	Tetrazine, 20
Phosphinate, 89	Theoretical calculations, 1
Phosphine oxide, cyclic, 89	Thioformamides, 86
Photocyclisation, anilide, 96	Thiophene dimers, 10
Photoreactions, enantioselective, solid state, 95	Triazine, 9
solid-state, 75	Trihydroxyisocyanuric acid, 99
Phthalocyanine, 113	inclusion ability, 99
Pincers, 38	Trimethylsilyldiazomethane, cycloaddition
Polyhalocarbon guest molecules, 60	reactions, 136
Powder X-ray diffraction (PXRD), 82	Triphenolics, 75
Pyridine dimer, metal-coordinated, 15	macrocyclic hosts, 99
Pyridine-methanol, 30	Triptycene derivative, 14
Pyrimidine dimer, 9	Trisoxazoline, chiral, 132
Pyrrole dimers, 11	Tröger's bases, 42
	Tubuland diols, helical, 39
	Tweezers, 38, 41
Q	
Quinolines, 15	
	$\mathbf{V}$
	V-shaped molecules, heterocyclic, 37
R	Vesicles, oligothiophene-based, 109
Rocaglamides, 98	
	$\mathbf{W}$
S	Water-benzene, 25
Sandwich structures, 23	Wheel and axle compounds, 39
Selenoformamides, 86	
Serotonin (5-HT), 19	
Solid-state photoreactions, 75	X
Spherands, 38	$X/\pi$ interactions, 1
Supramolecular synthons, 37	X-ray analysis, 75
Supramolecules, 2	X-ray diffraction, powder (PXRD), 82
Symmetry requirements, 39	X-ray structure, 1
	XABOX, 126
T	
TADDOLs, 75, 77	$\mathbf{Z}$
Tartaric acid, optically active heterocyclic	Zinc-2,4,6-tris(di-2-picorylamino)-1,3,5-
hosts, 82	triazine, 23